frontiers | Research Topics

Mycobacterial dormancy, culturability, and resuscitation: State-of-the-art, challenges, and future prospects

Edited by
Elena G. Salina, Tatyana L. Azhikina and Bavesh Kana

Published in
Frontiers in Cellular and Infection Microbiology

ISSN 1664-8714
ISBN 978-2-8325-2367-4
DOI 10.3389/978-2-8325-2367-4

About Frontiers

Frontiers is more than just an open access publisher of scholarly articles: it is a pioneering approach to the world of academia, radically improving the way scholarly research is managed. The grand vision of Frontiers is a world where all people have an equal opportunity to seek, share and generate knowledge. Frontiers provides immediate and permanent online open access to all its publications, but this alone is not enough to realize our grand goals.

Frontiers journal series

The Frontiers journal series is a multi-tier and interdisciplinary set of open-access, online journals, promising a paradigm shift from the current review, selection and dissemination processes in academic publishing. All Frontiers journals are driven by researchers for researchers; therefore, they constitute a service to the scholarly community. At the same time, the *Frontiers journal series* operates on a revolutionary invention, the tiered publishing system, initially addressing specific communities of scholars, and gradually climbing up to broader public understanding, thus serving the interests of the lay society, too.

Dedication to quality

Each Frontiers article is a landmark of the highest quality, thanks to genuinely collaborative interactions between authors and review editors, who include some of the world's best academicians. Research must be certified by peers before entering a stream of knowledge that may eventually reach the public - and shape society; therefore, Frontiers only applies the most rigorous and unbiased reviews. Frontiers revolutionizes research publishing by freely delivering the most outstanding research, evaluated with no bias from both the academic and social point of view. By applying the most advanced information technologies, Frontiers is catapulting scholarly publishing into a new generation.

What are Frontiers Research Topics?

Frontiers Research Topics are very popular trademarks of the *Frontiers journals series*: they are collections of at least ten articles, all centered on a particular subject. With their unique mix of varied contributions from Original Research to Review Articles, Frontiers Research Topics unify the most influential researchers, the latest key findings and historical advances in a hot research area.

Find out more on how to host your own Frontiers Research Topic or contribute to one as an author by contacting the Frontiers editorial office: frontiersin.org/about/contact

Mycobacterial dormancy, culturability, and resuscitation: State-of-the-art, challenges, and future prospects

Topic editors

Elena G. Salina — Bach Institute of Biochemistry, Research Center of Biotechnology of the Russian Academy of Sciences, Russia

Tatyana L. Azhikina — Institute of Bioorganic Chemistry (RAS), Russia

Bavesh Kana — University of the Witwatersrand, South Africa

Citation

Salina, E. G., Azhikina, T. L., Kana, B., eds. (2023). *Mycobacterial dormancy, culturability, and resuscitation: state-of-the-art, challenges, and future prospects*. Lausanne: Frontiers Media SA. doi: 10.3389/978-2-8325-2367-4

Table of contents

frontiers | Frontiers in Cellular and Infection Microbiology

TYPE Editorial
PUBLISHED 24 April 2023
DOI 10.3389/fcimb.2023.1201012

OPEN ACCESS

EDITED AND REVIEWED BY
Thomas Rudel,
Julius Maximilian University of Würzburg, Germany

*CORRESPONDENCE
Elena G. Salina
elenasalina@yandex.ru

SPECIALTY SECTION
This article was submitted to Bacteria and Host, a section of the journal Frontiers in Cellular and Infection Microbiology

RECEIVED 05 April 2023
ACCEPTED 17 April 2023
PUBLISHED 24 April 2023

CITATION
Salina EG, Azhikina TL and Kana B (2023) Editorial: Mycobacterial dormancy, culturability, and resuscitation: state-of-the-art, challenges, and future prospects. *Front. Cell. Infect. Microbiol.* 13:1201012. doi: 10.3389/fcimb.2023.1201012

Editorial: Mycobacterial dormancy, culturability, and resuscitation: state-of-the-art, challenges, and future prospects

Elena G. Salina[1,2*], Tatyana L. Azhikina[2] and Bavesh Kana[3]

[1]Bach Institute of Biochemistry, Research Center of Biotechnology, Russian Academy of Sciences, Moscow, Russia, [2]Shemyakin-Ovchinnikov Institute of Bioorganic Chemistry, Russian Academy of Sciences, Moscow, Russia, [3]Department of Science and Innovation/National Research Foundation Centre of Excellence for Biomedical Tuberculosis Research, School of Pathology, Infectious Diseases and Oncology Research Institute, Faculty of Health Sciences, University of the Witwatersrand and the National Health Laboratory Service, Johannesburg, South Africa

KEYWORDS

persistence, resuscitation, mycobacteria, dormancy, non-replicative state

Editorial on the Research Topic:
Mycobacterial dormancy, culturability, and resuscitation: state-of-the-art, challenges, and future prospects

Mycobacterial pathogens cause a variety of diseases such as tuberculosis (TB), Buruli ulcer and leprosy, with the success of these pathogens primarily being driven by a plethora of mechanisms that facilitate escape from host immunity, ultimately leading to disease progression. In addition, mycobacteria can enter non-replicative states that limit their susceptibility to drug treatment, enhance immune subversion and affect recovery of bacteria on routine laboratory media (Batyrshina and Schwartz, 2019). With TB, the combination of these adaptations has driven a global epidemic of staggering proportion, primarily affecting the poor and placing strain on healthcare systems in resource limited settings. This situation has worsened due to the Covid-19 pandemic (WHO, 2022). The complexity associated with clinical presentation of TB, manifesting as asymptomatic infection, subclinical disease, incipient TB or active disease, has long been associated with altered metabolic states of the prevailing tubercle bacilli, but definitive evidence for these associations remains somewhat lacking (Lipworth et al., 2016; Drain et al., 2018; Behr et al., 2021). Tackling this, and appending issues, emerges as an important global priority to enhance diagnostic pickup, tailor prophylaxis approaches, shorten chemotherapy and reduce recurrent disease. This research topic, "Mycobacterial Dormancy, Culturability, and Resuscitation: State-of-the-art, Challenges, and Future Prospects" broadly focuses on mycobacterial adaptation to the non-replicative state, and subsequent resuscitation, together with efforts to identify molecular mechanisms related to these phenomena. Also included are studies aimed at developing novel therapies against drug tolerant bacteria. These, and other studies, are summarized in this editorial.

As model systems to replicate host conditions encountered by tubercle bacilli during pathogenesis continue to evolve, the review by Parbhoo et al. details adaptive strategies employed by *M. tuberculosis* to sense and coordinate physiological responses following exposure to various host-associated stressors that induce persister formation. The authors

focus on exploring animal models for investigating different aspects of the immune response and the impact of the host environment, together with bacterial adaptation in contributing to recalcitrance of infection. Building on some of these aspects, their research article identified the importance of pathogen recognition, phagocytosis, phagosome acidification and maturation as host strategies in inhibiting intracellular growth of *M. tuberculosis*, with important consequences for persister formation. Parbhoo et al. studied how these host factors could impact intracellular bacterial burden, adaptive mechanisms and persistence in macrophages. Their findings provide important information that will direct future strategies targeting persisters to enhance bacterial clearance.

In the last decade, pathways involved in energy metabolism in mycobacteria have gained prominence as tractable areas for TB drug discovery. Plocinska et al. investigated the intracellular function of the Rv3143 protein, which influences the efficiency of the respiratory chain in mycobacteria and controls the switch to nitrate respiration, which is crucial at various stages of infection. Although the precise mechanism of action of Rv3143 requires further detailed analysis, this protein was identified as a component of the proton-pumping type I dehydrogenase complex (NDH-1) possibly modulating its activity.

Shifting to exploring molecular mechanisms that underpin mycobacterial dormancy, the review by Verma et al. focuses on detailing gaps in the understanding of mechanisms that are important for bacterial transition from dormancy to the replicative state and vice versa. Although several bacterial proteins have been identified as playing a key role in dormancy from a variety of studies using different models, how this information can be used to develop next generation therapies and vaccines is unclear. The review highlights novel drug candidates that are potent against non-replicating tubercle bacilli and discusses the potential of these agents to shorten the duration of treatment.

Characteristics of new vaccines and host factors that play an important role in modulating bacterial growth are also discussed. Extending on this idea, Sharma et al. identified phytomolecules that were specifically screened against dormant *M. smegmatis* obtained after prolonged incubation under low oxygen, low pH and nutrient limitation. The authors performed an in silico analysis focused on identifying the modes of action of these hits and found that some of them potentially target well known proteins/regulators involved in dormancy or cell cycle control.

The ability of *M. tuberculosis* to adopt non-culturable states, akin to those seen in laboratory models of dormancy, has important implications for the diagnosis of TB and mapping of transmission events. In this regard, the article by Chengalroyen et al. highlights this problem through detection of a heterogenous population of Differentially Culturable Tubercle Bacilli (DCTB) in sputum specimens from TB infected individuals. DCTB do not recover in routine laboratory media and this differential detection can influence diagnostic outcome and treatment regimens. The authors demonstrate that distinct *M. tuberculosis* lineages emerge differentially in liquid limiting dilution DCTB assays. These assays were supplemented with culture filtrate derived from *M. tuberculosis* as a source of growth stimulatory molecules. Their findings suggest that routine culture likely misses a large proportion of mixed TB infections, with important implications for selection of treatment regimens and in general, for key aspects of TB epidemiology such as transmission mapping. Related to this, Beltran et al. found that supplementation of cultures, with culture filtrate, from extrapulmonary clinical specimens can substantially improve culture positivity rates, with benefits for the diagnosis of spinal tuberculosis, which is usually paucibacillary nature and difficult to detect with routine approaches.

Diabetes is now considered an important risk factor for TB disease. Verma et al. studied the immunological cross-talk between diabetes and TB using the murine model of TB infection, with low bacterial loads in chronic infection to best mimic latent infection in humans. After establishing infection, diabetes was induced in a subset of animals using multiple doses of streptozotocin, followed by assessment of gene expression and cytokine production. The authors found that diabetes in TB infected animals led to a decrease in levels of monocyte chemotactic protein-1 (MCP-1), together with increased expression of matrix metalloprotease-1 (*mmp-1*), and a reduction in expression of *mmp-9*. These combined effects likely affect granulomatous containment of bacilli.

The search for master regulators that enable mycobacteria to respond to environmental stresses that trigger non-replicating persistence, such as hypoxia, has identified the DosR (dormancy regulon regulator), together with DosS and DosT as sensors (Sivaramakrishnan and De Montellano, 2013). In this article collection, Simcox et al. explore the function of DosR in the opportunistic pathogen *Mycobacterium abscessus* that is able to establish chronic infection in cystic fibrosis patients. The authors demonstrate that this regulatory circuit appears to coordinate a much larger set of genes (>1000) than those described in *M. tuberculosis*. Deletion of the DosRS homologues in *M. abscessus* led to attenuated growth of bacilli under low oxygen conditions, a shift from smooth to rough colony morphotype, and the down-regulation of numerous genes, thus providing the first outlook at the global transcriptomic response of this important pathogen.

Together, this research topic highlights important new data, providing a broad and diverse overview of challenges and prospects in area mycobacterial dormancy, culturability, and resuscitation. The Research Topic will be of interest to a wide audience, including researchers, physicians and clinicians, who study *M. tuberculosis* and other mycobacterial species that cause clinically relevant diseases.

Author contributions

All authors listed have made a substantial, direct, and intellectual contribution to the work and approved it for publication.

Funding

ES and TA were funded by the Russian Science Foundation, Grant 22-14-00235; BK was funded by the South African Department of Science and Innovation, the National Research Foundation and the South African Medical Research Council with funds from the Department of Health.

Acknowledgments

We acknowledge the participation of all contributing authors and are grateful for discussions related to the focus of the thematic issue and content of specific articles.

Conflict of interest

The authors declare that the research was conducted in the absence of any commercial or financial relationships that could be construed as a potential conflict of interest.

Publisher's note

References

Batyrshina, Y. R., and Schwartz, Y. S. (2019). Modeling of *Mycobacterium tuberculosis* dormancy in bacterial cultures. *Tuberculosis (Edinb)* 117, 7–17. doi: 10.1016/j.tube.2019.05.005

Behr, M. A., Kaufmann, E., Duffin, J., Edelstein, P. H., and Ramakrishnan, L. (2021). Latent tuberculosis: two centuries of confusion. *Am. J. Respir. Crit. Care Med.* 204, 142–148. doi: 10.1164/rccm.202011-4239PP

Drain, P. K., Bajema, K. L., Dowdy, D., Dheda, K., Naidoo, K., Schumacher, S. G., et al. (2018). Incipient and subclinical tuberculosis: a clinical review of early stages and progression of infection. *Clin. Microbiol. Rev.* 31 (4), e00021–18. doi: 10.1128/CMR.00021-18

Lipworth, S., Hammond, R. J. H., Baron, V. O., Hu, Y., Coates, A., and Gillespie, S. H. (2016). Defining dormancy in mycobacterial disease. *Tuberculosis (Edinb)* 99, 131–142. doi: 10.1016/j.tube.2016.05.006

Sivaramakrishnan, S., and De Montellano, P. R. (2013). The DosS-DosT/DosR mycobacterial sensor system. *Biosensors (Basel)* 3, 259–282. doi: 10.3390/bios3030259

WHO. (2022). *Global tuberculosis report 2022*. Available at: https://www.who.int/teams/global-tuberculosis-programme/tb-reports/global-tuberculosis-report-2022.

frontiers | Frontiers in Cellular and Infection Microbiology

ORIGINAL RESEARCH
published: 28 June 2022
doi: 10.3389/fcimb.2022.909507

The Orphan Response Regulator Rv3143 Modulates the Activity of the NADH Dehydrogenase Complex (Nuo) in *Mycobacterium tuberculosis via* Protein–Protein Interactions

*Renata Płocińska[1], Karolina Wasik[1], Przemysław Płociński[1,2], Ewelina Lechowicz[1], Magdalena Antczak[1], Ewelina Błaszczyk[1], Bożena Dziadek[3], Marcin Słomka[4], Anna Rumijowska-Galewicz[1] and Jarosław Dziadek[1]**

[1] Department of Genetics and Physiology of Mycobacteria, Institute of Medical Biology of the Polish Academy of Sciences, Łódź, Poland, [2] Department of Immunology and Infectious Biology, Faculty of Biology and Environmental Protection, University of Łódz, Łódź, Poland, [3] Department of Molecular Microbiology, Faculty of Biology and Environmental Protection, University of Łódź, Łódź, Poland, [4] Biobank Lab, Department of Molecular Biophysics, Faculty of Biology and Environmental Protection, University of Łódź, Łódź, Poland

Two-component signal transduction systems enable mycobacterial cells to quickly adapt and adequately respond to adverse environmental conditions encountered at various stages of host infection. We attempted to determine the role of the Rv3143 "orphan" response regulator in the physiology of *Mycobacterium tuberculosis* and its orthologue Msmeg_2064 in *Mycobacterium smegmatis*. We identified the Rv3143 protein as an interaction partner for NuoD, a member of the type I NADH dehydrogenase complex involved in oxidative phosphorylation. The mutants Δ*rv3143* and Δ*msmeg_2064* were engineered in *M. tuberculosis* and *M. smegmatis* cells, respectively. The Δ*msmeg_2064* strain exhibited a significant reduction in growth and viability in the presence of reactive nitrogen species. The Rv3143-deficient strain was sensitive to valinomycin, which is known to reduce the electrochemical potential of the cell and overexpressed genes required for nitrate respiration. An increased level of reduction of the 2,3,5-triphenyltetrazolium chloride (TTC) electron acceptor in Δ*rv3143* and Δ*msmeg_2064* cells was also evident. The silencing of *ndh* expression using CRISPRi/dCas9 affected cell survival under limited oxygen conditions. Oxygen consumption during entry to hypoxia was most severely affected in the double-mutant Δ*msmeg_2064 ndh*$^{CRISPRi/dCas9}$. We propose that the regulatory protein Rv3143 is a component of the Nuo complex and modulates its activity.

Keywords: tuberculosis, oxidative respiration, orphan two-component regulators, signal transduction, respiratory chain, NADH dehydrogenase

OPEN ACCESS

Edited by:
Bavesh Kana, University of the Witwatersrand, South Africa

Reviewed by:
Kyle Rohde, University of Central Florida, United States
Martin I. Voskuil, University of Colorado Denver, United States

***Correspondence:**
Jarosław Dziadek
jdziadek@cbm.pan.pl

Specialty section:
This article was submitted to Bacteria and Host, a section of the journal Frontiers in Cellular and Infection Microbiology

Received: *31 March 2022*
Accepted: *23 May 2022*
Published: *28 June 2022*

Citation:
Płocińska R, Wasik K, Płociński P, Lechowicz E, Antczak M, Błaszczyk E, Dziadek B, Słomka M, Rumijowska-Galewicz A and Dziadek J (2022) The Orphan Response Regulator Rv3143 Modulates the Activity of the NADH Dehydrogenase Complex (Nuo) in Mycobacterium tuberculosis via Protein–Protein Interactions. Front. Cell. Infect. Microbiol. 12:909507. doi: 10.3389/fcimb.2022.909507

INTRODUCTION

The success of *Mycobacterium tuberculosis* as a human pathogen is based on its ability to adapt to dynamic changes in intracellular and extracellular environments during the infection process. The fundamental feature of this adaptation is the ability to respire and generate energy, at both the replicative and non-replicative stages. To effectively respond to changing environmental conditions, mycobacteria exploit two-component signal transduction systems (TCSSs). A typical TCSS is composed of a membrane-bound histidine sensor kinase that upon detecting environmental signal undergoes autophosphorylation and can transfer the phosphoryl group onto the regulatory domain of the cytosolic response regulator. *M. tuberculosis* possesses 12 such two-component systems, e.g., SenX3/RegX3, PhoP/PhoR, DosR/DosS, MtrA/MtrB, and PdtaS/PdtaR (Zahrt and Deretic, 2000; Morth et al., 2005; Dadura et al., 2017). The genome of *M. tuberculosis* possesses information for six response regulators (Rv0195, Rv0260c, Rv0818, PdtaR, Rv2884, and Rv3143). Antczak and colleagues reported the role of NnaR (Msmeg_0432) as a regulator of nitrogen metabolism in *Mycobacterium smegmatis* (Antczak et al., 2018). *rv3143* gene was found to be upregulated in DosR mutant, in *M. tuberculosis* (Kendall et al., 2004). Recently, it was shown that Rv3143 increases antibiotic sensitivity by regulating cell wall permeability in *M. smegmatis* (Dong et al., 2020). The role of orphaned elements in bacteria is very fragmentary and remains to be determined. In microorganisms such as mycobacteria, similar to human mitochondria, membrane-bound ATPase catalyzes the synthesis of ATP when an electrochemical gradient (proton motive force (PMF)) is imposed across the cell membrane (Maloney et al., 1974). PMF is generated by an electron transport chain that acts as a proton pump across the membrane during respiration. The respiratory chain in *M. tuberculosis* is composed of nine respiratory dehydrogenases and four terminal oxidoreductases (for review, see (Cook et al., 2014). Since PMF is essential for the viability of replicative and dormant *M. tuberculosis*, the respiratory chain is considered a promising drug target for new anti-tuberculosis drug development. Under aerobic conditions, the major respiratory terminal oxidoreductase in mycobacteria is the bc_1-aa_3 cytochrome *c* supercomplex (Matsoso et al., 2005; Megehee et al., 2006). Menaquinol-cytochrome *c* oxidoreductase (bc_1), encoded by *qcr*CAB, and aa_3-cytochrome *c* oxidase, encoded by *cta*BCDE, belong to the heme-copper respiratory oxidase family (Boshoff and Barry, 2005; Matsoso et al., 2005; Megehee et al., 2006). The inactivation of the bc_1-aa_3 complex in *Mycobacterium* (*Mycolicibacterium*) *smegmatis* leads to the upregulation of cytochrome *bd*-type menaquinol oxidase, encoded by *cydABDC*, which is also present in other species of the *Mycobacterium* genus (Matsoso et al., 2005). A *cydC* mutant of *M. tuberculosis* was attenuated under transition from acute to chronic infection in mice, and CydC is involved in the persistence of *M. tuberculosis* in isoniazid-treated mice (Shi et al., 2005; Dhar and McKinney, 2010). Imidazopyridine amide, Q203, targeting the respiratory cytochrome bc1 complex, was reported to be efficacious in a mouse model of tuberculosis at a dose lower than 1 mg per kg of body weight (Pethe et al., 2013). More recently, despite the affinity of Q203 for the bc_1-aa_3 complex, the drug was shown to be only bacteriostatic and is not able to affect drug-tolerant persisters (Kalia et al., 2017). However, Q203 presented bactericidal activity against an *M. tuberculosis* mutant carrying inactivated *cyd*AB genes encoding cytochrome *bd* oxidase (Kalia et al., 2017). Furthermore, the downregulation or inactivation of *ctaE-qcrCAB*, *cta*C, and *ctaD* reduced but did not prevent the growth of mutants. The Δ*ctaE-qcrCAB M. tuberculosis* mutant was attenuated in the acute phase of mouse infection, but by day 28 post-infection, the strain had reached the same titer as control wild-type *M. tuberculosis* and showed no persistent defect thereafter (Beites et al., 2019). The upregulation of *cydA* in the bc_1-aa_3 mutant strain as well as the construction and analysis of mutants defective in the synthesis of both bc_1-aa_3 and *bd* oxidases clearly demonstrated that *M. tuberculosis* requires the bc_1-aa_3 complex to achieve an optimal growth rate; however, *bd* oxidase alone can support *M. tuberculosis* growth and persistence *in vitro* and *in vivo* (Beites et al., 2019). The use of a marmoset (non-primate monkey) tuberculosis infection model confirmed that the efficient inhibition of cytochrome bc_1-aa_3 oxidase allows the reduction of inflammation, but only a subset of bacilli were affected, while the bacilli present in granulomas exacerbate disease by increasing cavitation (Beites et al., 2019).

Tubercle bacilli possess a single copy of proton-pumping type I dehydrogenase (NDH-1, Nuo) and two copies of NADH dehydrogenases type II (NDH-2), encoded by *ndh* and *ndhA* genes, that transfer electrons to the quinone pool *via* a ping-pong reaction mechanism (Yano et al., 2006). Fast-growing *M. smegmatis* possesses only a single copy of NDH-2 (Ndh), but it carries approximately 95% of the total NADH oxidation measured in this model organism (Vilchèze et al., 2005). NADH-oxidizing activity in *M. tuberculosis* is also mediated mainly by NDH-2, with NDH-1 activity lower than 50% (Cook et al., 2014). NDH-1 of *M. tuberculosis* is encoded by a *nuo* operon consisting of 14 subunits (*nuoA-N*). This operon, except for the pseudogene *nuoN*, is missing in *Mycobacterium leprae* (Cole et al., 2001). NuoB–G are peripheral membrane proteins located on the cytoplasmic side, while NuoA, H, and J–N are located in the membrane section of the complex (Cook et al., 2014; Schut et al., 2016). The *nuo* operon in *M. tuberculosis* was reported to be essential for neither growth nor persistence under oxygen depletion conditions in a Wayne model (Sassetti et al., 2003; Rao et al., 2008; Griffin et al., 2011; DeJesus et al., 2017). The construction and analysis of various *M. tuberculosis* mutants defective in the synthesis of one or more NADH dehydrogenases (Ndh, NdhA, and/or Nuo) showed that Ndh is the main NADH dehydrogenase in tubercle bacilli (Vilchèze et al., 2018). The authors were able to inactivate *ndhA*, *nuoAN*, and both dehydrogenases together with no serious phenotype determined. In contrast, mutants defective in the synthesis of Ndh or both Ndh and NuoAN presented several growth defects *in vitro* as well as *in vivo*, with the Δ*ndh*Δ*nuoAN* double mutant most severely attenuated in mice (Vilchèze et al., 2018). The authors were not able to inactivate both NDH-2 dehydrogenases in *M. tuberculosis*, concluding that at least one NDH-2 dehydrogenase might be essential for the viability of mycobacteria (Vilchèze et al., 2018). Since NDH-2 seems to be

the major NADH dehydrogenase in *M. tuberculosis*, it is considered an attractive target for new drug development (Weinstein et al., 2005; Shirude et al., 2012; Harbut et al., 2018; Murugesan et al., 2018). More recently, the essentiality of NDH-2 was shown to be conditional and dependent on the presence of fatty acids. The *M. tuberculosis* mutant Δ*ndh-2* appeared to be attenuated in the acute phase of infection, but its persistence was not significantly affected (Beites et al., 2019). Since NDH-2 is not required for *M. tuberculosis* in media containing short-chain fatty acids or cholesterol, the treatment of tuberculosis by targeting NADH dehydrogenase might require efficient inactivation of all three enzymes, Ndh, NdhA, and the Nuo complex.

Here, we applied a suite of microbiology, molecular biology, and biochemistry methods to identify the role of an "orphan" regulatory protein of the two-component system family, Rv3143, which we found to be a component of the NDH-1 dehydrogenase complex. The inactivation of *rv3143*, as well as its ortholog *msmeg_2064* in *M. smegmatis*, especially in the context of *ndh* depletion, affects the functionality of the respiratory chain in mycobacteria.

MATERIALS AND METHODS

Bacterial Strains and Growth Conditions

The *Escherichia coli* strains used in this study were cultured in Luria–Bertani (LB) broth or on agar plates supplemented with ampicillin (50 μg/ml), kanamycin (50 μg/ml), hygromycin (200 μg/ml), and chloramphenicol (34 μg/ml) (Sigma-Aldrich, Missouri, USA). The *M. tuberculosis* strains were grown in 7H9 Middlebrook liquid media supplemented with 10% OADC enrichment (oleic acid, albumin, dextrose, and catalase) and Tween-80 (0.05%) or 7H10/OADC agar plates (Difco, Baltimore, USA). The *M. smegmatis* strains were propagated in Middlebrook 7H10 agar or 7H9 media with OADC and Tween-80 except for experiments under hypoxia where AD enrichment was used. The following antibiotics were used to culture the *M. tuberculosis* and *M. smegmatis* strains: kanamycin (25 μg/ml) and hygromycin (50 μg/ml). To induce *ndh* depletion in *M. smegmatis* strains, anhydrotetracycline (aTc; 100 ng/ml; Sigma-Aldrich, Missouri, USA) was added. All strains used in this study are listed in **Supplementary Table S4**.

Gene Cloning Strategies

All procedures associated with gene cloning into vectors (plasmid isolation, ligation, and transformation) were performed according to the protocols by Sambrook and Russell 2001 (Joseph Sambrook, 2001). All PCR products were generated using KAPA HiFi DNA Polymerase (KAPA Biosystems, Wilmington, MA, USA) and directly cloned into the linearized vector pJET 1.2/blunt (Thermo Fisher Scientific, Waltham, MA, USA). The genes of interest were sequenced, released using restriction endonucleases, and cloned into final vectors. The plasmids and primers used in this study are listed in **Supplementary Table S4**.

Construction of Gene Replacement Vectors and Complementation Plasmids

Mutant strains lacking functional Rv3143 and MSMEG_2064 proteins were constructed according to the homologous recombination protocol by Parish and Stocker (Parish and Stoker, 2000). First, non-functional *msmeg_2064* and *rv3143* genes containing an internal deletion region and marker cassette enabling easy selection of recombinants were cloned into a suicidal p2Nil vector. The 5′ fragments of *msmeg_2064* and *rv3143* (35 and 85 bp, respectively) genes with upstream regions (1,020 and 1,268 bp, respectively) were cloned into the suicidal recombination vector p2Nil. Next, the 3′ fragments of genes of interest (224 and 193 bp) with downstream regions (1,380 and 1,472 bp) along with the PacI screening cassette carrying *lacZ* and *sacB* genes from the pGOAL17 vector were cloned as described previously (Dadura et al., 2017; Antczak et al., 2018). The final plasmids pKW5 and pKW10 were used for a two-step mutant selection protocol. The complementation plasmids carrying native *msmeg_2064* and *rv3143* genes along with their putative promoter sequences were cloned into the pKW08Lx and pMV306 vectors and transformed into the appropriate mutant cells.

Disruption of the *Mycobacterium tuberculosis rv3143* and *Mycobacterium smegmatis msmeg_2064* Genes at Their Native Chromosomal Loci

The final gene replacement vectors pKW5 carrying an internal deletion in *msmeg_2064* and pKW10 (deletion in *rv3143*) were treated with 0.2 mM of NaOH and electroporated into *M. smegmatis* and *M. tuberculosis* cytoplasm. The obtained blue colonies sensitive to sucrose and Kan^R were single crossover (SCO) recombinants possessing the wild-type and mutant copies of the studied genes. The SCO strains were further processed for selection of double crossover (DCO) mutants that were white, resistant to sucrose, Kan^S, and retaining only one copy of the wild-type or mutated gene. The genotypes of the obtained DCO mutants Δ*msmeg_2064* and Δ*rv3143* were confirmed by Southern blotting hybridization using probes homologous to the investigated genes and the Amersham ECL Direct Nucleic Acid Labelling System (Amersham Pharmacia Biotech UK Ltd., Buckinghamshire, UK).

Growth Kinetics and Survival Analyses in the Presence of Reactive Oxygen and Nitrogen

The *M. smegmatis* strains grown in 7H9/AD medium up to the logarithmic stage were diluted to OD_{600} 0.1 and further propagated at 37°C in addition to reactive nitrogen forms–DETA NONOate and reactive oxygen species–menadione at final concentrations of 1,000 and 150 μM, respectively. The absorbance at 600 nm was measured every 3 h throughout the duration of the experiment. To determine the number of viable cells (colony-forming units (CFU) per ml) after 6, 9, 12, and 24 h of growth, bacteria were diluted and spread on 7H10 agar plates. The colonies obtained were counted after 3–5 days of incubation at 37°C, and an Excel file was used for calculations. The *M. tuberculosis* strains were cultured in the same media with the addition of DETA NONOate (25 μM) and

menadione (10 μM). As we reported earlier, the growth of *M. tuberculosis* wild-type cells, propagated in the presence of 25 and 50 μM of DETA NONOate, was inhibited by approximately 30% and 50%, respectively. The growth of *M. tuberculosis* was reduced by about 50% and 10% in the presence of menadione in the concentration of 40 and 10 μM, respectively (Brzostek et al., 2014). In the case of the *M. smegmatis* wild-type strain, 1,000 μM of DETA NONOate was required to achieve a growth reduction of about 50%. Bacterial growth was monitored by measuring the turbidity (OD_{600}) of each culture for 11 days of the experiment. Mycobacterial viable counts were determined as CFU per ml on days 4 and 9 of incubation, as described above.

Minimum Inhibitory Concentration

The microplate Alamar blue assay (MABA test) was applied to define the minimum inhibitory concentration (MIC) value (the lowest concentration of compound that prevents the growth of microorganisms) as described by Franzblau et al. (1998) and Dadura et al. (2017). The *M. tuberculosis* wild-type and Δ*rv3143* strains were propagated in a 7H9/OADC medium supplemented with casein hydrolysate (0.1%) and Tween-80 (0.05%) up to the logarithmic phase. Next, the cells were diluted to a 1.0 McFarland turbidity and 10-fold further in the same media. Thus, the prepared bacterial suspension (100 μl) was transferred to 96-well flat-bottom plates containing 100 μl of 7H9 medium with 2-fold dilutions of the concentration ranges of the tested compounds: valinomycin (1.5–0.125 μg/ml), CCCP-carbonyl cyanide *m*-chlorophenyl hydrazine (10-0.312 ug/ml), and trifluoperazine (28-0.437 ug/ml) (Sigma-Aldrich, St. Louis, MO, USA). The microtiter plate was incubated at 37°C for 7 days, and 25 μl of Alamar blue solution (Thermo Fisher Scientific, Waltham, MA, USA) was added to each well and incubated for an additional 48 h. The susceptibility of the tested strains was assessed based on the change in color from blue to pink, based on visual inspection. Wells containing only bacteria, medium, or compound were used as controls in this experiment, and the MABA test was repeated independently three times.

Construction of CRISPR-Cas Strains

The CRISPR-Cas system was applied to lower the expression level of *ndh* gene in the presence of the inducer in the Δ*msmeg_2064* mutant and *M. smegmatis* wild-type strain (Rock et al., 2017; Korycka-Machała et al., 2020). For this purpose, a 20-nucleotide DNA sequence complementary to the *M. smegmatis ndh* gene (*msmeg3621*) and 2 nucleotides away from the PAM sequence (5′-AGAAG-3′) was synthesized and cloned into the pLJR962 vector linearized with BsmBI endonuclease. The obtained pKW16 plasmid (**Supplementary Table S4**) was electroporated into *M. smegmatis* wild-type and Δ*msmeg_2064* mutant competent cells. Sequences of primers used to silence *ndh* gene are listed in **Supplementary Table S4**.

Survival Assessment of CRISPR-Cas Strains Under Hypoxia and Discoloration of Methylene Blue

The survival of mycobacterial strains was determined by growth kinetics and the viable CFU/ml. All studied strains were grown in 7H9 media supplemented with 10% AD and 0.05% Tween-80 up to OD_{600} 0.6–0.8 at 37°C. To silence *ndh* gene, the strains were propagated in the presence of aTc (100 ng/ml) for 16 h. Next, to obtain hypoxic conditions, cells were diluted to an OD_{600} of 0.3, and 12 ml of each culture was transferred to a 15-ml Falcon tube, tightly closed, sealed with parafilm, and incubated at 37°C for 6 h, 24 h, and 10 days with shaking. The different Falcon tubes have been prepared for each time point, in order not to disturb the hypoxic condition. To the control tube, the oxygen consumption indicator methylene blue was added at a final concentration of 6 μg/ml. The kinetics of growth was determined by measuring the optical density at 600 nm at 6 h, 24 h, and 10 days. Serial dilutions of the cells at the same time points were plated on 7H10 agar plates, colonies were counted, and CFU/ml was calculated. The discoloration of methylene blue was determined by measuring the absorbance at 600 nm every hour until the complete discoloration of the indicator. The experiment was repeated three times. Hypoxic conditions and *ndh* depletion were performed in the same way as described above.

Cloning, Expression, and Purification of Rv3143 and NuoD Proteins

The sequence coding the Rv3143 was cloned into pGEX-6P-2 (Addgene, Watertown, MA, USA), enabling purification of the tested protein fused to a glutathione S-transferase (GST) tag, and the sequence coding NuoD protein was cloned into pE-SUMO (LifeSensors Inc., Malvern, PA, USA) expression vector fused to a His tag. The overexpression of Rv3143-GST and pE-SUMO-NuoD was carried out in the *E. coli* BL21 (DE3) strain in LB media at 37°C with shaking until the OD_{600} reached 0.6–0.8. Next, the cells were cooled to 20°C, the expression was induced with isopropyl β-D-1-thiogalactopyranoside (IPTG) measuring 0.4 mM (Rv3143-GST) and 0.2 mM (pE-SUMO-NuoD), and the cells were cultured overnight at 20°C. Purification of recombinant proteins was performed from cell pellets obtained from 1 L of induced culture using affinity chromatography. The cell pellet was suspended in phosphate-buffered saline (PBS) buffer, sonicated using an ultrasonic probe (10 × 10 s), and centrifuged. Rv3143-GST was purified using agarose resin with immobilized glutathione, GST GraviTrap™ columns (GE Healthcare, Chicago, IL, USA), and elution buffer (50 mM of Tris-HCl, pH 8.0, 10 mM of reduced glutathione). Thirty milliliters of washing buffer (50 mM of Tris-HCl, pH 8.0, 10% glycerol) was used to remove reduced glutathione, and chosen fractions of purified Rv3143-GST protein were concentrated on a Vivaspin® 6, 10 kDa MWCO concentrator (GE Healthcare, IL, USA). The harvested cells of pESUMO-NuoD were suspended in binding buffer, pH 7.5 (50 mM of Tris-HCl, 500 mM of NaCl, and 0.1% sodium dodecyl sulfate (SDS)) with 100 μg/ml of lisozyme, disintegrated by sonication, and precleared by centrifugation, and supernatant with 2 M of hexylene glycol was incubated in an ice bath for 1.5 h with shaking. The recombinant protein was purified by applying His pure Ni-NTA resin (Thermo Fisher Scientific, Waltham, MA, USA) and elution buffer containing 500 mM of imidazole. To obtain

a purer protein preparation, a HiTrap SP FF column with an AKTA start (GE Healthcare, IL, USA) system was applied, and the pSUMO-NuoD protein was eluted in a NaCl gradient with buffers containing 50 mM of Tris-HCl and 10% glycerol. To remove imidazole, the protein was passed through a Sephadex G-25 column and concentrated on a Vivaspin® 6, 10 kDa MWCO concentrator.

Preparation of Mouse Polyclonal Anti-Rv3143 Antibodies

The Rv3143 recombinant protein was concentrated on a Novagen concentrator (Merck KGaA, Darmstadt, Germany) to a final concentration of 1 mg/ml and then used for immunization of 8- to 12-week-old female mice of the BALB/c strain. The recombinant protein was emulsified with incomplete Freund's adjuvant (IFA) (Sigma-Aldrich, Missouri, USA) at a ratio of 1:1 (v/v), and the protein/adjuvant mixture was administered subcutaneously using three doses at 2-week intervals. The final amounts of mycobacterial recombinant antigen used for immunization were 100 μg (1st dose) and 80 μg (2nd and 3rd doses). Two weeks after the last booster injection, mice were anesthetized with 40 mg per kilogram of body weight sodium pentobarbital, blood samples were collected from the orbital sinus, and laboratory animals were further euthanized using barbiturate overdose. Mouse sera were prepared from the collected blood samples, and both the titers and optimal working dilutions of polyclonal anti-Rv3143 IgG immunoglobulins (primary antibodies) were determined using indirect ELISA with recombinant Rv3143 protein as a coating antigen (20 μg/ml) and horseradish peroxidase (HRP)-labeled goat polyclonal antimouse IgG immunoglobulins as secondary antibodies (Jackson ImmunoResearch, West Grove, PA, USA) diluted 1:2,000. The resulting immune complexes were detected using a mixture of ABTS chromogen (2,2′-azino-bis(3-ethylbenzothiazoline-6-sulfonic) acid at a concentration of 1 mg/ml (Sigma-Aldrich, St. Louis, MO, USA) and H_2O_2 (Sigma-Aldrich, St. Louis, MO, USA) as an HRP substrate in phosphate-citrate buffer, pH 4.5. The optimal working dilution of secondary antibodies was established in the preliminary titration experiments.

The laboratory BALB/c mice used for immunization were raised under standard conventional conditions approved by the Polish Ministry of Science and Higher Education Animal Facility of the Institute Microbiology, Biotechnology and Immunology, Faculty of Biology and Environmental Protection, University of Lodz. The applied experimental procedures were approved and conducted according to guidelines provided by the appropriate Polish Local Ethics Commission for Experiments on Animals No. 9 in Lodz (Agreement 54/ŁD1/2011).

Protein Complex Purification

To identify the protein complexes for Rv3143, the integration pKW08 vector possessing the *rv3143* sequence fused with enhanced green fluorescent protein (eGFP) under a tetracycline-induced promoter was constructed. The final plasmid pKW17 was electroporated into *M. tuberculosis*-competent cells. The overexpression of Rv3143-eGFP and purification of protein complexes were performed according to a published protocol (Płociński et al., 2014). Actively growing *M. tuberculosis* cells expressing Rv3143-eGFP in Middlebrook 7H9/OADC media with an optical density $OD_{600\ of}$ 0.6 were induced with 50 ng/ml of tetracycline and incubated at 37°C for 48 h. Three hundred milliliters of induced cells was centrifuged at 4,500 rpm for 10 min at 4°C and washed twice with 30 ml of washing buffer (50 mM of HEPES, pH 7.4, 150 mM of NaCl). The cell pellet obtained was suspended in 9 ml of cold lysis buffer, transferred to BIGB-Lysing MATRIX B-tube (MP Biomedicals, Irvine, CA, USA), and homogenized five times for 20 s at 6.0 m/s using Ms disruptor system with Quick prep adapter (MP Biomedicals, Irvine, CA, USA) with a 5-min break between cycles on ice. Next, the clarified supernatant after spinning was incubated with GFP-trap agarose resin (ChromoTek, Planegg-Martinsried, Germany) for 2 h in a cold room with rotation. The column was washed three times with 10 ml of IPP150 buffer. In some experiments, bis(sulfosuccinimidyl)suberate (BS3) was added at a final concentration of 2 mM (Thermo Fisher Scientific, Waltham, MA, USA); a crosslinker was added according to the manufacturer's instructions (Thermo Fisher Scientific, Waltham, MA, USA), incubated for 45 min at room temperature in the dark and washed twice with 10 ml of tobacco etch virus (TEV) buffer. Next, 3 μl of TEV protease (Promega, Madison, WI, USA) in 400 μl of TEV buffer was incubated with the column for 4 h at room temperature followed by overnight incubation at 4°C. To precipitate the protein complexes obtained, pyrogallol red–molybdate (PRM) buffer was added and incubated for 5 h at room temperature followed by overnight incubation at 4°C. Samples were centrifuged for 25 min at 12,000 rpm at 25°C, and the resulting pellet was subjected to high-performance liquid chromatography coupled to tandem mass spectrometry (LC-MS/MS) analysis using Orbitrap Velos as a service at the Institute of Biochemistry and Biophysics Polish Academy of Sciences in Warsaw. The procedure is described in detail elsewhere (Płociński et al., 2014). The raw MS data were analyzed with MaxQuant 1.6.17.0 using default settings and label-free analysis against an *M. tuberculosis* proteome (mycobrowser v.3 *M. tuberculosis* database). Raw data for samples treated with BS3 crosslinker were converted to mzML format with the MSConvert application of the ProteoWizard, and protein–protein crosslinks were identified using Kojak version 1.5.3.

Phylogenetic Analysis of NuoD Proteins

NuoD phylogenetic analysis was performed with an online ETE3 pipeline provided by the database of the Kyoto Encyclopedia of Genes and Genomes (KEGG). First, the *M. tuberculosis* NuoD gene cluster analysis function was applied to pull out all the bacterial NuoD proteins that were most relevant to the downstream analyses. The threshold was set to 100, and the gap size was set to 0. NuoD alignment and phylogenetic reconstructions were performed using the function "build" of ETE3 v3.1.1 (Huerta-Cepas et al., 2016) as implemented on GenomeNet (https://www.genome.jp/tools/ete/). Alignment was

performed with MAFFT v6.861b with the default options (Katoh and Standley, 2013). The tree was constructed using FastTree v2.1.8 with default parameters (Price et al., 2009). Values at nodes are SH-like local support. The ETE3 Python programming package, with necessary dependencies, was used for data visualization. The co-occurrence of NuoD variants with Rv3143 orthologs was calculated from the gene cluster information and visualized on the phylogenetic tree.

Pull-Down Assay

A pulldown assay was performed to investigate the interaction between Rv3143 and NuoD proteins. A 200-µl solution of Rv3143-GST (50 µg) suspended in binding buffer (50 mM of Tris-HCl, pH 8.0, 150 mM of NaCl, 0.5% TitonX, and 10% glycerol) was mixed with GST magnetic beads and incubated for 1 h in an ice bath with swinging. The non-bound fraction was removed using a magnetic separator, and beads were washed six times with 1 ml of washing buffer (50 mM of Tris-HCl, pH 8.0, 150 mM of NaCl, 0.5% TitonX, 20 mM of imidazole, and 10% glycerol). Next, NuoD-His (50 µg) in binding buffer was incubated with magnetic beads for 1 h and washed six times, and protein complexes were eluted with 90 µl of buffer containing 0.3 M of imidazole. Incubation of proteins with magnetic beads to which they did not show affinity was the control in this experiment. Protein fractions were resolved on a 12% SDS–polyacrylamide gel electrophoresis (PAGE) gel and transferred to polyvinylidene difluoride (PVDF) membranes, and protein complexes were immunodetected with rabbit anti-GST (Sigma, St. Louis, MO, USA) and anti-His (Sigma, St. Louis, MO, USA) antibodies, washed with TBS-T (6 × 5 min), and probed with anti-rabbit secondary antibodies for 1.5 h. Immunoblots were processed with enhanced chemiluminescence (ECL) solution as a substrate for HRP following the manufacturer's instructions (Western Sun Luinol-Enhancer Solution, Cyanagen, Bologna, Italy), exposed to X-ray film, and scanned using a Medical X-ray Processor (Kodak, Rochester, NY, USA).

Analysis of Respiratory Efficiency of Mutant Cells by Reduction of 2,3,5-Triphenyltetrazolium Chloride

The Δ*rv3143* and Δ*msmeg_2064* cells from the logarithmic phase of growth were diluted in 7H9/OADC media to 1×10^6 cells/ml and transferred to a microtiter 96-well plate (200 µl). Sterile 2,3,5-triphenyltetrazolium chloride (TTC) solution at a final concentration of 0.625 mg/ml was added, and the plate was incubated at 37°C for 0, 2, and 6 h. The Benchmark Plus Microplate Spectrophotometer (Bio-Rad Laboratories, Hercules, CA, USA) was used to measure the amount of red formazan at a 480-nm wavelength. The significant differences between the studied strains were estimated using Student's *t*-test.

RNA Isolation, Quantitative Real-Time PCR, and Total RNA Sequencing

M. smegmatis cells were cultured in Middlebrook 7H9 liquid medium supplemented with AD for 16 h at 37°C with or without aTc. When the OD_{600} reached 0.6, 50 ml of culture was centrifuged at 4,500 rpm at 4°C for 20 min, and the cell pellet was stored at −70° C. Total RNA was extracted using TRIzol LS reagent (Thermo Fisher Scientific, Waltham, MA, USA), 0.1-mm silica spheres, and an MP disruptor system (MP Biomedicals, Irvine, CA, USA) as previously described (Pawelczyk et al., 2011; Dadura et al., 2017; Antczak et al., 2018). A Turbo DNA-*free*™ Kit (Ambion Inc., Austin, TX, USA) was used to remove DNA contamination following the manufacturer's instructions, and RNA quantity was assessed using a NanoDrop 2000 spectrophotometer (MP Biomedicals, Irvine, CA, USA). Reverse transcription was performed using SuperScript III First-Strand Synthesis Super Mix (MP Biomedicals, Irvine, CA, USA) and random hexamers. The expression profile of the studied genes was analyzed by qRT-PCR using Maxima SYBR green qPCR master mix (MP Biomedicals, Irvine, CA, USA) and a 7900HT real-time PCR system (Applied Biosystems, Foster City, CA, USA) as described previously (Pawelczyk et al., 2011; Dadura et al., 2017; Antczak et al., 2018). The total reaction of 25 µl containing 1× Maxima SYBR green qPCR master mix, 50 ng of cDNA, and 0.3 µM of each primer was activated at 95°C for 10 min. Next, 40 cycles of denaturation at 95°C for 20 s were followed by annealing at 60°C for 30 s and extension at 72°C for 30 s. After qRT-PCR, the melting curve was determined to verify that a single specific product was generated. The relative fold changes in gene expression were calculated using the double-delta method ($2^{-\Delta\Delta CT}$). The number of tested transcripts was normalized to the reference gene *msmeg_2758* (*sigA*) and then compared to the control strain.

The total RNA sequencing libraries were prepared as described in detail in our previous work (Płociński et al., 2019). Briefly, 2 µg of DNAse Turbo-treated, AMPure XP bead purified RNA was ribodepleted with a RiboZero Bacteria kit (Illumina, San Diego, CA, USA). Sequencing libraries were generated with a KAPA-stranded RNA-Seq kit according to the manufacturer's protocol (Roche Diagnostics, Rotkreuz, Switzerland). The resulting adapter-ligated, PCR-amplified cDNA libraries were subjected to sequencing on a NextSeq500 sequencer using the NextSeq500/550 v.2 sequencing kit (Illumina, San Diego, CA, USA), and approximately 5 to 10 million paired-end reads were sequenced for each sample. The sequencing data were processed using a suite of bioinformatic scripts and programs and mapped to the H37Rv reference genome as previously published (Płociński et al., 2019). Differential gene expression analysis was performed with the Degust RNA-Seq analysis platform using default parameters (http://degust.erc.monash.edu/, originally designed by D. R. Powell). The numerical data obtained from transcriptomic analysis were imported into Python Pandas data frame format, and the Seaborn package was used to draw the results as figure elements (Płociński et al., 2019).

RESULTS

Rv3143 Protein Interacts With NADH Dehydrogenase Type I Complex Proteins

Rv3143 is annotated as a putative "orphan" response regulator of a two-component system, and the protein contains no DNA-

binding domain, which indicates that it does not operate as a transcription factor. To identify the function of Rv3143, we employed our previously published method to screen for potential partners of the protein investigated in *M. tuberculosis*. The gene fusion encoding Rv3143 tagged to *eGFP-tag* (eGFP) was constructed, cloned into the integration pKW08 vector under control of the P_{tet} promoter, and then introduced into *M. tuberculosis*. The recombinant strain was cultured to the logarithmic phase of growth (OD_{600} at 0.6) when the expression of the bait protein was induced with tetracycline. Bacterial cells were allowed to overproduce GFP-Rv3143 protein and were collected and lysed, and the released proteins were purified on anti-GFP agarose resin, as described in the *Materials and Methods*. GFP-Rv3143 fusion protein and the potential interacting proteins binding to the bait, Rv3143, were recovered from the resin with TEV protease cleavage, and one of the samples was crosslinked with the BS3 crosslinker, which introduces stable amide bonds. The interacting proteins were discovered by MS analysis. The specificity of the purification process was confirmed by Rv3143 being among the top three most abundant proteins identified in the MS samples. Both samples containing the BS3 crosslinker and devoid of the crosslinker were rich in cytoplasmic components of the Nuo protein complex. Among the 30 most abundant proteins copurified with bait, we identified NuoE, NuoG, NuoF, NuoI, NuoD, NuoC, and NuoB (**Figure 1A** and **Supplementary Table S1A**). While much less abundant, we could also identify NuoL, NuoH, NuoN, and NuoK membrane proteins copurified with Rv3143. Mapping the interaction network with the BS3 crosslinker allowed us to identify a possible interaction between Rv3143 and the NuoD protein. Not only did the NuoD and Rv3143 pair have the highest number of crosslink instances identified, but the crosslinks were also assigned the highest score by Kojak software (**Figure 1C** and **Supplementary Table S1B**). Since the orthologs of Rv3143 are often within the same operon as the NuoA–N proteins in actinobacteria (e.g., *M. smegmatis*), we tested the co-occurrence of NuoD and Rv3143 orthologs in other bacteria. Based on a KEGG gene cluster search performed with mycobacterial NuoD, 3,503 orthologs were identified, and their sequences were fetched for phylogenetic analysis with the ETE3 pipeline. Interestingly, NuoD orthologs containing insertions inside the protein sequence clustered

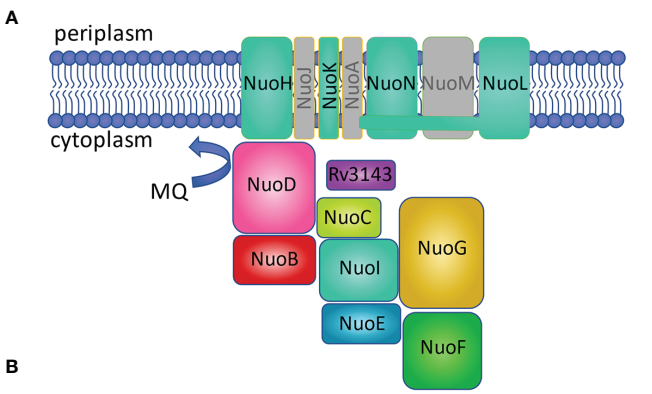

B

>NuoD *Mycobacterium tuberculosis*
MTAIADSAGGAGETVLVAGGQDWQQVVDAARSADPGERIVVNMGPQHPSTHGVLRLILEI
EGETVVEARCGIGYLHTGIEKNLEYRYWTQGVTFVTRMDYLSPFFNETAYCLGVEKLLGI
TDEIPERVNVIRVLMMELNRISSHLVALATGGMELGAMTPMFVGFRAREIVLTLFEKITG
LRMNSAYIRPGGVAQDLPPNAATEIAEALKQLRQPLREMGELLNENAIWKARTQGVGYLD
LTGCMALGITGPILRSTGLPHDLRKSEPYCGYQHYEFDVITDDSCDAYGR*YMIRVKEMWE*
*SMK*IVEQCLDKLRPGPTMISDRKLAWPADLQV*GPDGLGNSPKHIAKIM*GSSMEALIHHFK
LVTEGIRVPAGQVYVAVESPRGELGVHMVSDGGTRPYRVHYRDPSFTNLQSVAAMCEGGM
VADLIAAVASIDPVMGGVDR

>Rv3143
MPDSSTALRILVYSDNVQTRERVMRALGKRLHPDLPDLTYVEVATGPMVIRQMDRGGIDL
AILDGEATPTGGMGIAKQLKDELASCPPILVLTGRPDDTWLASWSRAEAAVPHPVDPIVL
GRTVLSLLRAPAH

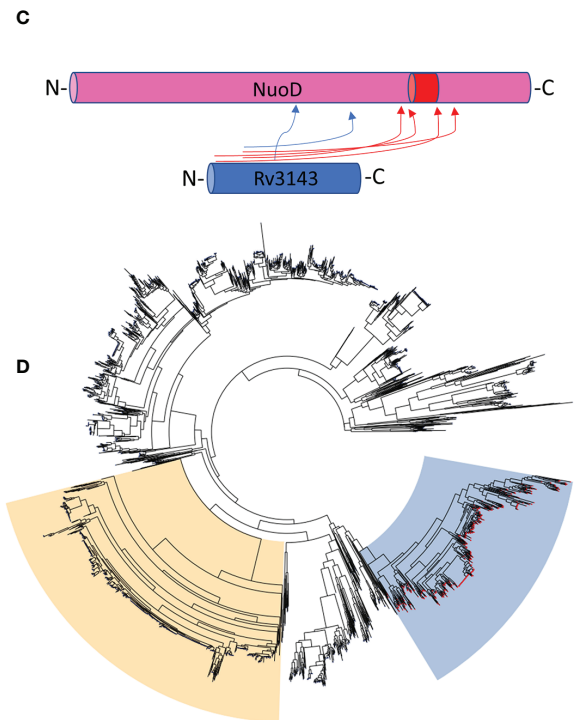

FIGURE 1 | The orphan response regulator Rv3143 is a component of the NuoA–N complex in actinobacteria. **(A)** Graphical summary of the interaction network of Rv3143 with NADH dehydrogenase complex I in *Mycobacterium tuberculosis* based on a single-step affinity purification method coupled with mass spectrometry. Nuo components that were not copurified with eGFP-Rv3143 used as bait were grayed out (the figure layout was modified from Schut et al. [(Schut et al., 2016)]. **(B)** Sequences of *M. tuberculosis* NuoD and Rv3143 are shown. Putative, conserved phosphorylation site (D, aspartic acid) is marked in blue on the Rv3143 sequence. The amino acid insertion sequence (marked in red) found in actinobacterial NuoD proteins may be involved in mediating the interaction between NuoD and Rv3143, as indicated by mass spectrometry BS3 crosslinking analysis performed with Kojak software. Crosslinks with Kojak scores higher than 0.5 are shown in the rudimentary cartoon figure **(C)**. Insertion of the amino acid stretch depicted in panel B is common in actinobacteria, and its presence correlates with the co-occurrence of Rv3143 orthologs in these bacteria. The phylogenetic tree is shown **(D)**, where the blue background indicates the NuoD cluster for which genomic co-occurrence of Rv3143 orthologs is evident (red nodes on each tree leaf). The phylogenetic cluster for NuoCD and NuoBCD chimeric proteins, common in proteobacteria, is indicated with moccasin color for comparison.

separately from other ortholog sequences (insertion marked in **Figure 1B**). The co-occurrence of our putative response regulator was addressed at the same time. The results clearly indicated that the actinobacterial NuoD orthologs, for which an ortholog of Rv3143 co-occurs on the bacterial genome, cluster away from other bacterial species (**Figure 1D**). Of 516 NuoD variants containing the extra stretch of amino acids in their sequence and thus forming a phylogenetic cluster, 513 were linked with co-occurrence of Rv3143 ortholog on their genomes at the same time.

To verify the protein–protein interaction identified by MS, we purified recombinant versions of His-NuoD and GST-Rv3143 as full-length polypeptides. NuoD was purified as a fusion protein with the N-terminal polyhistidine (6-His) tag, and Rv3143 was tagged with a GST tag. GST-Rv3143 and His-NuoD were incubated with anti-GST magnetic beads. We also immobilized His-NuoD protein with Ni-NTA magnetic beads and incubated it with Rv3143 protein. Western blotting analysis with tag-specific antibodies revealed the presence of both tested proteins in eluates obtained from anti-GST and Ni-NTA magnetic beads after extensive washing, confirming the interaction between Rv3143 and NuoD proteins (**Figure 2**). In the control experiments, the potential non-specific interaction of the tested proteins with no-affinity resin was verified, with no detection of the investigated proteins by Western blotting (**Figures 2E, F**). We have also performed the pull down between GST alone and NuoD with no interactions detected. The results are introduced into the Supplementary materials **Figure S2**.

Rv3143/MSMEG_2064 Is Not Essential for the Viability of Mycobacteria, and Its Removal Causes Transcriptional Changes Related to the Induction of Nitrate Respiration

We applied homologous recombination to replace intact *rv3143* and its ortholog in *M. smegmatis msmeg_2064* with non-functional copies carrying large internal deletions. Then, the mutants were complemented with accessory copies of intact *rv3143*/*msmeg_2064* genes carrying the upstream sequences as putative promoters. The functionality of complementation was verified by qRT-PCR (*M. smegmatis*) or immunodetection (*M. tuberculosis*) (**Supplementary Figure S1**). The Western blotting analysis demonstrated no detectable level of Rv3143 protein in the Δ*rv3143* knockout *M. tuberculosis* strain and overproduction of Rv3143 in the complementing strain when compared to the control wild-type *M. tuberculosis* (**Supplementary Figure S1A**). qRT-PCR revealed the expected depletion of *msmeg_2064* gene expression in the mutant lacking the functional *msmeg_2064* gene and strong significant overexpression of *msmeg_2064* transcripts in the complementing strain compared to the control wild-type strain (**Supplementary Figure S1B**).

M. tuberculosis and *M. smegmatis* mutants defective in the synthesis of Rv3143/MSMEG_2064, as well as control wild-type strains grown in rich media, were examined for kinetics of growth by measuring the optical density of the culture at 600 nm (OD_{600}) and viability by determining CFU/ml. The growth kinetics and viability of the mutants were not affected compared

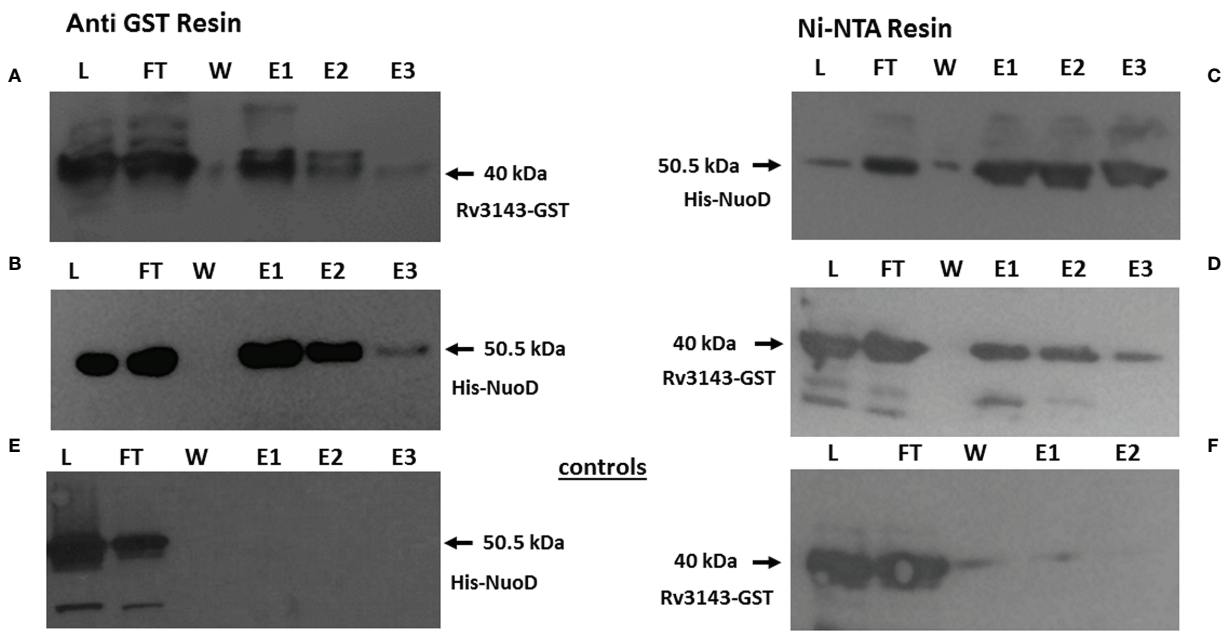

FIGURE 2 | Rv3143 protein interacts with NuoD *in vitro*. Immunoblots of NuoD pulled down with Rv3143 on anti-glutathione S-transferase (anti-GST) resin **(A, B)**. Immunoblots of Rv3143 pulled down with NuoD on Ni-NTA resin **(C, D)**. Bound proteins were eluted with imidazole, resolved on sodium dodecyl sulfate–polyacrylamide gel electrophoresis (SDS-PAGE) gels, transferred to polyvinylidene difluoride (PVDF) membranes, and probed with α-His and α-GST antibodies. L, load; FT, flow-through; W, wash; E, elution. **(E, F)** Non-specific interactions of the tested proteins.

to those of the wild-type *M. smegmatis* (**Supplementary Figures S2A, B**) and *M. tuberculosis* strains (**Supplementary Figures S2C, D**). We concluded that Rv3143 and MSMEG_2064 are not essential for the growth and survival of mycobacteria propagated in a rich medium.

Total RNA sequencing revealed that depletion of Rv3143 in *M. tuberculosis* caused a reduction in expression of 34 genes and overexpression of 74 genes (Log2-fold change threshold set to ±1.58, with false discovery rate (FDR) <0.05) when compared to the wild-type strain grown under standard conditions (**Supplementary Table S2**). Interestingly, when the changes from RNA-Seq were inspected with the use of the transcription factor overexpression analysis tool TFOE spreadsheet from www.tbdb.com, the tool indicated a significant number of genes belonging to the putative NnaR regulon (Rv0260c). Among them, there were genes encoding proteins primarily involved in nitrogen metabolism and assimilation, particularly important since nitrogen is used by mycobacteria in the respiratory chain when oxygen availability is limited. The transcripts for NarU and NarX were overexpressed nearly 12 times and 3.5 times, respectively, and NarK2 was upregulated 2.5 times, falling just below the threshold level set in our analysis. A summary of the RNA sequencing analysis is shown in **Figure 3**. Deletion of Rv3143 also led to downregulation of the hypoxic TCSS regulator Rv0195 and overexpression of the Rv0601c and Rv0600c histidine kinases that cooperate with the TcrA transcriptional regulator. Other changes on the transcriptional level included overexpression of the mym operon (Rv3083-3089) and Rv3612c-3616c (RD1 region associated with ESX-1 system), whereas *prpCD* locus (Rv1128c-1129c, Rv1130-1131) was downregulated. Several changes in the levels of individual small regulatory RNAs were also noticeable, with ESX-associated ncrMT1234, ncRv3648c, ncRv1298, ASdes, and mcr16 found among the 10 most significantly upregulated transcripts.

The MSMEG_2064-Defective Strain Is Sensitized to Reactive Nitrogen Species

The interaction between Rv3143 and the Nuo complex might suggest that MSMEG_2064 and/or Rv3143 proteins affect the function of complex I of the respiratory chain in mycobacteria. To study the respiratory chain activity of the Δ*msmeg_2064* and

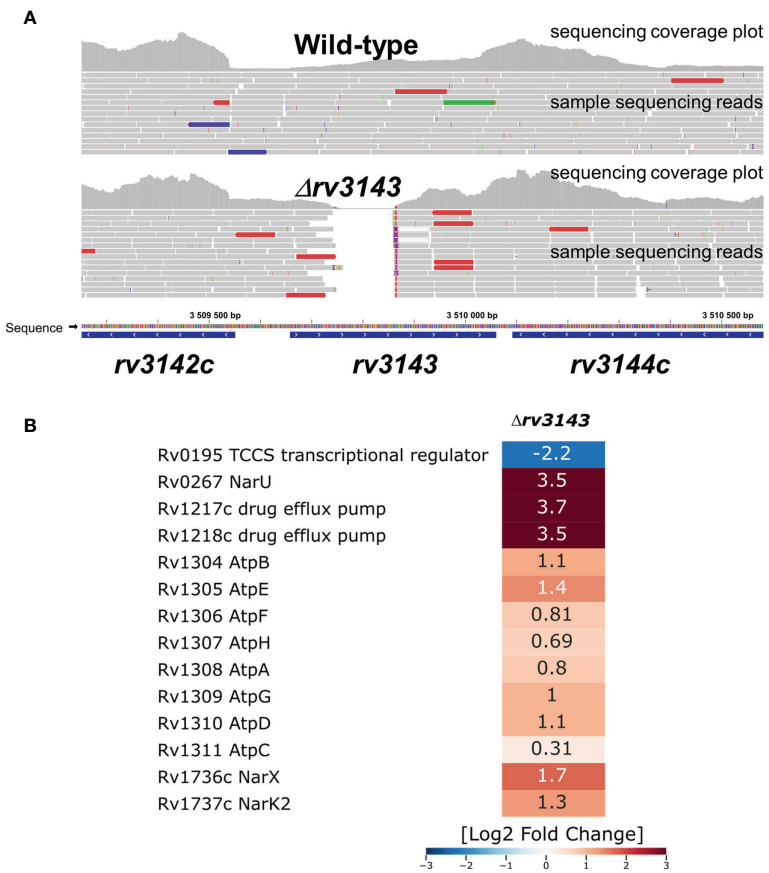

FIGURE 3 | Selected transcriptional changes observed in the Δ*rv3143* mutant strain grown under standard laboratory conditions compared to the wild-type H37Rv *Mycobacterium tuberculosis* strain. **(A)** Confirmation of *rv3143* deletion from sequencing reads, image modified from Integrative Genomics Viewer v2.8.13. Regular paired-end sequencing reads are represented as gray bars. Colored reads either contain insertions (red) and deletions (blue) or have an opposite read pair orientation (green). **(B)** Log2-fold change values are shown in a heatmap generated in Seaborn software based on total RNA sequencing and differential expression estimation from the Degust online RNA-Seq analysis platform.

Δ*rv3143* strains, we attempted to use TTC as an electron acceptor. The reduction of colorless TTC to red 1,3,5-triphenylformazan (TPF) was monitored by recording the absorbance at 480 nm. The potential defect in the entry point of electrons (Nuo) into the electron transport system could lead to a reduced cytosolic environment resulting in the reduced cytosolic TTC. Increased metabolic activity in the cells of the investigated mutants was observed. We noticed a modest but statistically significant increase in the utilization of TTC by approximately 12% in Δ*msmeg_2064* cells after 2 and 6 h of incubation at 37°C compared to the reduction in TTC measured in the wild-type cells (**Figure 4A**).

An increased level of TTC reduction (17% after 2 h and 20% after 6 h) was also observed in Δ*rv3143* cells compared to the control *M. tuberculosis* strain (**Figure 4B**). Furthermore, we observed the restoration of the phenotype to the wild-type strain of both complementing strains Δ*rv3143-attB::*P_{3143}*rv3143* and Δ*msmeg_2064-attB::*P_{2064}*msmeg_2064* encoding intact *rv3143* and *msmeg_2064* genes, respectively.

Reactive nitrogen species treatment and hypoxia were reported to affect cellular respiration, causing a switch from the transcription of type I to type II NADH dehydrogenase and switching to nitrate respiration (Shi et al., 2005). Nitrate respiration is in fact believed to protect hypoxic mycobacteria against reactive nitrogen species (Tan et al., 2010). To evaluate the role of the MSMEG_2064 response regulator in the respiration process, we decided to examine the sensitivity of the investigated strains to reactive nitrogen (DETA NONOate 1,000 μM) and oxygen species (menadione 150 μM). In the presence of DETA NONOate, the growth of the Δ*msmeg_2064* mutant was significantly inhibited compared to that of the wild-type and complementation strains (**Figure 5A**). Additionally, the number of CFU was reduced by approximately 50% in the mutant exposed to DETA NONOate compared to the strains carrying an intact *msmeg*_2064 gene (**Figure 5B**). However, the inactivation of *msmeg_2064* did not affect the kinetics of *M. smegmatis* growth in the presence of reactive oxygen species generated by menadione or the viability CFU of the Δ*msmeg_2064* mutant compared to the control strains carrying an intact *msmeg_2064* gene (**Figures 5C, D**). We did not observe any significant difference in the survival of *M. tuberculosis* mutant in comparison to the wild-type strain upon exposure to DETA NONOate and menadione (**Supplementary Figure S3**).

Deficiency of Rv3143 or MSMEG_2064 Affects the Membrane Redox Potential and Sensitivity to Valinomycin

To further investigate whether Rv3143/MSMEG_2064 affects the activity of complex I of the respiratory chain, we applied the microplate Alamar blue assay (MABA) to examine the sensitivity of the Δ*rv3143 M. tuberculosis* strain to compounds disrupting the electrochemical potential of membranes such as monensin and valinomycin. Monensin transports sodium ions through the membrane in an electrogenic and electroneutral manner. Valinomycin functions as a potassium-specific transporter and

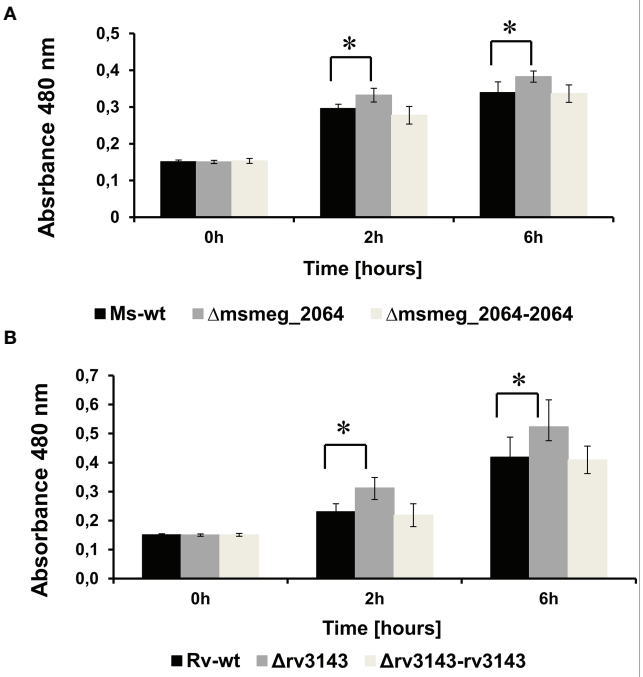

FIGURE 4 | Measurement of reduction rates of a redox indicator—TTC—in Δ*msmeg_2064 Mycobacterium smegmatis* **(A)** and Δ*rv3143 Mycobacterium tuberculosis* **(B)** strains. Absorbance values at 480-nm values are the means ± SDs from three independent experiments. Statistical significance was determined using Student's t-test **(A)** (*$p < 0.001$); **(B)** (*$p < 0.001$).

facilitates the movement of potassium ions through lipid membranes, disrupting the electrochemical potential gradient. We also tested the selected efflux pump inhibitors carbonyl cyanide *m*-chlorophenyl hydrazine (CCCP), an oxidative phosphorylation inhibitor, and trifluoperazine, which affect calcium-dependent ATPase. The strain defective in the synthesis of Rv3143 was not sensitized to monensin, CCCP, or trifluoperazine; however, the Δ*rv3143* mutant appeared to be 3 times more resistant to valinomycin (MIC_{90} 0.75 μg/ml) than the wild-type strain (MIC_{90} 0.25 μg/ml) (**Table 1**; **Supplementary Figure S4**).

However, the increased level of resistance to valinomycin observed in the Δ*rv3143* mutant was abolished in the presence of CCCP or trifluoperazine (**Table 1**). We additionally tested the sensitivity of the Δ*rv3143* mutant to the selected antituberculosis drugs, including ethionamide, isoniazid, capreomycin, ofloxacin, rifampicin, and streptomycin, which affect various molecular targets in the cells with no detectable differences in sensitivity compared to the wild-type strain (**Supplementary Table S3**).

Deficiency of MSMEG_2064 in the Ndh Depletion Background Affects the Viability of *Mycobacterium smegmatis* Under Hypoxia and Reaeration Conditions

The transfer of electrons through the respiratory chain to the quinone pool in mycobacteria depends mainly on NADH

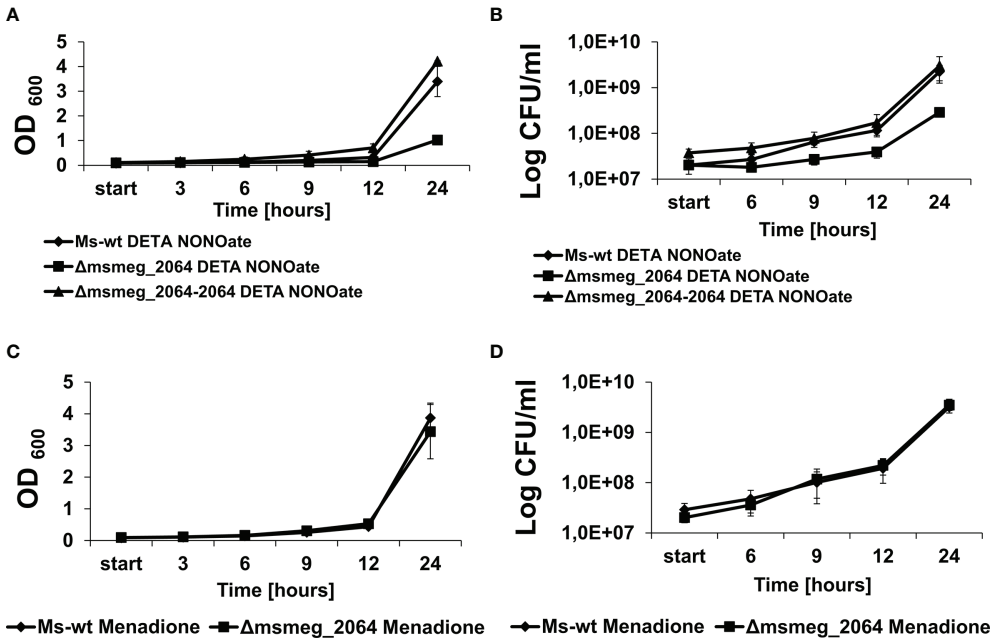

FIGURE 5 | Kinetics of growth and viability of *Mycobacterium smegmatis* strains treated with DETA NONOate or menadione. The mutant Δ*msmeg_2064*, wild-type Ms-wt, and complementing Δ*msmeg_2064–2064* strains were grown in 7H9 Middlebrook-rich medium in the presence of reactive nitrogen (DETA NONOate) **(A, B)** and oxygen species (menadione) **(C, D)**. The growth of strains was evaluated by measuring the OD_{600} at the indicated time points **(A, C)**, and the numbers of viable cells were determined as bacterial colony-forming units (CFU) per ml on 7H10/OADC plates **(B, D)**. Means ± SDs are shown from three independent experiments.

dehydrogenases type II encoded by *ndh* (*M. smegmatis*) or *ndh* and *ndhA* (*M. tuberculosis*) (Yano et al., 2006). To visualize the potential modulatory effect of MSMEG_2064 on respiratory complex I, we decided to construct a Δ*msmeg_2064* mutant with downregulated expression of *ndh* by using the CRISPRi-dCas9 system. The recombinant *M. smegmatis* strains Δ*msmeg_2064-ndh*$^{CRISPRi/dCas9}$ and *ndh*$^{CRISPRi/dCas9}$ were analyzed with respect to the expression level of *ndh* by qRT-PCR compared to the control Δ*msmeg_2064* and wild-type carrying an "empty" CRISPRi/dCas9 vector (**Supplementary Figure S5**).

Both mutants carrying *ndh*$^{CRISPRi/dCas9}$ appeared to express between 5 and 10 times less mRNA carrying information for *ndh* as compared to the control strains. The constructed mutants and control strains were grown under hypoxia and reaeration conditions as described in the *Materials and Methods*. In the absence of aTc (inducing CRISPRi/dCas9 expression), with an unaffected expression of *ndh*, the kinetics of the growth and survival of mutants were not different as compared to the control strains (**Supplementary Figures S6A, B**). However, growth inhibition was observed for Δ*msmeg_2064-ndh*$^{CRISPRi/dCas9}$ and *ndh*$^{CRISPRi/dCas9}$ mutants if aTc was supplemented into the media (**Figure 6A**).

CFU analysis revealed a significant decrease in the number of viable cells of both mutants depleted of Ndh compared to the controls (**Figure 6B**). Moreover, after 10 days of growth under hypoxic conditions, the number of viable cells of the *ndh*$^{CRISPRi/dCas9}$ mutant decreased significantly more (−11.3-fold change vs. wild type carrying the CRISPRi/dCas9 vector, $p < 0.001$) than the number of viable cells of the Δ*msmeg_2064-ndh*$^{CRISPRi/dCas9}$ mutant defective in the synthesis of MSMEG_2064 and depleted of Ndh (−2.64-fold difference vs. Δ*msmeg_2064* carrying the CRISPRi/dCas9 vector, $p < 0.001$; +2.24-fold difference vs. *ndh*$^{CRISPRi/dCas9}$ mutant, $p < 0.001$).

TABLE 1 | Minimum inhibitory concentration (MIC) of selected compounds used in these studies.

Selected compounds	MIC (μg/ml)	
	H37Rv	**Δ*rv3143***
Monensin	3.125	3.125
Valinomycin	**0.25**	**0.75**
CCCP	5	5
Trifluoperazine	14	14
Valinomycin+CCCP	0.25	0.25
Valinomycin+trifluoperazine	0.25	0.25

The presented MIC values were obtained repeatable in three biological repeats. The bold numbers represent the difference in MIC value between control H37Rv and mutant strain.

Furthermore, to reactivate the bacilli, the oxygen-depleted cultures were diluted in 7H9/AD rich medium and incubated at 37°C with intensive shaking for 39 h in conditions with free access to oxygen. All cultures not supplemented with aTc presented no differences in growth and viability after reaeration (**Supplementary Figures S6C, D**). However, the depletion of Ndh significantly inhibited the growth of the *ndh*$^{CRISPRi/dCas9}$ mutant but not the mutant defective in the synthesis of MSMEG_2064 with depleted Ndh (Δ*msmeg_2064-ndh*$^{CRISPRi/dCas9}$). Moreover, the number of viable bacilli detected 20 h after reaeration decreased significantly (9-fold, $p = 0.005$) in the *ndh*$^{CRISPRi/dCas9}$ mutant compared to the control strains and in the Δ*msmeg_2064-ndh*$^{CRISPRi/dCas9}$ mutant (**Figures 6 C, D**). We did not observe the effect of hypoxia on the efficacy of CRISPR system. The qRT-PCR confirmed the downregulation of *ndh* expression under hypoxic conditions (24 h and 10 days) in *M. smegmatis ndh*$^{CRISPRi/dCas9}$ and Δ*msmeg_2064-ndh*$^{CRISPRi/dCas9}$ strains compared to the control strain carrying an "empty" CRISPRi/dCas9 vector (**Supplementary Figures S7A, B**).

Depletion of Ndh But Not Inactivation of *msmeg_2064* Affects the Expression Level of *nuoA* and *nuoD*

NDH-2 in *M. tuberculosis* is conditionally essential and might be compensated by the activity of the NDH-1 complex. We asked the question about the expression level of the selected proteins of the Nuo complex in the Ndh depletion genetic background. The expression levels of *nuoA* and *nuoD* genes were analyzed in the *M. smegmatis* mutant with inducible depletion of Ndh (*ndh*$^{CRISPRi/dCas9}$), in the mutant defective in the synthesis of MSMEG_2064 (Δ*msmeg_2064*), and the double-mutant Δ*msmeg_2064-ndh*$^{CRISPRi/dCas9}$. Both analyzed genes were significantly overproduced (14-fold increase in *nuoA* and 30-fold increase in *nuoD* transcript levels) in both mutants with depleted Ndh compared to the control strain (wild-type strain carrying an "empty" CRISPRi/dCas9 vector). The expression of the investigated *nuo* genes was not affected at the transcriptional level by the inactivation of *msmeg_2064* (**Figure 7**).

MSMEG_2064 Deficiency in the Ndh Depletion Background Affects Oxygen Consumption

The oxygen consumption in the culture was monitored by discoloration of methylene blue as an indicator. We compared the dynamics of oxygen consumption in the culture of *M. smegmatis* mutants defective in the synthesis of MSMEG_2064 (Δ*msmeg_2064*) and strains with inducible depletion of Ndh (*ndh*$^{CRISPRi/dCas9}$, Δ*msmeg_2064-ndh*$^{CRISPRi/dCas9}$) in comparison to the control wild-type strain with or without an "empty" *CRISPRi/dCas9* vector as well as Δ*msmeg_2064* complemented

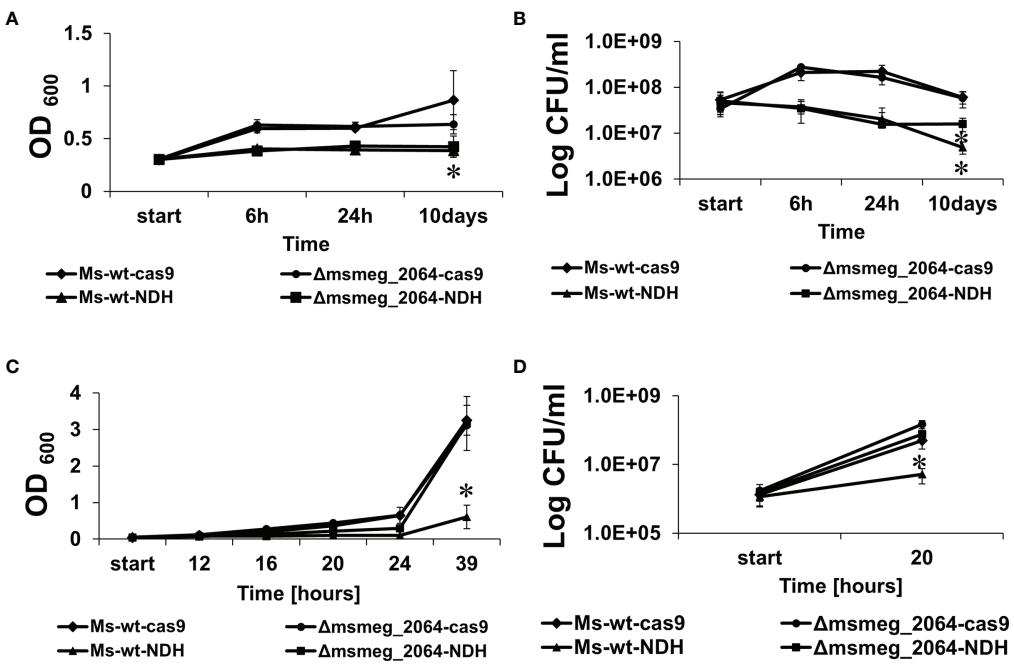

FIGURE 6 | Kinetics of growth and viability of *Mycobacterium smegmatis* strains expressing decreased levels of *ndh* gene. The mutant strains *ndh*$^{CRISPRi/dCas9}$ (Ms-wt-NDH) and Δ*msmeg_2064-ndh*$^{CRISPRi/dCas9}$ (Δ*msmeg_2064*-NDH) and control strains CRISPRi/dCas9 (Ms-wt-cas9) and Δ*msmeg_2064*$^{CRISPRi/dCas9}$ (Δ*msmeg_2064*-cas9) were grown in 7H9/AD Middlebrook medium for 16 h at 37°C with the addition of anhydrotetracycline to deplete *ndh*. Then, bacteria were cultured in limited oxygen access for 10 days **(A, B)** and subjected to reaeration for 39 h (C,D). The growth of strains was evaluated by measuring the OD_{600} at the indicated time points (A,C), and the numbers of viable cells were determined as bacterial colony-forming units (CFU) per ml on 7H10/OADC plates (B, D). Mean ± SD from three independent experiments are shown. Statistical significance was determined using Student's t-test **(A)** (*$p < 0.01$); **(B)** (*$p < 0.0001$); **(C)** (*$p < 0.001$); **(D)** (*$p < 0.0001$).

with an intact *msmeg_2064* gene (P_{tet}-*msmeg_2064*). All strains growing without aTc as an inducer of Ndh depletion presented a similar time of methylene blue discoloration as was monitored by OD_{600} readings. In the presence of aTc, oxygen consumption was dramatically slowed down in the $ndh^{CRISPRi/dCas9}$ mutant (6 vs. 12 h compared to the control). The inactivation of *msmeg_2064* in the Ndh depletion background further delayed oxygen consumption by approximately 2 h (**Table 2**).

DISCUSSION

The bioinformatics analyses of the Rv3143 protein, annotated as an "orphan" regulatory protein of the two-component regulatory system, indicate the presence of an N-terminal receiving domain REC and the absence of nucleic acid-binding domains in its structure. As reported, 70% of regulatory proteins contain the DNA binding domain and act as transcription regulators (Zschiedrich et al., 2016). Moreover, the Rv3143 protein was not phosphorylated by selected histidine kinases belonging to the already known TCSSs, and under the influence of acetyl phosphate, the compound presents a high potential for transferring phosphate groups (Agrawal et al., 2015). Hence, we postulated that Rv3143 acts as an auxiliary protein or an intermediary binding to other proteins. Importantly, Rv3143 was previously found to be overexpressed in multidrug-resistant tuberculosis strains, along with the DevR, MtrA, and RegX3 two-component system regulators (Zhou et al., 2015).

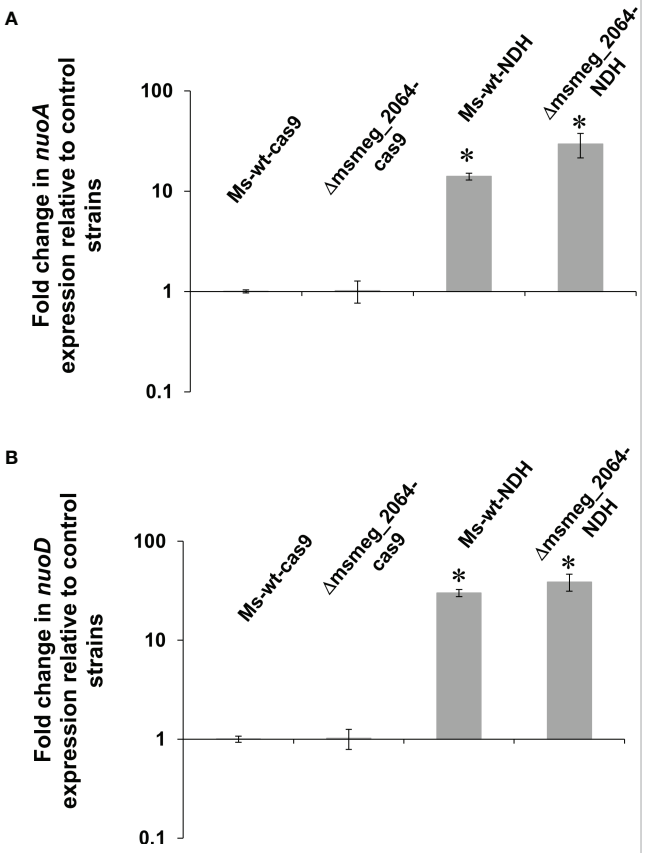

FIGURE 7 | Expression profile of *nuoA* **(A)** and *nuoD* **(B)** genes in *Mycobacterium smegmatis* strains expressing depleted *ndh*. Mutant strains $ndh^{CRISPRi/dCas9}$ (Ms-wt-NDH) and Δ*msmeg_2064-*$ndh^{CRISPRi/dCas9}$ (Δ*msmeg_2064*-NDH) and control strains CRISPRi/dCas9 (Ms-wt-cas9) and Δ*msmeg_2064*$^{CRISPRi/dCas9}$ (Δ*msmeg_2064*-cas9) were grown in 7H9/AD broth for 16 h at 37°C with the addition of anhydrotetracycline. Transcript levels were determined using qRT-PCR and SYBR green chemistry. The expression levels of *nuoA*/*nuoD* were normalized to the *sigA* housekeeping gene and compared to the control strain. Statistical significance was determined using Student's t-test **(A)** (*$p < 0.001$); **(B)** (*$p < 0.001$).

The aim of this study was to determine the role of the Rv3143 response regulator in the physiology of *M. tuberculosis*. Due to the high pathogenicity and slow growth of *M. tuberculosis*, part of this work was performed in its fast-growing, saprophytic cousin, *M. smegmatis*. To investigate the function of Rv3143, we decided to search for proteins interacting with the putative response regulator. Expression of Rv3143 protein fused with GFP as bait and analysis of purified protein complexes by MS/MS allowed identification of potential partner proteins for Rv3143 as soluble protein components of NADH dehydrogenase I, Nuo, or complex I: NuoB, NuoC, NuoD, NuoE, NuoF, NuoG, and NuoI. The MS analyses, repeated in the presence of a crosslinking agent, confirmed direct interactions of Rv3143 with proteins belonging to the Nuo complex and indicated NuoD as the most likely direct partner of Rv3143. The interaction between Rv3143 and NuoD was confirmed further by pull-down assays and was screened for direct interactors using MS facilitated by BS3 crosslinking. The pair of NuoD and Rv3143 had the highest number of crosslinks identified by Kojak software, which suggests the location of Rv3143 in respiratory complex I and its role in oxidative phosphorylation. It is interesting that in actinobacteria, the orthologs of *rv3143* gene are located in direct or very close proximity to the operon of *nuo* genes, encoding NuoA–N subunits of NADH dehydrogenase type I. The CheY protein, which is the closest equivalent of the Rv3143 protein in *E. coli*, possesses a phosphate-binding domain in its structure, but similarly to Rv3143, it does not have the effector domain. The CheY protein is an element of the system responsible for controlling flagella in the chemotaxis process, and when phosphorylated, it binds to the FliM protein, which then interacts with the NuoCD protein. Additionally, flagella, requiring energy for their movement, associate with the oxidative phosphorylation chain in the cell membrane (Rajagopala et al., 2007; Zarbiv et al., 2012). These findings may suggest that while the flagellar system was reduced in mycobacteria resulting in the loss of FliM protein, the link between CheY-like regulator and the Nuo complex, and NuoD protein, in particular, was sustained for other purposes, possibly oxygen sensing, redox sensing, or related sensing mechanisms. The majority of crosslinks found between the Rv3143 protein and NuoD appeared in the amino acid insertion region of NuoD, which does not occur in *Proteobacteria*. Importantly, the presence of this additional stretch of amino acids is specific to actinobacteria and allows their separate clustering in phylogenetic analysis. We used a collection of bacterial NuoD proteins to perform such analysis, and upon marking the co-

TABLE 2 | Monitoring of oxygen consumption by methylene blue discoloration under hypoxic conditions.

Strain	i	3 h	4 h	5 h	8 h	9 h	10 h	11 h	12 h	13 h
Ms-wt	–	0.609 ± 0.023	0.363 ± 0.084	0.067 ± 0.008						
Δ*msmeg_2064*	–	0.626 ± 0.023	0.578 ± 0.052	0.085 ± 0.002						
Δ*msmeg_2064*::2064	–	0.636 ± 0.045	0.558 ± 0.034	0.093 ± 0.006						
Ms-wt CRISPRi/dCas9	–	0.632 ± 0.031	0.432 ± 0.165	0.055 ± 0.017						
Δ*msmeg_2064*CRISPRi/dCas9	–	0.419 ± 0.191	0.18 ± 0.025	0.045 ± 0.028						
Ms-wt-ndhCRISPRi/dCas9	–	0.636 ± 0.008	0.287 ± 0.063	0.048 ± 0.000						
Δ*msmeg_2064*ndhCRISPRi/dCas9	–	0.184 ± 0.042	0.108 ± 0.077	0.031 ± 0.002						
Ms-wtCRISPRi/dCas9	+	0.647 ± 0.047	0.312 ± 0.279	0.065 ± 0.028						
Δ*msmeg_2064*CRISPRi/dCas9	+	0.213 ± 0.034	0.144 ± 0.076	0.017 ± 0.005						
Ms-wt-ndhCRISPRi/dCas9	+				0.629 ± 0.002	0.624 ± 0.004	0.435 ± 0.167	0.085 ± 0.005		
Δ*msmeg_2064*ndhCRISPRi/dCas9	+				0.554 ± 0.032	0.622 ± 0.012	0.476 ± 0.196	0.516 ± 0.066	0.278 ± 0.052	0.065 ± 0.005

The results are the absorbance readings at 600 nm and mean ± SD from three independent experiments. The addition of anhydrotetracycline as an inducer of CRISPRi/Cas9-driven gene expression silencing is indicated in the "i" column.

occurrence of Rv3143 orthologs in the investigated species, it became very clear that there is a correlation between NuoD clustering and the presence of the response regulator we investigated.

As expected based on high-density transposon mutagenesis (Sassetti et al., 2003; DeJesus et al., 2017), Rv3143 and its ortholog in *M. smegmatis* (MSMEG_2064) were not essential for viability, and the genes encoding these proteins could be replaced with non-functional forms. The constructed mutants and control strains were analyzed under various conditions of growth. In the presence of reactive nitrogen species generated by DETA NONOate, the Δ*msmeg_2064* mutant exhibited a significant reduction in growth kinetics and viability compared to the wild-type strain. Free radicals generated by DETA NONOate under standard laboratory conditions were previously reported to have minor bacteriostatic effects on clinical *M. tuberculosis* strains (Voskuil et al., 2011). Interestingly, tubercle bacilli under the influence of reactive nitrogen species in anaerobic conditions inhibit the transcription of NADH dehydrogenase type I *in vitro* while inducing the transcription of NADH type II. Under similar conditions but *in vivo*, fourfold repression of *nuoB* gene, encoding the subunit of NDH-1 dehydrogenase, was observed (Shi et al., 2005). Similarly, we noticed a correlation between the depletion of Rv3143 and the expression of NarU, NarK2, and NarX, which was overexpressed in the mutant strain lacking Rv3143 altogether. All three nitrogen metabolism enzymes listed above are postulated to be crucial to nitrate respiration in *M. tuberculosis* (Sohaskey and Wayne, 2003; Huang et al., 2015) and are typically overexpressed during hypoxia (Kundu and Basu, 2021). In contrast, Nuo complex proteins are typically downregulated under hypoxic conditions, when nitrate respiration is switched on, and are overexpressed during growth reactivation, when bacterial cultures are switched back to oxygen-rich growth conditions (Kundu and Basu, 2021). This may suggest that even though the Nuo complex is not the dominant NADH dehydrogenase in mycobacteria, bacilli lacking Rv3143 activate alternative respiratory mechanisms, and the Nuo complex with Rv3143 may be critical to oxygen sensing and downstream signaling.

To further characterize the biological effect of the identified interactions between Rv3143 and respiratory complex I, we further investigated the sensitivity of the Δ*rv3143* strain to the selected compounds disrupting the oxidative phosphorylation process and the membrane potential. While testing the sensitivity of bacterial strains to monensin, valinomycin, CCCP, and trifluoperazine, we noticed a threefold increase in the resistance of the Δ*rv3143* mutant to valinomycin. However, the observed increased resistance to valinomycin was abolished to the wild-type level in the presence of CCCP and trifluoperazine. Valinomycin reduces the natural electrochemical potential of the cell, decoupling the processes of oxidative phosphorylation. Valinomycin is highly selective for potassium cations, which are transported through cell membranes. CCCP inhibits the activity of the proton pump by reducing the membrane potential and inhibits oxidative phosphorylation, which causes a decrease in the activity of ATP synthase (Pule et al., 2016). The addition of the protonophore CCCP to *M. tuberculosis* strains resistant to ofloxacin has previously been reported to increase their sensitivity, suggesting the importance of proton pumps for resistance to fluoroquinolones (Singh et al., 2011; Sun et al., 2014). Moreover, Gupta and colleagues observed decreased resistance to rifampicin, isoniazid, and streptomycin in *M. tuberculosis* cells cultured in the presence of CCCP (Gupta

et al., 2006). CCCP at higher concentrations affects not only the transport of hydrogen cations but also other ions, including potassium ions (Rao et al., 2001). In turn, trifluoperazine belongs to the class of phenothiazine compounds and shows a pleiotropic effect in mycobacteria, affecting the synthesis of lipids and proteins, DNA processes, and respiration, including calcium-dependent ATPases or inhibition of type II NADH dehydrogenase (Advani et al., 2012; Black et al., 2014). As reported in *M. tuberculosis*, trifluoperazine inhibits growth and reduces resistance to rifampicin, contributing to the elimination of mycobacteria residing in macrophages (Crowle et al., 1992; Reddy et al., 1996). Our findings suggest that the Rv3143 interaction with the Nuo complex may interfere with resistance to antibiotics and reactive radicals in mycobacteria.

We then decided to determine the metabolic activity of the Δ*msmeg_2064*/Δ*rv3142* mutants using the known electron acceptor TTC. The assessment of TTC reduction by microorganisms is exploited for screening for cells that have a dysfunctional respiratory chain (Rich et al., 2001). The observed increased level of reduction of TTC by the mutant cells confirmed a potential defect in the electron transport system. In contrast, Dadura and colleagues (2017) reported a decreased level of reduction in TTC, indicating a slowdown in the respiration process in the Δ*pdtaS M. smegmatis* mutant lacking the functional histidine kinase PdtaS. Mutants of Δ*pdtaS* exhibited altered susceptibility to aminoglycoside antibiotics targeting 30S ribosomes as well as to tetracycline (Dadura et al., 2017).

As previously reported elsewhere, the *nuo* operon is not essential for the growth and survival of mycobacteria *in vitro* under hypoxic conditions (Rao et al., 2008; Vilchèze et al., 2018). Limited oxygen access leads to the overproduction of dehydrogenase type II, Ndh, and cytochrome oxidase bd and a reduction in the production of NADH dehydrogenase type I (Schubert et al., 2015; Prosser et al., 2017). In addition to respiratory complex I (NDH-1), *M. tuberculosis* transfers electrons to quinone by NADH dehydrogenases type II (NDH-2), which are encoded by *ndh* and *ndhA* genes (Yano et al., 2006). Fast-growing *M. smegmatis* possesses only a single copy of NDH-2 (Ndh), but it represents 95% of the total NADH oxidation measured (Vilchèze et al., 2005). Therefore, we decided to extend our research by demonstrating the role of the Rv3143 protein in the respiration process and examining the phenotypic effect of the lack of MSMEG_2064 protein in a strain with a silenced expression of *ndh* gene coding for NADH type II dehydrogenase. Downregulation of *ndh* expression was achieved using the CRISPR-Cas system. Studies on the growth kinetics and survival of mutant strains under conditions of limited access to oxygen revealed a slowdown in the rate of growth and a significant decrease in the viability of strains with silenced *ndh* genes compared to control strains. After hypoxia, the tested strains were reactivated by changing the growth conditions from anaerobic to aerobic. We observed a significant slowdown in the growth kinetics and decreased viability in mutants expressing the functional *msmeg_2064* gene and silenced *ndh*. In the reaeration process, the inhibition of growth and decreased viability were observed for mutants with depleted Ndh; however, the inactivation of *msmeg_2064* reversed this effect to the level of the control strain. Homology search databases such as KEGG recognize the Rv3143 protein as an ortholog of the response regulator domain of eubacterial aerobic respiration sensor-response proteins (ArcAs), and we think that oxygen sensing is the most plausible function of Rv3143 in mycobacteria. The ArcAB oxygen sensing system is not present in mycobacteria, and its function is fulfilled by other regulators, such as SenX-RegX3 (Singh and Kumar, 2015), and possibly other proteins. While the mechanisms of oxygen sensing are enormously important to the physiology and survival of this intracellular pathogen, they are not yet completely understood.

Our study sheds light on the intracellular function of the Rv3143 protein, which influences the efficiency of the respiratory chain in *Mycobacterium* and controls the nitrate respiration switch in this bacterium. However, the precise mechanism of action of the protein studied here requires further detailed analysis to fully understand the above-described phenomena.

DATA AVAILABILITY STATEMENT

The datasets presented in this study can be found in online repositories. The names of the repository/repositories and accession number(s) can be found in the article/**Supplementary Material**. The RNA-seq related data have been deposited to the GEO database and are accessible at https://www.ncbi.nlm.nih.gov/geo/query/acc.cgi?acc=GSE193950.

ETHICS STATEMENT

The animal study was reviewed and approved by Polish Local Ethics Commission for Experiments on Animals No. 9 in Lodz (Agreement 54/ŁD1/2011).

AUTHOR CONTRIBUTIONS

RP: conceptualization, investigation, visualization, writing—original draft, and funding acquisition. KW: investigation. PP: conceptualization, investigation, visualization, and writing. EL: investigation. MA: investigation. EB: investigation. BD: investigation. MS: investigation. AR-G: investigation. JD: conceptualization, writing—review and editing, and supervision. All authors listed have made a substantial, direct, and intellectual contribution to the work and approved it for publication.

FUNDING

This work was supported by the National Science Centre, Republic of Poland, SONATA 6—2013/11/D/NZ6/02888 (to RP) and by Foundation for Polish Science, PARENT-BRIDGE

Program, co-financed by the European Union with European Regional Development, BRIDGE/2013-8/10 (to RP).

ACKNOWLEDGMENTS

The authors thank Dominik Cysewski and the mass spectrometry service at the Institute of Biochemistry and Biophysics PAS in Warsaw for MS analysis. The MS analysis equipment used for the analysis was sponsored in part by the Centre for Preclinical Research and Technology (CePT), a project co-sponsored by European Regional Development Fund and Innovative Economy, The National Cohesion Strategy of Poland.

SUPPLEMENTARY MATERIAL

The Supplementary Material for this article can be found online at: https://www.frontiersin.org/articles/10.3389/fcimb.2022.909507/full#supplementary-material

REFERENCES

Advani, M. J., Siddiqui, I., Sharma, P., and Reddy, H. (2012). Activity of Trifluoperazine Against Replicating, Non-Replicating and Drug Resistant M. Tuberculosis. *PloS One* 7, e44245. doi: 10.1371/journal.pone.0044245

Agrawal, R., Pandey, A., Rajankar, M. P., Dixit, N. M., and Saini, D. K. (2015). The Two-Component Signalling Networks of Mycobacterium Tuberculosis Display Extensive Cross-Talk In Vitro. *Biochem. J.* 469, 121–134. doi: 10.1042/BJ20150268

Antczak, M., Płocińska, R., Płociński, P., Rumijowska-Galewicz, A., Żaczek, A., Strapagiel, D., et al. (2018). The NnaR Orphan Response Regulator is Essential for the Utilization of Nitrate and Nitrite as Sole Nitrogen Sources in Mycobacteria. *Sci. Rep.* 8, 17552. doi: 10.1038/s41598-018-35844-z

Beites, T., O'Brien, K., Tiwari, D., Engelhart, C. A., Walters, S., Andrews, J., et al. (2019). Plasticity of the Mycobacterium Tuberculosis Respiratory Chain and its Impact on Tuberculosis Drug Development. *Nat. Commun.* 10, 4970. doi: 10.1038/s41467-019-12956-2

Black, P. A., Warren, R. M., Louw, G. E., van Helden, P. D., Victor, T. C., and Kana, B. D. (2014). Energy Metabolism and Drug Efflux in Mycobacterium Tuberculosis. *Antimicrob. Agents Chemother.* 58, 2491–2503. doi: 10.1128/AAC.02293-13

Boshoff, H. I. M., and Barry, C. E.3rd (2005). Tuberculosis - Metabolism and Respiration in the Absence of Growth. *Nat. Rev. Microbiol.* 3, 70–80. doi: 10.1038/nrmicro1065

Brzostek, A., Szulc, I., Klink, M., Brzezinska, M., Sulowska, Z., and Dziadek, J. (2014). Either Non-Homologous Ends Joining or Homologous Recombination Is Required to Repair Double-Strand Breaks in the Genome of Macrophage-Internalized Mycobacterium Tuberculosis. *Plos One* 9(3), e92799. doi: 10.1371/journal.pone.0092799

Cole, S. T., Eiglmeier, K., Parkhill, J., James, K. D., Thomson, N. R., Wheeler, P. R., et al. (2001). Massive Gene Decay in the Leprosy Bacillus. *Nature* 409, 1007–1011. doi: 10.1038/35059006

Cook, G. M., Hards, K., Vilchèze, C., Hartman, T., and Berney, M. (2014). Energetics of Respiration and Oxidative Phosphorylation in Mycobacteria. *Microbiol. Spectr.* 2, 1–30. doi: 10.1128/microbiolspec.MGM2-0015-2013

Crowle, A. J., Douvas, G. S., and May, M. H. (1992). Chlorpromazine: A Drug Potentially Useful for Treating Mycobacterial Infections. *Chemotherapy* 38, 410–419. doi: 10.1159/000239036

Dadura, K., Płocińska, R., Rumijowska-Galewicz, A., Płociński, P., Żaczek, A., Dziadek, B., Zaborowski, A, and Dziadek, J. (2017). PdtaS Deficiency Affects Resistance of Mycobacteria to Ribosome Targeting Antibiotics. *Front. Microbiol.* 8. doi: 10.3389/fmicb.2017.02145

DeJesus, M. A., Gerrick, E. R., Xu, W., Park, S. W., Long, J. E., Boutte, C. C., et al. (2017). Comprehensive Essentiality Analysis of the Mycobacterium Tuberculosis Genome via Saturating Transposon Mutagenesis. *mBio* 8, 1–17. doi: 10.1128/mBio.02133-16

Dhar, N., and McKinney, J. D. (2010). Mycobacterium Tuberculosis Persistence Mutants Identified by Screening in Isoniazid-Treated Mice. *Proc. Natl. Acad. Sci. U.S.A.* 107, 12275–12280. doi: 10.1073/pnas.1003219107

Dong, W., Wang, R., Li, P., Wang, G., Ren, X., Feng, J., et al. (2020). Orphan Response Regulator Rv3143 Increases Antibiotic Sensitivity by Regulating Cell Wall Permeability in Mycobacterium Smegmatis. *Arch. Biochem. Biophysics* 692, 108522. doi: 10.1016/J.ABB.2020.108522

Franzblau, S. G., Witzig, R. S., McLaughlin, J. C., Torres, P., Madico, G., Hernandez, A., et al. (1998). Rapid, Low-Technology MIC Determination With Clinical Mycobacterium Tuberculosis Isolates by Using the Microplate Alamar Blue Assay. *J. Clin. Microbiol.* 36, 362–366. doi: 10.1128/JCM.36.2.362-366.1998

Griffin, J. E., Gawronski, J. D., Dejesus, M. A., Ioerger, T. R., Akerley, B. J., and Sassetti, C. M. (2011). High-Resolution Phenotypic Profiling Defines Genes Essential for Mycobacterial Growth and Cholesterol Catabolism. *PloS Pathog.* 7, e1002251. doi: 10.1371/journal.ppat.1002251

Gupta, A. K., Chauhan, D. S., Srivastava, K., Das, R., Batra, S., Mittal, M., et al. (2006). Estimation of Efflux Mediated Multi-Drug Resistance and its Correlation With Expression Levels of Two Major Efflux Pumps in Mycobacteria. *J. Commun. Dis.* 38, 246–254.

Harbut, M. B., Yang, B., Liu, R., Yano, T., Vilchèze, C., Cheng, B., et al. (2018). Small Molecules Targeting Mycobacterium Tuberculosis Type II NADH Dehydrogenase Exhibit Antimycobacterial Activity. *Angew. Chem. Int. Ed. Engl.* 57, 3478–3482. doi: 10.1002/anie.201800260

Huang, Q., Abdalla, A. E., and Xie, J. (2015). Phylogenomics of Mycobacterium Nitrate Reductase Operon. *Curr. Microbiol.* 71, 121–128. doi: 10.1007/s00284-015-0838-2

Huerta-Cepas, J., Serra, F., and Bork, P. (2016). ETE 3: Reconstruction, Analysis, and Visualization of Phylogenomic Data. *Mol. Biol. Evol.* 33, 1635–1638. doi: 10.1093/molbev/msw046

Joseph Sambrook, D. W. R. (2001). *Molecular Cloning: A Laboratory Manual* (New York, USA: Cold Spring Harbor Laboratory).

Kalia, N. P., Hasenoehrl, E. J., Ab Rahman, N. B., Koh, V. H., Ang, M. L. T., Sajorda, D. R., et al. (2017). Exploiting the Synthetic Lethality Between Terminal Respiratory Oxidases to Kill Mycobacterium Tuberculosis and Clear Host Infection. *Proc. Natl. Acad. Sci. U.S.A.* 114, 7426–7431. doi: 10.1073/pnas.1706139114

Katoh, K., and Standley, D. M. (2013). MAFFT Multiple Sequence Alignment Software Version 7: Improvements in Performance and Usability. *Mol. Biol. Evol.* 30, 772–780. doi: 10.1093/molbev/mst010

Kendall, S. L., Movahedzadeh, F., Rison, S. C. G., Wernisch, L., Parish, T., Duncan, K., et al. (2004). The Mycobacterium Tuberculosis dosRS Two-Component System is Induced by Multiple Stresses. *Tuberculosis* 84, 247–255. doi: 10.1016/j.tube.2003.12.007

Korycka-Machała, M., Pawełczyk, J., Borówka, P., Dziadek, B., Brzostek, A., Kawka, M., et al. (2020). PPE51 Is Involved in the Uptake of Disaccharides by Mycobacterium Tuberculosis. *Cells* 9, 1–16. doi: 10.3390/cells9030603

Kundu, M., and Basu, J. (2021). Applications of Transcriptomics and Proteomics for Understanding Dormancy and Resuscitation in Mycobacterium Tuberculosis. *Front. Microbiol.* 12. doi: 10.3389/fmicb.2021.642487

Maloney, P. C., Kashket, E. R., and Wilson, T. H. (1974). A Protonmotive Force Drives ATP Synthesis in Bacteria. *Proc. Natl. Acad. Sci. U.S.A.* 71, 3896–3900. doi: 10.1073/pnas.71.10.3896

Matsoso, L. G., Kana, B. D., Crellin, P. K., Lea-Smith, D. J., Pelosi, A., Powell, D., et al. (2005). Function of the Cytochrome Bc1-Aa3 Branch of the Respiratory Network in Mycobacteria and Network Adaptation Occurring in Response to its Disruption. *J. Bacteriol.* 187, 6300–6308. doi: 10.1128/JB.187.18.6300-6308.2005

Megehee, J. A., Hosler, J. P., and Lundrigan, M. D. (2006). Evidence for a Cytochrome Bcc-Aa3 Interaction in the Respiratory Chain of Mycobacterium Smegmatis. *Microbiol. (Reading)* 152, 823–829. doi: 10.1099/mic.0.28723-0

Morth, J. P., Gosmann, S., Nowak, E., and Tucker, P. A. (2005). A Novel Two-Component System Found in Mycobacterium Tuberculosis. *FEBS Letters* 579, 4145–4148 doi: 10.1016/j.febslet.2005.06.043

Murugesan, D., Ray, P. C., Bayliss, T., Prosser, G. A., Harrison, J. R., Green, K., et al. (2018). 2-Mercapto-Quinazolinones as Inhibitors of Type II NADH Dehydrogenase and Mycobacterium Tuberculosis: Structure-Activity Relationships, Mechanism of Action and Absorption, Distribution, Metabolism, and Excretion Characterization. *ACS Infect. Dis.* 4, 954–969. doi: 10.1021/acsinfecdis.7b00275

Parish, T., and Stoker, N. G. (2000). Use of a Flexible Cassette Method to Generate a Double Unmarked Mycobacterium Tuberculosis tlyA plcABC Mutant by Gene Replacement. *Microbiol. (Reading)* 146, 1969–1975. doi: 10.1099/00221287-146-8-1969

Pawelczyk, J., Brzostek, A., Kremer, L., Dziadek, B., Rumijowska-Galewicz, A., Fiolka, M., et al. (2011). AccD6, a Key Carboxyltransferase Essential for Mycolic Acid Synthesis in Mycobacterium Tuberculosis, is Dispensable in a Nonpathogenic Strain. *J. Bacteriol.* 193, 6960–6972. doi: 10.1128/JB.05638-11

Pethe, K., Bifani, P., Jang, J., Kang, S., Park, S., Ahn, S., et al. (2013). Discovery of Q203, a Potent Clinical Candidate for the Treatment of Tuberculosis. *Nat. Med.* 19, 1157–1160. doi: 10.1038/nm.3262

Płociński, P., Laubitz, D., Cysewski, D., Stoduś, K., Kowalska, K., and Dziembowski, A. (2014). Identification of Protein Partners in Mycobacteria Using a Single-Step Affinity Purification Method. *PloS One* 9, e91380. doi: 10.1371/journal.pone.0091380

Płociński, P., Macios, M., Houghton, J., Niemiec, E., Płocińska, R., Brzostek, A., et al. (2019). Proteomic and Transcriptomic Experiments Reveal an Essential Role of RNA Degradosome Complexes in Shaping the Transcriptome of Mycobacterium Tuberculosis. *Nucleic Acids Res.* 47, 5892–5905. doi: 10.1093/nar/gkz251

Price, M. N., Dehal, P. S., and Arkin, A. P. (2009). FastTree: Computing Large Minimum Evolution Trees With Profiles Instead of a Distance Matrix. *Mol. Biol. Evol.* 26, 1641–1650. doi: 10.1093/molbev/msp077

Prosser, G., Brandenburg, J., Reiling, N., Barry, C. E.3rd, Wilkinson, R. J., and Wilkinson, K. A. (2017). The Bacillary and Macrophage Response to Hypoxia in Tuberculosis and the Consequences for T Cell Antigen Recognition. *Microbes Infect.* 19, 177–192. doi: 10.1016/j.micinf.2016.10.001

Pule, C. M., Sampson, S. L., Warren, R. M., Black, P. A., van Helden, P. D., Victor, T. C., et al. (2016). Efflux Pump Inhibitors: Targeting Mycobacterial Efflux Systems to Enhance TB Therapy. *J. Antimicrob. Chemother.* 71, 17–26. doi: 10.1093/jac/dkv316

Rajagopala, S. V., Titz, B., Goll, J., Parrish, J. R., Wohlbold, K., McKevitt, M. T., et al. (2007). The Protein Network of Bacterial Motility. *Mol. Syst. Biol.* 3, 128. doi: 10.1038/msb4100166

Rao, S. P. S., Alonso, S., Rand, L., Dick, T., and Pethe, K. (2008). The Protonmotive Force is Required for Maintaining ATP Homeostasis and Viability of Hypoxic, Nonreplicating Mycobacterium Tuberculosis. *Proc. Natl. Acad. Sci. U.S.A.* 105, 11945–11950. doi: 10.1073/pnas.0711697105

Rao, M., Streur, T. L., Aldwell, F. E., and Cook, G. M. (2001). Intracellular pH Regulation by Mycobacterium Smegmatis and Mycobacterium Bovis BCG. *Microbiol. (Reading)* 147, 1017–1024. doi: 10.1099/00221287-147-4-1017

Reddy, M. V., Nadadhur, G., and Gangadharam, P. R. (1996). In-Vitro and Intracellular Antimycobacterial Activity of Trifluoperazine. *J. Antimicrob. Chemother.* 37, 196–197. doi: 10.1093/jac/37.1.196

Rich, P. R., Mischis, L. A., Purton, S., and Wiskich, J. T. (2001). The Sites of Interaction of Triphenyltetrazolium Chloride With Mitochondrial Respiratory Chains. *FEMS Microbiol. Lett.* 202, 181–187. doi: 10.1111/j.1574-6968.2001.tb10801.x

Rock, J. M., Hopkins, F. F., Chavez, A., Diallo, M., Chase, M. R., Gerrick, E. R., et al. (2017). Programmable Transcriptional Repression in Mycobacteria Using an Orthogonal CRISPR Interference Platform. *Nat. Microbiol.* 2, 16274. doi: 10.1038/nmicrobiol.2016.274

Sassetti, C. M., Boyd, D. H., and Rubin, E. J. (2003). Genes Required for Mycobacterial Growth Defined by High Density Mutagenesis. *Mol. Microbiol.* 48, 77–84. doi: 10.1046/j.1365-2958.2003.03425.x

Schubert, O. T., Ludwig, C., Kogadeeva, M., Zimmermann, M., Rosenberger, G., Gengenbacher, M., et al. (2015). Absolute Proteome Composition and Dynamics During Dormancy and Resuscitation of Mycobacterium Tuberculosis. *Cell Host Microbe* 18, 96–108. doi: 10.1016/j.chom.2015.06.001

Schut, G. J., Zadvornyy, O., Wu, C.-H., Peters, J. W., Boyd, E. S., and Adams, M. W. W. (2016). The Role of Geochemistry and Energetics in the Evolution of Modern Respiratory Complexes From a Proton-Reducing Ancestor. *Biochim. Biophys. Acta (BBA) Bioenerg.* 1857, 958–970. doi: 10.1016/j.bbabio.2016.01.010

Shirude, P. S., Paul, B., Roy Choudhury, N., Kedari, C., Bandodkar, B., and Ugarkar, B. G. (2012). Quinolinyl Pyrimidines: Potent Inhibitors of NDH-2 as a Novel Class of Anti-TB Agents. *ACS Med. Chem. Lett.* 3, 736–740. doi: 10.1021/ml300134b

Shi, L., Sohaskey, C. D., Kana, B. D., Dawes, S., North, R. J., Mizrahi, V., et al. (2005). Changes in Energy Metabolism of Mycobacterium Tuberculosis in Mouse Lung and Under *In Vitro* Conditions Affecting Aerobic Respiration. *Proc. Natl. Acad. Sci. U.S.A.* 102, 15629–15634. doi: 10.1073/pnas.0507850102

Singh, M., Jadaun, G. P. S., Ramdas, B., Srivastava, K., Chauhan, V., Mishra, R., et al. (2011). Effect of Efflux Pump Inhibitors on Drug Susceptibility of Ofloxacin Resistant Mycobacterium Tuberculosis Isolates. *Indian J. Med. Res.* 133, 535–540.

Singh, N., and Kumar, A. (2015). Virulence Factor SenX3 is the Oxygen-Controlled Replication Switch of Mycobacterium Tuberculosis. *Antioxid. Redox Signal* 22, 603–613. doi: 10.1089/ars.2014.6020

Sohaskey, C. D., and Wayne, L. G. (2003). Role of Nark2x and narGHJI in Hypoxic Upregulation of Nitrate Reduction by Mycobacterium Tuberculosis. *J. Bacteriol.* 185, 7247–7256. doi: 10.1128/jb.185.24.7247-7256.2003

Sun, Z., Xu, Y., Sun, Y., Liu, Y., Zhang, X., Huang, H., et al. (2014). Ofloxacin Resistance in Mycobacterium Tuberculosis Is Associated With Efflux Pump Activity Independent of Resistance Pattern and Genotype. *Microb. Drug Resist.* 20, 525–532. doi: 10.1089/mdr.2013.0171

Tan, M. P., Sequeira, P., Lin, W. W., Phong, W. Y., Cliff, P., Ng, S. H., et al. (2010). Nitrate Respiration Protects Hypoxic Mycobacterium Tuberculosis Against Acid- and Reactive Nitrogen Species Stresses. *PloS One* 5, e13356. doi: 10.1371/journal.pone.0013356

Vilchèze, C., Weinrick, B., Leung, L. W., and Jacobs, W. R. J. (2018). Plasticity of Mycobacterium Tuberculosis NADH Dehydrogenases and Their Role in Virulence. *Proc. Natl. Acad. Sci. U.S.A.* 115, 1599–1604. doi: 10.1073/pnas.1721545115

Vilchèze, C., Weisbrod, T. R., Chen, B., Kremer, L., Hazbón, M. H., Wang, F., et al. (2005). Altered NADH/NAD+ Ratio Mediates Coresistance to Isoniazid and Ethionamide in Mycobacteria. *Antimicrob. Agents Chemother.* 49, 708–720. doi: 10.1128/AAC.49.2.708-720.2005

Voskuil, M. I., Bartek, I. L., Visconti, K., and Schoolnik, G. K. (2011). The Response of Mycobacterium Tuberculosis to Reactive Oxygen and Nitrogen Species. *Front. Microbiol.* 2. doi: 10.3389/fmicb.2011.00105

Weinstein, E. A., Yano, T., Li, L.-S., Avarbock, D., Avarbock, A., Helm, D., et al. (2005). Inhibitors of Type II NADH:menaquinone Oxidoreductase Represent a Class of Antitubercular Drugs. *Proc. Natl. Acad. Sci. U.S.A.* 102, 4548–4553. doi: 10.1073/pnas.0500469102

Yano, T., Li, L.-S., Weinstein, E., Teh, J.-S., and Rubin, H. (2006). Steady-State Kinetics and Inhibitory Action of Antitubercular Phenothiazines on Mycobacterium Tuberculosis Type-II NADH-Menaquinone Oxidoreductase (NDH-2). *J. Biol. Chem.* 281, 11456–11463. doi: 10.1074/jbc.M508844200

Zahrt, T. C., and Deretic, V. (2000). An Essential Two-Component Signal Transduction System in Mycobacterium Tuberculosis. *J. Bacteriol.* 182, 3832–3838. [Accessed May 18, 2022]. doi: 10.1128/JB.182.13.3832-3838.2000

Zarbiv, G., Li, H., Wolf, A., Cecchini, G., Caplan, S. R., Sourjik, V., et al. (2012). Energy Complexes are Apparently Associated With the Switch-Motor Complex of Bacterial Flagella. *J. Mol. Biol.* 416, 192–207. doi: 10.1016/j.jmb.2011.12.027

Zhou, L., Yang, L., Zeng, X., Danzheng, J., Zheng, Q., Liu, J., et al. (2015). Transcriptional and Proteomic Analyses of Two-Component Response Regulators in Multidrug-Resistant Mycobacterium Tuberculosis. *Int. J. Antimicrob. Agents* 46, 73–81. doi: 10.1016/j.ijantimicag.2015.02.018

Zschiedrich, C. P., Keidel, V., and Szurmant, H. (2016). Molecular Mechanisms of Two-Component Signal Transduction. *J. Mol. Biol.* 428, 3752–3775. doi: 10.1016/j.jmb.2016.08.003

Conflict of Interest: The authors declare that the research was conducted in the absence of any commercial or financial relationships that could be construed as a potential conflict of interest.

Publisher's Note: All claims expressed in this article are solely those of the authors and do not necessarily represent those of their affiliated organizations, or those of the publisher, the editors and the reviewers. Any product that may be evaluated in

this article, or claim that may be made by its manufacturer, is not guaranteed or endorsed by the publisher.

frontiers | Frontiers in Cellular and Infection Microbiology

TYPE Review
PUBLISHED 27 September 2022
DOI 10.3389/fcimb.2022.956607

OPEN ACCESS

EDITED BY
Bavesh Kana,
University of the Witwatersrand,
South Africa

REVIEWED BY
Lee-Ann H Allen,
University of Missouri, United States
Wendy Mok, University of Connecticut
Health Center, United States

*CORRESPONDENCE
Samantha L. Sampson
ssampson@sun.ac.za

SPECIALTY SECTION
This article was submitted to
Bacteria and Host,
a section of the journal
Frontiers in Cellular and
Infection Microbiology

RECEIVED 30 May 2022
ACCEPTED 24 August 2022
PUBLISHED 27 September 2022

CITATION
Parbhoo T, Mouton JM
and Sampson SL (2022)
Phenotypic adaptation of
Mycobacterium tuberculosis to
host-associated stressors that
induce persister formation.
Front. Cell. Infect. Microbiol. 12:956607.
doi: 10.3389/fcimb.2022.956607

Phenotypic adaptation of *Mycobacterium tuberculosis* to host-associated stressors that induce persister formation

Trisha Parbhoo, Jacoba M. Mouton and
Samantha L. Sampson*

Department of Science and Technology (DSI)-NRF Centre of Excellence for Biomedical Tuberculosis Research (CBTBR); South African Medical Research Council Centre (SAMRC) Centre for Tuberculosis Research; Division of Molecular Biology and Human Genetics, Faculty of Medicine and Health Sciences, Stellenbosch University, Cape Town, South Africa

Mycobacterium tuberculosis exhibits a remarkable ability to interfere with the host antimicrobial response. The pathogen exploits elaborate strategies to cope with diverse host-induced stressors by modulating its metabolism and physiological state to prolong survival and promote persistence in host tissues. Elucidating the adaptive strategies that *M. tuberculosis* employs during infection to enhance persistence is crucial to understanding how varying physiological states may differentially drive disease progression for effective management of these populations. To improve our understanding of the phenotypic adaptation of *M. tuberculosis*, we review the adaptive strategies employed by *M. tuberculosis* to sense and coordinate a physiological response following exposure to various host-associated stressors. We further highlight the use of animal models that can be exploited to replicate and investigate different aspects of the human response to infection, to elucidate the impact of the host environment and bacterial adaptive strategies contributing to the recalcitrance of infection.

KEYWORDS

***Mycobacterium tuberculosis*, persistence, persisters, bacterial heterogeneity, host-pathogen interaction**

1 Introduction

The interaction between a pathogen and its host is extremely complex. During infection with *Mycobacterium tuberculosis*, bacilli reside in various host microenvironments, which influence their physiological and metabolic state (Liu et al., 2016; Vijay et al., 2017a). As an adaptive mechanism in response to host-associated stressors, heterogeneous bacterial responses at a single-cell and population-wide level

may drive the formation of phenotypically diverse subpopulations that enable survival in the host for prolonged periods. The majority of antibiotic-susceptible bacteria will succumb to host immune pressures, whilst a subpopulation of *M. tuberculosis* may transition into a persister state (Jain et al., 2016; Mouton et al., 2016). Persister bacteria are defined here as viable, but non- or slowly replicating, reversibly drug-tolerant subpopulations, with the potential to later resuscitate and cause active tuberculosis (TB) (Balaban et al., 2019; Moldoveanu et al., 2021). Persisters are able to survive exposure to high concentrations of antibiotics and/or host-associated stressors without known genetic mutations (Balaban et al., 2019). This is distinct from genetic resistance, which describes the ability of bacteria to grow at high concentrations of antibiotics through acquisition of resistance-conferring mutations. It is important to make the fine distinction between persister bacteria, and persistence of the infection. While the two are not mutually exclusive, in this review, the term "persistence" refers to failure to clear the infection.

M. tuberculosis has evolved to cope with diverse stressors in the host by manipulating specific host processes, in addition to modulating its metabolism to promote persister formation, enhance virulence, and ultimately prolong survival (persistence) within the host (Zimmermann et al., 2017; Huang et al., 2018; Russell et al., 2019). Improved knowledge regarding the strategies employed by *M. tuberculosis* to establish a persistent infection in the host, more specifically to sense and coordinate a physiological response, and trigger persister formation, is essential. The use of animal models (rabbits, guinea pigs, various mice and non-human primates) that recapitulate conditions experienced in the host, in combination with improved imaging technology is shedding light on the multifactorial mechanisms that contribute to *M. tuberculosis* persistence (Via et al., 2008; Lin et al., 2013; Gregg et al., 2018). Such animals display similarities in the pathophysiology and progression of infection compared to humans, however each model presents drawbacks, as highlighted in Table 1. Dependent on the animal model used,

TABLE 1 *M. tuberculosis* progression of infection in animal models.

Associated clinical phenotype	Cynomolgus macaque	Rabbit	Guinea pig	Mice (BALB/C, C57BL/6)	Kramnik mice (C3HeB/FeJ)	Zebrafish Larvae model
Hypoxia	Present	Present	Present	Absent	Present	Present
Granuloma formation	Present	Present	Present	Absent	Present	Present
Caseous necrosis	Present	Present	Present	Absent	Present	Present
TAG accumulation	Present	Present	Present	Absent	Present	Present
Pulmonary pathology	Present	Present	Present	Present	Present	Absent
Dissemination (Intracellular and extracellular bacilli)	Present	Present	Present	Absent	Present	Present
Advantages	• Wide-spectrum of lesions observed, similar to humans • Latent infection observed	• Mid-range cost • Granuloma development and histopathology similar to humans	• Mid-range cost, easy to handle • Granuloma development and histopathology similar to humans	• Inexpensive, fast generation time (weeks) • Genetic variant strains available	• Inexpensive, fast generation time (weeks) • Genetic variant strains available • Lesion diversity observed, immune cells involved similar to humans • Latent infection observed • Evaluation of drug efficacy	• Easily bred and genetically manipulated, inexpensive • Small, fast grower • Transparency allows *in vivo* real-time visualization of infection
Disadvantages	• Expensive, difficult to handle, long generation time	• Limited availability of immunological tools • Does not establish latent infection	• Limited availability of immunological tools • Extremely vulnerable to infection, unable to tolerate certain drug classes • Does not establish latent infection	• Lack of granuloma structure and organization, no extracellular dissemination • Does not establish latent infection	• Increased frequency of drug resistance observed • Research unknown how immune susceptibility may be altered due to inactivation of the *Ipr1* gene	• Lung structure and lymphocytes are absent • *Mycobacterium marinum* used as a surrogate bacterium
References	Lin et al., 2006; Via et al., 2008	Via et al., 2008; Guerrini et al., 2018	Via et al., 2008	Via et al., 2008; Driver et al., 2012	Driver et al., 2012; Irwin et al., 2015	Commandeur et al., 2020; Liu et al., 2020

TAG, triacylglycerol; Ipr1, intracellular pathogen resistance-1.

response to infection could differ, as observed in C3HeB/FeJ (Kramnik) versus BALB/c mice (Driver et al., 2012). The former model more accurately recapitulates certain aspects of human pathophysiology of infection progression where granuloma formation is observed. Further, C3HeB/FeJ mice display an increased susceptibility to *M. tuberculosis*, whilst the BALB/c model does not develop granuloma formation nor necrotic lesions (Table 1). However, the mycobacterial physiological state and adaptive mechanisms that promote a persister state during different stages of infection are largely unknown, and may be characterized by exploiting animal models that replicate different aspects of the human response to *M. tuberculosis* infection.

Elucidating the impact of the host environment and bacterial adaptive strategies during infection may guide future research into the recalcitrance of infection to treatment. To improve our understanding of the physiological state of *M. tuberculosis* persisters, this review will focus on the phenotypic adaptation of *M. tuberculosis* in response to various host-associated stressors and the strategies exploited by *M. tuberculosis* to not only survive, but to enter a persister state and ultimately drive disease progression.

2 Host environment encountered by *M. tuberculosis*

Upon inhalation, *M. tuberculosis* bacilli are transported to lung alveoli where alveolar macrophages engulf bacilli into phagosomal compartments. Dependent on the polarization state of alveolar macrophages, bacterial replication may occur in these compartments (Refai et al., 2018; Huang et al., 2019). Alveolar macrophages respond rapidly to *M. tuberculosis* through the secretion of cytokines [Interleukin (IL)-12, IL-23, IL-18] to induce interferon-gamma (IFN-γ) and tumor necrosis factor alpha (TNF-α) production by natural killer and T-cells (de Martino et al., 2019). Following activation by IFN-γ and TNF-α, macrophages undergo a considerable phenotypic transformation, leading to the increased production of chemokines, cytokines and pro-angiogenic factors to assist with mycobacterial killing (Flynn and Chan, 2001). This exposes *M. tuberculosis* to a nutrient-limited macrophage environment, where the bacilli experience acid stress, hypoxia, and exposure to reactive oxygen and nitrogen intermediates (Manina et al., 2015). The unique metabolism and immune profile of macrophages is critical for promoting either a restrictive (M1 polarized) or permissive (M2 polarized) environment for *M. tuberculosis* (Marino et al., 2015; Huang et al., 2018; Pisu et al., 2020). These host environments have shown to alter *M. tuberculosis* growth and induce persister formation in *M. tuberculosis*, and will be discussed in the following sections.

A hallmark feature of *M. tuberculosis* infection is the formation of granulomas, organized immunological structures rich in immune cells that are recruited to the site of inflammation. Granulomas are composed of lymphocytes, neutrophils and macrophages; *M. tuberculosis* primarily inhabits the latter. Growth restriction and extracellular dissemination of *M. tuberculosis* is contained by granulomas, which acts in synergy with IFN-γ and TNF-α for structural maintenance of granulomas during early and late stages of infection (Mezouar et al., 2019). Mature macrophages may additionally undergo phenotypic alterations by fusing into multinucleated giant cells and differentiating into lipid-loaded foam cells (Sia and Rengarajan, 2019). Whilst *M. tuberculosis* is largely contained within the granuloma, the phagosome becomes highly vulnerable to rupture during later stages of infection, leading to cytosolic escape of *M. tuberculosis* (Simeone et al., 2015).

Changes in oxygen tension within the granuloma result in a shift to anaerobic metabolism whereby *M. tuberculosis* adapts to exploit alternative pathways and enzymes [such as regulation of the stringent response (Dutta et al., 2019), cytochrome bd oxidase, cytochrome bcc/aa3 (Mascolo and Bald, 2019), fumarate reductase, nitrate reductase, isocitrate lyase, and succinate] (Supplementary Table 1), which are functional at lower metabolic rates (Salina et al., 2014). These pathways are however regarded as energetically demanding, implying that alternative metabolites are being utilized for the maintenance of the proton motive force (PMF), adenosine triphosphate (ATP) and cofactor recycling (Prosser et al., 2017).

M. tuberculosis shifts its metabolism to the glyoxylate shunt when β-oxidation of fatty acids provides the main carbon and energy source (Hoff et al., 2011). Additionally, the presence of the non-proton-translocating electron donor, NADH dehydrogenase 2, along with nitrate reduction (NAD+ recycling) (Eoh and Rhee, 2013; Prosser et al., 2017) plays a key role in maintaining an energized membrane, ATP production and carbon precursors during hypoxia and nutrient limitation. These cofactors may additionally serve as a reserve of metabolic energy that can facilitate the extracellular spread of *M. tuberculosis* (Tan et al., 2010). The thick cell wall of *M. tuberculosis* additionally offers protection from reactive oxygen species (ROS) by scavenging oxygen radicals (Ehrt and Schnappinger, 2009). Remodeling of bacterial respiration additionally mitigates intracellular redox stress, as excessive accumulation of NADH/NADPH enhances ROS *via* the Fenton reaction, which can induce intracellular damage to bacterial proteins and DNA (Vilchèze et al., 2013; Vilchèze et al., 2017).

Further research to identify host factors manipulated by *M. tuberculosis* will enhance our understanding of how *M. tuberculosis* modulates the antimicrobial host response. The host-pathogen interaction may be crucial for determining the fate of infection, and whether specific pathways are manipulated

for eradication of bacilli, containment and persistence, or bacterial dissemination.

2.1 Initial uptake of *M. tuberculosis* into phagosomes

Phagocytosis of *M. tuberculosis* by macrophages plays a crucial role in pathogen detection, engulfment and immune regulation. Depending on the host cell receptors engaged (e.g. antigen- and pattern recognition receptors), specific microbial ligand sequences will be recognized, which could alter the initial interaction between host and pathogen, and subsequent intracellular processing (Kumar et al., 2019). Following internalization into the phagosome, *M. tuberculosis* exhibits a remarkable ability to interfere with the host antimicrobial response and inhibit phagosome-lysosome fusion (Figure 1, Supplementary Table 1).

M. tuberculosis possesses a diverse array of cell-surface ligands and attempts to manipulate host cell recognition and internalization through pathogen-associated molecular patterns (PAMPs, Figure 1), including trehalose-6,6-dimycolate (TDM, cord factor) (Patin et al., 2017; Lerner et al., 2020), phosphatidylinositol mannoside (PIM) and mannose-capped lipoarabinomannan (ManLam) (Torrelles and Schlesinger, 2010; Marakalala and Ndlovu, 2017; Queval et al., 2017a). Phagocytosis of beads coated with ManLam (Fratti et al., 2003; Kang et al., 2005; Shui et al., 2011) and TDM (Geisel et al., 2005; Axelrod et al., 2008) has been shown to interfere with phagosome maturation and promote granuloma formation, respectively.

TDM is a significant contributor to intracellular cording of *M. tuberculosis*, whereby large lipid pellicles aggregate on the cell surface, preventing cytosolic recognition and phagocytosis into space-constrained vacuoles (Lerner et al., 2020). In contrast, dead bacilli are rapidly transported to lysosomes for degradation (Malik et al., 2000; Kyei et al., 2006). Since host immune cells express varying combinations of receptors, their interaction with PAMPS may differ (Liu et al., 2017; Dubé et al., 2021). *M. tuberculosis* may preferentially target specific host cell receptors to manipulate the host immune response, however, the mechanism of how manipulation by PAMPs influences macrophage metabolism, the delay of phagosome-lysosome fusion and subsequent intracellular processing, remains to be explored.

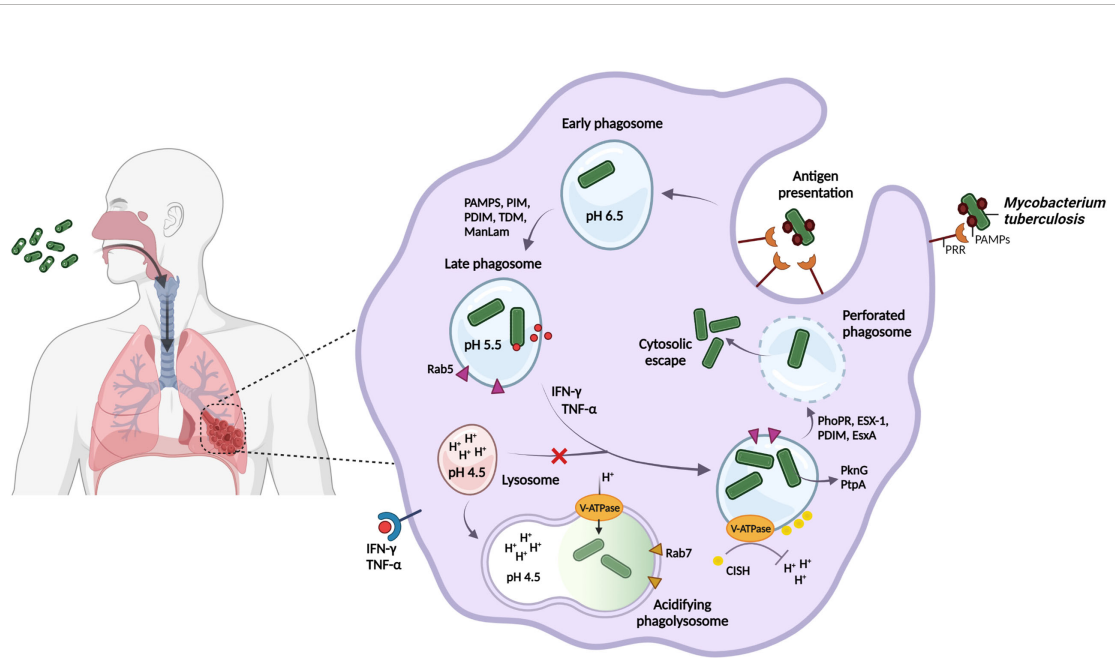

FIGURE 1
M. tuberculosis regulates phagosomal pH and blocks phagolysosome formation to avoid degradation by host acidic stressors and promote persister formation. *M. tuberculosis* is spread through the inhalation of aerosolized droplets that are released into the air when an infected individual coughs or sneezes. Host recognition of *M. tuberculosis*-specific PAMPs results in the internalization into the phagosome of alveolar macrophages for bacterial containment. *M. tuberculosis* may however interfere with host cellular processing and the host immune response by retaining its interaction with the host early phagosomal marker, Rab5, and by selectively engaging host receptors, as a strategy to enhance intracellular survival in the phagosome. Following host immune activation by IFN-γ and TNF-α, phagosomal acidification to pH 4.5 is proposed. *M. tuberculosis* inhibits phagolysosomal fusion and regulates the phagosomal pH by the V-ATPase proton pump to resist degradation by the acidic environment. *M. tuberculosis* recruits the host CISH protein to degrade V-ATPase for neutralization of the vacuole. Finally, ESX-1 and the mycobacterial cell envelope lipid PDIM, act in synergy to perforate the phagosome, which promotes cytosolic displacement of bacteria, and is a crucial step for intracellular persistence. Created with BioRender.com.

2.2 Phagosome acidification

Phagosome acidification represents a dynamic antimicrobial defense strategy used by the host, and despite *M. tuberculosis* being sensitive to high acidity (low pH), the pathogen appears to resist being killed in macrophages by maintaining its intra-bacterial pH (Vandal et al., 2008; Levitte et al., 2016). Several mechanisms that assist in neutralizing phagosomal pH have been proposed (Figure 1), including membrane proteins, proton pumps, ammonia production, amino acid decarboxylation and cell wall modifications (Vandal et al., 2008; Singh et al., 2019).

During phagosomal maturation, highly conserved vacuolar-type ATPase (V-ATPase) proton pumps are rapidly recruited to the phagosomal membrane to promote acidification. *M. tuberculosis* has however developed the ability to target and trigger degradation of the V-ATPase complex by inducing the expression of the host cytokine-inducible SH2-containing protein (CISH) (Queval et al., 2017b). This allows the phagosomal pH to remain above that required for the activity of lysosomal digestive enzymes and ROS (Pauwels et al., 2017; Baker et al., 2019).

The ability of *M. tuberculosis* to rapidly sense and respond to the external pH is crucial for pathogenesis, and involves strong induction of the PhoPR two-component regulatory system *in vitro* and in macrophages (Abramovitch et al., 2011). PhoPR is further required for intracellular pathogenesis and redox homeostasis, such as induction of the type VII secretion system ESX-1, regulation of heat shock-responsive genes (Sevalkar et al., 2019), and lipid biosynthesis regulated by the cytoplasmic redox sensor, WhiB3 (Johnson et al., 2015; Mehta et al., 2016; Feng et al., 2018) (Figures 1, 2).

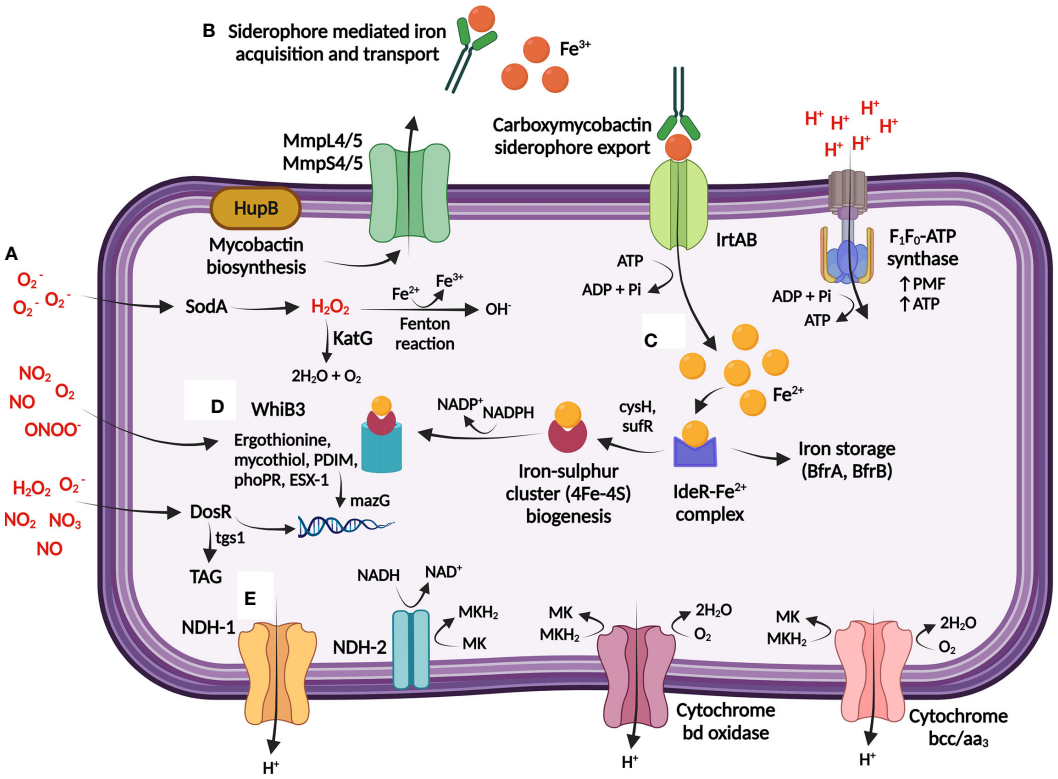

FIGURE 2
M. tuberculosis maintains bioenergetic metabolism to ensure redox homeostasis during persistence. **(A)** The host generates toxic reactive oxygen species (ROS) and reactive nitrogen species (RNS) [shown in red] through single-electron reactions, which can result in damage to *M. tuberculosis* DNA and proteins. **(B)** Redox homeostasis is maintained through the sensing and regulation of iron, obtained from the host *via* Fe^{3+}-specific iron scavenging siderophores that is imported into *M. tuberculosis* by the ABC exporter, IrtAB. **(C)** Iron is either stored or utilized directly for generation of iron sulphur clusters (4Fe-4S), and further encoded to 4Fe-4S redox sensor proteins by WhiB3. **(D)** WhiB3 produces detoxification buffers (ergothionine and mycothiol) and in combination with DosR directs the reducing equivalents produced during β-oxidation of fatty acids to produce cell wall lipids and protect DNA from oxidation. DosR further regulates lipid storage within *M. tuberculosis* through the regulation of TAG, providing a lipid rich nutrient source. **(E)** Proton balance during redox homeostasis is maintained through regulation of internal protons which can be utilised for the production of menaquinol (MKH_2) [via NDH-1/NDH-2], which is subsequently transferred to the respiratory complexes (cytochrome bd and cytochrome bcc/aa_3) to maintain the PMF and ATP production *via* F_1F_0-ATP synthase. TAG: triacylglycerol; MK: Menaquinone; NDH: NADH dehydrogenase; Fe^{3+}: ferric ion; Fe^{2+}: ferrous ion; O_2^-: superoxide; NO: nitric oxide; NO_2: nitrogen dioxide; $ONOO^-$: peroxynitrite; H_2O_2: hydrogen peroxide; MmpL: mycobacterial membrane protein large; MmpS: mycobacterial membrane protein small. Created with BioRender.com.

Transport of the ESX-1-dependent 6-kDa early secretory antigenic target (ESAT-6/EsxA) to the host cytosol (Simeone et al., 2015; Conrad et al., 2017) acts synergistically with the mycobacterial cell envelope lipid phthiocerol dimycocerosate (PDIM) in perforating the phagosome (Augenstreich et al., 2017; Barczak et al., 2017; Quigley et al., 2017; Lerner et al., 2020) and preventing recruitment of V-ATPase, thereby neutralizing the vacuole (Astarie-Dequeker et al., 2009; Passemar et al., 2014). Further membrane damage by continued perforation or complete rupture of the phagosome will allow translocation of the bacilli to the host cytosol (Jamwal et al., 2016; Schnettger et al., 2017) (Figure 1). This is crucial for intracellular persistence, as PDIM or *esxA* mutants failed to perforate the phagosomal membrane, possessed altered PAMPs, and were attenuated in human monocyte-derived macrophages (hMDMs) (Augenstreich et al., 2017). This suggests that remodeling of the cell envelope and central metabolism pathways may improve intracellular survival of persisters during acid stress by controlling the flux of lipid precursors and reducing equivalents (Baker and Abramovitch, 2018; Singh et al., 2019).

2.3 Oxidative and nitrosative stress

Host immune activation of macrophages stimulates multiple antimicrobial defense pathways, exposing *M. tuberculosis* to an environment where hydrolases, reactive nitrogen species (RNS), and ROS effectively function (Ehrt et al., 2001; Jamaati et al., 2017). *M. tuberculosis* effectively resists degradation by these reactive molecules by activating detoxification and redox buffering mechanisms to maintain bioenergetic homeostasis (Saini et al., 2016) (Figure 2; Supplementary Table 1).

Exposure to toxic nitric oxides slows bacterial growth by competing for oxygen binding, and in the process, reversibly inhibits cytochrome c oxidase, and thus aerobic respiration (Voskuil et al., 2003). *M. tuberculosis* metabolically adapts to acquire nitrate *via* oxidation of nitric oxide, thereby restoring survival due to maintenance of the PMF and ATP (Sohaskey, 2008; Tan et al., 2010). Induction of cytochrome *bd* by *M. tuberculosis* additionally plays a respiratory protective role against ROS/RNS by scavenging oxygen radicals upon breakdown of oxidative species (Small et al., 2013; Boot et al., 2017).

Host maintenance of the oxidative balance in the lung is controlled *via* antioxidant mechanisms, and *M. tuberculosis* utilizes the ROS scavenging enzymes, superoxide dismutase (SOD) and catalase-peroxidase (KatG) to degrade superoxide (O_2^-) to water and molecular oxygen to neutralize the free radicals generated in the host (Kumar et al., 2011) (Figure 2). Subsequent downregulation of ATP synthase genes may further slow bacterial growth by restricting proton translocation into the cytoplasm, thereby replenishing pools of oxidized cofactors to maintain redox and pH homeostasis (Baker et al., 2014; Baker et al., 2019). These metabolic adaptations prevent an excess of RNS/ROS, which may trigger damage to proteins, lipids and nucleic acids.

The pyrimidine-specific housekeeping enzyme, MazG, prevents DNA mutagenesis by specifically degrading and preventing the incorporation of oxidized deoxynucleotides into genomic DNA (Lyu et al., 2013; Shi et al., 2019) (Figure 2). Deletion of *mazG* decreases the NADH/NAD+ redox balance towards an oxidizing state, resulting in DNA instability, disruption to pyrimidine metabolism, and hindrance to iron and carbon uptake *in vitro* (Shi et al., 2019) and in mice (Lyu et al., 2013).

Free intracellular iron within *M. tuberculosis* catalyses ROS formation, thus homeostasis of iron is maintained by *M. tuberculosis* in a tightly regulated manner *via* the iron-dependent regulator (IdeR) (Rodriguez et al., 2002; Pandey and Rodriguez, 2014). Mycobactin and cysteine biosynthesis is maintained by *M. tuberculosis* to replace iron (Rodriguez et al., 2002) and sulphur (Song and Niederweis, 2012), respectively, for reconstruction of the damaged iron-sulphur clusters (Figure 2). This is essential for persister adaptation as iron-sulphur clusters are highly susceptible to oxidative and nitrosative stress as they undergo various oxidation-reduction reactions (Pandey et al., 2018). Paradoxically, iron uptake and cysteine synthesis promote DNA damage by forming reactive and damaging hydroxyl radicals *via* the Fenton reaction (Figure 2). However, the requirement of these proteins to repair damage appears to outweigh the negative effects of intermediate hydrogen peroxide and nitric oxide levels (Ford et al., 2011; Voskuil et al., 2011; Lyu et al., 2013).

Protection against ROS (Bhaskar et al., 2014) and nutrient starvation (Richard-Greenblatt et al., 2015; Saini et al., 2016) respectively involves WhiB3-dependent upregulation of the *M. tuberculosis* redox buffers, mycothiol and ergothioneine (Figure 2; Supplementary Table 1). These low molecular weight buffers maintain redox and bioenergetic homeostasis, including consumption of excess NADH/NADPH (Singh et al., 2009; Saini et al., 2016; Mehta and Singh, 2019). Lipid anabolism may therefore counteract reductive stress by oxidizing NADH/NADPH, as *phoP* mutants displayed a structurally altered cell envelope consisting of limited methyl branched fatty acids and diminished acid-fast staining (Walters et al., 2006).

2.4 Hypoxic environment within granulomas

As granulomas mature, gradual accumulation of necrotic cellular debris from lysed or damaged host and bacterial cells forms a caseous core (Hoff et al., 2011). Enlargement of the caseum during advanced stages of active TB disease compresses

the adjacent lung tissue, damaging the vasculature in the process, and distributing extracellular *M. tuberculosis* to the caseous center (Blanc et al., 2018; Dartois, 2014). The reduced vascularization additionally decreases oxygen availability (Datta et al., 2016), and in response, *M. tuberculosis* undergoes rapid and substantial metabolic and phenotypic adaptations (Qualls and Murray, 2016; Sershen et al., 2016) (Figure 3; Supplementary Table 1).

Foamy macrophages in necrotic regions accumulate triacylglycerol (TAG) within lipid droplets, a process exploited by *M. tuberculosis* to store host TAG intracellularly, providing a lipid-rich microenvironment for the persistence of *M. tuberculosis* during hypoxia (Guerrini et al., 2018; Del Portillo et al., 2019). Additionally, *M. tuberculosis* expression of triacylglycerol synthase (*tgs1*) induces lipid body formation in persisters, whereby lipid body-positive *M. tuberculosis* has been detected in sputum prior to the onset of treatment (Figure 3). The respiratory state of these bacilli displayed a shift from oxygen electron transfer to anaerobic respiration, thus challenging the belief that all bacilli in sputum respire aerobically (Garton et al., 2008).

ATP production in aerobic and anaerobic conditions is responsible for generating the membrane potential and proton concentration gradient that drives the PMF (Rao et al., 2008; Reichlen et al., 2017). Inhibitors of the membrane potential and proton concentration gradient are cidal towards persisters and lead to a loss in viability, suggesting that the cytoplasmic membrane of non-replicating hypoxic *M. tuberculosis*, induced in the Wayne model, is energized (Rao et al., 2008). The mechanisms

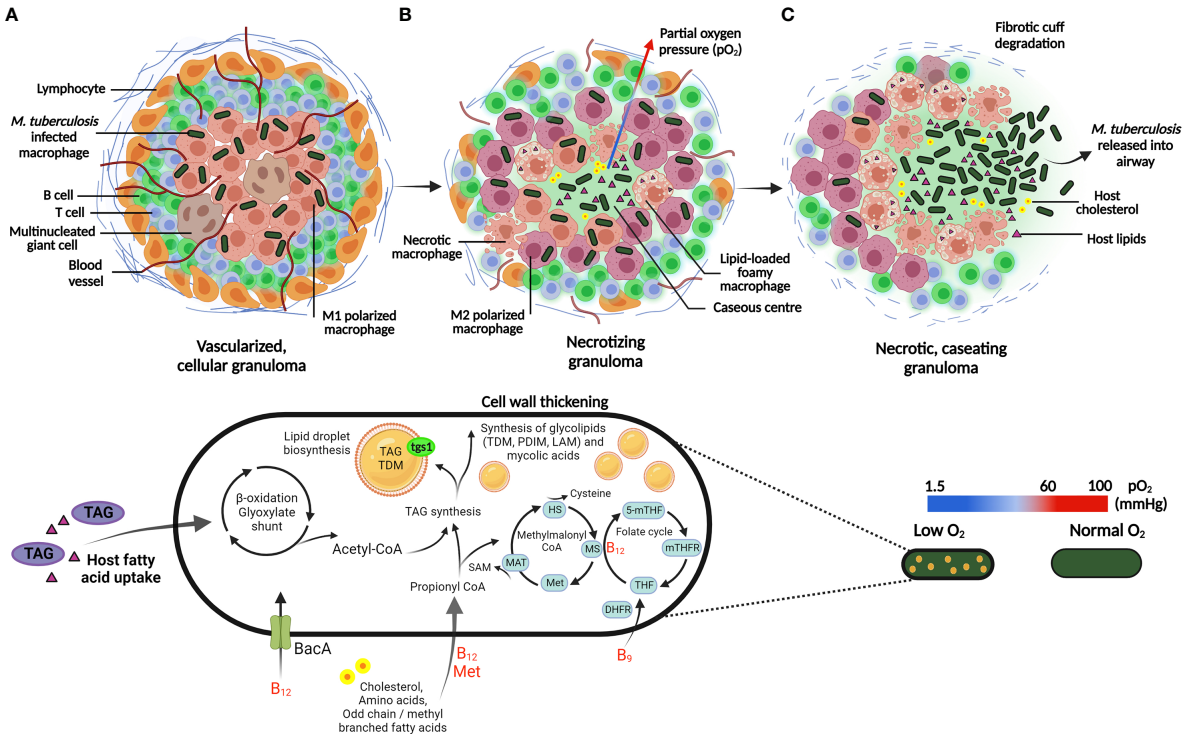

FIGURE 3
Adaptation of *M. tuberculosis* to the host granuloma environment and associated stressors. **(A)** *M. tuberculosis* is phagocytosed by alveolar macrophages and contained within the center of the granuloma, which is an organized aggregate of immune cells recruited to the site of inflammation. The pro-inflammatory cytokines, IFN-γ and TNF-α activate macrophages (M1 polarized; pink macrophages), which is essential for the control of infection. Following host immune activation, recruitment of lymphocytes, largely comprising of T and B cells, surround the periphery of the granuloma. **(B)** Mature granulomas develop heterogeneous vasculature, displaying a gradient of pro-inflammatory host cells (M1 and M2 polarized; pink and purple macrophages, respectively) and a decreasing oxygen gradient toward the caseum. In response to hypoxia, *M. tuberculosis* exploit lipid-loaded foamy macrophages to store host TAG during persistence. Host fatty acids and cholesterol are metabolized by the β-oxidation and methylmalonyl CoA pathway respectively, which generates a nutritional carbon source that can be stored in lipid droplets or utilized to generate mycobacterial cell wall components. Essential vitamins utilized in the respective metabolic pathways (shown in red) are acquired by *M. tuberculosis* from the host environment *via* the ABC-transporter, BacA. **(C)** Necrotic macrophages contributes to an accumulation of lipid debris, resulting in central caseation in mature granulomas. Eventual rupture of the granuloma leads to extracellular dissemination of *M. tuberculosis*. HS: homocysteine; MS: methionine synthase; Met: methionine; MAT: methionine adenosyltransferase; 5-mTHF: 5-methyltetrahydrofolate; mTHFR: methylenetetrahydrofolate reductase; THF: tetrahydrofolate; DHFR: dihydrofolate reductase. Created with BioRender.com.

involved in the maintenance of ATP suggest this process as essential for the survival of non-replicating *M. tuberculosis* under hypoxic conditions.

2.5 Adaptation during nutrient deprivation

Emerging evidence suggests that the active depletion of nutrients by the host immune system may create a nutrient-scarce environment within the phagosome (Appelberg, 2006; Eisenreich et al., 2013). Restricted access to transition metals (Kehl-Fie and Skaar, 2010; Hood and Skaar, 2012), carbon (Pandey and Sassetti, 2008; MacMicking, 2014), and amino acids (Zhang et al., 2013; MacMicking, 2014) drives the downregulation of key metabolism and replication machinery, possibly leading to auxotrophy in *M. tuberculosis*.

Auxotrophy is described as the inability of an organism to synthesize a specific metabolite required for its growth. *M. tuberculosis* auxotrophs for methionine (Berney et al., 2015), threonine (Hasenoehrl et al., 2019), lysine (Pavelka et al., 2003), leucine (Hondalus et al., 2000), and arginine (Tiwari et al., 2018) are severely attenuated *in vivo* due to their inability to scavenge these metabolites from the host. The *M. tuberculosis* stringent response pathway RelMtb, initiates production of the alarmones (p)ppGpp during amino acid deprivation, hypoxia and oxidative stress (Dutta et al., 2019). (p)ppGpp assists in enhancing survival during nutrient starvation in mice (Dahl et al., 2003) and guinea pigs (Klinkenberg et al., 2010; Thayil et al., 2011; Dutta et al., 2019) by inhibiting RNA synthesis for conservation of energy. Therefore, *M. tuberculosis* is incapable of entering persistence upon disruption to its stringent response (Dutta et al., 2019).

Certain metabolic processes are energetically expensive; *M. tuberculosis* has however developed elaborate strategies to synthesize or sequester essential host nutrients to satisfy its bioenergetic and biosynthetic requirements (Eisenreich et al., 2013). *M. tuberculosis* additionally exploits specific nutrients or metabolic processes that facilitate adaptation to persistence (Supplementary Table 1, Supplementary Table 2).

2.5.1 Essential amino acids act as structural components, co-factors and building blocks

Amino acids represent a critical source of nutrients used to fuel central metabolic pathways, and many pathogens are required to scavenge them in the host. The host compartments either restrict metabolite availability, or *M. tuberculosis* attempts to evade host detection by remaining metabolically independent from the host (Berney et al., 2015). *M. tuberculosis* has evolved to synthesize all 20 proteinogenic amino acids (Cole et al., 1998), of which certain amino acids are rapidly metabolized as carbon, sulphur, nitrogen or energy sources, whilst others are stored. Amino acids may additionally function as both carbon and nitrogen sources, indicating that the pathways required for their degradation and assimilation could differ (Lofthouse et al., 2013). *M. tuberculosis* furthermore exploits amino acids for their ability to provide cofactors for generating intermediate molecules or proteins, which are integral components for metabolic adaptation (Supplementary Table 2).

Amino acids acquired from the macrophage, such as alanine, glutamate and asparagine/aspartate contribute to the intracellular nutrition of *M. tuberculosis* (Beste et al., 2013). Alanine is an essential structural component of peptidoglycan (Beste et al., 2013); cell wall homeostasis is maintained by *M. tuberculosis* during persistence by conversion of L-alanine to D-alanine, whilst an impaired conversion severely restricts intracellular growth in bone marrow-derived macrophages (BMDMs) and mice (Awasthy et al., 2012). During persistence, regulation of the aspartate pathway is involved in essential cell wall processes, such as biosynthesis of the cell wall cofactor, S-adenosylmethionine (SAM), generation of the essential amino acids methionine, isoleucine, threonine and lysine, and the precursor metabolite homoserine (Hasenoehrl et al., 2019). The majority of the methionine pool is converted to SAM *via* the aspartate pathway (Berney et al., 2015; Hasenoehrl et al., 2019), therefore it is suggested that metabolic regulation of the aspartate pathway is essential for *M. tuberculosis* persistence.

2.5.2 Carbon and lipid metabolism: exploitation of the host niche

M. tuberculosis preferentially utilizes carbon-based metabolism during persistence. C-flux metabolism analysis indicates the adaptation of intracellular *M. tuberculosis* to simultaneously co-catabolize multiple carbon sources, including amino acids, carbon dioxide, vitamins and fatty acids; the latter derived from host lipids and cholesterol (de Carvalho et al., 2010; Beste et al., 2013; Noy et al., 2016; Borah et al., 2021). *M. tuberculosis* possesses the unusual ability to metabolize host fatty acids as substrates for β-oxidation. This yields substrates required for production of mycolic acids, or enables assimilation directly into TAG and phospholipids for maintenance of the cytoplasmic membrane integrity (Pandey and Sassetti, 2008) (Figure 2).

Lipid storage becomes the primary energy-conserving metabolic process in *M. tuberculosis* persisters, whereby intracellular accumulation of TAG has been observed (Russell et al., 2009; Daniel et al., 2011; Maurya et al., 2018). *M. tuberculosis* persisters may rapidly accumulate host lipids to form lipid bodies in resting macrophages, whilst access to lipid bodies is limited once macrophages are IFN-γ activated due to production of host protective eicosanoids (Knight et al., 2018). Instead, *M. tuberculosis* accumulates lipids from host macrophage lipid bodies stimulated by extracellular free fatty acids or by hypoxia (Daniel et al., 2011; Knight et al., 2018).

Observed within necrotic lesions, lipid-loaded foamy macrophages further represent a lipid-rich niche whereby host cholesterol serves as a carbon source for persisters (Pandey and Sassetti, 2008; Russell et al., 2009; Singh et al., 2012) (Figure 3).

2.5.3 Vitamins and cofactors central to nucleic acid and amino acid metabolism

β-oxidation of fatty acids accumulated by *M. tuberculosis*, generates a pool of coenzyme-A carriers and carbon units; even-chain fatty acids are degraded to acetyl coenzyme A (acetyl-CoA) *via* oxidation by the glyoxylate shunt to replenish central metabolites, whilst odd-chain fatty acids are degraded to propionyl-CoA (Warner et al., 2007; Savvi et al., 2008). Detoxification of the latter *via* the methylmalonyl-CoA and methyl citrate cycle is a vitamin B_{12}-dependent and B_{12}-independent mechanism, respectively (Figure 3). Additionally, MetH and MetE involved in methionine biosynthesis encode vitamin B_{12}-dependent and B_{12}-independent methionine synthase, respectively (Warner et al., 2007; Savvi et al., 2008). This indicates the essentiality of methionine biosynthesis, as *M. tuberculosis* may need to rapidly detect vitamin B_{12} bioavailability for prevention of toxic accumulation of propionyl-CoA (Figure 3). It is proposed that *M. tuberculosis* scavenges vitamin B_{12} from the host *via* the ATP-binding cassette (ABC) transporter, BacA (Gopinath et al., 2013). Deletion of *bacA* is speculated to contribute to the accumulation of cholesterol-rich lipid bodies (Gopinath et al., 2013), and since cholesterol provides a source of propionyl-CoA, efficient assimilation of propionyl-CoA is required for effective cholesterol metabolism (Supplementary Table 2).

An imbalance in vitamin B_{12} and methionine synthase is often associated with disruption to folate (Vitamin B_9) metabolism, as methionine synthase utilizes 5-methyltetrahydrofolate (5-MTHF) as a one-carbon (methyl group) donor to catalyze the methylation of homocysteine to methionine (Nixon et al., 2014). This is essential for production of purines, thymidine, methionine, glycine, serine, homocysteine and SAM. Inhibitors of folate synthesis exhibit distinct metabolic disruptions to methionine and SAM *in vitro*, with an upregulation of genes associated with DNA repair (Nixon et al., 2014). Disruption to SAM may be attributed to imbalances in DNA methylation, thereby introducing single nucleotide polymorphisms (SNPs) and DNA damage. This subsequently starved cells of crucial reduced folate precursors critical for the synthesis of DNA, RNA and protein (Chakraborty et al., 2013; Zheng et al., 2013; Minato et al., 2015). It has been suggested that methionine-mediated antagonism of anti-folate drugs may enhance methylation by increasing SAM abundance (Howe et al., 2018). This could be an adaptive process; however, the antagonistic mechanism has yet to be characterized. This further confirms that metabolic remodeling may offer an advantageous adaptation mechanism for conserving carbon and energy sources for prolonged persistence and possibly resuscitation.

2.5.4 Scavenging of host iron is tightly regulated

Persistence of *M. tuberculosis* during iron starvation is controlled by strict regulation of iron utilization and storage *via* the iron-dependent regulator IdeR; following acquisition, iron not immediately utilized is stored in the host as protein-bound iron in the form of ferritin to prevent the generation of toxic free radicals *via* the Fenton reaction (Pandey and Rodriguez, 2014) (Figure 2). Key cellular processes such as electron transfer, DNA replication and repair, and regulation of gene expression in response to ROS/RNS are dependent on iron and iron-sulphur clusters as a cofactor (Rodriguez and Smith, 2003). Iron is however not only restricted within granulomas, but the abundance of free iron is scarce due to its low solubility (Kurthkoti et al., 2017).

M. tuberculosis strongly promotes sequestration of iron following macrophage uptake (Abreu et al., 2018), and in necrotic and cavitary granulomas, where *M. tuberculosis* synthesizes and secretes high-affinity Fe^{3+}-specific siderophores (mycobactins) to actively compete for host iron (Kurthkoti et al., 2017) (Figure 2, Supplementary Table 2). This process is further dependent on the ESX-3 secretion system, as *M. tuberculosis* lacking the ESX-3 secretion system are defective in acquisition of bound iron from siderophores, and display severely impaired growth in THP-1 macrophages (Serafini et al., 2013), murine macrophages (Siegrist et al., 2009), and human granulomas (Kurthkoti et al., 2017).

Upon iron starvation, the *M. tuberculosis* heme enzyme KatG is downregulated, therefore reduced bioactivation of isoniazid (INH) likely mediates enhanced tolerance, contributing to antibiotic-tolerant persister formation (Kurthkoti et al., 2017). Metabolic reprogramming of iron-starved bacilli displayed repression in the majority of enzyme-encoding genes from the citric acid cycle (TCA) and oxidative phosphorylation, since these pathways require iron-sulphur clusters or heme proteins (Kurthkoti et al., 2017). DNA repair genes, including iron-sulphur cluster repair proteins were upregulated, poising bacteria to respond to oxidative damage (Tyagi et al., 2015). Additionally, biosynthesis of most amino acids decreased, with exception to lysine (Kurthkoti et al., 2017), which is the backbone of siderophore biosynthesis (McMahon et al., 2012).

2.5.5 Sulphur metabolism is intricately tied to oxidative stress

Sulphur assimilation pathways in *M. tuberculosis* produce reduced sulphur-containing metabolites, such as cysteine and methionine, and have been shown to play a critical role in facilitating bacterial adaptation and protection during

persistence (Rhee et al., 2005; Senaratne et al., 2006), and upon exposure to oxidative stress and hypoxia (Pinto et al., 2004; Voskuil et al., 2011). Controlled by *cys* genes, sulphur is required to maintain redox reactions through iron-sulphur clusters, translation initiation, methylation of DNA and RNA, biotin and menaquinone synthesis, and mycolic acid modification by SAM-dependent methyltransferases (Hasenoehrl et al., 2019).

Disruption in CysH renders *M. tuberculosis* unable to utilize inorganic sulphate for the synthesis of the cytosolic reducing buffer, mycothiol (Senaratne et al., 2006), which serves in detoxification of bactericidal agents and host oxidative damage (Buchmeier et al., 2003; Senaratne et al., 2006; Mishra et al., 2019). Perturbation in mycothiol redox homeostasis elevated endogenous ROS, inducing a long-lasting and irreversible oxidative shift in *M. tuberculosis* (Tyagi et al., 2015). Adaptation may have favored the release of secretory antioxidants in the phagosome to neutralize exogenous oxidative stress as a defense mechanism, playing a role in facilitating persistence (Tyagi et al., 2015).

To further neutralize host-mediated oxidative stress, *M. tuberculosis* overexpresses cysteine desulfurase to repair oxidatively damaged iron-sulphur clusters (Ayala-Castro et al., 2008; Tyagi et al., 2015). Accordingly, *sufR* enabled persistence in the host by maintaining iron homeostasis, and downregulating genes responsible for iron-sulphur cluster biogenesis (Pandey et al., 2018).

2.5.6 Co-metabolism of multiple nitrogen sources

M. tuberculosis appears to not require tight control of its nitrogen sources, as it has evolved the ability to co-metabolize a variety of alternate amino acids as nitrogen sources during infection (Agapova et al., 2019; Borah et al., 2019). It has been established that *M. tuberculosis* utilizes asparagine and glutamate as sole nitrogen sources during persistence (Song et al., 2011; Song and Niederweis, 2012). Originally described as a porin-forming protein, OmpATb (Song et al., 2011), and the asparaginase transporter AnsA (Gouzy et al., 2014) rapidly mediates ammonia secretion from these amino acids, thus neutralizing the acidic phagosomal pH. This may be an adaptive mechanism for pH homeostasis and indicates that asparaginase has evolved two independent key functions, to conduct nitrogen metabolism and counteract the host defense acidification (Figure 2, Supplementary Table 2).

To circumvent nitric oxide toxicity in macrophages, *M. tuberculosis* acquires nitrate by oxidation of nitric oxide. Upon persister formation, an increase in nitrate reductase occurs, indicating that *M. tuberculosis* utilizes nitrate as an alternative electron acceptor during anaerobic respiration since reduction in electron flow associated with decreasing oxygen levels results in an increased concentration of reduced cofactors, such as NADH (Sohaskey, 2008; Williams et al., 2015). Furthermore, PhoP and DosR regulates expression of nitrite and nitrate reductases for persistence during hypoxia (Singh et al., 2020).

2.5.7 Potassium metabolism tightly regulates the membrane potential

Potassium (K^+) is a crucial cation required for maintenance of an electrochemical gradient and PMF, and regulation of intracellular pH and osmotic pressure. During phagosome maturation, a change in host ions and K^+ uptake occurs, thus *M. tuberculosis* tightly controls regulation of its ionic signals *via* the Trk and Kdp K^+ uptake systems. Disruption of K^+ homeostasis results in the inability of *M. tuberculosis* to respond to low pH and high chloride levels in BMDMs (MacGilvary et al., 2019), and has been shown to negatively affect *M. tuberculosis* growth rate, as determined by uracil incorporation as a measure of transcriptional activity (Salina et al., 2014).

Interestingly, exposure to low environmental K^+ repressed iron uptake in *M. tuberculosis*, subsequently exposing bacilli to oxidative stress (MacGilvary et al., 2019). Following K^+ deficiency, *M. tuberculosis* persisters maintained a stable, yet low abundance of transcripts coding for biosynthetic enzymes or proteins involved in adaptation, repair, and management of transcription initiation. Once reintroduced into K^+ supplemented media, these mRNA transcripts likely assisted in rapid translation following resuscitation (Ignatov et al., 2015).

2.5.8 Phosphate metabolism and the stringent response

Phosphorous is essential for the synthesis of nucleotides, DNA, RNA and phospholipids, and is acquired from the host *via* the phosphate-specific transporter (Pst) to form phosphate compounds through interaction with the two-component regulatory system SenX3-RegX3 (Rifat et al., 2009; Tischler et al., 2013; Namugenyi et al., 2017). SenX3-RegX3 likely plays a role in virulence during persistence as deletion of *pstA1* constitutively activates RegX3, regardless of phosphate availability, and subsequently triggers the ESX-5 secretion system, resulting in hypersecretion of ESX-5 substrates in Irgm1-deficient mice (Elliott et al., 2019). While the ESX-5 system is required for virulence, tight control in secretion of ESX-5 substrates may limit recognition by the host immune system or prevent secretion of harmful cytokines (Elliott et al., 2019). This may represent a defense mechanism to evade the host adaptive immune response, however it is unknown whether ESX-5 substrates directly assist in phosphate scavenging or whether constitutive secretion of specific ESX-5 antigens may explain the impaired intracellular survival of *M. tuberculosis*.

During nutrient starvation, polyphosphate (polyP) accumulation provides a reservoir of energy and a phosphate donor, and may be the preferential energy store since decreased

ATP levels were observed during most stress conditions in guinea pigs (Singh et al., 2013). This was associated with down-regulation of reductive TCA cycle intermediates (succinate, fumarate, malate), and up-regulation of oxidative TCA intermediates, as indicated using ^{13}C isotope labelling (Dutta et al., 2019). Additionally, regulation of polyP is dependent on (p)ppGpp levels, as disruption to the stringent response pathway contributed to enhanced antibiotic susceptibility and defective bacterial growth in guinea pig lungs (Singh et al., 2013; Chuang et al., 2015). This suggests that tight regulation of Rel_{Mtb} and polyP homeostasis is critical for *M. tuberculosis* persister formation following exposure to host-induced stressors and/or antibiotics.

2.6 Impact of heterogeneous granuloma lesions on bacterial adaptation

Granulomas develop a spectrum of lesion types, driven by variable cytokine profiles and lesion histopathology (Lin et al., 2013; Martin et al., 2017). Importantly, previous work has shown that granuloma lesions harbor physiologically distinct bacterial populations with varying rates of replication and different metabolic states (Lenaerts et al., 2007; Hoff et al., 2011). Since heterogeneity within lung lesion types influences the bacterial phenotype, this could provide essential information about the microenvironment and how this impacts the bacterial physiology to favor and induce persistence (Dartois, 2014; Irwin et al., 2015; Gregg et al., 2018).

M. tuberculosis may exploit the host response by tweaking the inflammatory balance within granulomas. Detailed immunohistochemical analysis of granulomatous lesions from *M. tuberculosis*-infected cynomolgus macaques demonstrated a pro-inflammatory phenotype to be localized to the center of the granuloma (Mattila et al., 2013), which has been shown to contribute to persistence and extracellular survival of *M. tuberculosis* (Tan and Russell, 2015) (Figure 3). Contrarily, the tissue within the granuloma surrounding the caseum displays a gradient of anti-inflammatory phenotypes and gradually increasing oxygen tension (Mattila et al., 2013). This suggests that the pathways involved in macrophage metabolism influence the inflammatory signals and effector functions generated in response to infection.

Macrophage heterogeneity attributed to ontogeny and polarization states can further influence macrophage function, and the subsequent progression of varying granuloma types that coexist in individual patients. Using experimental data from nonhuman primates, the development of a computational model was used to investigate the temporal dynamics and spatial organization of M1 and M2 polarized macrophages to determine how cytokine signaling impacts the outcome of infection (Marino et al., 2015). Independent of adaptive immunity, alveolar macrophages in the mouse lung exhibit an M2 phenotype and favor fatty acid oxidation, therefore providing a metabolic and nutritional advantage for intracellular *M. tuberculosis* compared to bacilli residing in interstitial macrophages (Huang et al., 2018). Whilst this mechanism could protect the host against excessive inflammation, it is unclear how *M. tuberculosis* alters the metabolic state of macrophages towards M2 polarization to enhance intracellular persistence and sequestration of host nutrients.

M. tuberculosis increases TAG accumulation in the caseum, which contributes to antibiotic tolerance (Daniel et al., 2011; Sarathy et al., 2018), and correlates with the presence of lipid-body positive *M. tuberculosis* in sputum (Sloan et al., 2015). It is thought that foamy macrophages surround the caseum, as their lipid composition resembles the environment encountered in the caseum (Peyron et al., 2008; Kim et al., 2010). Additionally, necrotic death of foamy macrophages would release lipid droplets and cellular debris at the caseum interface (Peyron et al., 2008). Since foamy macrophages have lost their phagocytic ability (Peyron et al., 2008), it is suggested that their formation is exploited by *M. tuberculosis* to enhance cavitation of the granuloma.

2.7 Adaptation to antibiotic exposure within the granuloma

Histopathological analysis of lesions indicates that antibiotic treatment induces changes in the granuloma structure, whereby the majority of caseous granulomas evolve to fibrotic or necrotizing tissue that lack proper structure. Hypoxic conditions and poor antibiotic diffusion into the devascularized caseous center lead to heterogeneous susceptibility of bacteria, whereby residual bacterial growth remains in the caseum or acellular rim of necrotic granulomas following treatment in guinea pigs (Lenaerts et al., 2007), rabbits (Sarathy et al., 2018) and macaques (Lin et al., 2014). These bacilli were found to grow as multicellular pellicles, characteristic of biofilms (Ojha et al., 2008; Islam et al., 2012; Wright et al., 2017). It is hypothesized that this cording phenotype contributes to mycobacterial persistence in the host as the abundance of extracellular free mycolic acids during pellicle maturation creates a waxy-layered lipid-rich matrix that harbors and protects drug-tolerant bacilli (Ojha et al., 2008; Islam et al., 2012; Wright et al., 2017).

The host tissue environment and complex granuloma composition likely drives heterogeneous bacterial susceptibility and antibiotic-tolerant persister formation, as some lesions are sterilized prior to antibiotic treatment in macaques (Lin et al., 2014), whilst other lesions may endure following completion of treatment in humans (Malherbe et al., 2016). Differential drug partitioning between cellular and necrotic lesions (Irwin et al., 2016; Sarathy et al., 2016; Zimmerman et al., 2017; Blanc et al.,

2018) result in sub-inhibitory antibiotic concentrations, thereby impacting the rate of sterilization and treatment success. The prodrugs isoniazid and pyrazinamide additionally require bioactivation by *M. tuberculosis* KatG and PncA, respectively, to be functional. Whilst decreased expression of KatG is associated with isoniazid-treated persisters (Wakamoto et al., 2013; Kurthkoti et al., 2017), genes other than *pncA*, such as *sigE* and *panD* are implicated in pyrazinamide resistance (Thiede et al., 2022). It remains to be determined whether the latter genes mediate tolerance in *M. tuberculosis*. Inhibition of F_1F_0-ATP synthase following treatment with bedaquiline involves rapid metabolic adaptation by *M. tuberculosis*, whereby multiple metabolic pathways associated with the *dosR* dormancy regulon, lipid homeostasis and cell wall remodeling contribute to antibiotic tolerance (Peterson et al., 2016).

Persister formation and associated antibiotic tolerance may be triggered by host exposure, independent of antibiotic exposure. Increased antibiotic tolerance may thus be attributed to a combination of alternative metabolic pathways being utilized that may not be bioactivated, and inconsistent drug distribution attributed to lesional heterogeneity. In previous work from our group, macrophage uptake resulted in enrichment for non- or slowly replicating *M. tuberculosis*. Treatment with D-cycloserine revealed that this population is highly enriched for persisters, based on its antibiotic tolerant phenotype (Mouton et al., 2016). This is in line with work from Jain et al. (2016) who observed the presence of persisters in sputum from TB patients prior to antibiotic treatment. Vilchèze et al. (2017) additionally demonstrated that compounds that enhanced respiration and induced ROS in *M. tuberculosis* persisters prevented *M. tuberculosis* from entering a low metabolic state and rendered mycobacteria susceptible to bactericidal antibiotics (Vilchèze et al., 2017). This suggests that host pressures drive formation of antibiotic-tolerant persisters, and may be exploited by targeting processes required during maintenance of persistence in the host.

To mimic intracellular confinement and spatially monitor the impact of phagosomes on *M. tuberculosis* antibiotic-tolerant persister formation, space-confined cell culture chambers (Luthuli et al., 2015) and zebrafish larval models (Adams et al., 2011) have been exploited. This revealed differential progression of lesions in response to antibiotic treatment. Following macrophage uptake, drug tolerance arose within a few days, whereby antibiotic-tolerant persisters residing in macrophages exploited granulomas for their expansion or migrated to disseminate infection (Adams et al., 2011; Luthuli et al., 2015). Recent approaches to tracking the fate of individual lesions provides insight into the heterogeneous granuloma formation and size, and lesion-specific dissemination (Martin et al., 2017; Gregg et al., 2018; Cicchese et al., 2020), which may guide our understanding of how specific tissue environments influence responses to antibiotics.

3 Phenotypic adaptation of *M. tuberculosis* to host-associated stressors

The varying microenvironments that *M. tuberculosis* colonizes greatly enhance phenotypic adaptations that enable host evasion and promotes intracellular survival and persistence. A major adaptation is an altered growth rate. A slower growth rate has been associated with modifications to the mycobacterial cell wall architecture, whereby *M. tuberculosis* reconstructs its surface lipid and mycolic acid structure by undergoing mycolic acid biosynthesis and cell wall thickening (Hampshire et al., 2004; Rohde et al., 2012; Vilchèze and Kremer, 2017; Zimmermann et al., 2017; Baker and Abramovitch, 2018). An altered colony morphology (Salina et al., 2014) and cell length distribution observed in sputum (Vijay et al., 2017b) have been further shown to influence heterogeneity in metabolism, antibiotic sensitivity and response to stressors.

3.1 Structural adaptation

Prolonged periods under multiple stress conditions drastically increases the number of intracellular lipid bodies *in vitro* (Deb et al., 2009) and in sputum (Garton et al., 2008; Vijay et al., 2018), whereby a correlation between TAG accumulation and loss of acid fastness is observed (Deb et al., 2009; Daniel et al., 2011). Interestingly, transcriptomic analyses of these bacilli revealed downregulation of *kasB*, one of two *M. tuberculosis* genes encoding distinct ß-ketoacyl-ACP synthases, during persistence (Deb et al., 2009; Vilchèze et al., 2014). Deletion of *kasB* led to alterations in mycolic acid structure by producing mycolic acids that were two to four carbons shorter, and resulted in the loss of cording and acid-fastness (Gao et al., 2003; Bhatt et al., 2007). This may negatively affect cell wall permeability since these mycolic acids were not synthesized in dense bundles (Yamada et al., 2012). The precise mechanism resulting in loss of acid fastness is however not well understood, and it is uncertain whether retention of the acid-fast stain is hindered or whether reorganization of the cell wall components prevents access of the stain.

The current acid-fast staining approach is dependent on mycolic acid chain length and structure, which has been shown to substantially differ in the cell wall of *M. tuberculosis* (Barry et al., 1998; Beken et al., 2011). Persisters residing in the caseum frequently go undetected and appear acid-fast negative in guinea pigs (Hoff et al., 2011), highlighting the inconsistencies of acid-fast staining. Histological representation of various lung lesions from patients non-compliant to treatment display heterogeneous

morphology and distribution of acid-fast bacilli. Acid-fast bacilli were largely located at the granuloma surface, with connection to airways, whereas acid-fast bacilli in necrotizing granulomas were scarcely detected (Kaplan et al., 2003; Lenaerts et al., 2007). Interestingly, following resuscitation of *M. tuberculosis* persisters generated *in vitro*, upregulation of genes responsible for fatty acid and mycolic acid biosynthesis was observed (Du et al., 2016; Salina et al., 2019), whilst pathways involved in lipid uptake and catabolism were down-regulated (Du et al., 2016). This characteristic may reflect differences in the cell wall components and lipid profiles prior to resuscitation; it is thus intriguing whether these bacilli regained their acid-fastness.

Nutrient availability further influences variations in morphology, whereby phosphate- (Rifat et al., 2014) or potassium-starved bacilli (Salina et al., 2014) display a more elongated, or spherical and shorter morphology, respectively. This may alter the ultrastructure and could explain the loss in acid-fastness of *M. tuberculosis* persisters. The enhancement in surface-to-volume ratio for elongated cells may be advantageous in sequestering additional nutrients from its environment.

3.2 Cell division and growth rate

Asymmetric cellular division is commonly observed in mycobacteria during cell elongation and division (Aldridge et al., 2012). As bacterial cells divide, the progeny inherits an 'old pole' generated from previous cell divisions, and a 'new pole' from the most recent cell division. Cell length heterogeneity introduced by asymmetrical cell division has been associated with differential susceptibility to host- and antibiotic-induced stressors (Aldridge et al., 2012; Vijay et al., 2017a). Asymmetry-promoting proteins LamA and Wag31 regulate polar growth and cell elongation at each pole (Rego et al., 2017). Cells inheriting the old pole generate longer cells with faster elongation rates than cells that inherit the new pole (Aldridge et al., 2012; Richardson et al., 2016; Nair et al., 2019; Vijay et al., 2017a). Unequal partitioning of cells, with a stronger bias towards daughter cells inheriting the old pole, display higher tolerance to host and antibiotic stress (Richardson et al., 2016; Nair et al., 2019). Similarly, multidrug-resistant (MDR) strains were observed to increase their cell length distribution in macrophages (Vijay et al., 2017b), whilst shorter cells with slower elongation rates were more antibiotic susceptible (Aldridge et al., 2012; Nair et al., 2019). Computational tools that cytologically profile *M. tuberculosis* response to antibiotic treatment (Smith et al., 2020) may further be adapted to predict whether specific cell morphologies prior to treatment influence treatment outcome.

Synthesis of cell envelope components such as peptidoglycan and arabinogalactan varies in polar localization (Botella et al., 2017), thus asymmetrical division may impact on cell envelope assembly, resulting in distinct localization of cellular or metabolic machinery near poles that will allow for efficient growth. Repeated inheritance of the old poles at cellular division has been linked to limited growth rates, increased antibiotic susceptibility and cell death (Dhar and McKinney, 2007; Aldridge et al., 2012). This may be attributed to partitioning of damaged cell components, which would describe replicative aging and cell death. However, whether pole age influences survival or entry into persistence is unknown.

Alternative carbon sources (Priestman et al., 2017) or nutrient starvation (Hayashi et al., 2018) may further reflect variations in growth rate and cell length. Oxidative stress and iron deficiency have been shown to increase cell length heterogeneity in sensitive and MDR strains (Vijay et al., 2017b). A higher level of NADH oxidase in shorter cells generates significantly higher hydroxyl radical levels *via* the Fenton reaction. Since this occurs to a lesser extent in normal/long-length cells, this inherent predisposition could offer a survival advantage attributed to differential antibiotic susceptibility, and may provide a mechanism underlying tolerance (Vijay et al., 2017b). Interestingly, shorter cells possessed a lower buoyant density fraction in Percoll gradient, indicative of a high lipid content. The presence of lipid-rich membrane vesicles on the bacilli cell surface of shorter cells may indicate molecular differences to normal/long-length cells (Vijay et al., 2017a). Regardless of the growth media, the short and normal/long-length cells comprised ~ 10% and ~ 90% of the population, respectively, *in vitro* and in clinical isolates (Vijay et al., 2017a). Stressed *M. tuberculosis* additionally distributes irreversibly oxidized proteins asymmetrically (Vaubourgeix et al., 2015). This may represent an inherent mechanism for regulation of mycobacterial cell growth, further enhancing population heterogeneity, and requires further investigation.

4 Conclusion

Bacterial phenotypic heterogeneity signifies a survival strategy to allow rapid adaptation and persister formation in response to altering conditions (Ryan et al., 2010). *M. tuberculosis* is simultaneously exposed to multiple host-related stressors, contributing to the spectrum of adaptive responses that induce phenotypically heterogeneous subpopulations. Research highlights the induction of overlapping adaptive responses that may assist *M. tuberculosis* persisters to flourish in various microenvironments within the host, and further contributes to antibiotic tolerance (Kurthkoti et al., 2017; Huang et al., 2018; Pisu et al., 2020). *M. tuberculosis* appears to exploit macrophages and granuloma formation for its expansion. Therefore, utilizing animal models that reflect the diversity within lesion phenotypes as observed in humans can divulge how host interactions drive bacterial phenotypic heterogeneity, and subsequent disease progression (Driver et al., 2012; Martin et al., 2017). Many technical challenges are however associated with investigation of *M. tuberculosis* persisters, thus approaches involving flow cytometry and high-content imaging-based techniques in combination with *M. tuberculosis*-specific probes

could improve the characterization of persisters (Parbhoo et al., 2020). This could highlight specific mechanisms utilized by *M. tuberculosis* for adaptation to the host environment; understanding and exploiting such pathways may highlight key mechanisms utilized by *M. tuberculosis* to maintain persistence, possibly providing a target for therapeutic intervention.

Author contributions

TP researched data, constructed figures, wrote and edited the manuscript. JM and SS critically reviewed the manuscript and provided insightful discussions and ideas. All authors contributed to the article and approved the submitted version.

Funding

This work was supported by funding from the South African Medical Research Council (SA MRC), and the South African National Research Foundation (NRF). SS is funded by the South African Research Chairs Initiative of the Department of Science and Technology and NRF of South Africa, award number UID 86539. TP was funded by the Deutscher Akademischer Austauschdienst and NRF of South Africa, award number UID 111868. This work was supported by the GCRF Networks in Vaccines Research and Development VALIDATE Network which was co-funded by the MRC and BBSRC (ref MR/R005850/1). This UK funded award is part of the EDCTP2 programme supported by the European Union.

Conflict of interest

The authors declare that the research was conducted in the absence of any commercial or financial relationships that could be construed as a potential conflict of interest.

Publisher's note

All claims expressed in this article are solely those of the authors and do not necessarily represent those of their affiliated organizations, or those of the publisher, the editors and the reviewers. Any product that may be evaluated in this article, or claim that may be made by its manufacturer, is not guaranteed or endorsed by the publisher.

Supplementary material

The Supplementary Material for this article can be found online at: https://www.frontiersin.org/articles/10.3389/fcimb.2022.956607/full#supplementary-material

References

Abramovitch, R. B., Rohde, K. H., Hsu, F.-F., and Russell, D. G. (2011). aprABC: A mycobacterium tuberculosis complex-specific locus that modulates pH-driven adaptation to the macrophage phagosome. *Mol. Microbiol.* 80, 678–694. doi: 10.1111/j.1365-2958.2011.07601.x

Abreu, R., Essler, L., Loy, A., Quinn, F., and Giri, P. (2018). Heparin inhibits intracellular mycobacterium tuberculosis bacterial replication by reducing iron levels in human macrophages. *Sci. Rep.* 8, 7296. doi: 10.1038/s41598-018-25480-y

Adams, K. N., Takaki, K., Connolly, L. E., Wiedenhoft, H., Winglee, K., Humbert, O., et al. (2011). Drug tolerance in replicating mycobacteria mediated by a macrophage-induced efflux mechanism. *Cell* 145, 39–53. doi: 10.1016/j.cell.2011.02.022

Agapova, A., Serafini, A., Petridis, M., Hunt, D. M., Garza-Garcia, A., Sohaskey, C. D., et al. (2019). Flexible nitrogen utilisation by the metabolic generalist pathogen mycobacterium tuberculosis. *eLife* 8, e41129. doi: 10.7554/eLife.41129

Aldridge, B. B., Fernandez-Suarez, M., Heller, D., Ambravaneswaran, V., Irimia, D., Toner, M., et al. (2012). Asymmetry and aging of mycobacterial cells lead to variable growth and antibiotic susceptibility. *Science* 335, 100–104. doi: 10.1126/science.1216166

Appelberg, R. (2006). Macrophage nutriprive antimicrobial mechanisms. *J. Leukoc. Biol.* 79, 1117–1128. doi: 10.1189/jlb.0206079

Astarie-Dequeker, C., Guyader, L. L., Malaga, W., Seaphanh, F.-K., Chalut, C., Lopez, A., et al. (2009). Phthiocerol dimycocerosates of m. tuberculosis participate in macrophage invasion by inducing changes in the organization of plasma membrane lipids. *PloS Pathog.* 5, e1000289. doi: 10.1371/journal.ppat.1000289

Augenstreich, J., Arbues, A., Simeone, R., Haanappel, E., Wegener, A., Sayes, F., et al. (2017). ESX-1 and phthiocerol dimycocerosates of mycobacterium tuberculosis act in concert to cause phagosomal rupture and host cell apoptosis. *Cell. Microbiol.* 19, e12726. doi: 10.1111/cmi.12726

Awasthy, D., Bharath, S., Subbulakshmi, V., and Sharma, U. (2012). Alanine racemase mutants of mycobacterium tuberculosis require d-alanine for growth and are defective for survival in macrophages and mice. *Microbiol. Read. Engl.* 158, 319–327. doi: 10.1099/mic.0.054064-0

Axelrod, S., Oschkinat, H., Enders, J., Schlegel, B., Brinkmann, V., Kaufmann, S. H. E., et al. (2008). Delay of phagosome maturation by a mycobacterial lipid is reversed by nitric oxide. *Cell. Microbiol.* 10, 1530–1545. doi: 10.1111/j.1462-5822.2008.01147.x

Ayala-Castro, C., Saini, A., and Outten, F. W. (2008). Fe-s cluster assembly pathways in bacteria. *Microbiol. Mol. Biol. Rev. MMBR* 72, 110–125. doi: 10.1128/MMBR.00034-07

Baker, J. J., and Abramovitch, R. B. (2018). Genetic and metabolic regulation of mycobacterium tuberculosis acid growth arrest. *Sci. Rep.* 8, 1–16. doi: 10.1038/s41598-018-22343-4

Baker, J. J., Dechow, S. J., and Abramovitch, R. B. (2019). Acid fasting: Modulation of mycobacterium tuberculosis metabolism at acidic pH. *Trends Microbiol.* 27, 942–953. doi: 10.1016/j.tim.2019.06.005

Baker, J. J., Johnson, B. K., and Abramovitch, R. B. (2014). Slow growth of mycobacterium tuberculosis at acidic pH is regulated by phoPR and host-associated carbon sources. *Mol. Microbiol.* 94, 56–69. doi: 10.1111/mmi.12688

Balaban, N. Q., Helaine, S., Lewis, K., Ackermann, M., Aldridge, B., Andersson, D. I., et al. (2019). Definitions and guidelines for research on antibiotic persistence. *Nat. Rev. Microbiol.* 17, 441–448. doi: 10.1038/s41579-019-0196-3

Barczak, A. K., Avraham, R., Singh, S., Luo, S. S., Zhang, W. R., Bray, M.-A., et al. (2017). Systematic, multiparametric analysis of mycobacterium tuberculosis intracellular infection offers insight into coordinated virulence. *PloS Pathog.* 13, e1006363. doi: 10.1371/journal.ppat.1006363

Barry, C. E., Lee, R. E., Mdluli, K., Sampson, A. E., Schroeder, B. G., Slayden, R. A., et al. (1998). Mycolic acids: structure, biosynthesis and physiological functions. *Prog. Lipid Res.* 37, 143–179. doi: 10.1016/s0163-7827(98)00008-3

Beken, S. V., Dulayymi, J. R. A., Naessens, T., Koza, G., Maza-Iglesias, M., Rowles, R. R., et al. (2011). Molecular structure of the mycobacterium tuberculosis virulence factor, mycolic acid, determines the elicited inflammatory pattern. *Eur. J. Immunol.* 41, 450–460. doi: 10.1002/eji.201040719

Berney, M., Berney-Meyer, L., Wong, K.-W., Chen, B., Chen, M., Kim, J., et al. (2015). Essential roles of methionine and s-adenosylmethionine in the autarkic lifestyle of mycobacterium tuberculosis. *Proc. Natl. Acad. Sci. U. S. A.* 112, 10008–10013. doi: 10.1073/pnas.1513033112

Beste, D. J. V., Nöh, K., Niedenführ, S., Mendum, T. A., Hawkins, N. D., Ward, J. L., et al. (2013). 13C-flux spectral analysis of host-pathogen metabolism reveals a mixed diet for intracellular mycobacterium tuberculosis. chem. *Biol.* 20, 1012–1021. doi: 10.1016/j.chembiol.2013.06.012

Bhaskar, A., Chawla, M., Mehta, M., Parikh, P., Chandra, P., Bhave, D., et al. (2014). Reengineering redox sensitive GFP to measure mycothiol redox potential of mycobacterium tuberculosis during infection. *PloS Pathog.* 10, e1003902. doi: 10.1371/journal.ppat.1003902

Bhatt, A., Fujiwara, N., Bhatt, K., Gurcha, S. S., Kremer, L., Chen, B., et al. (2007). Deletion of kasB in mycobacterium tuberculosis causes loss of acid-fastness and subclinical latent tuberculosis in immunocompetent mice. *Proc. Natl. Acad. Sci. U. S. A.* 104, 5157–5162. doi: 10.1073/pnas.0608654104

Blanc, L., Daudelin, I. B., Podell, B. K., Chen, P.-Y., Zimmerman, M., Martinot, A. J., et al. (2018). High-resolution mapping of fluoroquinolones in TB rabbit lesions reveals specific distribution in immune cell types. *eLife* 7, e41115. doi: 10.7554/eLife.41115

Boot, M., Jim, K. K., Liu, T., Commandeur, S., Lu, P., Verboom, T., et al. (2017). A fluorescence-based reporter for monitoring expression of mycobacterial cytochrome bd in response to antibacterials and during infection. *Sci. Rep.* 7, 1–10. doi: 10.1038/s41598-017-10944-4

Borah, K., Beyß, M., Theorell, A., Wu, H., Basu, P., Mendum, T. A., et al. (2019). Intracellular mycobacterium tuberculosis exploits multiple host nitrogen sources during growth in human macrophages. *Cell Rep.* 29, 3580–3591.e4. doi: 10.1016/j.celrep.2019.11.037

Borah, K., Mendum, T. A., Hawkins, N. D., Ward, J. L., Beale, M. H., Larrouy-Maumus, G., et al. (2021). Metabolic fluxes for nutritional flexibility of mycobacterium tuberculosis. *Mol. Syst. Biol.* 17, e10280. doi: 10.15252/msb.202110280

Botella, H., Yang, G., Ouerfelli, O., Ehrt, S., Nathan, C. F., and Vaubourgeix, J. (2017). Distinct spatiotemporal dynamics of peptidoglycan synthesis between mycobacterium smegmatis and mycobacterium tuberculosis. *mBio* 8, e01183–17. doi: 10.1128/mBio.01183-17

Buchmeier, N. A., Newton, G. L., Koledin, T., and Fahey, R. C. (2003). Association of mycothiol with protection of mycobacterium tuberculosis from toxic oxidants and antibiotics. *Mol. Microbiol.* 47, 1723–1732. doi: 10.1046/j.1365-2958.2003.03416.x

Chakraborty, S., Gruber, T., Barry, C. E., Boshoff, H. I., and Rhee, K. Y. (2013). Para-aminosalicylic acid acts as an alternative substrate of folate metabolism in mycobacterium tuberculosis. *Science* 339, 88–91. doi: 10.1126/science.1228980

Chuang, Y.-M., Bandyopadhyay, N., Rifat, D., Rubin, H., Bader, J. S., and Karakousis, P. C. (2015). Deficiency of the novel exopolyphosphatase Rv1026/PPX2 leads to metabolic downshift and altered cell wall permeability in mycobacterium tuberculosis. *mBio* 6, e02428–e02414. doi: 10.1128/mBio.02428-14

Cicchese, J. M., Dartois, V., Kirschner, D. E., and Linderman, J. J. (2020). Both pharmacokinetic variability and granuloma heterogeneity impact the ability of the first-line antibiotics to sterilize tuberculosis granulomas. *Front. Pharmacol.* 11. doi: 10.3389/fphar.2020.00333

Cole, S. T., Brosch, R., Parkhill, J., Garnier, T., Churcher, C., Harris, D., et al. (1998). Deciphering the biology of mycobacterium tuberculosis from the complete genome sequence. *Nature* 393, 537. doi: 10.1038/31159

Commandeur, S., Iakobachvili, N., Sparrius, M., Nur, M. M., Mukamolova, G. V., and Bitter, W. (2020). Zebrafish embryo model for assessment of drug efficacy on mycobacterial persisters. *Antimicrob. Agents Chemother.* 64, e00801–20. doi: 10.1128/AAC.00801-20

Conrad, W. H., Osman, M. M., Shanahan, J. K., Chu, F., Takaki, K. K., Cameron, J., et al. (2017). Mycobacterial ESX-1 secretion system mediates host cell lysis through bacterium contact-dependent gross membrane disruptions. *Proc. Natl. Acad. Sci. U. S. A.* 114, 1371–1376. doi: 10.1073/pnas.1620133114

Dahl, J. L., Kraus, C. N., Boshoff, H. I. M., Doan, B., Foley, K., Avarbock, D., et al. (2003). The role of RelMtb-mediated adaptation to stationary phase in long-term persistence of mycobacterium tuberculosis in mice. *Proc. Natl. Acad. Sci. U. S. A.* 100, 10026–10031. doi: 10.1073/pnas.1631248100

Daniel, J., Maamar, H., Deb, C., Sirakova, T. D., and Kolattukudy, P. E. (2011). Mycobacterium tuberculosis uses host triacylglycerol to accumulate lipid droplets and acquires a dormancy-like phenotype in lipid-loaded macrophages. *PloS Pathog.* 7, e1002093. doi: 10.1371/journal.ppat.1002093

Dartois, V. (2014). The path of anti-tuberculosis drugs: from blood to lesions to mycobacterial cells. *Nat. Rev. Microbiol.* 12, 159–167. doi: 10.1038/nrmicro3200

Datta, M., Via, L. E., Chen, W., Baish, J. W., Xu, L., Barry, C. E., et al. (2016). Mathematical model of oxygen transport in tuberculosis granulomas. *Ann. Biomed. Eng.* 44, 863–872. doi: 10.1007/s10439-015-1415-3

Deb, C., Lee, C.-M., Dubey, V. S., Daniel, J., Abomoelak, B., Sirakova, T. D., et al. (2009). A novel in vitro multiple-stress dormancy model for mycobacterium tuberculosis generates a lipid-loaded, drug-tolerant, dormant pathogen. *PloS One* 4, e6077. doi: 10.1371/journal.pone.0006077

de Carvalho, L. P. S., Fischer, S. M., Marrero, J., Nathan, C., Ehrt, S., and Rhee, K. Y. (2010). Metabolomics of mycobacterium tuberculosis reveals compartmentalized co-catabolism of carbon substrates. *Chem. Biol.* 17, 1122–1131. doi: 10.1016/j.chembiol.2010.08.009

Del Portillo, P., García-Morales, L., Menéndez, M. C., Anzola, J. M., Rodríguez, J. G., Helguera-Repetto, A. C., et al. (2019). Hypoxia is not a main stress when mycobacterium tuberculosis is in a dormancy-like long-chain fatty acid environment. *Front. Cell. Infect. Microbiol.* 8. doi: 10.3389/fcimb.2018.00449

de Martino, M., Lodi, L., Galli, L., and Chiappini, E. (2019). Immune response to mycobacterium tuberculosis: A narrative review. *Front. Pediatr.* 7. doi: 10.3389/fped.2019.00350

Dhar, N., and McKinney, J. D. (2007). Microbial phenotypic heterogeneity and antibiotic tolerance. *Curr. Opin. Microbiol.* 10, 30–38. doi: 10.1016/j.mib.2006.12.007

Driver, E. R., Ryan, G. J., Hoff, D. R., Irwin, S. M., Basaraba, R. J., Kramnik, I., et al. (2012). Evaluation of a mouse model of necrotic granuloma formation using C3HeB/FeJ mice for testing of drugs against mycobacterium tuberculosis. antimicrob. *Agents Chemother.* 56, 3181–3195. doi: 10.1128/AAC.00217-12

Dubé, J.-Y., Fava, V. M., Schurr, E., and Behr, M. A. (2021). Underwhelming or misunderstood? genetic variability of pattern recognition receptors in immune responses and resistance to mycobacterium tuberculosis. *Front. Immunol.* 12. doi: 10.3389/fimmu.2021.714808

Du, P., Sohaskey, C. D., and Shi, L. (2016). Transcriptional and physiological changes during mycobacterium tuberculosis reactivation from non-replicating persistence. *Front. Microbiol.* 7. doi: 10.3389/fmicb.2016.01346

Dutta, N. K., Klinkenberg, L. G., Vazquez, M.-J., Segura-Carro, D., Colmenarejo, G., Ramon, F., et al. (2019). Inhibiting the stringent response blocks mycobacterium tuberculosis entry into quiescence and reduces persistence. *Sci. Adv.* 5, eaav2104. doi: 10.1126/sciadv.aav2104

Ehrt, S., and Schnappinger, D. (2009). Mycobacterial survival strategies in the phagosome: Defense against host stresses. *Cell. Microbiol.* 11, 1170–1178. doi: 10.1111/j.1462-5822.2009.01335.x

Ehrt, S., Schnappinger, D., Bekiranov, S., Drenkow, J., Shi, S., Gingeras, T. R., et al. (2001). Reprogramming of the macrophage transcriptome in response to interferon-γ and mycobacterium tuberculosis. J. *Exp. Med.* 194, 1123–1140. doi: 10.1084/jem.194.8.1123

Eisenreich, W., Heesemann, J., Rudel, T., and Goebel, W. (2013). Metabolic host responses to infection by intracellular bacterial pathogens. *Front. Cell. Infect. Microbiol.* 3. doi: 10.3389/fcimb.2013.00024

Elliott, S. R., White, D. W., and Tischler, A. D. (2019). Mycobacterium tuberculosis requires regulation of ESX-5 secretion for virulence in Irgm1-deficient mice. *Infect. Immun.* 87, e00660–18. doi: 10.1128/IAI.00660-18

Eoh, H., and Rhee, K. Y. (2013). Multifunctional essentiality of succinate metabolism in adaptation to hypoxia in mycobacterium tuberculosis. *Proc. Natl. Acad. Sci.* 110, 6554–6559. doi: 10.1073/pnas.1219375110

Feng, L., Chen, S., and Hu, Y. (2018). PhoPR positively regulates whiB3 expression in response to low pH in pathogenic mycobacteria. *J. Bacteriol.* 200, e00766–17. doi: 10.1128/JB.00766-17

Flynn, J. L., and Chan, J. (2001). Immunology of tuberculosis. *Annu. Rev. Immunol.* 19, 93–129. doi: 10.1146/annurev.immunol.19.1.93

Ford, C. B., Lin, P. L., Chase, M., Shah, R. R., Iartchouk, O., Galagan, J., et al. (2011). Use of whole genome sequencing to estimate the mutation rate of mycobacterium tuberculosis during latent infection. *Nat. Genet.* 43, 482–486. doi: 10.1038/ng.811

Fratti, R. A., Chua, J., Vergne, I., and Deretic, V. (2003). Mycobacterium tuberculosis glycosylated phosphatidylinositol causes phagosome maturation arrest. *Proc. Natl. Acad. Sci.* 100, 5437–5442. doi: 10.1073/pnas.0737613100

Gao, L.-Y., Laval, F., Lawson, E. H., Groger, R. K., Woodruff, A., Morisaki, J. H., et al. (2003). Requirement for kasB in mycobacterium mycolic acid biosynthesis, cell wall impermeability and intracellular survival: implications for therapy. *Mol. Microbiol.* 49, 1547–1563. doi: 10.1046/j.1365-2958.2003.03667.x

Garton, N. J., Waddell, S. J., Sherratt, A. L., Lee, S.-M., Smith, R. J., Senner, C., et al. (2008). Cytological and transcript analyses reveal fat and lazy persister-like bacilli in tuberculous sputum. *PloS Med.* 5, e75. doi: 10.1371/journal.pmed.0050075

Geisel, R. E., Sakamoto, K., Russell, D. G., and Rhoades, E. R. (2005). In vivo activity of released cell wall lipids of mycobacterium bovis bacillus calmette-guérin is due principally to trehalose mycolates. *J. Immunol.* 174, 5007–5015. doi: 10.4049/jimmunol.174.8.5007

Gopinath, K., Venclovas, Č., Ioerger, T. R., Sacchettini, J. C., McKinney, J. D., Mizrahi, V., et al. (2013). A vitamin B12 transporter in mycobacterium tuberculosis. *Open Biol.* 3, 120175. doi: 10.1098/rsob.120175

Gouzy, A., Larrouy-Maumus, G., Bottai, D., Levillain, F., Dumas, A., Wallach, J. B., et al. (2014). Mycobacterium tuberculosis exploits asparagine to assimilate nitrogen and resist acid stress during infection. *PloS Pathog.* 10, e1003928. doi: 10.1371/journal.ppat.1003928

Gregg, R. W., Maiello, P., Borish, H. J., Coleman, M. T., Reed, D. S., White, A. G., et al. (2018). Spatial and temporal evolution of lung granulomas in a cynomolgus macaque model of mycobacterium tuberculosis infection. *Radiol. Infect. Dis.* 5, 110–117. doi: 10.1016/j.jrid.2018.08.001

Guerrini, V., Prideaux, B., Blanc, L., Bruiners, N., Arrigucci, R., Singh, S., et al. (2018). Storage lipid studies in tuberculosis reveal that foam cell biogenesis is disease-specific. *PloS Pathog.* 14, e1007223. doi: 10.1371/journal.ppat.1007223

Hampshire, T., Soneji, S., Bacon, J., James, B. W., Hinds, J., Laing, K., et al. (2004). Stationary phase gene expression of mycobacterium tuberculosis following a progressive nutrient depletion: a model for persistent organisms? *Tuberc. Edinb. Scotl.* 84, 228–238. doi: 10.1016/j.tube.2003.12.010

Hasenoehrl, E. J., Sajorda, D. R., Berney-Meyer, L., Johnson, S., Tufariello, J. M., Fuhrer, T., et al. (2019). Derailing the aspartate pathway of mycobacterium tuberculosis to eradicate persistent infection. *Nat. Commun.* 10, 1–12. doi: 10.1038/s41467-019-12224-3

Hayashi, J. M., Richardson, K., Melzer, E. S., Sandler, S. J., Aldridge, B. B., Siegrist, M. S., et al. (2018). Stress-induced reorganization of the mycobacterial membrane domain. *mBio* 9, e01823–17. doi: 10.1128/mBio.01823-17

Hoff, D. R., Ryan, G. J., Driver, E. R., Ssemakulu, C. C., De Groote, M. A., Basaraba, R. J., et al. (2011). Location of intra- and extracellular m. tuberculosis populations in lungs of mice and guinea pigs during disease progression and after drug treatment. *PloS One* 6, e17550. doi: 10.1371/journal.pone.0017550

Hondalus, M. K., Bardarov, S., Russell, R., Chan, J., Jacobs, W. R., and Bloom, B. R. (2000). Attenuation of and protection induced by a leucine auxotroph of mycobacterium tuberculosis. infect. *Immun.* 68, 2888–2898. doi: 10.1128/iai.68.5.2888-2898.2000

Hood, M. I., and Skaar, E. P. (2012). Nutritional immunity: Transition metals at the pathogen-host interface. *Nat. Rev. Microbiol.* 10, 525–537. doi: 10.1038/nrmicro2836

Howe, M. D., Kordus, S. L., Cole, M. S., Bauman, A. A., Aldrich, C. C., Baughn, A. D., et al. (2018). Methionine antagonizes para-aminosalicylic acid activity via affecting folate precursor biosynthesis in mycobacterium tuberculosis. front. *Cell. Infect. Microbiol.* 8, 399. doi: 10.3389/fcimb.2018.00399

Huang, L., Nazarova, E. V., and Russell, D. G. (2019). Mycobacterium tuberculosis: Bacterial fitness within the host macrophage. *Microbiol. Spectr.* 7. doi: 10.1128/microbiolspec.BAI-0001-2019

Huang, L., Nazarova, E. V., Tan, S., Liu, Y., and Russell, D. G. (2018). Growth of mycobacterium tuberculosis in vivo segregates with host macrophage metabolism and ontogeny. *J. Exp. Med.* 215, 1135–1152. doi: 10.1084/jem.20172020

Ignatov, D. V., Salina, E. G., Fursov, M. V., Skvortsov, T. A., Azhikina, T. L., and Kaprelyants, A. S. (2015). Dormant non-culturable mycobacterium tuberculosis retains stable low-abundant mRNA. *BMC Genomics* 16, 954. doi: 10.1186/s12864-015-2197-6

Irwin, S. M., Driver, E., Lyon, E., Schrupp, C., Ryan, G., Gonzalez-Juarrero, M., et al. (2015). Presence of multiple lesion types with vastly different microenvironments in C3HeB/FeJ mice following aerosol infection with mycobacterium tuberculosis. dis. *Model. Mech.* 8, 591–602. doi: 10.1242/dmm.019570

Irwin, S. M., Prideaux, B., Lyon, E. R., Zimmerman, M. D., Brooks, E. J., Schrupp, C. A., et al. (2016). Bedaquiline and pyrazinamide treatment responses are affected by pulmonary lesion heterogeneity in mycobacterium tuberculosis infected C3HeB/FeJ mice. *ACS Infect. Dis.* 2, 251–267. doi: 10.1021/acsinfecdis.5b00127

Islam, M. S., Richards, J. P., and Ojha, A. K. (2012). Targeting drug tolerance in mycobacteria: a perspective from mycobacterial biofilms. *Expert Rev. Anti Infect. Ther.* 10, 1055–1066. doi: 10.1586/eri.12.88

Jain, P., Weinrick, B. C., Kalivoda, E. J., Yang, H., Munsamy, V., Vilcheze, C., et al. (2016). Dual-reporter mycobacteriophages (Φ2DRMs) reveal preexisting mycobacterium tuberculosis persistent cells in human sputum. *mBio* 7, e01023-16. doi: 10.1128/mBio.01023-16

Jamaati, H., Mortaz, E., Pajouhi, Z., Folkerts, G., Movassaghi, M., Moloudizargari, M., et al. (2017). Nitric oxide in the pathogenesis and treatment of tuberculosis. *Front. Microbiol.* 8. doi: 10.3389/fmicb.2017.02008

Jamwal, S. V., Mehrotra, P., Singh, A., Siddiqui, Z., Basu, A., and Rao, K. V. S. (2016). Mycobacterial escape from macrophage phagosomes to the cytoplasm represents an alternate adaptation mechanism. *Sci. Rep.* 6, 23089. doi: 10.1038/srep23089

Johnson, B. K., Colvin, C. J., Needle, D. B., Mba Medie, F., Champion, P. A. D., and Abramovitch, R. B. (2015). The carbonic anhydrase inhibitor ethoxzolamide inhibits the mycobacterium tuberculosis PhoPR regulon and esx-1 secretion and attenuates virulence. *Antimicrob. Agents Chemother.* 59, 4436–4445. doi: 10.1128/AAC.00719-15

Kang, P. B., Azad, A. K., Torrelles, J. B., Kaufman, T. M., Beharka, A., Tibesar, E., et al. (2005). The human macrophage mannose receptor directs mycobacterium tuberculosis lipoarabinomannan-mediated phagosome biogenesis. *J. Exp. Med.* 202, 987–999. doi: 10.1084/jem.20051239

Kaplan, G., Post, F. A., Moreira, A. L., Wainwright, H., Kreiswirth, B. N., Tanverdi, M., et al. (2003). Mycobacterium tuberculosis growth at the cavity surface: a microenvironment with failed immunity. *Infect. Immun.* 71, 7099–7108. doi: 10.1128/IAI.71.12.7099-7108.2003

Kehl-Fie, T. E., and Skaar, E. P. (2010). Nutritional immunity beyond iron: a role for manganese and zinc. *Curr. Opin. Chem. Biol.* 14, 218–224. doi: 10.1016/j.cbpa.2009.11.008

Kim, M.-J., Wainwright, H. C., Locketz, M., Bekker, L.-G., Walther, G. B., Dittrich, C., et al. (2010). Caseation of human tuberculosis granulomas correlates with elevated host lipid metabolism. *EMBO Mol. Med.* 2, 258–274. doi: 10.1002/emmm.201000079

Klinkenberg, L. G., Lee, J.-H., Bishai, W. R., and Karakousis, P. C. (2010). The stringent response is required for full virulence of mycobacterium tuberculosis in guinea pigs. *J. Infect. Dis.* 202, 1397–1404. doi: 10.1086/656524

Knight, M., Braverman, J., Asfaha, K., Gronert, K., and Stanley, S. (2018). Lipid droplet formation in mycobacterium tuberculosis infected macrophages requires IFN-γ/HIF-1α signaling and supports host defense. *PloS Pathog.* 14, e1006874. doi: 10.1371/journal.ppat.1006874

Kumar, A., Farhana, A., Guidry, L., Saini, V., Hondalus, M., and Steyn, A. J. C. (2011). Redox homeostasis in mycobacteria: the key to tuberculosis control? *Expert Rev. Mol. Med.* 13, e39. doi: 10.1017/S1462399411002079

Kumar, R., Singh, P., Kolloli, A., Shi, L., Bushkin, Y., Tyagi, S., et al (2019). Immunometabolism of phagocytes during *Mycobacterium tuberculosis* infection. *Front. Mol. Biosci.* 6, 105. doi: 10.3389/fmolb.2019.00105

Kurthkoti, K., Amin, H., Marakalala, M. J., Ghanny, S., Subbian, S., Sakatos, A., et al. (2017). The capacity of mycobacterium tuberculosis to survive iron starvation might enable it to persist in iron-deprived microenvironments of human granulomas. *mBio* 8, e01092-17. doi: 10.1128/mBio.01092-17

Kyei, G. B., Vergne, I., Chua, J., Roberts, E., Harris, J., Junutula, J. R., et al. (2006). Rab14 is critical for maintenance of mycobacterium tuberculosis phagosome maturation arrest. *EMBO J.* 25, 5250–5259. doi: 10.1038/sj.emboj.7601407

Lenaerts, A. J., Hoff, D., Aly, S., Ehlers, S., Andries, K., Cantarero, L., et al. (2007). Location of persisting mycobacteria in a Guinea pig model of tuberculosis revealed by r207910. *Antimicrob. Agents Chemother.* 51, 3338–3345. doi: 10.1128/AAC.00276-07

Lerner, T. R., Queval, C. J., Lai, R. P., Russell, M. R. G., Fearns, A., Greenwood, D. J., et al. (2020). Mycobacterium tuberculosis cords within lymphatic endothelial cells to evade host immunity. *JCI Insight* 5, 136937. doi: 10.1172/jci.insight.136937

Levitte, S., Adams, K. N., Berg, R. D., Cosma, C. L., Urdahl, K. B., and Ramakrishnan, L. (2016). Mycobacterial acid tolerance enables phagolysosomal survival and establishment of tuberculous infection in vivo. *Cell Host Microbe* 20, 250–258. doi: 10.1016/j.chom.2016.07.007

Lin, P. L., Coleman, T., Carney, J. P. J., Lopresti, B. J., Tomko, J., Fillmore, D., et al. (2013). Radiologic responses in cynomolgus macaques for assessing tuberculosis chemotherapy regimens. *Antimicrob. Agents Chemother.* 57, 4237–4244. doi: 10.1128/AAC.00277-13

Lin, P. L., Ford, C. B., Coleman, M. T., Myers, A. J., Gawande, R., Ioerger, T., et al. (2014). Sterilization of granulomas is common in both active and latent tuberculosis despite extensive within-host variability in bacterial killing. *Nat. Med.* 20, 75–79. doi: 10.1038/nm.3412

Lin, P. L., Pawar, S., Myers, A., Pegu, A., Fuhrman, C., Reinhart, T. A., et al. (2006). Early events in mycobacterium tuberculosis infection in cynomolgus macaques. *Infect. Immun.* 74, 3790–3803. doi: 10.1128/IAI.00064-06

Liu, C. H., Liu, H., and Ge, B. (2017). Innate immunity in tuberculosis: host defense vs pathogen evasion. *Cell. Mol. Immunol.* 14, 963–975. doi: 10.1038/cmi.2017.88

Liu, Y., Tan, S., Huang, L., Abramovitch, R. B., Rohde, K. H., Zimmerman, M. D., et al. (2016). Immune activation of the host cell induces drug tolerance in mycobacterium tuberculosis both in vitro and in vivo. J. *Exp. Med.* 213, 809–825. doi: 10.1084/jem.20151248

Liu, D., Zhang, J., Pan, Z., Mai, J., Mei, H., Dai, Y., et al. (2020). Over-expression of Tgs1 in mycobacterium marinum enhances virulence in adult zebrafish. *Int. J. Med. Microbiol.* 310, 151378. doi: 10.1016/j.ijmm.2019.151378

Lofthouse, E. K., Wheeler, P. R., Beste, D. J. V., Khatri, B. L., Wu, H., Mendum, T. A., et al. (2013). Systems-based approaches to probing metabolic variation

within the mycobacterium tuberculosis complex. *PloS One* 8, e75913. doi: 10.1371/journal.pone.0075913

Luthuli, B. B., Purdy, G. E., and Balagaddé, F. K. (2015). Confinement-induced drug-tolerance in mycobacteria mediated by an efflux mechanism. *PloS One* 10, e0136231. doi: 10.1371/journal.pone.0136231

Lyu, L.-D., Tang, B.-K., Fan, X.-Y., Ma, H., and Zhao, G.-P. (2013). Mycobacterial MazG safeguards genetic stability via housecleaning of 5-OH-dCTP. *PloS Pathog.* 9, e1003814. doi: 10.1371/journal.ppat.1003814

MacGilvary, N. J., Kevorkian, Y. L., and Tan, S. (2019). Potassium response and homeostasis in mycobacterium tuberculosis modulates environmental adaptation and is important for host colonization. *PloS Pathog.* 15, e1007591. doi: 10.1371/journal.ppat.1007591

MacMicking, J. D. (2014). Cell-autonomous effector mechanisms against mycobacterium tuberculosis. *Cold Spring Harb. Perspect. Med.* 4, a018507. doi: 10.1101/cshperspect.a018507

Malherbe, S. T., Shenai, S., Ronacher, K., Loxton, A. G., Dolganov, G., Kriel, M., et al. (2016). Persisting positron emission tomography lesion activity and mycobacterium tuberculosis mRNA after tuberculosis cure. *Nat. Med.* 22, 1094–1100. doi: 10.1038/nm.4177

Malik, Z. A., Denning, G. M., and Kusner, D. J. (2000). Inhibition of Ca2+ signaling by mycobacterium tuberculosisIs associated with reduced phagosome–lysosome fusion and increased survival within human macrophages. *J. Exp. Med.* 191, 287–302. doi: 10.1084/jem.191.2.287

Manina, G., Dhar, N., and McKinney, J. D. (2015). Stress and host immunity amplify mycobacterium tuberculosis phenotypic heterogeneity and induce nongrowing metabolically active forms. *Cell Host Microbe* 17, 32–46. doi: 10.1016/j.chom.2014.11.016

Marakalala, M. J., and Ndlovu, H. (2017). Signaling c-type lectin receptors in antimycobacterial immunity. *PloS Pathog.* 13, e1006333. doi: 10.1371/journal.ppat.1006333

Marino, S., Cilfone, N. A., Mattila, J. T., Linderman, J. J., Flynn, J. L., and Kirschner, D. E. (2015). Macrophage polarization drives granuloma outcome during mycobacterium tuberculosis infection. *Infect. Immun.* 83, 324–338. doi: 10.1128/IAI.02494-14

Martin, C. J., Cadena, A. M., Leung, V. W., Lin, P. L., Maiello, P., Hicks, N., et al. (2017). Digitally barcoding mycobacterium tuberculosis reveals in vivo infection dynamics in the macaque model of tuberculosis. *mBio* 8, e00312–17. doi: 10.1128/mBio.00312-17

Mascolo, L., and Bald, D. (2019). Cytochrome bd in mycobacterium tuberculosis: A respiratory chain protein involved in the defense against antibacterials. *Prog. Biophys. Mol. Biol* 152, 55–63. doi: 10.1016/j.pbiomolbio.2019.11.002

Mattila, J. T., Ojo, O. O., Kepka-Lenhart, D., Marino, S., Kim, J. H., Eum, S. Y., et al. (2013). Microenvironments in tuberculous granulomas are delineated by distinct populations of macrophage subsets and expression of nitric oxide synthase and arginase isoforms. *J. Immunol.* 191, 773–784. doi: 10.4049/jimmunol.1300113

Maurya, R. K., Bharti, S., and Krishnan, M. Y. (2018). Triacylglycerols: Fuelling the hibernating mycobacterium tuberculosis. front. *Cell. Infect. Microbiol.* 8. doi: 10.3389/fcimb.2018.00450

McMahon, M. D., Rush, J. S., and Thomas, M. G. (2012). Analyses of MbtB, MbtE, and MbtF suggest revisions to the mycobactin biosynthesis pathway in mycobacterium tuberculosis. J. *Bacteriol.* 194, 2809–2818. doi: 10.1128/JB.00088-12

Mehta, M., Rajmani, R. S., and Singh, A. (2016). Mycobacterium tuberculosis WhiB3 responds to vacuolar pH-induced changes in mycothiol redox potential to modulate phagosomal maturation and virulence. *J. Biol. Chem.* 291, 2888–2903. doi: 10.1074/jbc.M115.684597

Mehta, M., and Singh, A. (2019). Mycobacterium tuberculosis WhiB3 maintains redox homeostasis and survival in response to reactive oxygen and nitrogen species. *Free Radic. Biol. Med.* 131, 50–58. doi: 10.1016/j.freeradbiomed.2018.11.032

Mezouar, S., Diarra, I., Roudier, J., Desnues, B., and Mege, J.-L. (2019). Tumor necrosis factor-alpha antagonist interferes with the formation of granulomatous multinucleated giant cells: New insights into mycobacterium tuberculosis infection. *Front. Immunol.* 10, 1947. doi: 10.3389/fimmu.2019.01947

Minato, Y., Thiede, J. M., Kordus, S. L., McKlveen, E. J., Turman, B. J., and Baughn, A. D. (2015). Mycobacterium tuberculosis folate metabolism and the mechanistic basis for para-aminosalicylic acid susceptibility and resistance. *Antimicrob. Agents Chemother.* 59, 5097–5106. doi: 10.1128/AAC.00647-15

Mishra, R., Kohli, S., Malhotra, N., Bandyopadhyay, P., Mehta, M., Munshi, M., et al. (2019). Targeting redox heterogeneity to counteract drug tolerance in replicating mycobacterium tuberculosis. *Sci. Transl. Med.* 11, eaaw6635. doi: 10.1126/scitranslmed.aaw6635

Moldoveanu, A. L., Rycroft, J. A., and Helaine, S. (2021). Impact of bacterial persisters on their host. *Curr. Opin. Microbiol.* 59, 65–71. doi: 10.1016/j.mib.2020.07.006

Mouton, J. M., Helaine, S., Holden, D. W., and Sampson, S. L. (2016). Elucidating population-wide mycobacterial replication dynamics at the single-cell level. *Microbiol. Read. Engl* 162, 966–78. doi: 10.1099/mic.0.000288

Nair, R. R., Sharan, D., and Ajitkumar, P. (2019). A minor subpopulation of mycobacteria inherently produces high levels of reactive oxygen species that generate antibiotic resisters at high frequency from itself and enhance resister generation from its major kin subpopulation. *Front. Microbiol* 10, 1842. doi: 10.3389/fmicb.2019.01842

Namugenyi, S. B., Aagesen, A. M., Elliott, S. R., and Tischler, A. D. (2017). Mycobacterium tuberculosis PhoY proteins promote persister formation by mediating Pst/SenX3-RegX3 phosphate sensing. *mBio* 8, e00494-17. doi: 10.1128/mBio.00494-17

Nixon, M. R., Saionz, K. W., Koo, M.-S., Szymonifka, M. J., Jung, H., Roberts, J. P., et al. (2014). Folate pathway disruption leads to critical disruption of methionine derivatives in mycobacterium tuberculosis. chem. *Biol.* 21, 819–830. doi: 10.1016/j.chembiol.2014.04.009

Noy, T., Vergnolle, O., Hartman, T. E., Rhee, K. Y., Jacobs, W. R., Berney, M., et al. (2016). Central role of pyruvate kinase in carbon Co-catabolism of mycobacterium tuberculosis. *J. Biol. Chem.* 291, 7060–7069. doi: 10.1074/jbc.M115.707430

Ojha, A. K., Baughn, A. D., Sambandan, D., Hsu, T., Trivelli, X., Guerardel, Y., et al. (2008). Growth of mycobacterium tuberculosis biofilms containing free mycolic acids and harbouring drug-tolerant bacteria. *Mol. Microbiol.* 69, 164–174. doi: 10.1111/j.1365-2958.2008.06274.x

Pandey, R., and Rodriguez, G. M. (2014). IdeR is required for iron homeostasis and virulence in mycobacterium tuberculosis. *Mol. Microbiol.* 91, 98–109. doi: 10.1111/mmi.12441

Pandey, A. K., and Sassetti, C. M. (2008). Mycobacterial persistence requires the utilization of host cholesterol. *Proc. Natl. Acad. Sci.* 105, 4376–4380. doi: 10.1073/pnas.0711159105

Pandey, M., Talwar, S., Bose, S., and Pandey, A. K. (2018). Iron homeostasis in mycobacterium tuberculosis is essential for persistence. *Sci. Rep.* 8, 17359. doi: 10.1038/s41598-018-35012-3

Parbhoo, T., Sampson, S. L., and Mouton, J. M. (2020). Recent developments in the application of flow cytometry to advance our understanding of mycobacterium tuberculosis physiology and pathogenesis. *Cytometry A* 97, 683–693. doi: 10.1002/cyto.a.24030

Passemar, C., Arbués, A., Malaga, W., Mercier, I., Moreau, F., Lepourry, L., et al. (2014). Multiple deletions in the polyketide synthase gene repertoire of mycobacterium tuberculosis reveal functional overlap of cell envelope lipids in host–pathogen interactions. *Cell. Microbiol.* 16, 195–213. doi: 10.1111/cmi.12214

Patin, E. C., Geffken, A. C., Willcocks, S., Leschczyk, C., Haas, A., Nimmerjahn, F., et al. (2017). Trehalose dimycolate interferes with FcγR-mediated phagosome maturation through mincle, SHP-1 and FcγRIIB signalling. *PLo One* 12, e0174973. doi: 10.1371/journal.pone.0174973

Pauwels, A.-M., Trost, M., Beyaert, R., and Hoffmann, E. (2017). Patterns, receptors, and signals: Regulation of phagosome maturation. *Trends Immunol.* 38, 407–422. doi: 10.1016/j.it.2017.03.006

Pavelka, M. S., Chen, B., Kelley, C. L., Collins, F. M., and Jacobs, W. R. (2003). Vaccine efficacy of a lysine auxotroph of mycobacterium tuberculosis. infect. *Immun.* 71, 4190–4192. doi: 10.1128/IAI.71.7.4190-4192.2003

Peterson, E. J. R., Ma, S., Sherman, D. R., and Baliga, N. S. (2016). Network analysis identifies Rv0324 and Rv0880 as regulators of bedaquiline tolerance in mycobacterium tuberculosis. nat. *Microbiol.* 1, 16078. doi: 10.1038/nmicrobiol.2016.78

Peyron, P., Vaubourgeix, J., Poquet, Y., Levillain, F., Botanch, C., Bardou, F., et al. (2008). Foamy macrophages from tuberculous patients' granulomas constitute a nutrient-rich reservoir for m. tuberculosis persistence. *PloS Pathog.* 4, e1000204. doi: 10.1371/journal.ppat.1000204

Pinto, R., Tang, Q. X., Britton, W. J., Leyh, T. S., and Triccas, J. A. (2004). The mycobacterium tuberculosis cysD and cysNC genes form a stress-induced operon that encodes a tri-functional sulfate-activating complex. *Microbiol. Read. Engl.* 150, 1681–1686. doi: 10.1099/mic.0.26894-0

Pisu, D., Huang, L., Grenier, J. K., and Russell, D. G. (2020). Dual RNA-seq of mtb-infected macrophages in vivo reveals ontologically distinct host-pathogen interactions. *Cell Rep.* 30, 335–350.e4. doi: 10.1016/j.celrep.2019.12.033

Priestman, M., Thomas, P., Robertson, B. D., and Shahrezaei, V. (2017). Mycobacteria modify their cell size control under Sub-optimal carbon sources. *Front. Cell Dev. Biol.* 5. doi: 10.3389/fcell.2017.00064

Prosser, G., Brandenburg, J., Reiling, N., Barry, C. E., Wilkinson, R. J., and Wilkinson, K. A. (2017). The bacillary and macrophage response to hypoxia in tuberculosis and the consequences for T cell antigen recognition. *Microbes Infect.* 19, 177–192. doi: 10.1016/j.micinf.2016.10.001

Qualls, J. E., and Murray, P. J. (2016). Immunometabolism within the tuberculosis granuloma: amino acids, hypoxia, and cellular respiration. *Semin. Immunopathol.* 38, 139–152. doi: 10.1007/s00281-015-0534-0

Queval, C. J., Brosch, R., and Simeone, R. (2017a). The macrophage: A disputed fortress in the battle against mycobacterium tuberculosis. *Front. Microbiol.* 8. doi: 10.3389/fmicb.2017.02284

Queval, C. J., Song, O.-R., Carralot, J.-P., Saliou, J.-M., Bongiovanni, A., Deloison, G., et al. (2017b). Mycobacterium tuberculosis controls phagosomal acidification by targeting CISH-mediated signaling. *Cell Rep.* 20, 3188–3198. doi: 10.1016/j.celrep.2017.08.101

Quigley, J., Hughitt, V. K., Velikovsky, C. A., Mariuzza, R. A., El-Sayed, N. M., and Briken, V. (2017). The cell wall lipid PDIM contributes to phagosomal escape and host cell exit of mycobacterium tuberculosis. *mBio* 8, e00148-17. doi: 10.1128/mBio.00148-17

Rao, S. P. S., Alonso, S., Rand, L., Dick, T., and Pethe, K. (2008). The protonmotive force is required for maintaining ATP homeostasis and viability of hypoxic, nonreplicating mycobacterium tuberculosis. *Proc. Natl. Acad. Sci. U. S. A.* 105, 11945–11950. doi: 10.1073/pnas.0711697105

Refai, A., Gritli, S., Barbouche, M.-R., and Essafi, M. (2018). Mycobacterium tuberculosis virulent factor ESAT-6 drives macrophage differentiation toward the pro-inflammatory M1 phenotype and subsequently switches it to the anti-inflammatory M2 phenotype. *Front. Cell. Infect. Microbiol* 8, 327. doi: 10.3389/fcimb.2018.00327

Rego, E. H., Audette, R. E., and Rubin, E. J. (2017). Deletion of a mycobacterial divisome factor collapses single-cell phenotypic heterogeneity. *Nature* 546, 153–157. doi: 10.1038/nature22361

Reichlen, M. J., Leistikow, R. L., Scobey, M. S., Born, S. E. M., and Voskuil, M. I. (2017). Anaerobic mycobacterium tuberculosis cell death stems from intracellular acidification mitigated by the DosR regulon. *J. Bacteriol.* 199, e00320-17. doi: 10.1128/JB.00320-17

Rhee, K. Y., Erdjument-Bromage, H., Tempst, P., and Nathan, C. F. (2005). S-nitroso proteome of mycobacterium tuberculosis: Enzymes of intermediary metabolism and antioxidant defense. *Proc. Natl. Acad. Sci. U. S. A.* 102, 467–472. doi: 10.1073/pnas.0406133102

Richard-Greenblatt, M., Bach, H., Adamson, J., Peña-Diaz, S., Li, W., Steyn, A. J. C., et al. (2015). Regulation of ergothioneine biosynthesis and its effect on mycobacterium tuberculosis growth and infectivity. *J. Biol. Chem.* 290, 23064–23076. doi: 10.1074/jbc.M115.648642

Richardson, K., Bennion, O. T., Tan, S., Hoang, A. N., Cokol, M., and Aldridge, B. B. (2016). Temporal and intrinsic factors of rifampicin tolerance in mycobacteria. *Proc. Natl. Acad. Sci. U. S. A.* 113, 8302–8307. doi: 10.1073/pnas.1600372113

Rifat, D., Belchis, D. A., and Karakousis, P. C. (2014). senX3-independent contribution of regX3 to mycobacterium tuberculosis virulence. *BMC Microbiol.* 14, 265. doi: 10.1186/s12866-014-0265-8

Rifat, D., Bishai, W. R., and Karakousis, P. C. (2009). Phosphate depletion: A novel trigger for mycobacterium tuberculosis persistence. *J. Infect. Dis.* 200, 1126–1135. doi: 10.1086/605700

Rodriguez, G. M., and Smith, I. (2003). Mechanisms of iron regulation in mycobacteria: role in physiology and virulence. *Mol. Microbiol.* 47, 1485–1494. doi: 10.1046/j.1365-2958.2003.03384.x

Rodriguez, G. M., Voskuil, M. I., Gold, B., Schoolnik, G. K., and Smith, I. (2002). ideR, an essential gene in mycobacterium tuberculosis: Role of IdeR in iron-dependent gene expression, iron metabolism, and oxidative stress response. *Infect. Immun.* 70, 3371–3381. doi: 10.1128/IAI.70.7.3371-3381.2002

Rohde, K. H., Veiga, D. F. T., Caldwell, S., Balázsi, G., and Russell, D. G. (2012). Linking the transcriptional profiles and the physiological states of mycobacterium tuberculosis during an extended intracellular infection. *PloS Pathog.* 8, e1002769. doi: 10.1371/journal.ppat.1002769

Russell, D. G., Cardona, P.-J., Kim, M.-J., Allain, S., and Altare, F. (2009). Foamy macrophages and the progression of the human TB granuloma. *Nat. Immunol.* 10, 943–948. doi: 10.1038/ni.1781

Russell, D. G., Huang, L., and VanderVen, B. C. (2019). Immunometabolism at the interface between macrophages and pathogens. *Nat. Rev. Immunol.* 19, 291–304. doi: 10.1038/s41577-019-0124-9

Ryan, G. J., Hoff, D.R., Driver, E.R., Voskuil, M.I., Gonzalez-Juarrero, M., Basaraba, R.J., et al (2010). Multiple *M. tuberculosis* Phenotypes in mouse and guinea pig lung tissue revealed by a dual-staining approach. *PLOS ONE* 5, e11108. doi: 10.1371/journal.pone.0011108

Saini, V., Cumming, B. M., Guidry, L., Lamprecht, D. A., Adamson, J. H., Reddy, V. P., et al. (2016). Ergothioneine maintains redox and bioenergetic homeostasis essential for drug susceptibility and virulence of mycobacterium tuberculosis. *Cell Rep.* 14, 572–585. doi: 10.1016/j.celrep.2015.12.056

Salina, E. G., Grigorov, A. S., Bychenko, O. S., Skvortsova, Y. V., Mamedov, I. Z., Azhikina, T. L., et al. (2019). Resuscitation of dormant "Non-culturable" mycobacterium tuberculosis is characterized by immediate transcriptional burst. *Front. Cell. Infect. Microbiol.* 9. doi: 10.3389/fcimb.2019.00272

Salina, E. G., Waddell, S. J., Hoffmann, N., Rosenkrands, I., Butcher, P. D., and Kaprelyants, A. S. (2014). Potassium availability triggers mycobacterium tuberculosis transition to, and resuscitation from, non-culturable (dormant) states. *Open Biol.* 4, 140106–140106. doi: 10.1098/rsob.140106

Sarathy, J. P., Via, L. E., Weiner, D., Blanc, L., Boshoff, H., Eugenin, E. A., et al. (2018). Extreme drug tolerance of mycobacterium tuberculosis in caseum. *Antimicrob. Agents Chemother.* 62, e02266–17. doi: 10.1128/AAC.02266-17

Sarathy, J. P., Zuccotto, F., Hsinpin, H., Sandberg, L., Via, L. E., Marriner, G. A., et al. (2016). Prediction of drug penetration in tuberculosis lesions. *ACS Infect. Dis.* 2, 552–563. doi: 10.1021/acsinfecdis.6b00051

Savvi, S., Warner, D. F., Kana, B. D., McKinney, J. D., Mizrahi, V., and Dawes, S. S. (2008). Functional characterization of a vitamin B12-dependent methylmalonyl pathway in mycobacterium tuberculosis: Implications for propionate metabolism during growth on fatty acids. *J. Bacteriol.* 190, 3886–3895. doi: 10.1128/JB.01767-07

Schnettger, L., Rodgers, A., Repnik, U., Lai, R. P., Pei, G., Verdoes, M., et al. (2017). A Rab20-dependent membrane trafficking pathway controls m. tuberculosis replication by regulating phagosome spaciousness and integrity. *Cell Host Microbe* 21, 619–628.e5. doi: 10.1016/j.chom.2017.04.004

Senaratne, R. H., Silva, A. D. D., Williams, S. J., Mougous, J. D., Reader, J. R., Zhang, T., et al. (2006). 5′-adenosinephosphosulphate reductase (CysH) protects mycobacterium tuberculosis against free radicals during chronic infection phase in mice. *Mol. Microbiol.* 59, 1744–1753. doi: 10.1111/j.1365-2958.2006.05075.x

Serafini, A., Pisu, D., Palù, G., Rodriguez, G. M., and Manganelli, R. (2013). The ESX-3 secretion system is necessary for iron and zinc homeostasis in mycobacterium tuberculosis. *PloS One* 8, e78351. doi: 10.1371/journal.pone.0078351

Sershen, C. L., Plimpton, S. J., and May, E. E. (2016). Oxygen modulates the effectiveness of granuloma mediated host response to mycobacterium tuberculosis: A multiscale computational biology approach. *Front. Cell. Infect. Microbiol.* 6. doi: 10.3389/fcimb.2016.00006

Sevalkar, R. R., Arora, D., Singh, P. R., Singh, R., Nandicoori, V. K., Karthikeyan, S., et al. (2019). Functioning of mycobacterial heat shock repressors requires the master virulence regulator PhoP. *J. Bacteriol.* 201, e00013–19. doi: 10.1128/JB.00013-19

Shi, K.-X., Wu, Y.-K., Tang, B.-K., Zhao, G.-P., and Lyu, L.-D. (2019). Housecleaning of pyrimidine nucleotide pool coordinates metabolic adaptation of nongrowing mycobacterium tuberculosis. emerg. *Microbes Infect.* 8, 40–44. doi: 10.1080/22221751.2018.1559706

Shui, W., Petzold, C. J., Redding, A., Liu, J., Pitcher, A., Sheu, L., et al. (2011). Organelle membrane proteomics reveals differential influence of mycobacterial lipoglycans on macrophage phagosome maturation and autophagosome accumulation. *J. Proteome Res.* 10, 339–348. doi: 10.1021/pr100688h

Sia, J. K., and Rengarajan, J. (2019). Immunology of mycobacterium tuberculosis infections. *Microbiol. Spectr.* 7. doi: 10.1128/microbiolspec.GPP3-0022-2018

Siegrist, M. S., Unnikrishnan, M., McConnell, M. J., Borowsky, M., Cheng, T.-Y., Siddiqi, N., et al. (2009). Mycobacterial esx-3 is required for mycobactin-mediated iron acquisition. *Proc. Natl. Acad. Sci. U. S. A.* 106, 18792–18797. doi: 10.1073/pnas.0900589106

Simeone, R., Sayes, F., Song, O., Gröschel, M. I., Brodin, P., Brosch, R., et al. (2015). Cytosolic access of mycobacterium tuberculosis: Critical impact of phagosomal acidification control and demonstration of occurrence in vivo. *PloS Pathog.* 11, e1004650. doi: 10.1371/journal.ppat.1004650

Singh, A., Crossman, D. K., Mai, D., Guidry, L., Voskuil, M. I., Renfrow, M. B., et al. (2009). *Mycobacterium tuberculosis* WhiB3 maintains redox homeostasis by regulating virulence lipid anabolism to modulate macrophage response. *PloS Pathog.* 5, e1000545. doi: 10.1371/journal.ppat.1000545

Singh, S., Goswami, N., Tyagi, A. K., and Khare, G. (2019). Unraveling the role of the transcriptional regulator VirS in low pH-induced responses of mycobacterium tuberculosis and identification of VirS inhibitors. *J. Biol. Chem.* 294, 10055–75. doi: 10.1074/jbc.RA118.005312

Singh, V., Jamwal, S., Jain, R., Verma, P., Gokhale, R., and Rao, K. V. S. (2012). Mycobacterium tuberculosis-driven targeted recalibration of macrophage lipid homeostasis promotes the foamy phenotype. *Cell Host Microbe* 12, 669–681. doi: 10.1016/j.chom.2012.09.012

Singh, R., Singh, M., Arora, G., Kumar, S., Tiwari, P., and Kidwai, S. (2013). Polyphosphate deficiency in mycobacterium tuberculosis is associated with enhanced drug susceptibility and impaired growth in Guinea pigs. *J. Bacteriol.* 195, 2839–2851. doi: 10.1128/JB.00038-13

Singh, P. R., Vijjamarri, A. K., and Sarkar, D. (2020). Metabolic switching of mycobacterium tuberculosis during hypoxia is controlled by the virulence regulator PhoP. *J. Bacteriol.* 202, e00705–19. doi: 10.1128/JB.00705-19

Sloan, D. J., Mwandumba, H. C., Garton, N. J., Khoo, S. H., Butterworth, A. E., Allain, T. J., et al (2015). Pharmacodynamic modeling of bacillary elimination rates and detection of bacterial lipid bodies in sputum to predict and understand

outcomes in treatment of pulmonary tuberculosis. *Clin. Infect. Dis. Off. Publ. Infect. Dis. Soc. Am.* 61, 1–8. doi: 10.1093/cid/civ195

Small, J. L., Park, S. W., Kana, B. D., Ioerger, T. R., Sacchettini, J. C., and Ehrt, S. (2013). Perturbation of cytochrome c maturation reveals adaptability of the respiratory chain in mycobacterium tuberculosis. *mBio* 4, e00475–00413. doi: 10.1128/mBio.00475-13

Smith, T. C., Pullen, K. M., Olson, M. C., McNellis, M. E., Richardson, I., Hu, S., et al. (2020). Morphological profiling of tubercle bacilli identifies drug pathways of action. *Proc. Natl. Acad. Sci.* 117, 18744–18753. doi: 10.1073/pnas.2002738117

Sohaskey, C. D. (2008). Nitrate enhances the survival of mycobacterium tuberculosis during inhibition of respiration. *J. Bacteriol.* 190, 2981–2986. doi: 10.1128/JB.01857-07

Song, H., Huff, J., Janik, K. E., Walter, K., Keller, C. E. M., Ehlers, S., et al. (2011). Expression of the ompATb operon accelerates ammonia secretion and adaptation of mycobacterium tuberculosis to acidic environments. *Mol. Microbiol.* 80, 900–918. doi: 10.1111/j.1365-2958.2011.07619.x

Song, H., and Niederweis, M. (2012). Uptake of sulfate but not phosphate by mycobacterium tuberculosis is slower than that for mycobacterium smegmatis. *J. Bacteriol.* 194, 956–964. doi: 10.1128/JB.06132-11

Tan, S., and Russell, D. G. (2015). Trans-species communication in the mycobacterium tuberculosis-infected macrophage. *Immunol. Rev.* 264, 233–248. doi: 10.1111/imr.12254

Tan, M. P., Sequeira, P., Lin, W. W., Phong, W. Y., Cliff, P., Ng, S. H., et al. (2010). Nitrate respiration protects hypoxic mycobacterium tuberculosis against acid- and reactive nitrogen species stresses. *PloS One* 5, e13356. doi: 10.1371/journal.pone.0013356

Thayil, S. M., Morrison, N., Schechter, N., Rubin, H., and Karakousis, P. C. (2011). The role of the novel exopolyphosphatase MT0516 in mycobacterium tuberculosis drug tolerance and persistence. *PloS One* 6, e28076. doi: 10.1371/journal.pone.0028076

Thiede, J. M., Dillon, N. A., Howe, M. D., Aflakpui, R., Modlin, S. J., Hoffner, S. E., et al. (2022). Pyrazinamide susceptibility is driven by activation of the SigE-dependent cell envelope stress response in mycobacterium tuberculosis. *mBio* 13, e00439-21. doi: 10.1128/mbio.00439-21

Tischler, A. D., Leistikow, R. L., Kirksey, M. A., Voskuil, M. I., and McKinney, J. D. (2013). Mycobacterium tuberculosis requires phosphate-responsive gene regulation to resist host immunity. *Infect. Immun.* 81, 317–328. doi: 10.1128/IAI.01136-12

Tiwari, S., Tonder, A. J., Vilchèze, C., Mendes, V., Thomas, S. E., Malek, A., et al. (2018). Arginine-deprivation–induced oxidative damage sterilizes mycobacterium tuberculosis. *Proc. Natl. Acad. Sci.* 115, 9779–9784. doi: 10.1073/pnas.1808874115

Torrelles, J. B., and Schlesinger, L. S. (2010). Diversity in mycobacterium tuberculosis mannosylated cell wall determinants impacts adaptation to the host. *Tuberc. Edinb. Scotl.* 90, 84–93. doi: 10.1016/j.tube.2010.02.003

Tyagi, P., Dharmaraja, A. T., Bhaskar, A., Chakrapani, H., and Singh, A. (2015). Mycobacterium tuberculosis has diminished capacity to counteract redox stress induced by elevated levels of endogenous superoxide. *Free Radic. Biol. Med.* 84, 344–354. doi: 10.1016/j.freeradbiomed.2015.03.008

Vandal, O. H., Pierini, L. M., Schnappinger, D., Nathan, C. F., and Ehrt, S. (2008). A membrane protein preserves intrabacterial pH in intraphagosomal mycobacterium tuberculosis. *Nat. Med.* 14, 849–854. doi: 10.1038/nmXXXX

Vaubourgeix, J., Lin, G., Dhar, N., Chenouard, N., Jiang, X., Botella, H., et al. (2015). Stressed mycobacteria use the chaperone ClpB to sequester irreversibly oxidized proteins asymmetrically within and between cells. *Cell Host Microbe* 17, 178–190. doi: 10.1016/j.chom.2014.12.008

Via, L. E., Lin, P. L., Ray, S. M., Carrillo, J., Allen, S. S., Eum, S. Y., et al. (2008). Tuberculous granulomas are hypoxic in Guinea pigs, rabbits, and nonhuman primates. *Infect. Immun.* 76, 2333–2340. doi: 10.1128/IAI.01515-07

Vijay, S., Hai, H. T., Thu, D. D. A., Johnson, E., Pielach, A., Phu, N. H., et al. (2018). Ultrastructural analysis of cell envelope and accumulation of lipid inclusions in clinical mycobacterium tuberculosis isolates from sputum, oxidative stress, and iron deficiency. *Front. Microbiol.* 8. doi: 10.3389/fmicb.2017.02681

Vijay, S., Nair, R. R., Sharan, D., Jakkala, K., Mukkayyan, N., Swaminath, S., et al. (2017a). Mycobacterial cultures contain cell size and density specific Sub-populations of cells with significant differential susceptibility to antibiotics, oxidative and nitrite stress. *Front. Microbiol.* 8. doi: 10.3389/fmicb.2017.00463

Vijay, S., Vinh, D. N., Hai, H. T., Ha, V. T. N., Dung, V. T. M., Dinh, T. D., et al. (2017b). Influence of stress and antibiotic resistance on cell-length distribution in mycobacterium tuberculosis clinical isolates. *Front. Microbiol.* 8. doi: 10.3389/fmicb.2017.02296

Vilchèze, C., Hartman, T., Weinrick, B., and Jacobs, W. R. (2013). Mycobacterium tuberculosis is extraordinarily sensitive to killing by a vitamin c-induced fenton reaction. *Nat. Commun.* 4, 1881. doi: 10.1038/ncomms2898

Vilchèze, C., Hartman, T., Weinrick, B., Jain, P., Weisbrod, T. R., Leung, L. W., et al. (2017). Enhanced respiration prevents drug tolerance and drug resistance in mycobacterium tuberculosis. *Proc. Natl. Acad. Sci. U. S. A.* 114, 4495–4500. doi: 10.1073/pnas.1704376114

Vilchèze, C., and Kremer, L. (2017). Acid-fast positive and acid-fast negative mycobacterium tuberculosis: The Koch paradox. *Microbiol. Spectr.* 5, 5.2.15. doi: 10.1128/microbiolspec.TBTB2-0003-2015

Vilchèze, C., Molle, V., Carrère-Kremer, S., Leiba, J., Mourey, L., Shenai, S., et al. (2014). Phosphorylation of KasB regulates virulence and acid-fastness in mycobacterium tuberculosis. *PloS Pathog.* 10, e1004115. doi: 10.1371/journal.ppat.1004115

Voskuil, M. I., Bartek, I. L., Visconti, K., and Schoolnik, G. K. (2011). The response of mycobacterium tuberculosis to reactive oxygen and nitrogen species. *Front. Microbiol.* 2, 105. doi: 10.3389/fmicb.2011.00105

Voskuil, M. I., Schnappinger, D., Visconti, K. C., Harrell, M. I., Dolganov, G. M., Sherman, D. R., et al. (2003). Inhibition of respiration by nitric oxide induces a mycobacterium tuberculosis dormancy program. *J. Exp. Med.* 198, 705–713. doi: 10.1084/jem.20030205

Wakamoto, Y., Dhar, N., Chait, R., Schneider, K., Signorino-Gelo, F., Leibler, S., et al. (2013). Dynamic persistence of antibiotic-stressed mycobacteria. *Science* 339, 91–95. doi: 10.1126/science.1229858

Walters, S. B., Dubnau, E., Kolesnikova, I., Laval, F., Daffe, M., and Smith, I. (2006). The mycobacterium tuberculosis PhoPR two-component system regulates genes essential for virulence and complex lipid biosynthesis. *Mol. Microbiol.* 60, 312–330. doi: 10.1111/j.1365-2958.2006.05102.x

Warner, D. F., Savvi, S., Mizrahi, V., and Dawes, S. S. (2007). A riboswitch regulates expression of the coenzyme B12-independent methionine synthase in mycobacterium tuberculosis: Implications for differential methionine synthase function in strains H37Rv and CDC1551. *J. Bacteriol.* 189, 3655–3659. doi: 10.1128/JB.00040-07

Williams, M. J., Shanley, C. A., Zilavy, A., Peixoto, B., Manca, C., Kaplan, G., et al. (2015). Bis-molybdopterin guanine dinucleotide is required for persistence of mycobacterium tuberculosis in Guinea pigs. *Infect. Immun.* 83, 544–550. doi: 10.1128/IAI.02722-14

Wright, C. C., Hsu, F. F., Arnett, E., Dunaj, J. L., Davidson, P. M., Pacheco, S. A., et al. (2017). The mycobacterium tuberculosis MmpL11 cell wall lipid transporter is important for biofilm formation, intracellular growth, and nonreplicating persistence. *Infect. Immun.* 85, e00131–17. doi: 10.1128/IAI.00131-17

Yamada, H., Bhatt, A., Danev, R., Fujiwara, N., Maeda, S., Mitarai, S., et al. (2012). Non-acid-fastness in mycobacterium tuberculosis ΔkasB mutant correlates with the cell envelope electron density. *Tuberculosis* 92, 351–357. doi: 10.1016/j.tube.2012.02.006

Zhang, Y. J., Reddy, M. C., Ioerger, T. R., Rothchild, A. C., Dartois, V., Schuster, B. M., et al. (2013). Tryptophan biosynthesis protects mycobacteria from CD4 T cell-mediated killing. *Cell* 155, 1296–1308. doi: 10.1016/j.cell.2013.10.045

Zheng, J., Rubin, E. J., Bifani, P., Mathys, V., Lim, V., Au, M., et al. (2013). Para-aminosalicylic acid is a prodrug targeting dihydrofolate reductase in mycobacterium tuberculosis. *J. Biol. Chem.* 288, 23447–23456. doi: 10.1074/jbc.M113.475798

Zimmerman, M., Lestner, J., Prideaux, B., O'Brien, P., Dias-Freedman, I., Chen, C., et al. (2017). Ethambutol partitioning in tuberculous pulmonary lesions explains its clinical efficacy. *Antimicrob. Agents Chemother.* 61, e00924–17. doi: 10.1128/AAC.00924-17

Zimmermann, M., Kogadeeva, M., Gengenbacher, M., McEwen, G., Mollenkopf, H.-J., Zamboni, N., et al. (2017). Integration of metabolomics and transcriptomics reveals a complex diet of mycobacterium tuberculosis during early macrophage infection. *mSystems* 2, e00057–17. doi: 10.1128/mSystems.00057-17

frontiers | Frontiers in Cellular and Infection Microbiology

TYPE Brief Research Report
PUBLISHED 24 November 2022
DOI 10.3389/fcimb.2022.1072073

OPEN ACCESS

EDITED BY
Anthony Baughn,
University of Minnesota Twin Cities, United States

REVIEWED BY
Anil Ojha,
Wadsworth Center, United States
Jianping Xie,
Southwest University, China

*CORRESPONDENCE
Bavesh Kana
bavesh.kana@nhls.ac.za

SPECIALTY SECTION
This article was submitted to Bacteria and Host, a section of the journal Frontiers in Cellular and Infection Microbiology

RECEIVED 17 October 2022
ACCEPTED 08 November 2022
PUBLISHED 24 November 2022

CITATION
Chengalroyen MD, Beukes GM, Otwombe K, Gordhan BG, Martinson N and Kana B (2022) The detection of mixed tuberculosis infections using culture filtrate and resuscitation promoting factor deficient filtrate.
Front. Cell. Infect. Microbiol. 12:1072073.
doi: 10.3389/fcimb.2022.1072073

The detection of mixed tuberculosis infections using culture filtrate and resuscitation promoting factor deficient filtrate

Melissa D. Chengalroyen[1], Germar M. Beukes[1], Kennedy Otwombe[2], Bhavna G. Gordhan[1], Neil Martinson[1,2,3] and Bavesh Kana[1]*

[1]National Health Laboratory Service, DST/NRF Centre of Excellence for Biomedical TB Research, University of the Witwatersrand, Johannesburg, South Africa, [2]Perinatal HIV Research Unit, Faculty of Health Sciences, University of the Witwatersrand, Johannesburg, South Africa, [3]Center for TB Research, Johns Hopkins University, Baltimore, MD, United States

Tuberculosis (TB) infected individuals harbor a heterogenous population of differentially culturable tubercle bacilli (DCTB). Herein, we describe how DCTB assays using culture filtrate either containing or deficient in resuscitation promoting factors can uncover mixed infections. We demonstrate that *Mycobacterium tuberculosis* (*Mtb*) strain genotypes can be separated in DCTB assays based on their selective requirement for growth stimulatory factors. Beijing mixed infections appear to be associated with a higher bacterial load and reduced reliance on growth stimulatory factors. These data have important implications for identifying mixed infections and hetero-resistance, which in turn can affect selection of treatment regimen and establishment of transmission links.

KEYWORDS

resuscitation promoting factor, *Mycobacterium tuberculosis*, mixed infection, differentially culturable tubercle bacteria, most probable number assay

Introduction

Mycobacterium tuberculosis (*Mtb*), the causative agent of tuberculosis (TB), is a pathogen whose successful adaptation to the human host has been paramount to its colonization of one-fourth of the globe's population (Cohen et al., 2019). Challenges contributing to the control of TB disease include a strong association with HIV infection in certain endemic settings, evolution of multi-drug resistance, infection with multiple

Mtb strains and the recent long term negative impact of the COVID-19 pandemic (Wingfield et al., 2021).

Traditionally, the commonly accepted modes of TB disease acquisition were associated with primary infection or reactivation with a single strain (Milburn, 2001; Ai et al., 2016). However, increased reports of mixed strain infections, particularly in retreatment cases (Warren et al., 2004) or in high TB incidence settings (Verver et al., 2005) have been documented. These are most likely acquired by simultaneous infection with more than one *Mtb* strain or endogenous reactivation and subsequent secondary infection with a distinct strain (Perez-Lago et al., 2015). Patients with mixed *Mtb* strains, particularly with different drug resistance profiles, may not respond well to standard anti-TB chemotherapy. As an example, the challenge of treating mixed infections was demonstrated in a case study where the treatment regimen cleared one strain but was ineffective against the second strain, resulting in prolonged persistence of that isolate (Abascal et al., 2021). *Mtb* mixed infections ultimately predict a higher probability of poor outcomes (Shin et al., 2018).

The ability to detect mixed infections is influenced by numerous factors. These include the timing of sputum sampling relative to treatment, the specific lesions open to the airway at the time of sampling, the specimen handling process which could lead to a reduction in prevalence of the minority variant, sensitivity of the assay being used and retreatment of TB disease (Cohen et al., 2012). In addition, broader aspects such as socio-economic conditions, TB-incidence rate (Richardson et al., 2002), host genetic predispositions and socio-demographics also influence the frequency of *Mtb* mixed infections. Considering the interplay of these complicated factors, its unsurprising that the prevalence of *Mtb* mixed infections documented in various settings is highly variable, ranging from 1.3% (2/160), 2.3% (3/131), 14.7% (15/102), 3% (14/466), 26.6% (20/75), 0.01% (9/703) to 19% (35/186) (Richardson et al., 2002; Warren et al., 2004; Mallard et al., 2010; Wang et al., 2010; Navarro et al., 2011; Hajimiri et al., 2016; Mustafa et al., 2016). In addition, another study observed an incidence of 51% (26/51) mixed infections, when comparing blood against sputum samples (Ssengooba et al., 2015).

Molecular typing methods used to distinguish mixed *Mtb* strains include 24 loci mycobacterial interspersed repetitive unit variable tandem repeat typing (MIRU-VNTR), spoligotyping, whole genome sequencing (WGS) or IS6110-RFLP (Das et al., 2004). These methods are useful, however most depend on the visualization of low intensity bands (corresponding to the minority strain) against prominent bands of the majority strain, which can be subjective. For WGS, conventional culturing of samples in liquid media often favors the growth of the predominant strain over the minority variant, thus minimizing the ability to detect multiple strain infections (Martin et al., 2010). Also, for most techniques, samples must constitute at least 10% of the minority strain for detection (de Boer et al., 2000), while for WGS, the minority population must be > 10% (Sobkowiak et al., 2018). Warren et al. (2004) developed a simple rapid PCR-based assay to detect mixed Beijing/non-Beijing infections for a more accurate measure of the proportion of individuals harboring multiple strains (Wang et al., 2010). To our knowledge no such method has been developed to distinguish mixed genotypes within the same lineage. Advancements in the identification of mixed infections will reconcile the true percentage of individuals infected with more than one *Mtb* strain, facilitating optimal treatment.

Our previous findings indicated that sputum from TB infected individuals contains Differentially Culturable Tubercle Bacilli (DCTB), a population of bacteria which have a requirement for growth stimulatory factors in culture filtrate (CF) to either recover from a damaged state or reawaken from a state that precludes growth on standard laboratory media (Chengalroyen et al., 2016). Within CF, the presence of resuscitation promoting factors (Rpfs), a group of growth stimulatory enzymes, has been associated with recovery of DCTB (Mukamolova et al., 2009; Chengalroyen et al., 2016). However, DCTB populations have also been shown to grow in CF deficient of Rpfs, suggesting that other molecules in CF also have a growth stimulatory effect (Chengalroyen et al., 2016; Gordhan et al., 2021). The presence of these differentially culturable populations suggests that use of routine culture media only allows for a subset of bacteria to emerge, possibly limiting the detection of all genotypes present in a sputum sample. In this study we used Most Probable Number (MPN) assays with growth factor supplementation to identify mixed strains in sputum obtained from TB infected individuals. Spoligotyping was used to identify the different strains, if any, from each participant. We demonstrate that this approach allows for the detection of mixed strain infections.

Materials and methods

Study population

This study was approved by the Human Research Ethics Committee of the University of Witwatersrand (M110532). One-hundred and ten drug sensitive TB infected patients from Soweto in Johannesburg, South Africa were enrolled. Participants provided written consent and were requested to provide a sputum sample prior to treatment initiation. Patients were older than 18 years with either a GeneXpert or smear positive TB result. For more comprehensive detail of the patient cohort, clinical characteristics and methodology used which includes sputum sample preparation, bacterial culturing and quality control checks, the reader is referred to (Chengalroyen et al., 2016).

MPN assay

The MPN assay was conducted as previously described (Chengalroyen et al., 2016). This technique involves performing a 10-fold serial dilution of bacilli and uses the Poisson distribution to estimate the number of viable cells based on the dilutions which show the presence vs the absence of visible growth. The experimental outline is given in Figure 1A. Briefly, sputum samples were decontaminated and resuspended in 7H9 media. Thereafter, the cells were dispersed by vortexing with glass beads. To determine the MPN, the sputum sample was added to the first well of a 48-well microtiter plate and subsequently diluted 10-fold to the end of the plate. The media was supplemented in a 1:1 ratio with i) CF harvested from *Mtb* H37Rv grown in 7H9 media, ii) Rpf $^{-}$ CF, CF harvested from *Mtb* BG1, a quintuple mutant deficient in all five *rpf*-encoding genes (Kana et al., 2008) and iii) standard 7H9 media as a control. Following the dilution, the microtiter plates were incubated for six weeks. Thereafter, the growth pattern in wells was recorded and used to determine bacterial count. The

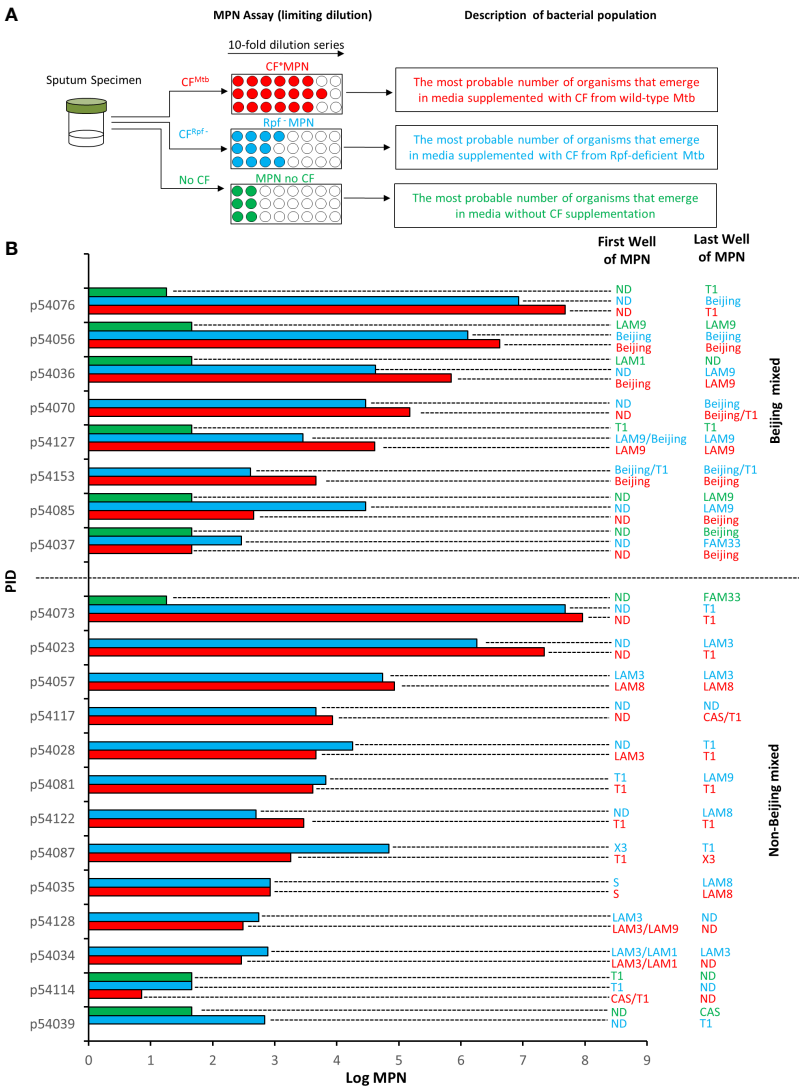

FIGURE 1
Mycobacterial family strains identified in Most Probable Number (MPN) assays. **(A)** Shown is a schematic representation of the experimental workflow. Sputum specimens were decontaminated and the same specimen was subjected to three MPN assays in the presence of culture filtrate (CF) from wild type *M. tuberculosis* (CF^{Mtb}), CF from an Rpf-deficient mutant of *M. tuberculosis* (CF^{Rpf-}) and no CF. The populations detected in this experimental set up are shown. **(B)** Shown is the strain identified in the first well and last well of CF^{+}MPN (red), Rpf $^{-}$ MPN (blue) and MPN no CF (green) assays. The absence of a MPN value reflects no growth under that condition. Wells in which Beijing strains were detected with another strain "Beijing Mixed" (top set) are delineated from those with only Non-Beijing strains "Non-Beijing mixed" (lower set) by the horizontal dashed line. Spoligotyping was used to genotype isolates present in the MPN wells. ND, not determined.

first and last well of the microtitre plate showing visible growth for each condition was harvested. An aliquot was used to extract DNA from the bacteria by heat killing at 95°C for 30 minutes, in preparation for spoligotyping. Additionally, in a select case (participant 54034), bacilli from the first and last wells were spread onto 7H10 plates to isolate individual colonies. After 3-4 weeks of incubation, individual colonies were picked, followed by heat killing at 95°C for 30 minutes to extract DNA in preparation for spoligotyping.

Spoligotyping

Spoligotyping was performed as per the manufacturer's instruction using a kit (Ocimum Biosolutions) to amplify IS6110 regions. Amplified IS6110 products were hybridized to 43 immobilized oligonucleotides on a membrane representing unique spacer regions. Hybridized DNA was detected by chemiluminescence (Amersham Biosciences) and exposed to X-ray film. Mycobacterial strain identification was conducted by comparison of the resulting pattern to the SPOTCLUST database (https://tbinsight.cs.rpi.edu/run_spotclust.html).

Data analysis

Specimens were categorized as harboring either *Mtb* Beijing mixed (simultaneous presence of a Beijing and non-Beijing strain) or *Mtb* non-Beijing mixed strains (simultaneous presence of two non-Beijing strains). Interquartile ranges were determined for each variable using the Kruskal-Wallis Test.

Results

Each sputum sample in our collection was subjected to three MPN assays supplemented with CF, Rpf-deficient CF and no CF (Figure 1A). The patterns of positive and negative growth were used to determine the MPN. The bacterial yield from these three assays for the specimens reported in this study are given in Figure 1B. From these assays, the first and last wells from MPN plates were sampled and where possible, a spoligotype was determined. Of the 102 spoligotype profiles obtained from our collection of specimens, 21% (21/102) carried mixed infections, as observed by the detection of a different strain in i) the culture obtained from the first well versus the last well in the CF^+ MPN or Rpf^- MPN condition, or ii) in any well of the CF^+ MPN when compared to either the Rpf^- CF or media control (MPN no CF) wells, Figure 1B. To further confirm the presence of mixed strains, the bacteria from the first and last MPN well, for a randomly selected isolate, was plated to single colonies and the individual colonies were spoligotyped. Two distinct strains emerged in the MPN assays (Figure 2). Spoligotyping of the entire bacterial population from the first well of the MPN plates identified the LAM9 strain however, the single colonies isolated from the culture showed the presence of a mixture of LAM1 and LAM3 suggesting that the LAM9 spoligotype pattern observed in the original analysis of the culture from the MPN well was the result of LAM1 and LAM3 superimposed spacer regions (Figure 2). These data indicate that the LAM3 strain outcompeted the LAM1 strain in the presence of CF containing Rpfs while the absence of Rpfs in CF exhibited a selective advantage for the LAM1 strain (Rpf^- MPN first well). It is likely however that LAM1 was diluted out in the last Rpf^-

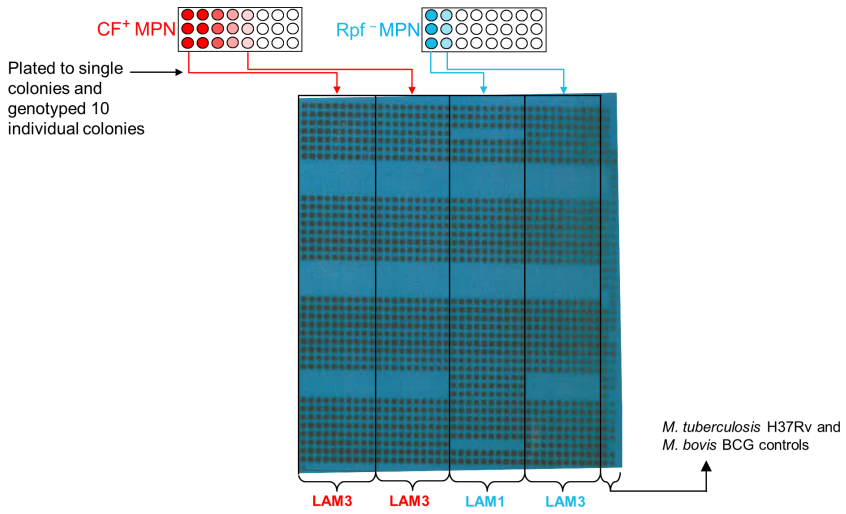

FIGURE 2
Detection of different strain types in MPN wells. Aliquots from the MPN wells from participant 54034 were plated to single colonies and 10 individual colonies were genotyped. Shown is the blot from the spoligotyping of these colonies.

MPN well since LAM3 re-emerged. These observations point to a complex interplay between infecting strains whereby particular strains emerge differentially in the presence or absence of CF or Rpf $^{-}$ CF.

To expand on this, we searched for correlations among pathology, immunology, diagnostics and DCTB profile relative to the 8 Beijing-mixed and 13 non-Beijing mixed infections in our cohort. Notably, the small sample size was a limitation, precluding extensive analysis and determination of statistical significance. Nevertheless, we observed that the Beijing mixed strains grew slightly better in the presence of CF containing Rpfs compared to the absence of Rpfs (MPN of 4.9 vs 3.5). We also noted that individuals harboring Beijing-mixed infections carried a higher quantum of CF^{+} MPN and Rpf $^{-}$ MPN organisms (MPN 4.9 and 4.5) compared to non-Beijing mixed carriers (MPN 3.5 and 3.7) (Table 1). Additionally, the propensity for spontaneous reactivation (without the requirement for additional growth factors), inferred from the MPN no CF media control, was observed strictly within Beijing mixed strains (Table 1). Furthermore, colony forming units were higher from Beijing mixed infections when compared to non-Beijing mixed carriers (640.0 vs 0.0) (Table 1). These observations should be explored in a larger cohort.

Discussion

The classification of TB as a binary disease of either active versus latent infection has evolved, with the current outlook suggesting that TB infection exists as a spectrum (Lin and Flynn, 2018) ranging from incipient or subclinical disease with/without symptoms to active disease (Migliori et al., 2021). We posit that underlying these disease states are heterogenous populations of bacteria, including DCTB that appear to be modulated by the host immune response (Chengalroyen et al., 2016). These have been identified in the sputum of drug sensitive (Mukamolova et al., 2010; Chengalroyen et al., 2016; McAulay et al., 2018) and drug resistant TB infected patients (Saito et al., 2017;

TABLE 1 Demographics and clinical characteristics of patient participants categorized as carriers of either Beijing or non-Beijing *Mtb* mixed infection.

Variable	Overall (n=21)	Beijing mixed (n=8)	Non-beijing mixed (n=13)
Demographics			
Female (%)	9.0 (42.9)	3.0 (37.5)	6.0 (46.2)
Male (%)	12.0 (57.1)	5.0 (62.5)	7.0 (53.8)
Median age in years (IQR)	39.0 (32.0-44.0)	36.0 (29.5-42.5)	40.0 (34.0-44.0)
Minimum, maximum	22.0-69.0	24.0-69.0	22.0-64.0
BMI (IQR) in kg/m^2			
Underweight (%)	6.0 (28.6)	3.0 (37.5)	3.0 (23.1)
Normal (%)	12.0 (57.1)	3.0 (37.5)	9.0 (69.2)
Overweight (%)	3.0 (14.3)	2.0 (25.0)	1.0 (7.7)
Median BMI (IQR)	20.3 (17.7-23.6)	18.8 (16.9-24.2)	20.5 (18.8-23.6)
Minimum, maximum	10.1-30.5	10.1-30.5	16.9-26.0
Lung pathology*			
No cavity (%)	2.0 (11.8)	1.0 (14.3)	1.0 (10.0)
Cavity (%)	15.0 (88.2)	6.0 (85.7)	9.0 (90.0)
Extent of disease†			
Limited (%)	3.0 (14.3)	2.0 (25.0)	1.0 (7.7)
Moderate (%)	9.0 (42.9)	2.0 (25.0)	7.0 (53.8)
Extensive (%)	5.0 (23.8)	3.0 (37.5)	2.0 (15.4)
Unknown (%)	4.0 (19.0)	1.0 (12.5)	3.0 (23.1)
Patient immunology‡			
HIV status			
Negative (%)	13.0 (61.9)	5.0 (62.5)	8.0 (61.5)
Positive (%)	8.0 (38.1)	3.0 (37.5)	5.0 (38.5)
Median CD4 count (IQR) cells/mm^3 (only HIV infected)	211.0 (116.0-300.0) n = 7.0	211.0 (34.0-223.0) n = 3.0	219.5 (127.5-357.0) n = 4.0
Minimum, maximum	34.0-414.0	34.0-223.0	116.0-414.0
HAART treatment (%) $^{\Pi}$	1.0 (12.5)	0.0 (0.0)	1.0 (20.0)

(Continued)

TABLE 1 Continued

Variable	Overall (n=21)	Beijing mixed (n=8)	Non-beijing mixed (n=13)
Conventional TB diagnosis			
Smear Grade negative (%)	5.0 (23.8)	1.0 (12.5)	4.0 (30.8)
Smear Grade positive (%)	16.0 (76.2)	7.0 (87.5)	9.0 (69.2)
GeneXpert result **§			
High (%)	2.0 (12.5)	1.0 (14.3)	1.0 (11.1)
Medium (%)	5.0 (31.3)	3.0 (42.9)	2.0 (22.2)
Low (%)	6.0 (37.5)	2.0 (28.6)	4.0 (44.4)
None (%)	3.0 (18.8)	1.0 (14.3)	2.0 (22.2)
Median GeneXpert cycle threshold (IQR)	18.7 (15.5-23.6) n = 16.0	18.2 (15.3-23.5) n =7.0	22.6 (15.8-23.6) n = 9.0
Minimum, maximum	0.0-28.6	0.0-23.6	0.0-28.6
Median MGIT days to positivity (IQR) ††	12.0 (10.5-21.0) n = 20.0	12.0 (10.0-13.0) n = 7.0	12.0 (11.0-29.0) n = 13.0
Minimum, maximum	5.0-42.0	8.0-22.0	5.0-42.0
Most probable number [MPN] (IQR)			
Log median CF^{+} MPN	3.7 (2.7-5.2)	4.9 (3.2-6.2)	3.5 (2.5-3.9)
Minimum, maximum	0.0-8.0	1.7-7.7	0.0-8.0
Log median Rpf^{-} MPN	3.8 (2.8-4.7)	4.5 (3.0-5.4)	3.7 (2.8-4.7)
Minimum, maximum	0.0-7.7	2.5-6.9	0.0-7.7
Log median MPN no CF	0.0 (0.0-1.3)	1.5 (0.0-1.7)	0.0 (0.0-0.0)
Minimum, maximum	0.0-1.7	0.0-1.7	0.0-1.7
Median MPN days to positivity (IQR)	14.0 (14.0-21.0)	14.0 (14.0–17.5)	14.0 (14.0-21.0)
Minimum, maximum	7.0-49.0	7.0-35.0	7.0-49.0
Median Colony forming units [CFU] (IQR)	50.0 (0.0-600.0)	640.0 (32.5-15750.0)	0.0 (0.0-70.0)
Minimum, maximum	0.0-32500	0.0-32500	0.0-29500

The sample size was too small to test statistical assumptions, hence the p-value was not calculated. IQR represents the interquartile range and bracketed numbers represent the percentage IQR.
*4 participants did not have cavitation data.
†4 participants did not have disease extent data.
‡1 participant did not have CD4 count data.
§5 participants had no GeneXpert data.
¶only 1 participant was on HAART.
**5 participants did not have GeneXpert data.
††1 participant had missing MGIT data.

Zainabadi et al., 2021; Gordhan et al., 2022) in addition to being present at extrapulmonary sites of infection (Rosser et al., 2018). In this study, using DCTB assays, we identified mixed infections at a prevalence of 21% in sputum samples from drug sensitive participants. Strains displayed growth stimulation/suppression in response to unidentified selective factors in CF and could be segregated using the MPN assay. Plazzotta et al. (2015) established a mathematical model showing that the initial quantity of a minor variant and its growth rate are the main factors which affect its detection, predicting that if the minority strain is present in < 3% of the sample, it will not be detected, thus misclassifying the patient with a single strain infection. Notably, in the MPN assay, dilution of the majority strain and favored growth of the minority strain may alleviate these limitations. Using this method, same family genotype mixed infections could be detected. However, to be able to distinguish modern and ancient Beijing mixed infections, this assay would need to be conducted in conjunction with a more sensitive genotyping method such as MIRU-VNTR or WGS.

The Beijing *Mtb* lineage is characterized by enhanced virulence, higher transmission rates and an increased association with drug resistance (Hanekom et al., 2011). Notably in this study, patients with Beijing mixed infection had a higher bacterial load as estimated by CFUs and MPN (Table 1) and did not require stimulatory factors for efficient growth. It is possible that the Beijing genotype exploits or suppresses the non-Beijing isolate to gain a growth advantage (von Groll et al., 2010; Wang et al., 2010), although the

mechanism/s underlying this remains to be determined. Further analysis of our patient cohort indicted that no host parameters were specifically associated with Beijing or non-Beijing DCTB mixed infection (Table 1).

Multiple infections can lead to discordant drug susceptibility profiles (Mei et al., 2015) with instances of patients carrying a drug sensitive and drug resistant strain (Baldeviano-Vidalon et al., 2005). Also, in mixed Beijing infections there exists a higher probability of resistance to at least one drug (Huang et al., 2010). The identification of dual/multiple strain infection could allow for a change in treatment regimen, a higher antibiotic dosage and lengthened treatment to improve outcomes. The separation of different *Mtb* genotypes with this assay premises a phenotypic and/or metabolic disparity between the strains. Consequently, this could be a gateway to better understanding competition, suppression and mutualism-based interactions between different *Mtb* genotypes.

Data availability statement

The original contributions presented in the study are included in the article/supplementary material. Further inquiries can be directed to the corresponding author.

Ethics statement

The studies involving human participants were reviewed and approved by Human Research Ethics Committee, University of the Witwatersrand. The patients/participants provided their written informed consent to participate in this study.

Author contributions

MC and GB performed the experiments. KO performed the statistical analysis. NM recruited patients for the study and assembled appropriate patient data. BG and BK designed the experiments. All authors contributed to the article and approved the submitted version.

Funding

This study was supported by the National Institutes of Health (U01 AI069453-07), National Research Foundation of South Africa, South African Medical Research Council, Centre for Aids Prevention Research in South Africa and the Howard Hughes Medical Institute.

Conflict of interest

The authors declare that the research was conducted in the absence of any commercial or financial relationships that could be construed as a potential conflict of interest.

Publisher's note

References

Abascal, E., Herranz, M., Ruiz Serrano, M. J., Fernandez-Gonzalez, F., Munoz, P., Gotuzzo, E., et al. (2021). In-depth analysis of a mixed mycobacterium tuberculosis infection involving a multidrug-resistant strain and a susceptible strain. *Clin. Microbiol. Infect.* 27, 641–643. doi: 10.1016/j.cmi.2020.09.032

Ai, J.-W., Ruan, Q.-L., Liu, Q.-H., and Zhang, W.-H. (2016). Updates on the risk factors for latent tuberculosis reactivation and their managements. *Emerg. Microbes Infect.* 5, 1–8. doi: 10.1038/emi.2016.10

Baldeviano-Vidalon, G. C., Quispe-Torres, N., Bonilla-Asalde, C., Gastiaburu-Rodriguez, D., Pro-Cuba, J. E., and Llanos-Zavalaga, F. (2005). Multiple infection with resistant and sensitive m. tuberculosis strains during treatment of pulmonary tuberculosis patients. *Int. J. Tuberc Lung Dis.* 9, 1155–1160.

Chengalroyen, M. D., Beukes, G. M., Gordhan, B. G., Streicher, E. M., Churchyard, G., Hafner, R., et al. (2016). Detection and quantification of differentially culturable tubercle bacteria in sputum from tuberculosis patients. *Am. J. Respir. Crit. Care Med.* 194, 1532–1540. doi: 10.1164/rccm.201604-0769OC

Cohen, A., Mathiasen, V. D., Schön, T., and Wejse, C. (2019). The global prevalence of latent tuberculosis: A systematic review and meta-analysis. *Eur. Respir. J.* 54, 1–14. doi: 10.1183/13993003.00655-2019

Cohen, T., Van Helden, P. D., Wilson, D., Colijn, C., Mclaughlin, M. M., Abubakar, I., et al. (2012). Mixed-strain mycobacterium tuberculosis infections and the implications for tuberculosis treatment and control. *Clin. Microbiol. Rev.* 25, 708–719. doi: 10.1128/CMR.00021-12

Das, S., Narayanan, S., Hari, L., Mohan, N. S., Somasundaram, S., Selvakumar, N., et al. (2004). Simultaneous infection with multiple strains of mycobacterium tuberculosis identified by restriction fragment length polymorphism analysis. *Int. J. Tuberc Lung Dis.* 8, 267–270.

de Boer, A. S., Kremer, K., Borgdorff, M. W., De Haas, P. E., Heersma, H. F., and Van Soolingen, D. (2000). Genetic heterogeneity in mycobacterium tuberculosis isolates reflected in IS6110 restriction fragment length polymorphism patterns as low-intensity bands. *J. Clin. Microbiol.* 38, 4478–4484. doi: 10.1128/jcm.38.12.4478-4484.2000

Gordhan, B. G., Peters, J. S., Mcivor, A., Machowski, E. E., Ealand, C., Waja, Z., et al. (2021). Detection of differentially culturable tubercle bacteria in sputum using mycobacterial culture filtrates. *Sci. Rep.* 11, 6493. doi: 10.1038/s41598-021-86054-z

Gordhan, B. G., Sewcharran, A., Letsoalo, M., Chinappa, T., Yende-Zuma, N., Padayatchi, N., et al. (2022). Detection of differentially culturable tubercle bacteria in sputum from drug-resistant tuberculosis patients. *Front. Cell. Infection Microbiol.* 12. doi: 10.3389/fcimb.2022.949370

Hajimiri, E. S., Masoomi, M., Ebrahimzadeh, N., Fateh, A., Hadizadeh Tasbiti, A., Rahimi Jamnani, F., et al. (2016). High prevalence of mycobacterium

tuberculosis mixed infection in the capital of moderate tuberculosis incidence country. *Microb. Pathog.* 93, 213–218. doi: 10.1016/j.micpath.2016.02.015

Hanekom, M., Gey Van Pittius, N. C., Mcevoy, C., Victor, T. C., Van Helden, P. D., and Warren, R. M. (2011). Mycobacterium tuberculosis Beijing genotype: A template for success. *Tuberc (Edinb)* 91, 510–523. doi: 10.1016/j.tube.2011.07.005

Huang, H. Y., Tsai, Y. S., Lee, J. J., Chiang, M. C., Chen, Y. H., Chiang, C. Y., et al. (2010). Mixed infection with Beijing and non-Beijing strains and drug resistance pattern of mycobacterium tuberculosis. *J. Clin. Microbiol.* 48, 4474–4480. doi: 10.1128/JCM.00930-10

Kana, B. D., Gordhan, B. G., Downing, K. J., Sung, N., Vostroktunova, G., Machowski, E. E., et al. (2008). The resuscitation-promoting factors of *Mycobacterium tuberculosis* are required for virulence and resuscitation from dormancy but are collectively dispensable for growth *in vitro*. *Mol. Microbiol.* 67, 672–684. doi: 10.1111/j.1365-2958.2007.06078.x

Lin, P. L., and Flynn, J. L. (2018). The end of the binary era: Revisiting the spectrum of tuberculosis. *J. Immunol.* 201, 2541–2548.. doi: 10.4049/jimmunol.1800993

Mallard, K., Mcnerney, R., Crampin, A. C., Houben, R., Ndlovu, R., Munthali, L., et al. (2010). Molecular detection of mixed infections of mycobacterium tuberculosis strains in sputum samples from patients in karonga district, Malawi. *J. Clin. Microbiol.* 48, 4512–4518. doi: 10.1128/jcm.01683-10

Martin, A., Herranz, M., Ruiz Serrano, M. J., Bouza, E., and Garcia De Viedma, D. (2010). The clonal composition of mycobacterium tuberculosis in clinical specimens could be modified by culture. *Tuberc (Edinb)* 90, 201–207. doi: 10.1016/j.tube.2010.03.012

McAulay, K., Saito, K., Warrier, T., Walsh, K. F., Mathurin, L. D., Royal-Mardi, G., et al. (2018). Differentially detectable *Mycobacterium tuberculosis* cells in sputum from treatment-naive subjects in Haiti and their proportionate increase after initiation of treatment. *mBio* 9, e02192–18. doi: 10.1128/mBio.02192-18

Mei, Z., Sun, Z., Bai, D., Xu, Y., Li, Z., Huang, H., et al. (2015). Discrepancies in drug susceptibility test for tuberculosis patients resulted from the mixed infection and the testing system. *BioMed. Res. Int.* 2015, 7. doi: 10.1155/2015/651980

Migliori, G. B., Ong, C. W. M., Petrone, L., Ambrosio, L., Centis, R., and Goletti, D. (2021). The definition of tuberculosis infection based on the spectrum of tuberculosis disease. *Breathe* 17, 210079. doi: 10.1183/20734735.0079-2021

Milburn, H. J. (2001). Primary tuberculosis. *Curr. Opin. Pulmonary Med.* 7, 133–141.

Mukamolova, G. V., Turapov, O., Malkin, J., Woltmann, G., and Barer, M. R. (2009). Resuscitation-promoting factors reveal an occult population of tubercle bacilli in sputum. *Am. J. Respir. Crit. Care Med.* 181, 174–180. doi: 10.1164/rccm.200905-0661OC

Mukamolova, G. V., Turapov, O., Malkin, J., Woltmann, G., and Barer, M. R. (2010). Resuscitation-promoting factors reveal an occult population of tubercle bacilli in sputum. *Am. J. Respir. Crit. Care Med.* 181, 174–180. doi: 10.1164/rccm.200905-0661OC

Mustafa, S., Javed, H., Hashmi, J., Jamil, N., Tahir, Z., and Akhtar, A. M. (2016). Emergence of mixed infection of Beijing/Non-Beijing strains among multi-drug resistant mycobacterium tuberculosis in Pakistan. *3 Biotech.* 6, 1–9. doi: 10.1007/s13205-016-0423-9

Navarro, Y., Herranz, M., Pérez-Lago, L., Martínez Lirola, M., Ruiz-Serrano Maria, J., Bouza, E., et al. (2011). Systematic survey of clonal complexity in tuberculosis at a populational level and detailed characterization of the isolates involved. *J. Clin. Microbiol.* 49, 4131–4137. doi: 10.1128/JCM.05203-11

Perez-Lago, L., Lirola, M. M., Navarro, Y., Herranz, M., Ruiz-Serrano, M. J., Bouza, E., et al. (2015). Co-Infection with drug-susceptible and reactivated latent multidrug-resistant mycobacterium tuberculosis. *Emerg. Infect. Dis.* 21, 2098–2100. doi: 10.3201/eid2111.150683

Plazzotta, G., Cohen, T., and Colijn, C. (2015). Magnitude and sources of bias in the detection of mixed strain m. tuberculosis infection. *J. Theor. Biol.* 368, 67–73. doi: 10.1016/j.jtbi.2014.12.009

Richardson, M., Carroll, N. M., Engelke, E., van der Spuy, G. D., Salker, F., Munch, Z., et al. (2002). Multiple mycobacterium tuberculosis strains in early cultures from patients in a high-incidence community setting. *J. Clin. Microbiol.* 40, 2750–2754. doi: 10.1128/jcm.40.8.2750-2754.2002

Rosser, A., Pareek, M., Turapov, O., Wiselka, M. J., and Mukamolova, G. V. (2018). Differentially culturable tubercule bacilli are generated during nonpulmonary tuberculosis infection. *Am. J. Respir. Crit. Care Med.* 197, 818–821. doi: 10.1164/rccm.201705-1048LE

Saito, K., Warrier, T., Somersan-Karakaya, S., Kaminski, L., Mi, J., Jiang, X., et al. (2017). Rifamycin action on RNA polymerase in antibiotic-tolerant *Mycobacterium tuberculosis* results in differentially detectable populations. *Proc. Natl. Acad. Sci. U.S.A.* 114, E4832–E4840. doi: 10.1073/pnas.1705385114

Shin, S. S., Modongo, C., Baik, Y., Allender, C., Lemmer, D., Colman, R. E., et al. (2018). Mixed mycobacterium tuberculosis–strain infections are associated with poor treatment outcomes among patients with newly diagnosed tuberculosis, independent of pretreatment heteroresistance. *J. Infect. Dis.* 218, 1974–1982. doi: 10.1093/infdis/jiy480

Sobkowiak, B., Glynn, J. R., Houben, R. M. G. J., Mallard, K., Phelan, J. E., Guerra-Assunção, J. A., et al. (2018). Identifying mixed mycobacterium tuberculosis infections from whole genome sequence data. *BMC Genomics* 19, 613. doi: 10.1186/s12864-018-4988-z

Ssengooba, W., Cobelens, F. G., Nakiyingi, L., Mboowa, G., Armstrong, D. T., Manabe, Y. C., et al. (2015). High genotypic discordance of concurrent mycobacterium tuberculosis isolates from sputum and blood of HIV-infected individuals. *PloS One* 10, e0132581. doi: 10.1371/journal.pone.0132581

Verver, S., Warren, R. M., Beyers, N., Richardson, M., van der Spuy, G. D., Borgdorff, M. W., et al. (2005). Rate of reinfection tuberculosis after successful treatment is higher than rate of new tuberculosis. *Am. J. Respir. Crit. Care Med.* 171, 1430–1435. doi: 10.1164/rccm.200409-1200OC

von Groll, A., Martin, A., Stehr, M., Singh, M., Portaels, F., Da Silva, P. E., et al. (2010). Fitness of mycobacterium tuberculosis strains of the W-Beijing and non-W-Beijing genotype. *PloS One* 5, e10191. doi: 10.1371/journal.pone.0010191

Wang, J. Y., Hsu, H. L., Yu, M. C., Chiang, C. Y., Yu, F. L., Yu, C. J., et al. (2010). Mixed infection with Beijing and non-Beijing strains in pulmonary tuberculosis in Taiwan: prevalence, risk factors, and dominant strain. *Clin. Microbiol. Infect.* 17, 1239–1245. doi: 10.1111/j.1469-0691.2010.03401.xS1198-743X(14)62961-X

Warren, R. M., Victor, T. C., Streicher, E. M., Richardson, M., Beyers, N., Gey Van Pittius, N. C., et al. (2004). Patients with active tuberculosis often have different strains in the same sputum specimen. *Am. J. Respir. Crit. Care Med.* 169, 610–614. doi: 10.1164/rccm.200305-714OC

Wingfield, T., Karmadwala, F., Macpherson, P., Millington, K. A., Walker, N. F., Cuevas, L. E., et al. (2021). Challenges and opportunities to end tuberculosis in the COVID-19 era. *Lancet Respir. Med.* 9, 556–558. doi: 10.1016/S2213-2600(21)00161-2

Zainabadi, K., Walsh, K. F., Vilbrun, S. C., Mathurin, L. D., Lee, M. H., Saito, K., et al. (2021). Characterization of differentially detectable *Mycobacterium tuberculosis* in the sputum of subjects with drug-sensitive or drug-resistant tuberculosis before and after two months of therapy. *Antimicrob. Agents Chemother.* 65, e0060821. doi: 10.1128/AAC.00608-21

frontiers | Frontiers in Cellular and Infection Microbiology

TYPE Brief Research Report
PUBLISHED 25 November 2022
DOI 10.3389/fcimb.2022.1065893

OPEN ACCESS

EDITED BY
Elena G. Salina,
Bach Institute of Biochemistry, Research Center of Biotechnology of the Russian Academy of Sciences (RAS), Russia

REVIEWED BY
Martin I. Voskuil,
University of Colorado Denver, United States
Dragana Vukovic,
Faculty of Medicine, University of Belgrade, Serbia

*CORRESPONDENCE
Caroline G. G. Beltran
cbeltran@sun.ac.za

SPECIALTY SECTION
This article was submitted to Bacteria and Host, a section of the journal Frontiers in Cellular and Infection Microbiology

RECEIVED 10 October 2022
ACCEPTED 14 November 2022
PUBLISHED 25 November 2022

CITATION
Beltran CGG, Venter R, Mann TN, Davis JH, Kana BD and Walzl G (2022) Culture filtrate supplementation can be used to improve *Mycobacterium tuberculosis* culture positivity for spinal tuberculosis diagnosis.
Front. Cell. Infect. Microbiol. 12:1065893.
doi: 10.3389/fcimb.2022.1065893

Culture filtrate supplementation can be used to improve *Mycobacterium tuberculosis* culture positivity for spinal tuberculosis diagnosis

Caroline G. G. Beltran[1*], Rouxjeane Venter[1], Theresa N. Mann[2], Johan H. Davis[2], Bavesh D. Kana[3,4] and Gerhard Walzl[1]

[1]Department of Science and Technology-National Research Foundation (DST-NRF) Centre of Excellence for Biomedical Tuberculosis Research, South African Medical Research Council Centre for Tuberculosis Research, Division of Molecular Biology and Human Genetics, Faculty of Medicine and Health Sciences, Stellenbosch University, Cape Town, South Africa, [2]Division of Orthopaedic Surgery, Department of Surgical Sciences, Faculty of Medicine and Health Sciences, Stellenbosch University, Cape Town, South Africa, [3]Department of Science and Technology-National Research Foundation (DST-NRF) Centre of Excellence for Biomedical TB Research, School of Pathology, Faculty of Health Sciences, University of the Witwatersrand and the National Health Laboratory Service, Johannesburg, South Africa, [4]Medical Research Council Centre for the Aids Programme of Research in South Africa (MRC-CAPRISA) HIV-TB Pathogenesis and Treatment Research Unit, Centre for the AIDS Programme of Research in South Africa, CAPRISA, Durban, South Africa

Culture remains the gold standard to diagnose spinal tuberculosis (STB) despite the paucibacillary nature of the disease. Current methods can take up to 42 days to yield a result, delaying the ability to rapidly detect drug resistance. Studies have demonstrated the use of supplementation with culture filtrate (CF) from an axenic culture of *Mycobacterium tuberculosis* (*Mtb*) as a source of growth factors to improve culture rates. Our objective was to test a modified culture assay, utilizing CF supplemented media (CFSM), to improve culture positivity rates for suspected STB. Twelve patients with suspected STB were assessed by conventional culture (BACTEC™ MGIT 960), GeneXpert™ and standard histopathological examination. Spinal biopsies were taken from areas of diseased vertebral tissue or abscess, predetermined from MRI. Additional biopsies were obtained to assess CFSM for improved detection and faster culture of Mtb. All cases were diagnosed as STB and treated empirically for tuberculosis based on either bacteriological evidence (GeneXpert™, MGIT and/or CFSM positive), or based on clinical presentation. 5 specimens (45.45%) were positive for *Mtb* DNA as detected by GeneXpert™ and 1 specimen (8.33%) was cultured using MGIT (time to detection; 18 days). CFSM was able to culture 7 specimens (58.3%), with all CFSM positive specimens yielding a culture within 14 days. Two samples were positive only using the CFSM assay pointing to additional yield for diagnostic workup. Modification of standard culture can improve detection of *Mtb* and reduce time to positivity in individuals with STB where culture material is a requirement.

KEYWORDS

spinal TB, extrapulmonary TB, culture, dormancy, resuscitation - methods, diagnostic

Introduction

Diagnosis of spinal tuberculosis (STB), an extra pulmonary tuberculosis (EPTB) disease, remains difficult due to the slow, insidious onset of symptoms, variation in clinical presentation and health system delays (Chen et al., 2016). STB accounts for ~50% of musculoskeletal-TB and involves the progressive destruction of spinal vertebrae (Garg and Somvanshi, 2011). While a combination of radiological and clinical findings are used to establish diagnosis, culturing of the etiological agent remains the gold standard (Agrawal et al., 2010). However, culture positivity rates for STB can vary and may take as long as 42 days (Agrawal et al., 2010; Colmenero et al., 2013; Watt and Davis, 2014; Mann et al., 2018), potentially contributing to treatment delays and poorer outcomes.

Given the concerns associated with standard culture, molecular diagnostics such as the GeneXpert™

MTB/RIF (GeneXpert™), are becoming routinely used for diagnosis of EPTB. However,

GeneXpert™ also has limitations. Reduced sensitivity for paucibacillary samples has been reported and test results may be confounded by DNA from dead bacilli, an important consideration for the assessment of treatment response (Kohli et al., 2018). Furthermore, at least 5% of STB cases in our setting have multi- and extensively-drug resistant STB, requiring further methods for drug susceptibility testing (DST). Line probe assays including the Genotype MTBDR*plus* and MTBDR*sl* (HAIN Lifesciences, Germany) can detect resistance to first– and second-line drugs, yet suffer from poor sensitivity in paucibacillary samples. Thus, it is recommended that these assays are done on cultured isolates for definitive DST (Kumari et al., 2016).

While the paucibacillary nature of the sample may contribute to poor culture rates, altered physiological growth states of *Mtb*, such as a dormancy related states, add another layer of complexity. The ability for *Mtb* to switch to a non-replicating state during periods of stress is well characterized and indicates a hidden population which are differentially culturable (DC), and thus undetectable, on routine culture mediums (Mukamolova et al., 2003). Recent studies have demonstrated the presence of these DC cells in sputa of TB patients (Mukamolova et al., 2010; Chengalroyen et al., 2016; Rosser et al., 2018; Beltran et al., 2020). These cells appear to be dependent on supplementation by culture filtrate (CF), sourced from actively growing *Mtb* cultures, to resume their growth. CF supplementation has been shown to reduce lag time of liquid culture and resuscitate populations of dormant *Mtb* which were otherwise undetectable by standard culture (Chengalroyen et al., 2016; Beltran et al., 2020).

The growth stimulatory effect of CF is primarily attributed to a family of lytic transglycosylase-like proteins, known as resuscitation promoting factors (RPFs), thought to cleave the cell wall of dormant cells and allowing division to resume (Kana and Mizrahi, 2010). Although RPFs have been demonstrated to play a key role in uncovering dormant cells, *Mtb* CF has been shown to have superior growth-stimulatory activity compared to recombinant RPF alone, most likely due to the biological stability of RPFs in CF (Chengalroyen et al., 2016).

The use of CF to culture EPTB samples is limited and has only been conducted in two studies (O'Connor et al., 2015; Gleeson et al., 2016). Conflicting results could not definitively demonstrate the utility of CF to increase culture detection for EPTB, possibly in part be due to differences in the sample collection (freshly acquired vs frozen). The utility of CF supplementation, and presence of altered *Mtb* cells in various EPTB samples, thus warrants further investigation.

Here, we report the use of a modified-culture assay, using CF supplementation, to investigate the utility of this approach in improving culture positivity rates for STB.

Materials and methods

Participant recruitment and sample collection

The study was approved by the Health Research Ethics Committee of Stellenbosch University (N16/02/029) and by Tygerberg Hospital. Treatment-naïve participants, > 18 years of age (8 men and 4 women, age mean ± standard deviation 42 ± 20 years), with clinical and radiological signs suggestive of STB were approached and provided written, informed consent prior to undergoing a diagnostic spinal biopsy.

Depending on the location of the lesion, percutaneous transpedicular core needle biopsies were performed in the lumbar -and thoracolumbar spine, with a small open costotransversectomy approach typically utilized in the thoracic spine, in order to gain access to the paravertebral abscess and diseased tissue. Spinal tissue biopsies were collected from the same diseased area under strict aseptic conditions, and placed into separate containers containing sterile saline for simultaneous processing. As far as possible, equal material was collected and sent for the following: 1) routine diagnostic pathology (haematoxylin and eosin stain), 2) standard liquid culture (BACTEC™ MGIT 960), 3) GeneXpert™ testing and finally, 4) CFSM assay. A trained pathologist experienced in reviewing and diagnosing TB reviewed the histopathological slides. Criteria for TB included caseous necrosis, presence of granulomas/granulomatous regions, epitheloid cells and Langerhans giant cells.The automated liquid BACTEC™ MGIT 960 by BD Diagnostic Systems, Sparks MD (Franklin Lakes, New Jersey) was used for standard culture. Tissue biopsies were processed according to the manufacturer's instructions. Briefly, tissue biopsies were agitated *via* vortexing and removed from the sterile saline using forceps and placed inside a MGIT tube containing

reconstituted antimicrobial mixture PANTA™ (Polymyxin B, Amphotericin B, Nalidixic Acid, Trimethoprim, Azlocillin). Tubes were placed inside a BACTEC™ MGIT 960 by BD Diagnostic System and monitored over a period of 42 days for growth.

GeneXpert™ testing was performed according to the manufacturer's instructions. Briefly, tissue biopsies were transferred to a 15mL falcon tube and 2mL lysis buffer was added to the sample and vortexed periodically during the 15-minute incubation period at room temperature. Following which, 2mL of the material was transferred into the cartridges and loaded into the machine for automated testing.

Preparation of culture filtrate supplemented media

A laboratory strain of *Mtb*, H37Rv, was used to produce CF and was prepared as described previously (Shleeva et al., 2002). Fresh 7H9 media was supplemented with CF (1:1) and PANTA antibiotic mixture (BD Biosciences). A 450 µL aliquot of the culture filtrate supplemented media (CFSM) was added to a 48-well multidish cell culture plate (Thermo Scientific Nunc). Neat CFSM aliquots were included as controls.

Addition of spinal biopsies to modified culture assay

Spinal biopsies were prepared for the CFSM assay within 24 hours of collection. Biopsies were removed aseptically from the collection container and transferred to a well containing 450 µL of CFSM. Culture plates were sealed with micropore-tape and incubated at 37°C for 8 weeks and checked for growth weekly. A positive well was determined visually, through development of turbidity, and presence of *Mtb* was subsequently confirmed [Ziehl-Neelsen staining, single colony isolation on Mycobacteria Selectatab media (Kirchner) and strain typed using spoligotyping (Molhuizen et al., 1998)]. A negative culture well was defined as one in which neither *Mtb* grew, nor contamination was observed.

Results

Assessment of modified culture assay for spinal biopsies

In total, 12 patients were assessed for spinal TB diagnosis using standard pathology, liquid culture (BACTEC™ MGIT 960), GeneXpert™ and the CFSM assay. All cases were diagnosed as STB and treated empirically for tuberculosis based on either bacteriological evidence (GeneXpert™ and/or MGIT and/or CFSM positive) or based on clinical presentation.

Of the 12 patients assessed, 4 (33.3%) had negative bacteriological spine-biopsy findings and were diagnosed based on clinical presentation alone, including spine MRI suggestive of TB (Table 1).

The remaining 8 patients (66.67%) could be diagnosed based on a bacteriological diagnosis (Table 1). *Mtb* DNA was detected in 5 samples (45.45%) using GeneXpert™, with one sample not being sent for analysis. Standard culture (BACTEC™ MGIT) only detected 1 sample (8.33%), with a time to positivity of 18 days (Figure 1), all other samples remained culture negative. The CFSM assay detected 7 positive samples (58.3%), with a median

TABLE 1 Suspected spinal TB cases (n=12) assessed by GeneXpert™, BACTEC™ MGIT 960, modified culture (CFSM) and/or histology.

PID	GeneXpert	MGIT (TTD)	CFSM assay (TTD)	Strain type	Histology	STB diagnosis
SP003	+	+ (18)	+ (11)	Beijing 1	ND	Bact.
SP002	+	–	+ (3)	156T1	No gran. infl.	Bact.
SP029	ND	–	+ (14)	LAM 33	Inconclusive	Bact.
SP031	–	–	+ (12)	Beijing 1	Chronic infl.	Bact.
SP037	+	–	+ (9)	LAM 33	Diffuse gran. infl.	Bact.
SP038	–	–	+ (11)	130 LAM 3	Necrotic bone, chronic infl.	Bact.
SP041	+	–	+ (12)	Beijing 1	Necrosis and acute infl.	Bact.
SP028	+	–	–	NA	Gran. infl.	Bact.
SP034	–	–	–	NA	Chronic infl.	Clin.
SP036	–	–	–	NA	Hypocellular bone, no gran. infl.	Clin.
SP046	–	–	–	NA	Osteitis, no gran. infl.	Clin.
SP047	–	–	–	NA	Necrotic material, no gran. infl.	Clin.
Percentage detected	45.45%	8.33%	58.3%			

(PID) patient identifier; (+) positive result; (-) negative result; (TTD) time to detection in days; (ND) not done; 257 (STB) Spinal Tuberculosis; (gran.) granulomatous; (infl.) inflammation; (Bact.) bacteriological; (Clin.) clinical; 258 (NA) Not Applicable; TTD (time to detection) shown in days for culture (MGIT 254 and CFSM). Strain type refers to the genotyping of the strains recovered by the modified culture 255 assay.

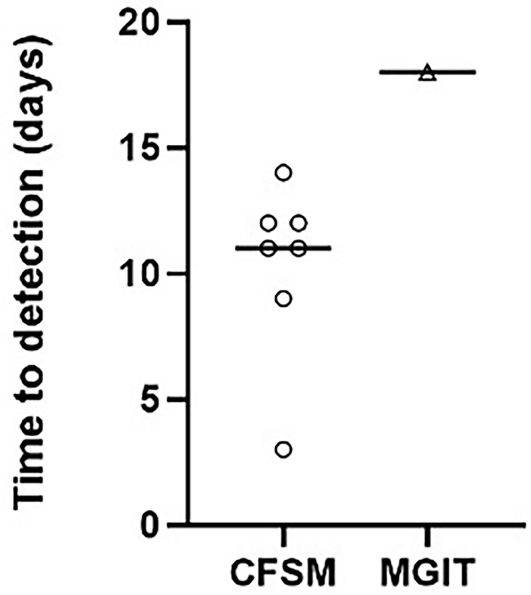

FIGURE 1
Scatter plot comparing the time to detection in days for positive cultures of *M. tuberculosis* from spinal biopsies using culture filtrate supplemented media vs standard liquid culture (Mycobacteria Indicator Growth Indicator Tube; MGIT). A negative culture result where no growth was detected was assigned as negative and not displayed on the graph. Median time to detection was 11 and 18 days for CFSM and MGIT culture, respectively.

time to detection of 9 days (Figure 1). Compared to GeneXpert™, CFSM was able to detect 2 samples as *Mtb* positive that were negative by GeneXpert™, whilst one sample was positive for GeneXpert only (Table 1).

Discussion

In this study, we have shown that a modified culture assay of spinal biopsies utilizing CFSM can be used to increase the culture yield and time-to-positivity for *Mtb* and could add value to the diagnostic workup of suspected STB, in conjunction with GeneXpert™. The positive STB samples all yielded detectable growth within 2 weeks using the CFSM assay. These results support an earlier study that used CFSM to culture a lymph node biopsy that was otherwise negative for all other diagnostic tests for TB (O'Connor et al., 2015), although this is in contrast to a later study that found that CF did not increase archived (frozen) specimens (Gleeson et al., 2016). This may indicate the requirement that a fresh sample is required for this assay, which may not always be practical in a clinical setting. This assay does have the advantage of detecting bacteria in a dormancy-related state which may be clinically relevant (Chengalroyen et al., 2016; Beltran et al., 2020; Gordhan et al., 2021). One of the main limitations of this assay is the requirement of fresh preparation of CF, which is laborious for a clinical laboratory to implement, though standardization of CF as a supplement to add to current MGIT tubes could be developed. Overall, the CFSM assay correlated well with GeneXpert™ results and performed better than standard MGIT culture. Two samples were positive only for the CFSM assay pointing to additional yield for diagnostic workup since further DST using the MTBDR*plus* and MTBDR*sl* LPA's can be done on the cultured isolate (Kumari et al., 2016).

These conclusions are limited by the assessment of the CFSM assay in a small cohort of participants however, whilst further investigation is needed, these results provide strong support that this assay could be applied to paucibacillary sample types where culture has proven difficult and can lead to earlier detection of *Mtb*.

Data availability statement

The original contributions presented in the study are included in the article/supplementary material. Further inquiries can be directed to the corresponding author.

Ethics statement

The studies involving human participants were reviewed and approved by Health Research Ethics Committee of Stellenbosch University. The patients/participants provided their written informed consent to participate in this study.

Author contributions

All authors listed, have made substantial, direct and intellectual contribution to the work, and approved it for publication. CB, TM, JD and GW contributed to the conception and design of the study. CB, RV and TM collected data, analyzed the results and wrote the manuscript. All authors contributed to the article and approved the submitted version.

Funding

CB was supported by the National Research Foundation South African Research Chair Initiative (SARChI) in TB Biomarkers (#86535) led by GW. GW was supported by the South African Medical Research Council (Strategic Health Innovation Program), the South African National Research Foundation (SARChi, grant 86535) and grant 1U01AI115619 – 01 from the NIH. BK was supported by funding from an International Early Career Scientist Award from the Howard

Hughes Medical Institute, the South African National Research Foundation, the South African Medical Research Council and the Bill and Melinda Gates Foundation. TM was supported by postdoctoral fellowships from the National Research Foundation and from the Vice Dean of Research in the Faculty of Medicine and Health Sciences, Stellenbosch University. RV was supported by the National Research Foundation and the Faculty of Medicine and Health Sciences.

Acknowledgments

We would like to thank all participants who participated in this study.

Conflict of interest

The authors declare that the research was conducted in the absence of any commercial or financial relationships that could be construed as a potential conflict of interest.

Publisher's note

All claims expressed in this article are solely those of the authors and do not necessarily represent those of their affiliated organizations, or those of the publisher, the editors and the reviewers. Any product that may be evaluated in this article, or claim that may be made by its manufacturer, is not guaranteed or endorsed by the publisher.

References

Agrawal, V., Patgaonkar,P. R., and Nagariya, S. P. (2010). Tuberculosis of spine. *J. Craniovertebr Junction Spine* 1, 74–85. doi: 10.4103/0974-8237.77671

Beltran, C. G. G., Heunis, T., Gallant, J., Venter, R., du Plessis, N., Loxton, A. G., et al. (2020). Investigating non-sterilizing cure in TB patients at the end of successful anti-TB therapy. *Front. Cell Infect. Microbiol.* 10, 10. doi: 10.3389/fcimb.2020.00443

Chen, C. H., Chen, Y. M., Lee, C. W., Chang, Y. J., Cheng, C. Y., and Hung, J. K. (2016). Early diagnosis of spinal tuberculosis. *J. Formosan Med. Assoc.* 115, 825–836. doi: 10.1016/j.jfma.2016.07.001

Chengalroyen, M. D., Beukes, G. M., Gordhan, B. G., Streicher, E. M., Churchyard, G., Hafner, R., et al. (2016). Detection and quantification of differentially culturable tubercle bacteria in sputum from patients with tuberculosis. *Am. J. Respir. Crit. Care Med.* 194, 1532–1540. doi: 10.1164/rccm.201604-0769OC

Colmenero, J. D., Ruiz-Mesa, J. D., Sanjuan-Jimenez, R., Sobrino, B., and Morata, P. (2013). Establishing the diagnosis of tuberculous vertebral osteomyelitis. *Eur. Spine J.* 22, 579–586. doi: 10.1007/s00586-012-2348-2

Garg, R. K., and Somvanshi, D. S. (2011). Spinal tuberculosis: A review. *J. Spinal Cord Med.* 34, 440–454. doi: 10.1179/2045772311Y.00000000237

Gleeson, L., Raftery, P., Fitzgibbon, M., Mukamolova, G. V., Rogers, T., and Keane, J. (2016). Resuscitation-promoting factor does not enhance mycobacterium tuberculosis culture yield in archival lymph node aspirates. *10.2 Tuberculosis (European Respir. Society)* 48, PA2790. doi: 10.1183/13993003.congress-2016.PA2790

Gordhan, B. G., Peters, J. S., McIvor, A., Machowski, E. E., Ealand, C., Waja, Z., et al. (2021). Detection of differentially culturable tubercle bacteria in sputum using mycob0acterial culture filtrates. *Sci. Rep.* 12, 11. doi: 10.1038/s41598-021-86054-z

Kana, B. D., and Mizrahi, V. (2010). Resuscitation-promoting factors as lytic enzymes for bacterial growth and signaling. *FEMS Immunol. Med. Microbiol.*, 58 39–50. doi: 10.1111/j.1574-695X.2009.00606.x

Kohli, M., Schiller, I., Dendukuri, N., Dheda, K., Denkinger, C. M., Schumacher, S. G., et al. (2018). Xpert® MTB/RIF assay for extrapulmonary tuberculosis and rifampicin resistance. *Cochrane Database Systematic Rev. 2018.* 8 (8), CD012768. doi: 10.1002/14651858.CD012768.pub2

Kumari, R., Tripathi, R., Pandey, A. P., Banerjee, T., Sinha, P., and Anupurba, S. (2016). Rapid screening of MDR-TB in cases of extra pulmonary tuberculosis using geno type MTBDRplus. *PloS One* 7, 11. doi: 10.1371/journal.pone.0159651

Mann, T. N., Schaaf, H. S., Dunn, R. N., Dix-Peek, S., du Preez, K., Lamberts, R. P., et al. (2018). Child and adult spinal tuberculosis at tertiary hospitals in the Western cape, south Africa: 4-year burden and trend. *Epidemiol. Infect.* 146, 2107–2115. doi: 10.1017/S0950268818002649

Molhuizen, H. O., Bunschoten, A. E., Schouls, L. M., and van Embden, J. D. (1998). Rapid detection and simultaneous strain differentiation of mycobacterium tuberculosis complex bacteria by spoligotyping. *Methods Mol. Biol.* 101, 381–394. doi: 10.1385/0-89603-471-2:381

Mukamolova, G. V., Kaprelyants, A. S., Kell, D. B., and Young, M. (2003). Adoption of the transiently non-culturable state — a bacterial survival strategy? *Adv. Microb. Physiol.* 47, 65–129. doi: 10.1016/S0065-2911(03)47002-1

Mukamolova, G. V., Turapov, O., Malkin, J., Woltmann, G., and Barer, M. R. (2010). Resuscitation-promoting factors reveal an occult population of tubercle bacilli in sputum. *Am. J. Respir. Crit. Care Med.* 181, 174–180. doi: 10.1164/rccm.200905-0661OC

O'Connor, B. D., Woltmann, G., Patel, H., Turapov, O., Haldar, P., and Mukamolova, G. V. (2015). Can resuscitation-promoting factors be used to improve culture rates of extra-pulmonary tuberculosis? *Int. J. Tuberculosis Lung Dis.* 19, 1556–1557. doi: 10.5588/ijtld.15.0682

Rosser, A., Pareek, M., Turapov, O., Wiselka, M. J., and Mukamolova, G. V. (2018). Differentially culturable tubercule bacilli are generated during nonpulmonary tuberculosis infection. *Am. J. Respir. Crit. Care Med.* 197, 818–821. doi: 10.1164/rccm.201705-1048LE

Shleeva, M. O., Bagramyan, K., Telkov, M. V., Mukamolova, G. V., Young, M., Kell, D. B., et al. (2002). Formation and resuscitation of 'non-culturable' cells of rhodococcus rhodochrous and mycobacterium tuberculosis in prolonged stationary phase. *Microbiology* 148, 1581–1591. doi: 10.1099/00221287-148-5-1581

Watt, J. P., and Davis, J. H. (2014). Percutaneous core needle biopsies: The yield in spinal tuberculosis. *South Afr. Med. J.* 104, 29–32. doi: 10.7196/SAMJ.6868

frontiers | Frontiers in Cellular and Infection Microbiology

TYPE Original Research
PUBLISHED 02 December 2022
DOI 10.3389/fcimb.2022.981827

OPEN ACCESS

EDITED BY
Bavesh Kana,
University of the Witwatersrand,
South Africa

REVIEWED BY
Suraj P. Parihar,
University of Cape Town, South Africa
Luiz Bermudez,
Oregon State University, United States

*CORRESPONDENCE
Samantha L. Sampson
ssampson@sun.ac.za

SPECIALTY SECTION
This article was submitted to Bacteria and Host, a section of the journal Frontiers in Cellular and Infection Microbiology

RECEIVED 29 June 2022
ACCEPTED 17 November 2022
PUBLISHED 02 December 2022

CITATION
Parbhoo T, Schurz H, Mouton JM and Sampson SL (2022) Persistence of *Mycobacterium tuberculosis* in response to infection burden and host-induced stressors.
Front. Cell. Infect. Microbiol. 12:981827.
doi: 10.3389/fcimb.2022.981827

Persistence of *Mycobacterium tuberculosis* in response to infection burden and host-induced stressors

Trisha Parbhoo, Haiko Schurz, Jacoba M. Mouton and Samantha L. Sampson*

Department of Science and Technology (DSI)- National Research Foundation (NRF) Centre of Excellence for Biomedical Tuberculosis Research (CBTBR), South African Medical Research Council Centre (SAMRC) Centre for Tuberculosis Research, Division of Molecular Biology and Human Genetics, Faculty of Medicine and Health Sciences, Stellenbosch University, Cape Town, South Africa

Introduction: As infection with Mycobacterium tuberculosis progresses, the bacilli experience various degrees of host stressors in the macrophage phagosome such as low pH, nutrient deprivation, or exposure to toxic agents, which promotes cell-to-cell phenotypic variation. This includes a physiologically viable but non- or slowly replicating persister subpopulation, which is characterised by a loss of growth on solid media, while remaining metabolically active. Persisters additionally evade the host immune response and macrophage antimicrobial processes by adapting their metabolic pathways to maintain survival and persistence in the host.

Methods: A flow cytometry-based dual-fluorescent replication reporter assay, termed fluorescence dilution, provided a culture-independent method to characterize the single-cell replication dynamics of M. tuberculosis persisters following macrophage infection. Fluorescence dilution in combination with reference counting beads and a metabolic esterase reactive probe, calcein violet AM, provided an effective approach to enumerate and characterize the phenotypic heterogeneity within M. tuberculosis following macrophage infection.

Results: Persister formation appeared dependent on the initial infection burden and intracellular bacterial burden. However, inhibition of phagocytosis by cytochalasin D treatment resulted in a significantly higher median percentage of persisters compared to inhibition of phagosome acidification by bafilomycin A1 treatment.

Discussion: Our results suggest that different host factors differentially impact the intracellular bacterial burden, adaptive mechanisms and entry into persistence in macrophages.

KEYWORDS

***Mycobacterium tuberculosis*, persistence, persisters, bacterial heterogeneity, host-pathogen interaction, phagocytosis, phagosome acidification**

Introduction

Macrophages represent the first line of defence against *Mycobacterium tuberculosis*, and recognize invading bacteria *via* cell surface receptors [e.g. pattern recognition receptors (PRRs), complement receptors and antibody binding *via* Fc receptors]. This process initiates a series of dynamic host antimicrobial strategies, such as phagocytosis and phagosome acidification, for bacterial engulfment, and antigen presentation (Sia and Rengarajan, 2019).

The phagocytic process is initiated upon pathogen recognition of *M. tuberculosis* pathogen-associated molecular patterns (PAMPs) by host PRRs. *M. tuberculosis* PAMPs include the cell wall components lipoarabinomannan (LAM), mannose-capped lipoarabinomannan (ManLAM), phthiocerol dimycocerosate (PDIM) and mycolic acids, which possess an array of ligands and antigenic moieties that facilitate host recognition in addition to providing a complex lipid structure that enables protection from host defence mechanisms (Stamm et al., 2015). Maturation of the phagosome into the acidic phagolysosome represents an essential host process for degradation of invading microbes by enhancing the antimicrobial capacity and immune signalling processes of macrophages (Rohde et al., 2012). This exposes *M. tuberculosis* to the oxidative and lytic activities of reactive oxygen species (ROS), nitric oxide (NO), and low pH through activity of proton-pumping vacuolar-ATPase (V-ATPase) complexes.

M. tuberculosis has the remarkable ability to persist in the host for long periods of time by undergoing growth arrest and metabolic adaptation in preparation for long-term persistence (Zimmermann et al., 2017; Maurya et al., 2018). Persisters are defined here in accordance with the definition by Balaban et al. (2019), whereby persisters represent a subpopulation of non- or slowly replicating drug-tolerant bacteria within an isogenic population (Balaban et al., 2019). Clinically, this population has been regarded as a pre-existing drug-tolerant population that is actively enriched for during cell division, or during adaption to host stressors prior to antibiotic treatment (Garton et al., 2008; Jain et al., 2016). Persisters remain undetected by current diagnostic tests, yet provide a reservoir for infection relapse during favourable growth conditions (Kana et al., 2008; Chengalroyen et al., 2016).

In this study, calcein violet acetoxymethyl (CV-AM) was utilized as a marker for metabolic esterase activity. CV-AM has previously been utilized for mammalian systems (Lis et al., 2011), and more recently applied to *M. tuberculosis* (Hendon-Dunn et al., 2016; Mishra et al., 2019). Esterase activity, as measured by CV-AM, is suggested to facilitate survival by providing an important intracellular source of energy and carbon for *M. tuberculosis* (Supplementary Table 1). Many *M. tuberculosis* esterases/lipases appear to be upregulated during stress, suggesting the importance of these lipolytic enzymes during adaptation to intracellular survival and persistence (Ghazaei, 2018). CV-AM will thus provide a measure of intracellular enzyme hydrolysis and substrate reactivity of esters containing short-medium chain fatty acids.

A flow cytometry-based technique, termed fluorescence dilution, provided a culture-independent method to characterize the single-cell replication dynamics of *M. tuberculosis* persisters following macrophage infection (Mouton et al., 2016). Fluorescence dilution was utilized in combination with flow cytometry and CV-AM staining to provide insight into the heterogeneous nature of persisters, and for characterization of esterase activity in differentially replicating subpopulations. We further aimed to investigate whether varying infection burdens, and inhibition of phagocytosis and phagosome acidification influences the abundance of persisters internalized by macrophages.

Material and methods

Bacterial strains and plasmids

All reagents were purchased from Sigma-Aldrich (St. Louis, MO, USA), unless otherwise specified. All strains and plasmids utilized in this study is listed in Table 1.

Mycobacterium tuberculosis H37Rv (ATCC, 27294) was cultured in Middlebrook 7H9 media supplemented with 10% OADC (oleic acid-albumin-dextrose-catalase supplement), 0.2% (v/v) glycerol and 0.05% (w/v) Tween-80 (7H9-OGT). An attenuated strain of *M. tuberculosisΔleuDΔpanCD*, as previously constructed (Sampson et al., 2004), was grown at 37°C in 7H9-OGT supplemented with 50 µg/ml leucine and 24 µg/ml pantothenate, with shaking at 180 rpm, until an optical density at 600 nm (OD_{600nm}) of 0.8 (≈ $8x10^7$ CFU/ml) was reached. Selective antibiotics, kanamycin and hygromycin (Thermo Scientific, USA) was added to the cultures when required, at a final concentration of 25 µg/ml and 50 µg/ml, respectively.

For induction of fluorescent proteins under control of the riboswitch promoter, 7H9-OGT was supplemented with 4 mM theophylline for 7 days during culturing.

Mammalian cell culture

RAW 264.7 (ATCC TIB-71) murine macrophages were cultured in Dulbecco's Modified Eagle's Medium (DMEM), supplemented with 10% heat-inactivated fetal bovine serum (FBS) and incubated at 37°C in 5% CO_2 until 80% confluent. Cells were passaged every 2-3 days or upon reaching 80% confluency, at a ratio of 1:6 in DMEM-10% FBS (D10) and incubated at 37°C in 5% CO_2.

Twenty hours prior to infection, 48-well plates were seeded with $2.5x10^5$ macrophages per well, and incubated overnight (37°C, 5% CO_2). Non-adherent macrophages were removed the

TABLE 1 Strains and plasmids utilized in this study.

	Relevant characteristics	Source/Reference
Bacterial strains		
M. tuberculosis H37Rv	Pathogenic lab strain	ATCC 27294
M. tuberculosis Δ*leuD*Δ*panCD*	Double leucine and pantothenate auxotroph, Hyg^R	Sampson et al., 2004
Plasmids		
pTiGc	Dual fluorescent reporter construct, Kan^R Constitutive GFP, TurboFP635 under control of the theophylline inducible riboswitch	Mouton et al., 2016
pST5552	Bacterial Expression vector, Kan^R GFP under control of the theophylline inducible riboswitch	Addgene, USA (Plasmid #36255); Seeliger et al., 2012
pSTCHARGE	Bacterial Expression vector, Kan^R TurboFP635 under control of the theophylline inducible riboswitch	Mouton et al., 2016

Kan^R, Kanamycin resistance; Hyg^R, Hygromycin resistance.

following day by gentle washing with D10, thereafter macrophages were immunologically activated by supplementing D10 with 100 ng/ml lipopolysaccharide (LPS), and incubated at 37°C in 5% CO_2 for 60 min.

Single-cell suspensions of early-exponentially replicating *M. tuberculosis* and *M. tuberculosis* Δ*leuD*Δ*panCD* were prepared for infection by brief sonication in an ultrasonic waterbath (UC-1D, Zeus Automation, South Africa) at 37 kHz for 12 min, followed by filtering through a 40 µm cell strainer (Corning, USA) to reduce cell clumping. *M. tuberculosis* cultures were washed twice in D10 supplemented with 2 mM theophylline and added to the macrophage monolayers at a multiplicity of infection (MOI) of 1:1, 5:1 or 10:1 to obtain varying infection burdens, and incubated for 3 hours (37°C, 5% CO_2). Following bacterial uptake, monolayers were washed with PBS, and the media replaced with D10 containing 2 mM theophylline and 100 U/ml penicillin-streptomycin. Cells were incubated for 60 min (37°C, 5% CO_2) for removal of any extracellular, non-phagocytosed bacteria. Cells were washed three times with PBS, followed by the addition of fresh D10 containing 2 mM theophylline. Theophylline was retained in the media for 24 hours to maintain expression of TurboFP635 under control of the riboswitch-based promoter; this ensured that dilution of fluorescence was detectable over 5 days. The day 0 time-point refers to harvesting of intracellular bacteria following treatment with 100 U/ml penicillin-streptomycin treatment on the day of infection. Treatment with penicillin-streptomycin was performed daily for 5 days. For *in vitro* measurements, bacterial suspensions was added to wells at the time of infection.

Recovery of intracellular bacteria for flow cytometry involved lysing the macrophages with 500 µl distilled sterile water, whereby plates were incubated for 5 min at room temperature to release the intracellular bacteria. For recovery of whole infected macrophages, macrophages were loosened with 100 µl Accutase, and incubated for 10 min at room temperature for optimal detachment. Infected macrophages or intracellular bacteria were transferred to 2 ml screw cap tubes, washed with Hanks' Balanced Salt Solution (HBSS), and transferred to 5 ml polypropylene flow cytometer tubes *via* 35 µm cell strainer caps (Corning, USA) prior to flow cytometric analysis. Where required, cells were fluorescently stained (described below), followed by fixation in 4% formaldehyde (v/v) for 30 min.

Inhibitors of phagocytosis and phagosome acidification

Cytochalasin D (CytD) and bafilomycin A1 (BafA1) were used to inhibit phagocytosis and phagosome acidification, respectively. Inhibitors were hydrated in dimethylsulfoxide (DMSO) for preparation of 1 mM CytD and 20 µM BafA1 master stocks, and stored at -20°C. The minimum optimal concentration for CytD and BafA1 were experimentally determined. To confirm that the DMSO concentration in CytD (0.607% DMSO) and BafA1 (0.05% DMSO) was not detrimental to macrophages, inhibitors were added to uninfected macrophages as a control. Macrophage viability was unaffected throughout infection, as assessed using an MTT assay (data not shown).

Macrophages were pre-treated with 100 ng/ml LPS for 60 min, and following 20 min of treatment, 6 µM CytD or 10 nM BafA1 was added to monolayers and incubated at 37°C in 5% CO_2 for 40 min. Monolayers were washed with PBS, and the media replaced with D10 containing 2 mM theophylline and either CytD or BafA1. *M. tuberculosis*Δ*leuD*Δ*panCD*::pTiGc, pre-induced with 4 mM theophylline 7 days prior to infection, was added to monolayers at MOI 10:1, and incubated for 3 hours (37°C, 5% CO_2). The infection procedure was carried out as described before. Importantly, the possibility of bacterial

reuptake following CytD treatment would have been minimized by daily removal of extracellular bacteria by penicillin-streptomycin treatment. Following the penicillin-streptomycin treatment, BafA1 was re-added to the fresh D10 media each day for 5 days. Uninfected macrophages treated with each inhibitor served as a negative control, and was maintained throughout the 5-day infection. Intracellular bacteria were harvested, fluorescently stained, formaldeyhyde-fixed and prepared for flow cytometric analysis.

Calcein violet-acetoxymethyl

CV-AM (Invitrogen, Life Technologies, USA) is a lipophilic non-fluorescent dye able to permeate the cell membranes of live cells, whereby intracellular esterases cleave the AM group to allow fluorescence. The fluorescent intensity is proportional to the level of functional esterases.

CV-AM was freshly prepared for each experiment by reconstituting a pre-warmed vial in DMSO to prepare a 1 µg/µl working stock. *M. tuberculosis* from *in vitro* cultures or recovered from lysed macrophages was stained with 5 ng/µl CV-AM in 500 µl HBSS for 30 min at 37°C with shaking. Samples were fixed in 4% formaldehyde for 30 min, resuspended in HBSS, and transferred to 5 ml polypropylene flow cytometer tubes *via* a 35 µm cell strainer cap (Corning, USA) for flow cytometric acquisition.

M. tuberculosis::pTiGc was cultured as described above, till OD_{600nm} = 0.5. Cultures were then inoculated at an OD_{600nm} = 0.05, following which the OD_{600nm} was assessed every 2 days for 21 days. Following sampling, an aliquot of culture was resuspended in HBSS to OD_{600nm} = 0.5 (≈ $5x10^7$ bacteria/ml) and stained with CV-AM to ensure a constant dye:cell distribution. To acquire dead cells for the control sample, 1 ml of cells was heat-killed at 95°C for 60 min, stained with CV-AM and formaldeyhyde-fixed prior to flow cytometric acquisition.

pHrodo Green STP ester

To confirm inhibition of phagosome acidification following BafA1 treatment, the pH responsive fluorescent probe, pHrodo Green STP ester (Life Technologies, USA) was utilised. pHrodo Green was hydrated in DMSO to generate 1 mM master stocks, and stored at -20°C. Pre-induced *M. tuberculosisΔleuDΔpanCD*:: pSTCHARGE with 4 mM theophylline for 7 days was adjusted to OD_{600nm} = 1, washed twice with HBSS before resuspending in a 10^{th} of the total volume of 100 mM sodium bicarbonate to stabilize the pH. Cells were stained with 0.5 mM pHrodo Green for 60 min at room temperature, with shaking. Following staining, cells were resuspended in HBSS to 1 ml and washed three times in 1 ml HBSS. To maintain fluorescence of TurboFP635, pHrodo-labelled cells were resuspended in 1 ml 7H9-OGT media containing 4 mM theophylline prior to macrophage infection.

To determine the pH response range of the conjugate, pre-induced pHrodo Green-labelled *M. tuberculosisΔleuDΔpanCD*:: pSTCHARGE with 4 mM theophylline for 7 days was diluted 1:5 to reach OD_{600nm} = 0.2 and exposed to 50 mM potassium phosphate buffers ranging from pH 4.5-7.5. Neutral pH conditions were reflected by non-fluorescence, and increasing fluorescent intensity was observed with increasing acidity. Samples were serially diluted in a black, clear bottom 96-well plate (Corning, USA), and fluorescence readings were taken to determine the signal limit of detection using the FLUOstar Omega 96-well microplate reader (BMG Labtech, Germany). Optical settings were applied using a 584/640 nm and 485/520 nm filter for excitation of TurboFP635 and pHrodo Green, respectively. To limit background noise, the auto-gain adjustment parameter was applied to the positive single-colour controls.

Fifty mM potassium phosphate buffer (pH 4.5-7.5) and 100 mM sodium bicarbonate (pH 8.5) were prepared in distilled water and the pH confirmed using a calibrated pH probe prior to usage. Buffers were filter-sterilized and stored at room temperature until use.

Flow cytometric acquisition

The BD fluorescence-activated cell sorter (FACS) Jazz (Becton Dickinson Biosciences, USA) was used for *M. tuberculosis* sample analysis. To calibrate fluorescence in each detector of the laser, quality control was performed using the 8-peak quality control beads (BD Biosciences, USA).

A primary gate was set on total bacteria based on forward scatter (FSC) and side scatter (SSC) properties and a second gate selected the reference bead population (See below; Invitrogen, USA) for flow cytometric quantification of samples (Figure 1). Fluorescence was acquired using logarithmic scaling in acquisition mode with the detection threshold set on SSC, using the parameters listed in Table 2. For each experiment, compensation was performed using unlabelled and single colour controls.

Thirty-thousand events were captured for all samples, and included a stopping gate selected on live cells (GFP positive). BD FACS Sortware software version 1.1.0.84 generated raw data, which was subsequently processed and analysed using FlowJo software version 10.0.8 (Tree Star Inc., USA). Dot plots were largely utilized for viability analysis, and for setting up gates to determine positivity in fluorescence. Histogram overlays of plots allowed visual detection of the shift in fluorescent signal, and statistical assessment using the median fluorescent intensity (MFI) of each gated population. The MFI of TurboFP635 at a given time was used to calculate the number of bacterial generations, as previously described (Mouton et al., 2016).

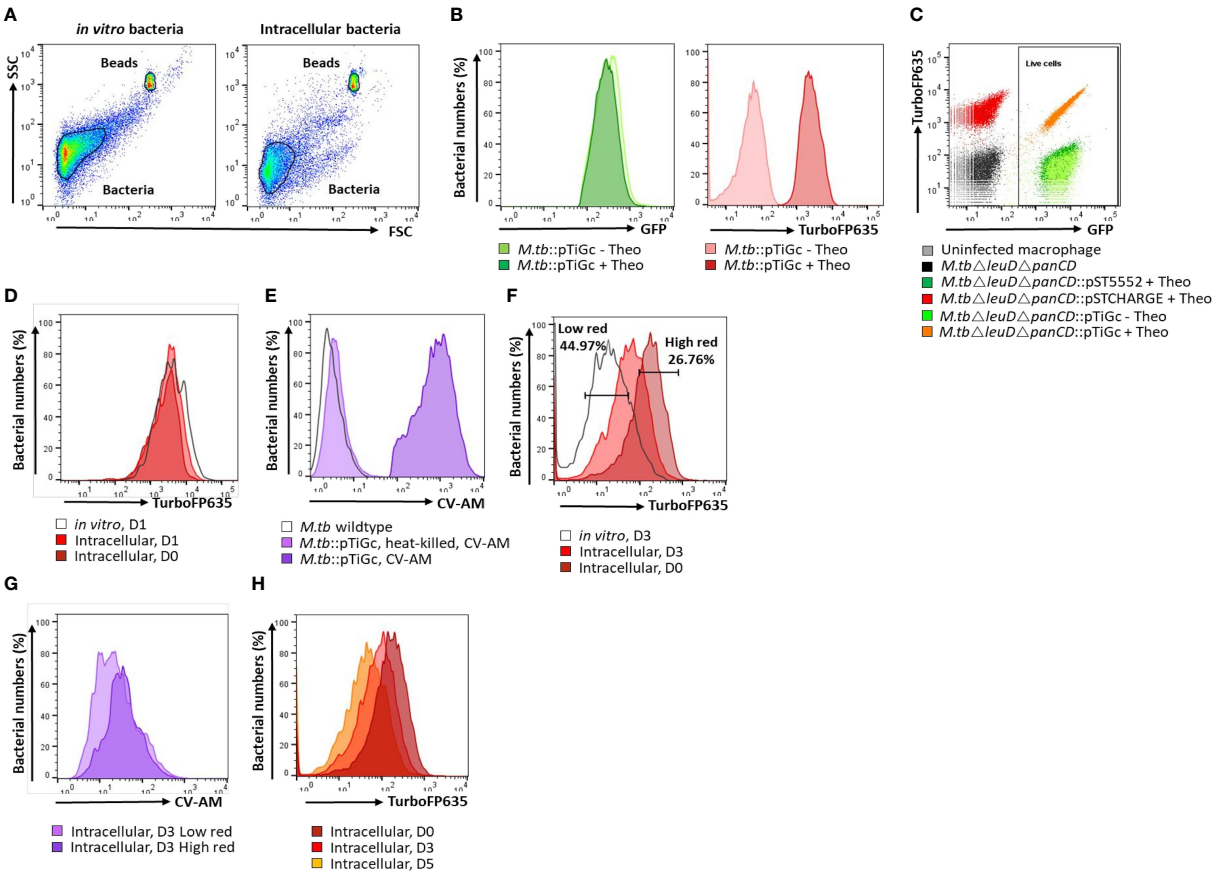

FIGURE 1
Flow cytometry gating strategy. **(A)** A primary gate was applied to the bacterial population according to forward scatter (FSC) and side scatter (SSC) properties. For cell enumeration, a secondary gate was applied to the non-fluorescent bead population. **(B)** *M. tuberculosisΔleuDΔpanCD*::pTiGc was cultured in the presence of 4 mM theophylline to allow induction of the riboswitch-based promoter for expression of TurboFP635. Constitutive expression of GFP is observed, whilst fluorescence of TurboFP635 is observed following induction with theophylline. **(C)** Selecting on the bacterial population, a rectangle gate was created to select for live cells, according to their GFP positivity. Single colour controls ensured optimal voltage settings for positive fluorescence of GFP (pST5552) and TurboFP635 (pSTCHARGE), above that of the autofluorescence of unstained cells. **(D)** The fluorescence dilution technique allows monitoring of bacterial replication for 5 generations. To improve detection of the fluorescent signal to allow measurement over 5 days, theophylline, was retained in culture for 24 hours. Bacterial replication could thus effectively be monitored from day 2 onwards since the fluorescent signal remained stable *in vitro* and intracellularly between day 0 and day 1. **(E)** Following harvesting of intracellular bacteria, cells were stained with CV-AM for analyses of metabolic esterase activity. CV-AM is a non-polar, cell permeable fluorogenic probe that is rapidly hydrolysed to a polar, fluorescent compound by intracellular esterases of live cells. Dead cells no longer possess esterase activity, and will thus not convert to the fluorescent calcein, whilst calcein is stably retained in live cells. **(F)** Selecting on the live cells population, dilution of the TurboFP635 fluorescent signal provided an indication of bacterial replication following removal of the inducer, theophylline (Theo). The high red gate was created based on maximum TurboFP635 fluorescence observed at D0 using the range tool and used to detect mycobacteria that retain their TurboFP635 fluorescence from later time points (D3 and D5), representing slow or non-growing bacteria. The low TurboFP635 gate was created to distinguish replicating intracellular bacteria, as visually assessed when overlayed with *in vitro* day 3 or day 5 bacteria. **(G)** Selecting on the high and low TurboFP635 subpopulations, the esterase activity of intracellular bacteria was assessed by overlaying on a histogram plot. **(H)** Fluorescence dilution of the TurboFP635 signal over time. The geometric median fluorescent intensity (MFI) of TurboFP635 enabled determination of the number of bacterial generations during infection. CV-AM, calcein violet AM.

A calibrated suspension of 6 µm non-fluorescent microsphere reference beads (suspended at $1x10^8$ beads/ml) supplied with the BacLight Live/Dead Bacterial Viability and Counting kit (Invitrogen, USA) was sonicated for 10 min and 5 µl (i.e. $5x10^5$ beads) was added to selected samples. The number of reference beads recorded by flow cytometry was used to enumerate bacterial populations using the following formula (Adapted from ThermoFisher Scientific, 2004):

TABLE 2 Excitation and emission properties of fluorescent probes utilized.

Fluorophore (s)	Ex/Em (nm)	Laser (nm)	Bandpass filter (nm)
GFP	408/509	488	530/40
TurboFP635	588/635	561	610/20
CV-AM	400/452	405	450/50
pHrodo Green	505/525	488	530/40

Ex/Em: excitation and emission wavelengths.

$$\text{Bacteria/ml} = \frac{\text{Bacterial events}}{\text{Bead events}} \times \frac{\#\text{ Beads per sample}}{\text{Sample volume}} \times \text{Bacterial dilution factor}$$

Statistical analysis

Bacterial numbers calculated using the reference beads was quality controlled (QC) and analysed using the R programming environment, version 4.0.3 (RStudio Team, 2020) and GraphPad Prism, version 8.0 (GraphPad Software, USA). QC of the macrophage infection data included removal of samples with outlying *in vitro* and intracellular bacterial counts at day 0, based on visual inspection of box and whisker plots. The cut-off for outliers was determined based on the distribution of the data, whereby data points outside 1.5 times of the interquartile range above the upper and below the lower quartile were removed.

To compare distributions, a one-way repeated measures ANOVA was implemented to detect significant differences in bacterial numbers or MFI (*in vitro* and intracellular) between three or more groups at different time points. Following a significant ANOVA result, a *post hoc* multiple comparison test was done to compare the distribution of data between two groups using the 2-sided (unpaired) Students t-test or Wilcoxon Rank-Sum test with Bonferroni multiple test correction for parametric or non-parametric data, respectively. Distribution of the data was inspected visually for normality using QQ-plots. The significance threshold for all analysis was set to a Bonferroni corrected p-value < 0.05.

To determine the extent of correlation between the infection burden and intracellular bacterial burden, against persister numbers at day 3 and day 5, the Pearson's product-moment correlation or Kendall Tau correlation test was utilised for parametric or non-parametric data, respectively. The strength of the correlation was assessed using the square of the Pearson product moment correlation coefficient (r^2) or Kendall's Tau correlation coefficient (τ) and associated p-value. For a visual comparison, non-linear local regression lines with 95% confidence interval were added to the correlation plots using the R loess function from the nlshelper package (Duursma, 2017).

Results

Influence of initial infection burden and subsequent intracellular bacterial burden on persister numbers

The double auxotrophic *M. tuberculosis*Δ*leuD*Δ*panCD* strain utilized in this study provides a model organism for *M. tuberculosis* research, which recapitulates salient features of the physiology, replication dynamics and response to treatment of *M. tuberculosis* H37Rv (Mouton et al., 2019). The attenuated strain is additionally safe for use in biosafety level 2 facilities (Sampson et al., 2004). In previous work, the non- or slowly replicating *M. tuberculosis* persister subpopulation was observed 3 days following macrophage uptake, as identified using fluorescence dilution in combination with flow cytometry (Mouton et al., 2016). The fluorescence dilution reporter, pTiGc, contains a constitutive reporter (GFP) for tracking of viable bacteria, whilst an inducible reporter (TurboFP635) allows measurement of bacterial replication (see gating strategy, Figure 1). This approach exploits the principle that following induction, the inducible fluorescent signal will halve with each successive cell division after removal of the inducer, and allows monitoring of bacterial replication for 5 generations. Bacterial cells not undergoing replication or existing in a slowly replicating state, such as persisters, will retain their TurboFP635 fluorescent signal (Helaine et al., 2010). Following flow cytometric detection, the persister subpopulation was confirmed to be antibiotic tolerant following exposure to the antibiotic D-cycloserine. Proportions of persisters were similar in D-cycloserine -treated *vs* non-treated samples, confirming that the non-replicating cells observed with fluorescence dilution are indeed drug-tolerant persisters (Mouton et al., 2016).

To determine whether the number and percent of persisters observed at day 3 and day 5 is influenced by the initial infection burden, macrophages were infected with varying bacterial numbers. Here, initial infection burden refers to the number of bacteria applied to infect the macrophages, and the initial intracellular burden refers to the number of bacteria taken up by macrophages (day 0). Retention of theophylline in the growth media for 24 hours following infection ensured that the fluorescent signal of TurboFP635 would remain detectable by day 5 should initial early replication and TurboFP635 dilution occur (Figure 1D). Enumeration of intracellular *M. tuberculosis*Δ*leuD*Δ*panCD* using reference beads in combination with flow cytometry provided an effective culture-free approach for counting heterogeneous populations.

To assess whether varying infection burdens influenced intracellular bacterial numbers, the intracellular live bacterial population was enumerated using reference beads, by flow cytometry. The initial infection burden (day 0 *in vitro* bacteria/ml) displayed a significant positive correlation with

the intracellular bacterial burden at day 0 ($p = 2.20e^{-16}$; Figure 2A). We next assessed the impact of different initial infection and later intracellular bacterial burdens on absolute persister numbers at day 3 and day 5. The initial infection burden significantly correlated with the number of actively replicating bacteria and persisters at day 3 (p-values = $2.20e^{-16}$; Figure 2B) and day 5 (p-values < $2.20e^{-16}$; Figure 2C). Similarly, the intracellular burden significantly correlated with the respective number of actively replicating bacteria and persisters at day 3 (p-values = $2.20e^{-16}$; Figure 3A) and day 5 (p-values = $2.20e^{-16}$; Figure 3B).

In support of the results above, a strong positive correlation between actively replicating bacteria and persister numbers was observed at day 3 ($p = 2.20e^{-16}$; Figure 4A) and day 5 ($p = 4.44e^{-16}$; Figure 4B) following infection. Whilst a strong linear correlation between actively replicating and persister numbers was observed at day 3, the correlation began to skew towards a non-linear relationship at day 5 (Figure 4C). Although the increase in actively replicating bacterial numbers was minimal and not significant ($p = 0.432$; Figure 4C), this does indicate continued growth of the actively replicating bacteria throughout the infection (Figure 2C, 3, 4). Persisters contrastingly possessed similar bacterial numbers between days 3 and 5 ($p = 0.321$; Figure 4C). Whilst persister numbers may appear greater for higher initial infection burdens, a similar median percentage of persisters, which is an absolute count of persisters relative to the overall intracellular burden was observed across all infection burdens from day 3 to day 5 (24.25% to 23.25%; $p = 0.784$; Figure 4D). This likely indicates a fixed frequency of bacteria in the starting population that go on to form persisters, irrespective of the infection burden.

Persister numbers are influenced by macrophage-associated antimicrobial responses

To determine the impact that selected host processes may have on the ability of *M. tuberculosisΔleuDΔpanCD* to enter a persister state, we exploited inhibitors of macrophage phagocytosis and phagosome acidification. Firstly, cytochalasin D (CytD) was used to inhibit F-actin polymerization, a process crucial for phagocytosis. Previous analysis showed that CytD

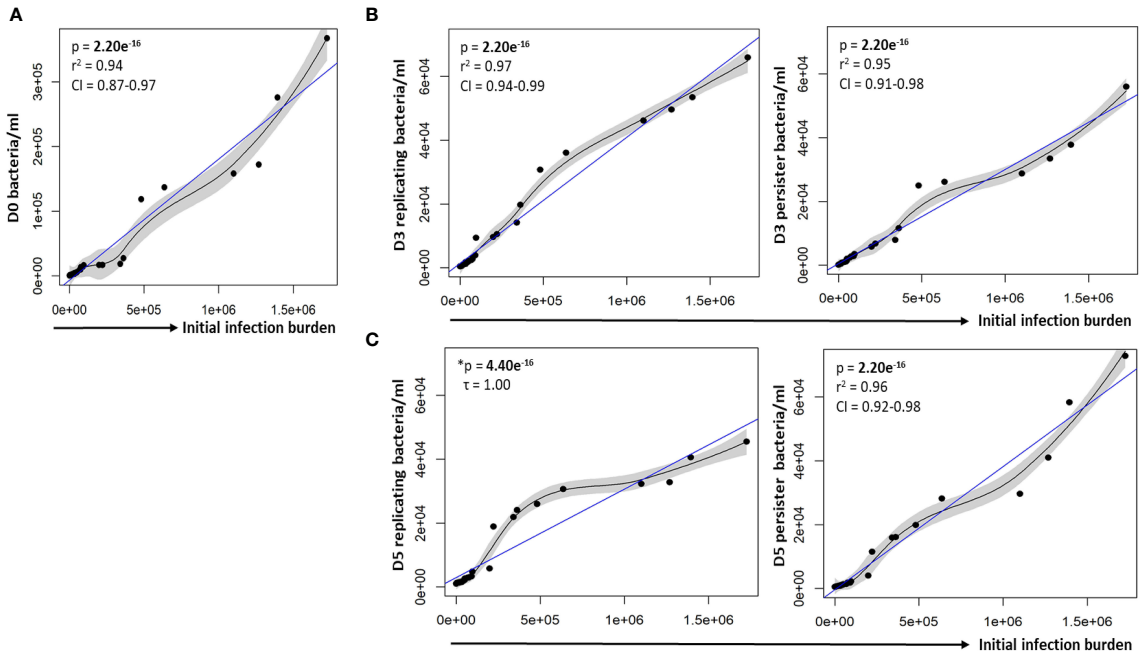

FIGURE 2
Correlation between the infection burden and growth of intracellular bacteria. **(A)** Macrophages were infected with varying bacterial burdens. Cell enumeration using reference counting beads was used to establish the correlation between the initial infection burden (D0 *in vitro* bacteria/ml) and intracellular bacteria following uptake. Significant positive correlations between the initial infection burden and actively replicating bacteria or persisters was observed at **(B)** day 3 and **(C)** day 5. Data was assessed using the Pearson's product-moment correlation (linear) and is representative of data independently conducted in 7 biological experiments, including technical triplicates. *The Kendall's Tau correlation was used to determine the non-linear correlation coefficient tau (τ). Significant p-values ($p < 0.05$) are shown in bold. The blue line represents the regression line for the correlation analyses (Pearson and Kendall), while the black line and associated shaded area represents the local non-linear regression and 95% confidence interval. r^2, Pearson's correlation coefficient squared; CI, 95% confidence interval; SEM, standard error of mean.

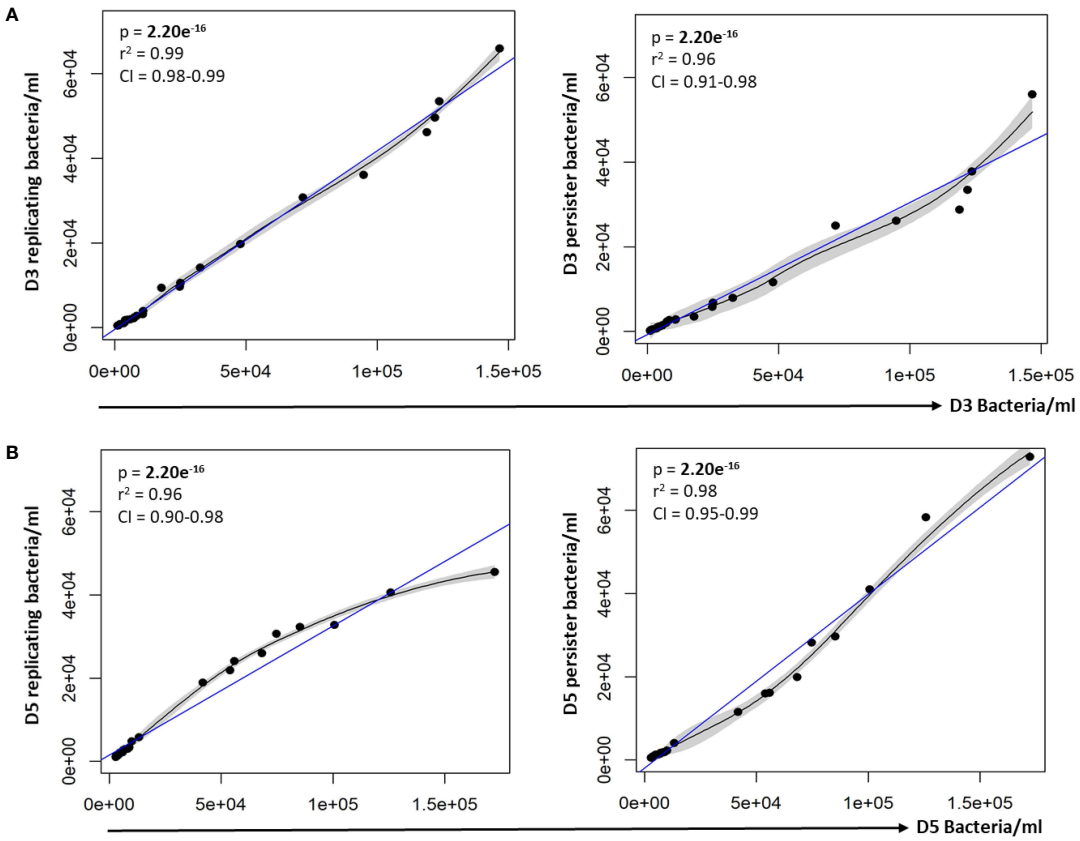

FIGURE 3
Persister numbers correlated with respective intracellular bacterial numbers. A strong correlation between the infection burden observed at **(A)** day 3 and **(B)** day 5 in relation to the respective persister numbers was observed on the scatter plot. Data was assessed using the Pearson's product-moment correlation (linear) and is representative of data independently conducted in 7 biological experiments, including technical triplicates. Significant p-values ($p < 0.05$) are shown in bold. The blue line represents the regression line for the correlation analyses (Pearson), while the black line and associated shaded area represents the local non-linear regression and 95% confidence interval. r^2, Pearson's correlation coefficient squared; CI, 95% confidence interval.

effectively decreased bacterial uptake, inhibited macrophage apoptosis and decreased secretion of pro-inflammatory cytokines (Ding et al., 2005; Basu et al., 2007; Rohde et al., 2007). Further, an inhibitor of the V-ATPase proton pump, Bafilomycin A1 (BafA1), was utilized to inhibit phagosome acidification. BafA1 has been shown to prevent phagosome acidification and autophagy by inhibiting V-ATPase (Simeone et al., 2015; Smyth et al., 2021).

As expected, following CytD treatment, significantly lower bacterial numbers were recovered from macrophages following internalization compared to untreated samples ($p = 1.15e^{-2}$; Figure 5A). The reduced uptake of bacteria was further confirmed by the significantly increased bacterial numbers harvested from the supernatant of CytD-treated macrophages compared to untreated macrophages following bacterial uptake ($p = 3.39e^{-2}$; Figure 5A). A 3.42 fold decrease in median bacterial numbers was observed following CytD treatment compared to bacterial numbers in untreated macrophages following internalization, confirming its ability to inhibit phagocytosis (Figure 5A).

A similar initial intracellular bacterial burden was observed between untreated and BafA1-treated macrophages at day 0, confirming that BafA1 treatment did not influence bacterial uptake ($p = 1.000$; Figure 5A). Inhibition of phagosome acidification was confirmed by labelling *M. tuberculosis* Δ*leuD*Δ*panCD* with a lipophilic pH-responsive fluorescent probe, pHrodo Green, which emits increasing fluorescence intensity with a decreasing pH environment (Figure 6). pHrodo-labelling was however not suited for monitoring the intracellular pH environment over multiple days due to reduction in pHrodo fluorescence with cell division (result not shown). In addition, formaldehyde fixation greatly reduced pHrodo fluorescence (result not shown). For these reasons, the pH environment could not be assessed throughout infection, although we could confirm reduced phagosome acidification at the start of infection.

10.3389/fcimb.2022.981827

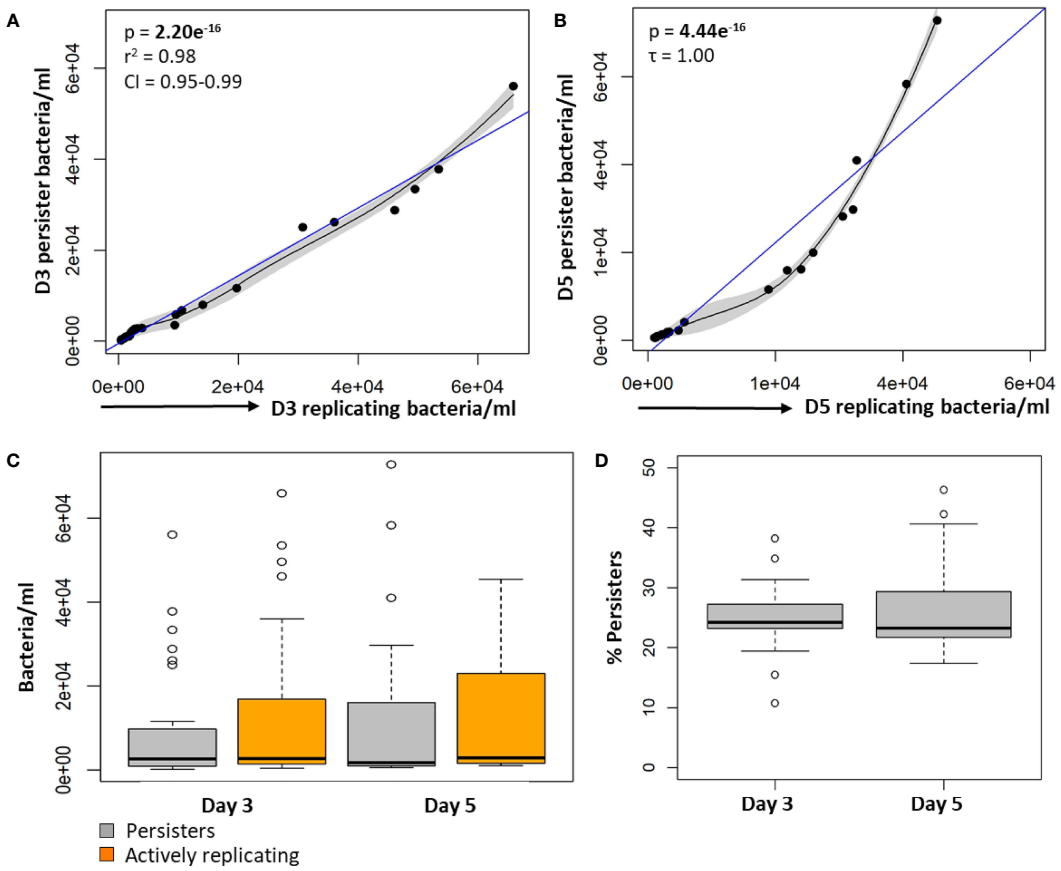

	D3 replicating vs D3 persister	D5 replicating vs D5 persister	D3 persister vs D5 persister	D3 replicating vs D5 replicating
p-value	0.448	0.179	0.321	0.432

FIGURE 4
Persister numbers correlated with the number of intracellular growing mycobacteria in macrophages. Significant positive correlations were observed between actively replicating bacteria and respective persister numbers at **(A)** day 3 and **(B)** day 5. **(C)** No significant difference between bacterial numbers was observed between day 3 and day 5 (Wilcoxon test). **(D)** The median percentage of persisters in relation to the respective intracellular bacterial numbers was assessed. No significant differences in the median percentage of persisters between days 3 and 5 was observed (p = 0.784; Wilcoxon test). Correlations were assessed using the Pearson's product-moment (linear), or Kendall's Tau correlation (non-linear). The blue line represents the regression line for the correlation analyses (Pearson and Kendall), while the black line and associated shaded area represents the local non-linear regression and 95% confidence interval. Box and whisker plots express distribution of data, indicating the median (bold line), interquartile range (box), and range (whiskers). The data was independently conducted in 7 biological experiments, including technical triplicates. Significant p-values ($p < 0.05$) are shown in bold. r^2, Pearson's correlation coefficient squared; CI, 95% confidence interval; τ, Tau correlation coefficient.

The fluorescence dilution reporter was subsequently exploited to calculate the number of bacterial generations at different time points, based on the TurboFP635 MFI. The number of bacterial generations in untreated macrophages increased over 5 days, displaying approximately 2 generations by day 3 (1.989 ± 0.083), and approximately 3 generations by day 5 (2.890 ± 0.066; Figure 5D). Despite the intracellular bacterial numbers steadily increasing over 5 days following CytD treatment, the lower number of bacterial generations observed between day 3 (1.486 ± 0.133) and day 5 (2.320 ± 0.093; Figure 5D) implies slower bacterial growth in CytD-treated macrophages compared to bacteria from untreated and BafA1-treated macrophages.

Significantly higher median numbers of actively replicating bacteria compared to persister numbers were observed in untreated samples at day 3 and day 5 (p-values $< 6.52e^{-3}$; Table 3). Contrastingly, no significant differences in median numbers between actively replicating and persister bacteria were observed at and between day 3 and day 5 following CytD treatment (p-values = 1.000; Figure 7A, B; Tables 3, 4).

10.3389/fcimb.2022.981827

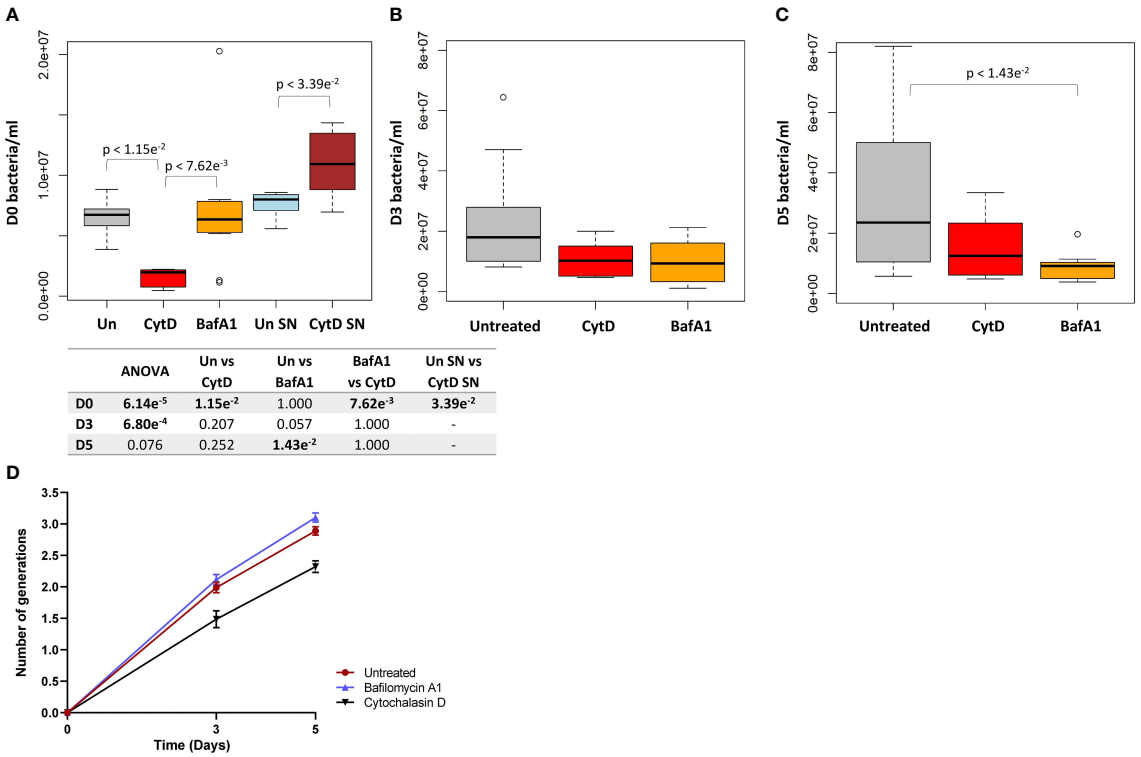

	ANOVA	Un vs CytD	Un vs BafA1	BafA1 vs CytD	Un SN vs CytD SN
D0	**6.14e^{-5}**	**1.15e^{-2}**	1.000	**7.62e^{-3}**	**3.39e^{-2}**
D3	**6.80e^{-4}**	0.207	0.057	1.000	-
D5	0.076	0.252	**1.43e^{-2}**	1.000	-

FIGURE 5
Intracellular bacterial growth following treatment with inhibitors of phagocytosis and phagosome acidification. Macrophages were either untreated or pre-treated with 6 μM CytD or 10 nM BafA1 for 40 min prior to infection with *M. tuberculosisΔleuDΔpanCD*::pTiGc pre-induced with 4 mM theophylline. **(A)** Following internalization, macrophages were lysed and intracellular bacteria was harvested for flow cytometry. A 3.42 fold decrease in the median bacterial uptake was detected following CytD treatment compared to untreated macrophages at day 0 ($p = 1.15e^{-2}$). The supernatant following bacterial uptake displayed significantly increased bacterial numbers following CytD treatment ($p = 3.39e^{-2}$), confirming inhibition of phagocytosis of *M. tuberculosisΔleuDΔpanCD*::pTiGc. Uptake of bacteria was unaffected by BafA1 treatment compared to bacterial numbers harvested from untreated macrophages (p = 1.000). The effect of the inhibitors on bacterial growth were assessed at **(B)** day 3 and **(C)** day 5 post infection. Bacterial numbers following CytD treatment remained similar to untreated macrophages at day 3 and day 5 (p-values > 0.207), whilst a significant decrease in bacterial numbers following BafA1 treatment was observed at day 5 compared to untreated macrophages ($p = 1.43e^{-2}$). Box and whisker plots express distribution of data independently conducted in biological triplicate, including technical triplicates, indicating the median (bold line), interquartile range (box), and range (whiskers). Significance testing between groups was assessed by repeated measures ANOVA and pairwise Students t-test with Bonferroni correction; significant p-values ($p < 0.05$) are shown in bold. **(D)** The number of intracellular bacterial generations from day 3 to day 5 for untreated (1.989 ± 0.083 to 2.890 ± 0.066), CytD (1.486 ± 0.133 to 2.320 ± 0.093), and BafA1 (2.115 ± 0.082 to 3.103 ± 0.074) increased over time. Despite lower bacterial numbers recorded following CytD treatment, the number of bacterial generations steadily increased, similarly to the untreated and BafA1-treated group. Plots represent data independently conducted in 4 biological experiments, including technical triplicates, indicating mean ± SEM. Un, untreated; SN, supernatant; SEM standard error of mean.

Comparisons of the median bacterial numbers between untreated and CytD-treated macrophages revealed no significant differences for either actively replicating or persister bacteria at day 3 and day 5 (p-values > 0.154; Figure 7A, B; Table 3). A significantly higher median percentage of persisters was however observed at day 5 following CytD treatment compared to the untreated group ($p = 8.10e^{-3}$; Figure 7D), but not at day 3 (p = 0.070; Figure 7C; Table 3).

Whilst BafA1 treatment did not influence initial bacterial uptake at day 0, (Figure 5A), significantly reduced bacterial numbers were recorded at day 5 ($p = 1.43e^{-2}$; Figure 5C), but not at day 3, compared to untreated macrophages (p = 0.057; Figure 5B). Following BafA1 treatment, an increased number of bacterial generations from day 3 (2.115 ± 0.082) to day 5 (3.103 ± 0.074) was observed, suggesting faster bacterial growth, similarly to bacteria recovered from untreated macrophages (Figure 5D).

Actively replicating bacterial numbers were significantly lower following BafA1 treatment compared to untreated bacteria at day 3 (p = 0.027; Figure 7A) and day 5 ($p = 1.33e^{-3}$; Figure 7B; Table 3). The stronger significant association at day 5 could be a direct result of the bacterial loss from the BafA1-

10.3389/fcimb.2022.981827

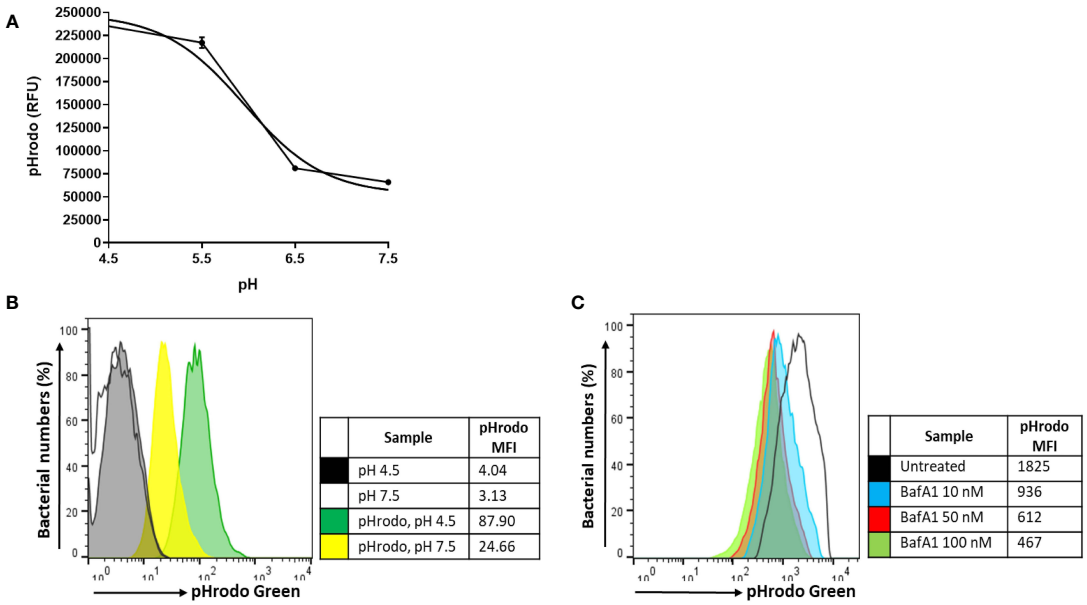

FIGURE 6
pH calibration of pHrodo Green. **(A)** Exponentially growing *M. tuberculosisΔleuDΔpanCD*::pSTCHARGE was labelled with 0.5 mM pHrodo Green, exposed to potassium phosphate buffers ranging between pH 4.5-7.5, and visualized spectrophotometrically. A sigmoidal line of best fit was applied to the graph using GraphPad Prism, generating a pH lookup table to accurately determine the pH (Supplementary Table 2). Results are representative of triplicate samples, displaying geometric mean ± SD, and involved the removal of background fluorescence from unstained cells. **(B)** Unfixed macrophages infected with unlabelled or pHrodo-labelled *M. tuberculosisΔleuDΔpanCD*::pSTCHARGE pre-induced with 4 mM theophylline were harvested and exposed for 60 min to pH 4.5 and pH 7.5 potassium phosphate buffers to determine whether a change in intracellular fluorescence could be observed using flow cytometry. The increase in pHrodo MFI reflects the decrease in pH. **(C)** Macrophages were pre-treated with increasing concentrations of BafA1 40 min prior to infection with pHrodo-labelled *M. tuberculosis ΔleuDΔpanCD*::pSTCHARGE pre-induced with 4 mM theophylline. Intact macrophages were harvested following internalization and resuspended in HBSS buffer (unfixed) prior to analysis using flow cytometry. Live cells were gated according to TurboFP635 positivity, thereafter pHrodo fluorescence was assessed. Increasing BafA1 concentrations led to a decrease in pH as detected by the decreasing pHrodo MFI. To minimize possible adverse effects associated with higher DMSO concentrations, 10 nM BafA1 was applied to subsequent experiments. Results are representative of data independently conducted in biological triplicate, including technical triplicates. MFI, median fluorescence intensity; RFU, relative fluorescence units.

treated macrophages. Despite this, no significant difference in median persister numbers (p-values > 0.539; Figure 7A, B; Table 3) and median percentage of persisters (p-values > 0.510; Figure 7C, D) were observed at day 3 and day 5 between untreated and BafA1-treated macrophages. Whilst actively replicating bacterial numbers significantly increased in the untreated group between days 3 and 5 (p = 0.039; Table 4), no significant increase in median numbers of actively replicating bacteria or persisters were observed following BafA1 treatment (p-values = 1.000; Table 4).

TABLE 3 Comparison of bacterial numbers at day 3 and day 5.

Group 1	Group 2	Day 3 p-value	Day 5 p-value
ANOVA		**0.006**	**0.034**
BafA1 persisters	BafA1 replicating	0.182	1.000
BafA1 persisters	CytD persisters	1.000	1.000
CytD persisters	CytD replicating	1.000	1.000
BafA1 persisters	Untreated persisters	0.539	1.000
CytD persisters	Untreated persisters	1.000	1.000
BafA1 replicating	Untreated replicating	**0.027**	**$1.33e^{-3}$**
CytD replicating	Untreated replicating	0.154	0.191
Untreated persisters	Untreated replicating	**$6.52e^{-3}$**	**$5.45e^{-4}$**

p-values below the statistical significance threshold ($p < 0.05$) are shown in bold; ANOVA repeated measures and *post-hoc* pairwise Students t-test (unpaired) with Bonferroni correction. p-values below the statistical significance threshold ($p < 0.05$) are shown in bold.

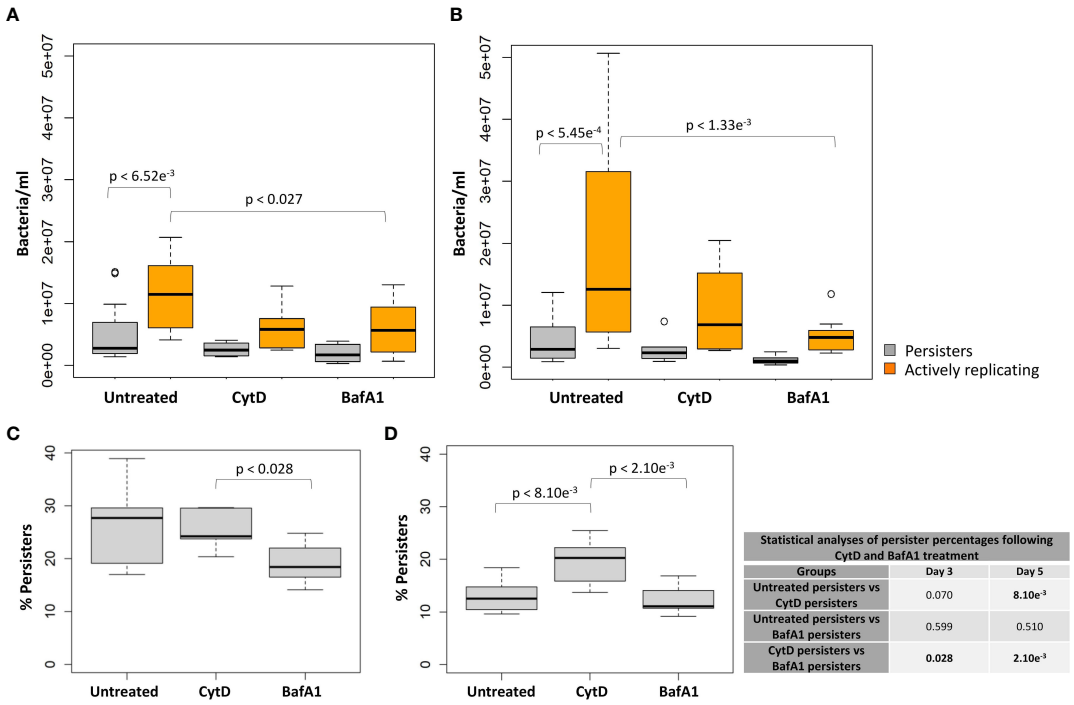

FIGURE 7
Macrophage antimicrobial processes impact *M. tuberculosis* persister formation. The persister subpopulation was visually assessed using flow cytometry at day 3 and day 5. Significant differences between groups was observed at **(A)** day 3 ($p = 0.006$) and **(B)** day 5 ($p = 0.034$; repeated measures ANOVA). p-values are listed in Table 3. The median percentage of persisters in relation to the respective intracellular bacterial numbers was assessed at **(C)** day 3 and **(D)** day 5. Significance testing between persister percentages was assessed using a pairwise Students t-test (unpaired) with Bonferroni correction; significant p-values ($p < 0.05$) are shown in bold. Box and whisker plots express distribution of data independently conducted in 4 biological experiments, including technical triplicates, indicating the median (bold line), interquartile range (box), and range (whiskers).

Significantly different intracellular bacterial numbers were observed between CytD and BafA1 groups at day 0 ($p = 7.62e^{-3}$; Figure 5A), but not at day 3 or day 5 (p-values = 1.000; Figure 5B, C). Despite similar numbers of intracellular bacteria between CytD- and BafA1-treated groups, a significantly higher median percentage of persisters was observed following CytD treatment at day 3 ($p = 0.028$; Figure 7C) and day 5 ($p = 2.10e^{-3}$; Figure 7D).

TABLE 4 Comparison of bacterial numbers between days 3 and 5.

Group 1	Group 2	p-value
ANOVA		**$6.877e^{-08}$**
D3 BafA1 persisters	D5 BafA1 persisters	1.000
D3 BafA1 replicating	D5 BafA1 replicating	1.000
D3 CytD persisters	D5 CytD persisters	1.000
D3 CytD replicating	D5 CytD replicating	1.000
D3 untreated persisters	D5 untreated persisters	1.000
D3 untreated replicating	D5 untreated replicating	**0.039**

p-values below the statistical significance threshold ($p < 0.05$) are shown in bold; ANOVA repeated measures and *post-hoc* pairwise Students t-test (unpaired) with Bonferroni correction. p-values below the statistical significance threshold ($p < 0.05$) are shown in bold.

M. tuberculosis persisters possess metabolic esterase activity

To establish the use of CV-AM as a metabolic marker, *M. tuberculosis*::pTiGc was sampled *in vitro* during varying growth states to determine the influence of growth phase on *M. tuberculosis* metabolic esterase activity (Supplementary Figure 1). Here, we applied CV-AM staining for assessment of the esterase activity in differentially replicating bacterial populations harvested from macrophages at day 3 and day 5 following internalization. The wide range in distribution of esterase activity is indicative of heterogeneous metabolic activity, whereby bacteria (actively replicating and persisters) may exist in varying metabolic states.

For the different bacterial burdens assessed, a significant positive correlation between the MFI of CV-AM for persisters and actively replicating bacteria was observed at day 3 and day 5

(p-values = $2.20e^{-16}$; Figure 8). As a result, there were no significant differences between the esterase activity of actively replicating bacteria and persisters at day 3 and day 5 (p-values > 0.188; Supplementary Figure 2). Furthermore, no significant difference in the esterase activity for actively replicating bacteria (p = 0.136) and persisters (p = 0.854) was detected between days 3 and 5 (Supplementary Figure 2).

Repeated measures ANOVA analysis revealed significant differences in the esterase activity of mycobacteria from untreated, CytD- and BafA1-treated groups at day 5 (p = $7.35e^{-8}$; Table 5) and between days 3 and 5 (p = $8.86e^{-9}$; Table 6). Persister bacteria displayed a significant increase in esterase activity compared to actively replicating bacteria for the untreated (p = 0.047) and BafA1-treated group (p = 0.046) at day 3, whilst no significant difference was observed at day 5 (p-values > 0.420; Table 5). Furthermore, a significant increase in the esterase activity of persisters was observed from days 3 to 5 following BafA1 treatment (p = $5.22e^{-4}$; Figure 9; Table 6).

Whilst the esterase activity of persisters in the CytD-treated group was slightly elevated compared to the actively replicating bacteria, this was not significant at day 3 or day 5 (p-values = 1.000; Figure 9; Table 5). Similarly, the higher esterase activity observed for persisters following BafA1 treatment was not significantly different to persisters following CytD treatment at day 3 and day 5 (p-values > 0.141).

Heterogeneity in esterase activity was observed in persisters and actively replicating bacteria. Together, this shows that persisters possess esterase activity inside macrophages; the change in esterase activity between day 3 and day 5 could further suggest the temporal nature of metabolic processes during intracellular infection.

Discussion

Diversity in lesion size and bacterial burden have previously been observed in granulomas from non-human primates, where bacilli within the same microenvironment may exist in varying physiological and metabolic states (Lin et al., 2014; Martin et al., 2017). This facilitates the selection of subpopulations more suited to adapt and persist during unfavourable conditions in the host by entering a non- or slowly replicating persistent state, which was effectively observed in macrophage infection models using fluorescence dilution in combination with flow cytometry, as reported in this study and previously (Mouton et al., 2016).

Persister numbers were strongly correlated to the initial infection burden, and the number of intracellular actively replicating bacteria at day 3 and day 5. Irrespective of the varying intracellular bacterial burden in macrophages, this did not lead to significantly different absolute numbers or median percentage of persisters at and between day 3 and day 5.

Since cytokines control macrophage activation and maturation (Marino et al., 2015), it is likely that immune signalling and the antimicrobial activity may be differentially regulated during inhibition of phagocytosis by CytD. Despite significantly lower bacterial numbers observed following inhibition of phagocytosis, CytD treatment resulted in a significantly higher median percentage of persisters at day 5

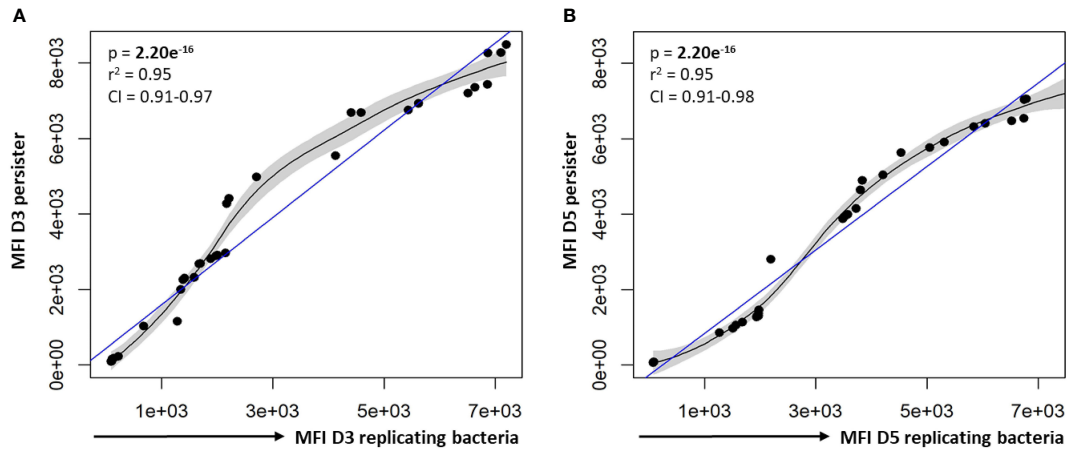

FIGURE 8
Correlation between the esterase activity of actively replicating bacteria and persisters. The esterase activity of intracellular bacteria was assessed following CV-AM staining and flow cytometric analysis. Significant positive correlations were observed between the esterase activity of actively replicating bacteria and persisters at **(A)** day 3 and **(B)** day 5. Data was assessed using the Pearson's product-moment correlation (linear) and is representative of data independently conducted in 7 biological experiments, including technical triplicates. Significant p-values ($p < 0.05$) are shown in bold. The blue line represents the regression line for the correlation analyses (Pearson), while the black line and associated shaded area represents the local non-linear regression and 95% confidence interval. r^2, Pearson's correlation coefficient squared; CI, 95% confidence interval; MFI, median fluorescent intensity.

TABLE 5 Metabolic activity between groups at day 3 and day 5.

Group 1	Group 2	Day 3 p-value	Day 5 p-value
ANOVA		0.198	**$7.35e^{-8}$**
BafA1 persisters	BafA1 replicating	**0.046**	0.420
BafA1 persisters	CytD persisters	0.141	0.159
BafA1 replicating	CytD replicating	1.000	0.461
CytD persisters	CytD replicating	1.000	1.000
BafA1 persisters	Untreated persisters	1.000	0.138
CytD persisters	Untreated persisters	0.557	1.000
CytD replicating	Untreated replicating	1.000	1.000
Untreated persisters	Untreated replicating	**0.047**	1.000

p-values below the statistical significance threshold ($p < 0.05$) are shown in bold; ANOVA repeated measures and *post-hoc* pairwise Students t-test (unpaired) with Bonferroni correction. p-values below the statistical significance threshold ($p < 0.05$) are shown in bold.

TABLE 6 Metabolic activity between days 3 and 5.Group 1.

	Group 2	p-value
ANOVA		**$8.865e^{-09}$**
D3 BafA1 persisters	D5 BafA1 persisters	**$5.22e^{-04}$**
D3 BafA1 replicating	D5 BafA1 replicating	**$3.02e^{-03}$**
D3 CytD persisters	D5 CytD persisters	0.502
D3 CytD replicating	D5 CytD replicating	1.000
D3 untreated persisters	D5 untreated persisters	0.696
D3 untreated replicating	D5 untreated replicating	1.000

p-values below the statistical significance threshold ($p < 0.05$) are shown in bold; ANOVA repeated measures and post-hoc pairwise Students t-test (unpaired) with Bonferroni correction. p-values below the statistical significance threshold ($p < 0.05$) are shown in bold.

post infection, compared to bacteria harvested from untreated macrophages. Accordingly, CytD-treated murine macrophages infected with *M. tuberculosis*, and *M. tuberculosis* clinical isolates associated with severe tuberculosis have been suggested to exploit mechanisms to inhibit cytosolic recognition, and subsequently lower host pro-inflammatory cytokine release (Sousa et al., 2020). *M. tuberculosis* furthermore promotes host macrophage differentiation towards the M2 macrophage phenotype, thereby subverting the host immune response by inhibiting inflammatory cytokine release, which enhances intracellular survival and persistence (Refai et al., 2018). *M. tuberculosis* thus appears to use macrophages as residence whilst overcoming host immune evasion strategies.

Following inhibition of phagosome acidification by BafA1 treatment, median persister percentages were not significantly different to untreated macrophages at day 3 and day 5. It is plausible that the reduction in intracellular bacterial numbers observed in our study at day 5 was attributed to extracellular release of *M. tuberculosis* due to continued cell replication and subsequent overburdening of the macrophage. Contrasting reports in the literature indicates that intracellular *M. tuberculosis* numbers are differentially impacted by the infection burden, host cell type and activation state (Lee et al., 2006; Welin et al., 2011; Sullivan et al., 2012; Mehta et al., 2016). Furthermore, *M. tuberculosis* induces an ESX-1-dependent secretion of host pro-inflammatory cytokines as an adaptive

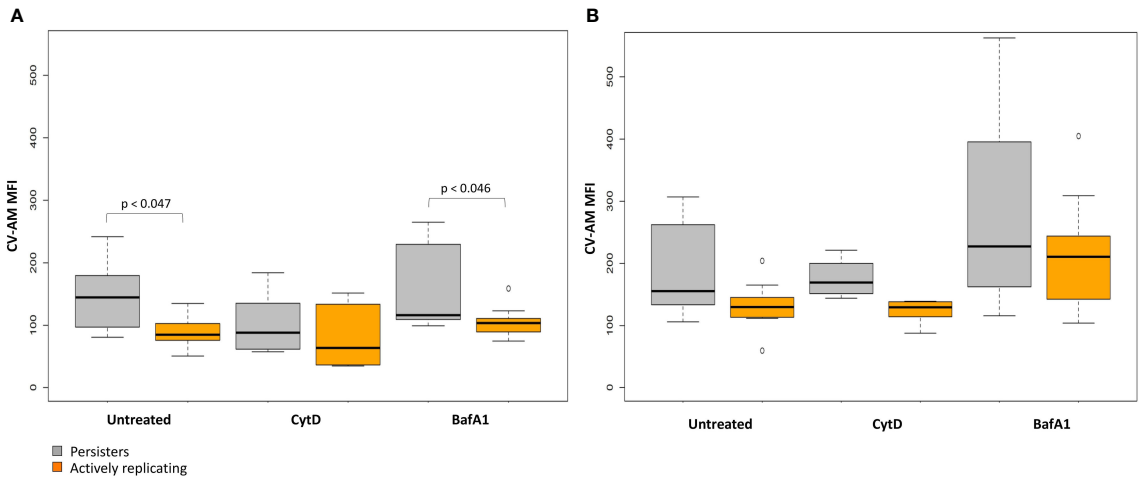

FIGURE 9
Metabolic esterase activity of persisters is influenced by macrophage antimicrobial processes. The MFI of CV-AM from the actively replicating and persister subpopulations was assessed at day 3 and day 5. No significant differences between groups was observed at **(A)** day 3 ($p = 0.198$), **(B)** whilst significant differences between groups was observed at day 5 ($p = 7.35e^{-8}$; repeated measures ANOVA). Significance testing between groups is listed in Table 5 and 6. Box and whisker plots express distribution of data independently conducted in 4 biological experiments, including technical triplicates, indicating the median (bold line), interquartile range (box), and range (whiskers). MFI, median fluorescent intensity.

strategy to mediate phagosomal rupture and cytosolic escape in mice lungs following treatment with BafA1 (Simeone et al., 2015). Extracellular release of *M. tuberculosis* may have contributed to the significantly reduced actively replicating bacterial numbers harvested from macrophages following BafA1 treatment compared to untreated macrophages at day 3 and day 5.

Genes required for phagosomal exclusion of V-ATPase (2011; Wong et al., 2018), protein synthesis and DNA repair during exposure to acidic pH intracellularly (Vilchèze et al., 2017), may not necessarily be expressed and required during BafA1 treatment. Since the median percentage of persisters were significantly different between CytD- and BafA1-treated groups, this highlights mechanisms whereby *M. tuberculosis* may differentially modulate macrophage metabolic processes and antimicrobial functions (or vice versa), thus affecting the capacity of the host to resolve infection (Gleeson et al., 2016; Martin et al., 2017). The pharmacokinetics of anti-*M. tuberculosis* drugs may furthermore be influenced following BafA1 treatment, as drugs that accumulate in acidic vacuoles possessed a reduced killing capacity (Schump et al., 2017), whilst treatment with isoniazid or rifampicin led to a rapid decrease in drug tolerant *M. tuberculosis* (Mishra et al., 2019; Jain et al., 2020). It would thus be intriguing to determine the influence of these host processes on *M. tuberculosis* gene regulation to provide insight into how *M. tuberculosis* manipulates host immune signals and cytokines to evade immune detection and clearance.

Furthermore, the overall replication rates of intracellular bacteria did not seem to provide an early indication for the onset of persistence, which is in agreement with previous findings where persister formation was shown to be independent of single-cell growth rates (Wakamoto et al., 2013; Raffetseder et al., 2014; Manina et al., 2015). However, variation in *M. tuberculosis* growth rate (Richardson et al., 2016; Nair et al., 2019) and single-cell phenotypic variation (Manina et al., 2015; Rego et al., 2017; Vijay et al., 2017) following exposure to host immune pressures has shown to enhance bacterial phenotypic heterogeneity. Since the pH distribution in macrophages is observed to be heterogeneous (Bhaskar et al., 2014; Dragotakes et al., 2020), it could be valuable to assess how the change in phagosomal pH during infection is linked to the physiological state of *M. tuberculosis* at a single-cell level.

Metabolic adaptation is integral to the intracellular survival and pathogenesis of *M. tuberculosis* (Zimmermann et al., 2017; Fernández-García et al., 2020; Vrieling et al., 2020). CV-AM provided a representation of overall esterase activity in actively replicating bacteria and persisters. Since esterases/lipases are involved in lipid degradation, this provides *M. tuberculosis* with an efficient source of energy and carbon for intracellular persistence (Maurya et al., 2018; Nazarova et al., 2019), as shown using recombinant strains (Lun and Bishai, 2007). Esterases/lipases are furthermore involved in remodelling of cell wall lipids, which have been shown to alter colony morphology, aggregation, and pellicle formation, thereby enhancing *M. tuberculosis* antibiotic tolerance and persistence (Singh et al., 2016; Kumar et al., 2017; Maan et al., 2018).

Overall, an increase in esterase activity was observed from days 3 to 5 for all infection burdens and inhibitor treatments, although this was less pronounced for untreated bacteria. Persisters in the untreated and BafA1-treated group exhibited significantly higher esterase activity compared to actively replicating bacteria at day 3. *M. tuberculosis* from BafA1-treated macrophages additionally demonstrated significantly higher esterase activity for both actively replicating bacteria and persisters from days 3 to 5. It is thus intriguing that although CytD treatment displayed a significantly higher median percentage of persisters at day 3 and day 5, these bacteria appeared to possess lower esterase activity compared to persisters from BafA1-treated macrophages, although this was not significant. This suggests that slowed growth does not account for a reduction in metabolic activity, as previously notioned (Gengenbacher et al., 2010). Literature has shown persisters to exhibit a diversity of metabolic pathways in macrophages (Zimmermann et al., 2017; Huang et al., 2018; Pisu et al., 2020).

The wide distribution in esterase activity observed highlights the dynamic and broad spectrum of metabolic processes that may be activated during differential bacterial replication, in accordance with findings from others (Vijay et al., 2017; Pisu et al., 2020). The change in esterase activity observed for intracellular bacteria from days 3 to 5 could further suggest continued metabolic adaptation to maintain intracellular survival and persistence. This is thought to occur in a temporal nature throughout infection (Rohde et al., 2007; Zulauf et al., 2018), however it has yet to be characterized how adaptation of metabolic pathways is regulated (directly or in response to external signals).

Whilst CV-AM staining may indicate that persisters are metabolically active, detailed characterization of specific *M. tuberculosis* esterases/lipases and their involvement in metabolic functions and adaptation during infection and persistence could prove useful for future work. This could be applied to assess whether specific esterases/lipases differentially influence PDIM production, phospholipid biosynthesis, lipid catabolism and amino acid metabolism during persistence, and how this facilitates bacterial intracellular survival when exposed to lipids of varying chain lengths. Varying chain lengths and trehalose analogues could be assessed for their antigenic potential, as they are suggested to represent novel adjuvants for subunit vaccines (Tima et al., 2017). This could assist in understanding how adaptation promotes remodelling or biosynthesis of specific cell wall components, which could be targeted as an intervention strategy, such as the development of an inhibitor that prevented hydrolysis of the esterase, triacylglycerol (TAG), which inhibited resuscitation of persistent *M. tuberculosis* (Ravindran et al., 2014).

Variation in the composition of *M. tuberculosis* cell wall glycolipids may impact phagocytosis; partial delipidation of the

M. tuberculosis cell envelope has been shown to enhance host receptor-ligand interactions and phagocytosis (Stokes et al., 2004). Comparatively, over-production of free trehalose led to increased macrophage adhesion, and decreased phagocytosis (Li et al., 2016), whilst overexpression of trehalose dimycolates (TDM, cord factor) promoted macrophage cell death and cytosolic escape (Raffetseder et al., 2019).

Conclusion

Heterogeneity within *M. tuberculosis* following macrophage uptake, with respect to intracellular bacterial numbers, percentage of persisters, replication dynamics and metabolic esterase activity was observed. The importance of pathogen recognition, phagocytosis, phagosome acidification and maturation as host strategies in inhibiting intracellular growth of *M. tuberculosis* further suggests these host processes as facilitators of persistence. Since adaptation to the host environment is advantageous for intracellular mycobacterial survival, it is unsurprising that the pathogen can exploit multiple routes to achieve this. Coordination between the immunometabolic processes and metabolic remodelling strategies used by *M. tuberculosis* requires further investigation, as heterogeneity at a single-cell level can influence the outcome at a population level. This will not only enhance our understanding of how *M. tuberculosis* interferes with the host immune response, but assist in strategies that effectively target persisters to enhance bacterial clearance.

Data availability statement

The raw data supporting the conclusions of this article will be made available by the authors, without undue reservation.

Author contributions

TP, JM and SS conceptualized the experiments. TP performed the experimental work and drafted the manuscript. TP and HS analysed and interpreted results. HS conducted the statistical analysis. HS, JM and SS provided constructive feedback and insightful discussions, and contributed to revising of the manuscript. All authors contributed to the article and approved the submitted version.

Funding

This work was supported by funding from the South African Medical Research Council (SA MRC), and the South African National Research Foundation (NRF). SLS is funded by the South African Research Chairs Initiative of the Department of Science and Technology and NRF of South Africa, award number UID 86539. HS was funded by Subcommittee C of the research committee at the Faculty of Medicine and Health Sciences of Stellenbosch University. TP was funded by the Deutscher Akademischer Austauschdienst and NRF of South Africa, award number UID 111868. This work was supported by the GCRF Networks in Vaccines Research and Development VALIDATE Network which was co-funded by the MRC and BBSRC (ref MR/R005850/1). This UK funded award is part of the EDCTP2 programme supported by the European Union.

Conflict of interest

The authors declare that the research was conducted in the absence of any commercial or financial relationships that could be construed as a potential conflict of interest.

Publisher's note

Supplementary material

The Supplementary Material for this article can be found online at: https://www.frontiersin.org/articles/10.3389/fcimb.2022.981827/full#supplementary-material

SUPPLEMENTARY FIGURE 1
Varying growth states influence the esterase activity of M. tuberculosis. (A) Metabolic esterase activity of M. tuberculosis::pTiGc was assessed over 21 days in vitro, by staining with CV-AM, followed by (B) flow cytometric analysis. Selecting on live cells according to GFP positivity, the esterase activity was assessed at i) day 2 (early exponential), ii) day 5 (mid exponential), iii) day 13 (late exponential), and iv) day 21 (stationary phase). To distinguish the change in CV-AM MFI, a gate was placed on each normally-distributed population (indicated by the dotted line). Growth curve results are expressed as the mean OD600nm of triplicate samples ± SD. Negligible cell death, as determined by loss of GFP positivity, was observed over 21 days (result not shown). CV-AM: calcein violet AM; MFI: median fluorescent intensity.

SUPPLEMENTARY FIGURE 2
Heterogeneity in metabolic esterase activity in response to varying bacterial burdens. The distribution of esterase activity was assessed for actively replicating bacteria and persisters at day 3 and day 5. No significant differences between groups was observed at and between day 3 and day 5, as assessed using a pairwise Students t-test (unpaired) with Bonferroni correction. Box and whisker plots express distribution of data conducted in 4 biological experiments, including technical triplicates, indicating the median (bold line), interquartile range (box), and range (whiskers).MFI: median fluorescent intensity.

References

Balaban, N. Q., Helaine, S., Lewis, K., Ackermann, M., Aldridge, B., Andersson, D. I., et al. (2019). Definitions and guidelines for research on antibiotic persistence. *Nat. Rev. Microbiol.* 17, 441–448. doi: 10.1038/s41579-019-0196-3

Basu, S., Pathak, S. K., Banerjee, A., Pathak, S., Bhattacharyya, A., Yang, Z., et al. (2007). Execution of macrophage apoptosis by PE_PGRS33 of *mycobacterium tuberculosis* is mediated by toll-like receptor 2-dependent release of tumor necrosis factor-α *. *J. Biol. Chem.* 282, 1039–1050. doi: 10.1074/jbc.M604379200

Bhaskar, A., Chawla, M., Mehta, M., Parikh, P., Chandra, P., Bhave, D., et al. (2014). Reengineering redox sensitive GFP to measure mycothiol redox potential of mycobacterium tuberculosis during infection. *PloS Pathog.* 10, e1003902. doi: 10.1371/journal.ppat.1003902

Chengalroyen, M. D., Beukes, G. M., Gordhan, B. G., Streicher, E. M., Churchyard, G., Hafner, R., et al. (2016). Detection and quantification of differentially culturable tubercle bacteria in sputum from patients with tuberculosis. *Am. J. Respir. Crit. Care Med.* 194, 1532–1540. doi: 10.1164/rccm.201604-0769OC

Ding, A., Yu, H., Yang, J., Shi, S., and Ehrt, S. (2005). Induction of macrophage-derived SLPI by *mycobacterium tuberculosis* depends on TLR2 but not MyD88. *Immunology* 116, 381–389. doi: 10.1111/j.1365-2567.2005.02238.x

Dragotakes, Q., Stouffer, K. M., Fu, M. S., Sella, Y., Youn, C., Yoon, O. I., et al. (2020). Macrophages use a bet-hedging strategy for antimicrobial activity in phagolysosomal acidification. *J. Clin. Invest.* 130, 3805–3819. doi: 10.1172/JCI133938

Duursma, R. (2017). *Nlshelper: Convenient functions for non-linear regression*. Available at: https://CRAN.R-project.org/package=nlshelper

Fernández-García, M., Rey-Stolle, F., Boccard, J., Reddy, V. P., García, A., Cumming, B. M., et al. (2020). Comprehensive examination of the mouse lung metabolome following *mycobacterium tuberculosis* infection using a multiplatform mass spectrometry approach. *J. Proteome Res.* 19, 2053–2070. doi: 10.1021/acs.jproteome.9b00868

Garton, N. J., Waddell, S. J., Sherratt, A. L., Lee, S.-M., Smith, R. J., Senner, C., et al. (2008). Cytological and transcript analyses reveal fat and lazy persister-like bacilli in tuberculous sputum. *PloS Med.* 5, e75. doi: 10.1371/journal.pmed.0050075

Gengenbacher, M., Rao, S. P. S., Pethe, K., and Dick, T. (2010). Nutrient-starved, non-replicating *mycobacterium tuberculosis* requires respiration, ATP synthase and isocitrate lyase for maintenance of ATP homeostasis and viability. *Microbiol. Read. Engl.* 156, 81–87. doi: 10.1099/mic.0.033084-0

Ghazaei, C. (2018). *Mycobacterium tuberculosis* and lipids: Insights into molecular mechanisms from persistence to virulence. *J. Res. Med. Sci. Off. J. Isfahan Univ. Med. Sci.* 23, 63. doi: 10.4103/jrms.JRMS_904_17

Gleeson, L. E., Sheedy, F. J., Palsson-McDermott, E. M., Triglia, D., O'Leary, S. M., O'Sullivan, M. P., et al. (2016). Cutting edge: *Mycobacterium tuberculosis* induces aerobic glycolysis in human alveolar macrophages that is required for control of intracellular bacillary replication. *J. Immunol.* 196, 2444–2449. doi: 10.4049/jimmunol.1501612

Helaine, S., Thompson, J. A., Watson, K. G., Liu, M., Boyle, C., and Holden, D. W. (2010). Dynamics of intracellular bacterial replication at the single cell level. *Proc. Natl. Acad. Sci.* 107, 3746–3751. doi: 10.1073/pnas.1000041107

Hendon-Dunn, C. L., Doris, K. S., Thomas, S. R., Allnutt, J. C., Marriott, A. A. N., Hatch, K. A., et al. (2016). A flow cytometry method for rapidly assessing *m. tuberculosis* responses to antibiotics with different modes of action. *Antimicrob. Agents Chemother.* 60, 3869. doi: 10.1128/AAC.02712-15

Huang, L., Nazarova, E. V., Tan, S., Liu, Y., and Russell, D. G. (2018). Growth of *mycobacterium tuberculosis in vivo* segregates with host macrophage metabolism and ontogeny. *J. Exp. Med.* 215, 1135–1152. doi: 10.1084/jem.20172020

Jain, N., Kalam, H., Singh, L., Sharma, V., Kedia, S., Das, P., et al. (2020). Mesenchymal stem cells offer a drug-tolerant and immune-privileged niche to *mycobacterium tuberculosis*. *Nat. Commun.* 11, 3062. doi: 10.1038/s41467-020-16877-3

Jain, P., Weinrick, B. C., Kalivoda, E. J., Yang, H., Munsamy, V., Vilcheze, C., et al. (2016). Dual-reporter mycobacteriophages (Φ2DRMs) reveal preexisting *mycobacterium tuberculosis* persistent cells in human sputum. *mBio* 7, e01023–e01016. doi: 10.1128/mBio.01023-16

Kana, B. D., Gordhan, B. G., Downing, K. J., Sung, N., Vostroktunova, G., Machowski, E. E., et al. (2008). The resuscitation-promoting factors of *mycobacterium tuberculosis* are required for virulence and resuscitation from dormancy but are collectively dispensable for growth *in vitro*. mol. *Microbiol* 67, 672–684. doi: 10.1111/j.1365-2958.2007.06078.x

Kumar, A., Saini, V., Kumar, A., Kaur, J., and Kaur, J. (2017). Modulation of trehalose dimycolate and immune system by Rv0774c protein enhanced the intracellular survival of mycobacterium smegmatis in human macrophages cell line. *Front. Cell. Infect. Microbiol.* 7. doi: 10.3389/fcimb.2017.00289

Lee, J., Remold, H. G., Ieong, M. H., and Kornfeld, H. (2006). Macrophage apoptosis in response to high intracellular burden of *mycobacterium tuberculosis* is mediated by a novel caspase-independent pathway. *J. Immunol.* 176, 4267–4274. doi: 10.4049/jimmunol.176.7.4267

Lin, P. L., Ford, C. B., Coleman, M. T., Myers, A. J., Gawande, R., Ioerger, T., et al. (2014). Sterilization of granulomas is common in active and latent tuberculosis despite within-host variability in bacterial killing. *Nat. Med.* 20, 75–79. doi: 10.1038/nm.3412

Lis, R., Touboul, C., Mirshahi, P., Ali, F., Mathew, S., Nolan, D. J., et al. (2011). Tumor associated mesenchymal stem cells protects ovarian cancer cells from hyperthermia through CXCL12. *Int. J. Cancer* 128, 715–725. doi: 10.1002/ijc.25619

Li, H., Wu, M., Shi, Y., and Javid, B. (2016). Over-expression of the mycobacterial trehalose-phosphate phosphatase OtsB2 results in a defect in macrophage phagocytosis associated with increased mycobacterial-macrophage adhesion. *Front. Microbiol.* 7. doi: 10.3389/fmicb.2016.01754

Lun, S., and Bishai, W. R. (2007). Characterization of a novel cell wall-anchored protein with carboxylesterase activity required for virulence in mycobacterium tuberculosis*. *J. Biol. Chem.* 282, 18348–18356. doi: 10.1074/jbc.M700035200

Maan, P., Kumar, A., Kaur, J., and Kaur, J. (2018). Rv1288, a two domain, cell wall anchored, nutrient stress inducible carboxyl-esterase of *mycobacterium tuberculosis*, modulates cell wall lipid. *Front. Cell. Infect. Microbiol.* 8. doi: 10.3389/fcimb.2018.00421

Manina, G., Dhar, N., and McKinney, J. D. (2015). Stress and host immunity amplify *mycobacterium tuberculosis* phenotypic heterogeneity and induce nongrowing metabolically active forms. *Cell Host Microbe* 17, 32–46. doi: 10.1016/j.chom.2014.11.016

Marino, S., Cilfone, N. A., Mattila, J. T., Linderman, J. J., Flynn, J. L., and Kirschner, D. E. (2015). Macrophage polarization drives granuloma outcome during *Mycobacterium tuberculosis* infection. *Infect. Immun.* 83, 324–338. doi: 10.1128/IAI.02494-14

Martin, C. J., Cadena, A. M., Leung, V. W., Lin, P. L., Maiello, P., Hicks, N., et al. (2017). Digitally barcoding mycobacterium tuberculosis reveals *In vivo* infection dynamics in the macaque model of tuberculosis. *mBio* 8, e00312-17. doi: 10.1128/mBio.00312-17

Maurya, R. K., Bharti, S., and Krishnan, M. Y. (2018). Triacylglycerols: Fuelling the hibernating *mycobacterium tuberculosis*. *Front. Cell. Infect. Microbiol.* 8. doi: 10.3389/fcimb.2018.00450

Mehta, M., Rajmani, R. S., and Singh, A. (2016). Mycobacterium tuberculosis WhiB3 responds to vacuolar pH-induced changes in mycothiol redox potential to modulate phagosomal maturation and virulence. *J. Biol. Chem.* 291, 2888–2903. doi: 10.1074/jbc.M115.684597

Mishra, R., Kohli, S., Malhotra, N., Bandyopadhyay, P., Mehta, M., Munshi, M., et al. (2019). Targeting redox heterogeneity to counteract drug tolerance in replicating mycobacterium tuberculosis. *Sci. Transl. Med.* 11, eaaw6635. doi: 10.1126/scitranslmed.aaw6635

Mouton, J. M., Helaine, S., Holden, D. W., and Sampson, S. L. (2016). Elucidating population-wide mycobacterial replication dynamics at the single-cell level. *Microbiol. Read. Engl.* 162, 966–978. doi: 10.1099/mic.0.000288

Mouton, J. M., Heunis, T., Dippenaar, A., Gallant, J. L., Kleynhans, L., and Sampson, S. L. (2019). Comprehensive characterization of the attenuated double auxotroph *mycobacterium tuberculosis*ΔleuDΔpanCD as an alternative to H37Rv. *Front. Microbiol.* 10. doi: 10.3389/fmicb.2019.01922

Nair, R. R., Sharan, D., and Ajitkumar, P. (2019). A minor subpopulation of mycobacteria inherently produces high levels of reactive oxygen species that generate antibiotic resisters at high frequency from itself and enhance resister generation from its major kin subpopulation. *Front. Microbiol* 10, 1842. doi: 10.3389/fmicb.2019.01842

Nazarova, E. V., Montague, C. R., Huang, L., La, T. T. T., Russell, D. G., and VanderVen, B. C. (2019). The genetic requirements of fatty acid import by *mycobacterium tuberculosis* within macrophages. *ELife* 8, e43621. doi: 10.7554/elife.43621

Pisu, D., Huang, L., Grenier, J. K., and Russell, D. G. (2020). Dual RNA-seq of mtb-infected macrophages *In vivo* reveals ontologically distinct host-pathogen interactions. *Cell Rep.* 30, 335–350.e4. doi: 10.1016/j.celrep.2019.12.033

Raffetseder, J., Pienaar, E., Blomgran, R., Eklund, D., Patcha Brodin, V., Andersson, H., et al. (2014). Replication rates of *mycobacterium tuberculosis* in human macrophages do not correlate with mycobacterial antibiotic susceptibility. *PloS One* 9, e112426. doi: 10.1371/journal.pone.0112426

Raffetseder, J., Iakobachvili, N., Loitto, V., Peters, P. J., and Lerm, M. (2019). Retention of EsxA in the capsule-like layer of *Mycobacterium tuberculosis* is associated with cytotoxicity and is counteracted by lung surfactant. *Infect. Immun.* 87, e00803–e00818. doi: 10.1128/IAI.00803-18

Ravindran, M. S., Rao, S. P. S., Cheng, X., Shukla, A., Cazenave-Gassiot, A., Yao, S. Q., et al. (2014). Targeting lipid esterases in mycobacteria grown under different physiological conditions using activity-based profiling with tetrahydrolipstatin (THL)*. *Mol. Cell. Proteomics* 13, 435–448. doi: 10.1074/mcp.M113.029942

Refai, A., Gritli, S., Barbouche, M.-R., and Essafi, M. (2018). *Mycobacterium tuberculosis* virulent factor ESAT-6 drives macrophage differentiation toward the pro-inflammatory M1 phenotype and subsequently switches it to the anti-inflammatory M2 phenotype. *Front. Cell. Infect. Microbiol.* 0. doi: 10.3389/fcimb.2018.00327

Rego, E. H., Audette, R. E., and Rubin, E. J. (2017). Deletion of a mycobacterial divisome factor collapses single-cell phenotypic heterogeneity. *Nature* 546, 153–157. doi: 10.1038/nature22361

Richardson, K., Bennion, O. T., Tan, S., Hoang, A. N., Cokol, M., and Aldridge, B. B. (2016). Temporal and intrinsic factors of rifampicin tolerance in mycobacteria. *Proc. Natl. Acad. Sci. U. S. A* 113, 8302–8307. doi: 10.1073/pnas.1600372113

Rohde, K. H., Abramovitch, R. B., and Russell, D. G. (2007). *Mycobacterium tuberculosis* invasion of macrophages: Linking bacterial gene expression to environmental cues. *Cell Host Microbe* 2, 352–364. doi: 10.1016/j.chom.2007.09.006

Rohde, K. H., Veiga, D. F. T., Caldwell, S., Balázsi, G., and Russell, D. G. (2012). Linking the transcriptional profiles and the physiological states of *mycobacterium tuberculosis* during an extended intracellular infection. *PloS Pathog.* 8, e1002769. doi: 10.1371/journal.ppat.1002769

RStudio Team (2020). *RStudio: Integrated development environment for r.* (Boston, MA: RStudio, PBC). Available at: http://www.rstudio.com/

Sampson, S. L., Dascher, C. C., Sambandamurthy, V. K., Russell, R. G., Jacobs, W. R., Bloom, B. R., et al. (2004). Protection elicited by a double leucine and pantothenate auxotroph of *mycobacterium tuberculosis* in Guinea pigs. *Infect. Immun.* 72, 3031–3037. doi: 10.1128/IAI.72.5.3031-3037.2004

Schump, M. D., Fox, D. M., Bertozzi, C. R., and Riley, L. W. (2017). Subcellular partitioning and intramacrophage selectivity of antimicrobial compounds against *mycobacterium tuberculosis*. *Antimicrob. Agents Chemother.* 61, e01639–e01616. doi: 10.1128/AAC.01639-16

Seeliger, J. C., Topp, S., Sogi, K. M., Previti, M. L., Gallivan, J. P., and Bertozzi, C. R. (2012). A riboswitch-based inducible gene expression system for mycobacteria. *PloS One* 7, e29266. doi: 10.1371/journal.pone.0029266

Sia, J. K., and Rengarajan, J. (2019). Immunology of *Mycobacterium tuberculosis* infections. *Microbiol. Spectr.* 7 (4), 10.1128/microbiolspec.GPP3-0022-2018. doi: 10.1128/microbiolspec.GPP3-0022-2018

Simeone, R., Sayes, F., Song, O., Gröschel, M. I., Brodin, P., Brosch, R., et al. (2015). Cytosolic access of *mycobacterium tuberculosis*: Critical impact of phagosomal acidification control and demonstration of occurrence *In vivo*. *PloS Pathog.* 11, e1004650. doi: 10.1371/journal.ppat.1004650

Singh, P., Rao, R. N., Reddy, J. R. C., Prasad, R. B. N., Kotturu, S. K., Ghosh, S., et al. (2016). PE11, a PE/PPE family protein of *mycobacterium tuberculosis* is involved in cell wall remodeling and virulence. *Sci. Rep.* 6, 21624. doi: 10.1038/srep21624

Smyth, R., Berton, S., Rajabalee, N., Chan, T., and Sun, J. (2021). Protein kinase r restricts the intracellular survival of *mycobacterium tuberculosis* by promoting selective autophagy. *Front. Microbiol.* 11. doi: 10.3389/fmicb.2020.613963

Sousa, J., Cá, B., Maceiras, A. R., Simões-Costa, L., Fonseca, K. L., Fernandes, A. I., et al. (2020). *Mycobacterium tuberculosis* associated with severe tuberculosis evades cytosolic surveillance systems and modulates IL-1β production. *Nat. Commun.* 11, 1949. doi: 10.1038/s41467-020-15832-6

Stamm, C. E., Collins, A. C., and Shiloh, M. U. (2015). Sensing of *mycobacterium tuberculosis* and consequences to both host and bacillus. *Immunol. Rev.* 264, 204–219. doi: 10.1111/imr.12263

Stokes, R. W., Norris-Jones, R., Brooks, D. E., Beveridge, T. J., Doxsee, D., and Thorson, L. M. (2004). The glycan-rich outer layer of the cell wall of *mycobacterium tuberculosis* acts as an antiphagocytic capsule limiting the association of the bacterium with macrophages. *Infect. Immun.* 72, 5676–5686. doi: 10.1128/IAI.72.10.5676-5686.2004

Sullivan, J. T., Young, E. F., McCann, J. R., and Braunstein, M. (2012). The *mycobacterium tuberculosis* SecA2 system subverts phagosome maturation to promote growth in macrophages. *Infect. Immun.* 80, 996–1006. doi: 10.1128/IAI.05987-11

ThermoFisher Scientific (2004) *LIVE/DEAD™ BacLight™ bacterial viability and counting kit*. Available at: https://www.thermofisher.com/order/catalog/product/L34856 (Accessed 9.23.20).

Tima, H. G., Dulayymi, J. R. A., Denis, O., Lehebel, P., Baols, K. S., Mohammed, M. O., et al. (2017). Inflammatory properties and adjuvant potential of synthetic glycolipids homologous to mycolate esters of the cell wall of *mycobacterium tuberculosis*. *J. Innate Immun.* 9, 162–180. doi: 10.1159/000450955

Vijay, S., Vinh, D. N., Hai, H. T., Ha, V. T. N., Dung, V. T. M., Dinh, T. D., et al. (2017). Influence of stress and antibiotic resistance on cell-length distribution in *mycobacterium tuberculosis* clinical isolates. *Front. Microbiol.* 8. doi: 10.3389/fmicb.2017.02296

Vilchèze, C., Hartman, T., Weinrick, B., Jain, P., Weisbrod, T. R., Leung, L. W., et al. (2017). Enhanced respiration prevents drug tolerance and drug resistance in mycobacterium tuberculosis. *Proc. Natl. Acad. Sci. U. S. A.* 114, 4495–4500. doi: 10.1073/pnas.1704376114

Vrieling, F., Kostidis, S., Spaink, H. P., Haks, M. C., Mayboroda, O. A., Ottenhoff, T. H. M., et al. (2020). Analyzing the impact of *mycobacterium tuberculosis* infection on primary human macrophages by combined exploratory and targeted metabolomics. *Sci. Rep.* 10, 7085. doi: 10.1038/s41598-020-62911-1

Wakamoto, Y., Dhar, N., Chait, R., Schneider, K., Signorino-Gelo, F., Leibler, S., et al. (2013). Dynamic persistence of antibiotic-stressed mycobacteria. *Science* 339, 91–95. doi: 10.1126/science.1229858

Welin, A., Raffetseder, J., Eklund, D., Stendahl, O., and Lerm, M. (2011). Importance of phagosomal functionality for growth restriction of *mycobacterium tuberculosis* in primary human macrophages. *J. Innate Immun.* 3, 508–518. doi: 10.1159/000325297

Wong, D., Bach, H., Sun, J., Hmama, Z., and Av-Gay, Y. (2011). *Mycobacterium tuberculosis* protein tyrosine phosphatase (PtpA) excludes host vacuolar-H +-ATPase to inhibit phagosome acidification. *Proc. Natl. Acad. Sci. U. S. A.* 108, 19371–19376. doi: 10.1073/pnas.1109201108

Wong, D., Li, W., Chao, J. D., Zhou, P., Narula, G., Tsui, C., et al. (2018). Protein tyrosine kinase, PtkA, is required for *mycobacterium tuberculosis* growth in macrophages. *Sci. Rep.* 8, 155. doi: 10.1038/s41598-017-18547-9

Zimmermann, M., Kogadeeva, M., Gengenbacher, M., McEwen, G., Mollenkopf, H.-J., Zamboni, N., et al. (2017). Integration of metabolomics and transcriptomics reveals a complex diet of mycobacterium tuberculosis during early macrophage infection. *mSystems* 2, e00057-17. doi: 10.1128/mSystems.00057-17

Zulauf, K. E., Sullivan, J. T., and Braunstein, M. (2018). The SecA2 pathway of *mycobacterium tuberculosis* exports effectors that work in concert to arrest phagosome and autophagosome maturation. *PloS Pathog.* 14, e1007011. doi: 10.1371/journal.ppat.1007011

frontiers | Frontiers in Cellular and Infection Microbiology

TYPE Review
PUBLISHED 22 December 2022
DOI 10.3389/fcimb.2022.1079569

OPEN ACCESS

EDITED BY
Bavesh Kana,
University of the Witwatersrand,
South Africa

REVIEWED BY
Abhishek Mishra,
Houston Methodist Research Institute,
United States
Ayan Chatterjee,
University of Texas Health Science
Center at Houston, United States

*CORRESPONDENCE
Ashima Bhaskar
ashimabhaskar@gmail.com;
ashimabhaskar23@gmail.com

†These authors have contributed
equally to this work

SPECIALTY SECTION
This article was submitted to
Bacteria and Host,
a section of the journal
Frontiers in Cellular and
Infection Microbiology

RECEIVED 25 October 2022
ACCEPTED 06 December 2022
PUBLISHED 22 December 2022

CITATION
Verma A, Ghoshal A, Dwivedi VP and
Bhaskar A (2022) Tuberculosis: The
success tale of less explored dormant
Mycobacterium tuberculosis.
Front. Cell. Infect. Microbiol.
12:1079569.
doi: 10.3389/fcimb.2022.1079569

Tuberculosis: The success tale of less explored dormant *Mycobacterium tuberculosis*

Akanksha Verma†, Antara Ghoshal†,
Ved Prakash Dwivedi and Ashima Bhaskar*

Immunobiology Group, International Centre for Genetic Engineering and Biotechnology, New Delhi, India

Mycobacterium tuberculosis (*M.tb*) is an intracellular pathogen that predominantly affects the alveolar macrophages in the respiratory tract. Upon infection, the activation of TLR2 and TLR4- mediated signaling pathways leads to lysosomal degradation of the bacteria. However, bacterium counteracts the host immune cells and utilizes them as a cellular niche for its survival. One distinctive mechanism of *M.tb* to limit the host stress responses such as hypoxia and nutrient starvation is induction of dormancy. As the environmental conditions become favorable, the bacteria resuscitate, resulting in a relapse of clinical symptoms. Different bacterial proteins play a critical role in maintaining the state of dormancy and resuscitation, namely, DevR (DosS), Hrp1, DATIN and RpfA-D, RipA, etc., respectively. Existing knowledge regarding the key proteins associated with dormancy and resuscitation can be employed to develop novel therapies. In this review we aim to highlight the current knowledge of bacterial progression from dormancy to resuscitation and the gaps in understanding the transition from dormant to active state. We have also focused on elucidating a few therapeutic strategies employed to prevent *M.tb* resuscitation.

KEYWORDS

***Mycobacterium tuberculosis (M.tb)*, Tuberculosis (TB), LTBI, dormancy, resuscitation, vaccines, drugs, Host-directed therapies (HDT)**

1 Introduction

The second most common infectious killer and 13th leading cause of death worldwide, behind COVID-19, is tuberculosis (TB). In 2022, the WHO stated that there were over 1.5 million annual deaths, further emphasizing the need to eradicate TB. *Mycobacterium tuberculosis* (*M.tb*), initially identified by Dr. Robert Koch in 1882 (Cambau and Drancourt, 2014), is the cause of tuberculosis. *M.tb* is a slow-growing, acid-fast aerobic bacterium, with a doubling time of 18-24 hours (Smith, 2003; Beste et al., 2009). It is one of the oldest bacteria on the planet, with origin dating back to around 150 million years ago. *M.tb* has been known by diverse names such

as *phthisis* in ancient Greece, *tabes* in ancient Rome, *schachepheth* in ancient Hebrew, *scrofula* in Middle Ages and *white plague* in the 1700s (Barberis et al., 2017). *M.tb* is a successful intracellular pathogen. When inhaled through aerosol droplets it affects primarily the lungs and can eventually disseminate to other organs such as the brain, liver, kidney, and pancreas. The pathogenesis of the bacterium has already been reviewed elsewhere (Smith, 2003; Bañuls et al., 2015; Ehrt et al., 2018). In a nutshell, the pathogenesis can be summed up as infection of the alveolar macrophages which phagocytose and attempt to eliminate the pathogen *via* lysosomal-dependent degradation of the phagosome containing the pathogen (Hmama et al., 2015). However, the bacteria have evolved various strategies to counteract the host defense systems. It inhibits the phagolysosome fusion and replicates within host macrophages, followed by slowing down to a low metabolic state called dormancy. The bacteria take advantage of the host factors and environment, due to which they remain in dormant state for years without showing clinical symptoms (Boom et al., 2021). Nonetheless, co-infections and other causes of immunosuppression can assist the bacteria to resuscitate and replicate thereby causing active TB and increasing the threat of transmission of *M.tb* to other healthy individuals.

To date, researchers are relentlessly trying to understand the exact mechanism of transition of bacteria from dormant to metabolically active state in the host. Battling the disease to enhance the safety of individuals requires a deep understanding of bacterial factors that utilize the host machinery to subvert host immune responses. The understanding of the twofold relationship between the host and bacteria can help design better therapeutics to augment existing anti-TB drugs.

Being a serious life-threatening disease, there are still major conundrums associated with TB. These include improper diagnosis of latent TB in endemic areas (Zellweger et al., 2020), prediction of reactivation in patients with latent infection, less efficient vaccine (the only available vaccine is BCG) (Brandt et al., 2002), and multi-drug resistant TB (MDR, XDR) (Singh et al., 2020; Hu et al., 2021). It is a pre-requisite to address the above-mentioned pitfalls to curtail TB transmission and eventually boost the WHO End TB campaign by 2035. To better understand the problems associated with latent TB and TB recurrence, in this review, we have highlighted the possible mechanisms and factors responsible for bacterial dormancy, persistence, and resuscitation. We have briefly summarised the existing models to study dormancy and resuscitation. We endeavour to underline the conventional and prospective novel targets of host and bacteria which can be employed to design an efficacious therapy against TB.

2 Dormancy, persistence, and models of dormancy

Dormancy in *M.tb* refers to the state of viability but metabolic inactivity under unfavorable physiological conditions and immune pressure faced in the host. Immunologically unfavorable conditions include challenges posed by various cells of innate and adaptive immune compartments *via* production of cytokines, chemokines, interleukins, increased phagocytosis, rapid antigen processing and presentation. Such stresses result in reduced metabolism to improve *M.tb* survival, but the bacteria can resume their basal metabolic pathways under favorable conditions. Dormant bacteria are also resistant to front line antibiotics such as isoniazid which primarily target metabolically active cells.

Attainment of dormant state by *M.tb* in the host instigates a state of latent TB infection (LTBI). LTBI can be further defined as a clinical state arising due to the host defense mechanisms whereby the host remains asymptomatic (Singh et al., 2020). There exists different school of thoughts regarding latency and its role in increasing the global TB burden. Further confirmation is required regarding persistence of the bacteria in humans. Several epidemiological studies have investigated the time period of the persisting infection i.e., infection after a span of about 2 years is majorly due to recently transmitted infection (Behr et al., 2019; Behr et al., 2021). The widely used tests for LTBI- the tuberculin skin test and interferon gamma release assay fails to give a clear-cut explanation about the spectrum of disease progression in TB endemic areas (Behr et al., 2018). The limitation to detect LTBI in TB endemic areas can prove fatal in patients undergoing Hematopoietic stem cell transplant (HSCT). Studies have shown that TB is one of the major complications associated with HSCT. The authors from one such prospective cohort study have suggested LTBI screening, detection, and prophylactic treatment with isoniazid (INH) of patients as a safer measure to avoid reactivation of TB after HSCT (de Oliveira Rodrigues et al., 2021).

Persisters refers to a bacterium population with non-heritable phenotypic resistance that arises due to antibiotic pressure through stochastic or deterministic epigenetic factors. Upon removal of antibiotic stress, they can still give rise to antibiotic-sensitive parent populations. The mechanism of persistence is due to survival strategies such as efflux pumps, biofilm formation, altered metabolism, etc. This can even have a role in the emergence of multi-drug resistant strains (Bhaskar et al., 2019).

Models of dormancy can be categorized into two types, *in vitro*, and *in vivo* models. The most used *in vitro* models are the Wayne model, starvation model, nitrous oxide-based model, *in vitro* granuloma model, low oxygen recovery assay, and whole cell nitrate reductase assay. *In vivo* models can be generated using mice, rats, rabbits, guinea pigs, zebrafish, and non-human primates (NHP). Cornell model and low-dose chronic mice infection model are the most widely used murine models for establishing dormancy phenotype. These have been reviewed in detail in various publications along with their limitations (Murphy and Brown, 2007; Alnimr, 2015; Bhaskar et al., 2019).

Singh et al. have proposed a new *ex vivo* dormancy model by using human mesenchymal stem cells (MSCs). Upon using a low multiplicity of infection, *M.tb* survived for 22 days in MSCs

without causing host cell death. There was an upregulation in the expression of HspX and increased tolerance to the anti-tubercular drug, isoniazid and rifampicin thus indicating a non-proliferative dormant-like phenotype (Singh et al., 2020).

NHPs are a better option for modeling human TB due to physiological and immunological similarities. In these, macaques such as rhesus and cynomolgus have been widely used (Mothé et al., 2015). Apart from these, the common marmoset (*Callithrix jacchus*) has recently been used (Via et al., 2015). It is susceptible to *M.tb* infection by aerosol and intra-tracheal methods. It demonstrates granulomas closer to humans and survives for greater than 300 days thus can be used for developing a chronic model of infection. Moreover, breeding pairs usually bear twin or triplet offspring allowing for a certain degree of homogeneity across studies (Via et al., 2013). Other *in-vivo* models that are under study for LTBI includes Wistar rat and minipigs and Chinese tree shrew (Gaonkar et al., 2010; Zhan et al., 2014; Rodrigues-Junior et al., 2017).

2.1 *Mycobacterial* genes upregulated during dormancy

To unravel the genes involved in dormancy, Iona et al. used the Wayne hypoxia model with forty days of dormancy. Upon studying the kinetics of gene expression during the dormancy period using quantitative real-time PCR (qPCR), they observed upregulation of dormancy regulon genes such as *devR*, alpha-crystallin (*acr*), triglycerol synthase *(tgs1*) in non-replicating persistence stage (NRP-1) after a week of log phase replication. Apart from this, genes involved in general metabolism like *fad26* and nitrate metabolism gene such as *narK2* were also unregulated. After around 11 days, entry of bacterium into the NRP-2 phase was confirmed through methylene decoloration assay. During the transition from NRP-1 to NRP-2, hypoxic genes such as sigma factors (*sigB, sigE, rpoB*), thioredoxin reductase *(trxB1)*, hexose monophosphate shunt pathway *(hmp)*, and *narX* were upregulated. Few genes such as sigma factors involved in transcription (*sigA, sigF, sigH)*, genes involved in general metabolism (Isocitrate lyase-*icl*, Phthiocerol Dimycocerosates-*fadD21*, Heparin-Binding Hemagglutinin Adhesin- *hbhA, fadD26, kasB, lipY*, Cyclopropane synthase gene-*cma2*), genes with miscellaneous functions (Superoxide dismutase-*sodC, relA, mprA*) were constantly expressed throughout forty days of dormancy period suggesting their requirement for survival and basal gene expression. Apart from this, genes such as early secretory target antigen- *esat-6*, Fibronectin binding protein-*fbpB*, culture filtrate protein-*cfp10, dnaA, Ftsz* were downregulated during hypoxic growth phase indicating reduced log phase replication (Iona et al., 2016).

RNA-seq at day 25 of hypoxia establishment revealed the activation of dormancy genes such as *DosRST, MprAB* alternative sigma factors *SigE, SigH*, genes involved in encoding isocitrate lyase (*icl-1)* and methylcitrate lyase (*prpC)*. Authors also observed induction of Caseinolytic protease gene regulator (*ClgR)* regulon including the Psp system in the *SigE* subnetwork which also presumably helps in maintaining membrane integrity under envelope perturbing conditions. The genes involved in uptake and catabolism of lipids were upregulated during persistence phase such as the genes involved in fatty acid beta-oxidation and degradation pathways, genes regulated by *KstR* that controls the expression of a cluster of mycobacterial genes involved in lipid degradation, *Mce* transport systems (*Mce1-4*), which encode putative ABC transporters involved in diverse lipid transportation across the cell wall, genes involved in glyoxylate and dicarboxylate metabolism which is a canonical pathway for lipid utilization (Du et al., 2016).

M.tb facing *in vitro* hypoxia in the low stirring sealed tubes was instrumental in elucidating the necessity of *de novo* ATP synthesis to maintain basal ATP level in hypoxic nonreplicating conditions. Anaerobic electron transport chain (ETC) with Type 2 NADH dehydrogenase (*ndh2)* as an initiation enzyme is also functional during hypoxia and is necessary for generating proton motive force (PMF) (Rao et al., 2008).

Microarray profiling of *M.tb* infected murine lungs and broth grown cultures by Talaat et al. has been successful in characterizing differential expressed genes between mice models like Balb/c, SCID and *in vitro* culture at different time points of 7, 14, 21, 28 days post infection. SCID mice with an immune-compromised phenotype showed expression profile like culture grown log phase bacterium. Core *in vivo* regulated genes included- *rubB, dinF*, and Ferredoxin reductase (*fdxA*) which were induced under condition of low pH, DNA damage stress, regardless of host immune status. Few genes were upregulated only in *in vivo* model of Balb/c such as sucrose *proZ* (transport system permease protein), *aceA* (probable isocitrate lyase involved in lipid metabolism), and genes encoding regulatory proteins such as *sigK, sigE*, and *kdpE* (transcriptional regulatory protein). Some genes were distinctly upregulated during *in vitro* growth only such as *cstA* (carbon starvation-induced stress response protein), *cysW* (sulfate transport system permease protein), *Rv3383c* (transferase involved in lipid biosynthesis), and gene-encoding regulatory proteins such as *sigJ* and *Rv1167c* or *Rv1994c* (transcriptional regulators). Transcript analysis of Balb/c at 21 days indicated macrophage activation characterized by low pH and stressors that could lead to a dormant phenotype of the bacilli. In this study *LipF* was identified as one of the important gene for mycobacterial persistence (Talaat et al., 2004). Hence, different transcript profiles were observed among different models of dormancy, suggesting the effect of environmental conditions in influencing bacterial transcription in dormancy regulation.

Another study analyzed the expression of *M.tb* mRNA in C57BL/6 mice model using qPCR and they revealed that the gene expression signature in the granulomatous lesion corresponded to cellular hypoxia, C2 carbon metabolism, and survival in a limited iron environment. Icl, an enzyme of glyoxylate cycle is required for the long-term persistence of *M.tb* in mice indicating a switch to the C2 cycle for long-term persistence. Pyruvate carboxykinase (*pckA*) was also elevated in aerosol-infected mice at 9 weeks post-infection, thus indicating growth on fatty acid substrates. Heat shock protein gene *hspX* which encodes alpha-crystallin with a role in adaptation to stimuli such as hypoxia and nitric oxide is also induced during the stationary growth phase (Timm et al., 2003). The mice model C3HeB/FeJ (Kramnik mice) closely replicates the human granuloma features, as it is hyper-susceptible to *M.tb* infection due to the presence of super susceptibility to tuberculosis 1 (*sst1*) locus (Poh et al., 2022). Research conducted by Harper et al. using the Kramnik mice model showed upregulation of several hypoxia-associated genes such as *dosR/devR, hspX, tgs1*, and *narK2* in bacteria obtained from necrotic lesions. *Rv1733c* which results in a strong T cell response in latently infected individuals also showed about 4-fold upregulation (Harper et al., 2012).

Recent work by Hudock et al. has delineated *M.tb* transcriptome during latent vs active TB using the NHP model. Hypoxic condition *in vivo* was characterized by marked upregulation of genes belonging to the *dosR* regulon, especially in that highly hypoxic areas. Genes belonging to PE/PPE family were expressed more in active TB (ATB) as compared to LTBI. The expression of toxin-antitoxin genes belonging to the *vapBC* family was upregulated within the granulomas. Alternate sigma factors such as *sigF, sigD, sigJ*, *sigI*, *sigB*, *sigK*, and *sigH* were enhanced to suit the changing environment milieu within the granuloma (Hudock et al., 2017).

Transcript profiling of human lung granulomas using resected tissue samples also revealed upregulation of genes such as *icl*, *narX*, *Rv2557*, and *Rv2558* (Fenhalls et al., 2002).

A proteomic study using the Wayne model of dormancy using the SWATH MS technique has helped in quantifying absolute proteome composition and dynamics during dormancy and resuscitation. The proteomic data correlated well with various available transcript-level data about gene modulation during dormancy. *DosR* regulon proteins, proteins with a role in cell wall synthesis such as (alanine dehydrogenase Ald), proteins involved in lipid metabolism (FadE5, DesA1/2, Tgs1/4, and Icl1), as well as the copper stress-related enzymes MymT (copper toxicity protection) and CsoR (copper-sensitive operon repressor) were found to be about 4-folds upregulated during hypoxia-induced dormancy. Various enzymes subnetworks of menaquinone metabolism, cholesterol degradation, fatty acid metabolism, mycolate biosynthesis, branched-chain fatty acid, sulfur compound metabolism, etc. were upregulated during hypoxia. Enzymes involved in the anaerobic electron transport chain such as narX, narK2, ndh2, and cytochrome bd oxidase were also upregulated (Schubert et al., 2015). The summary of genes up-regulated in various *in-vitro* and *in-vivo* models of dormancy have been tabulated and presented in Table 1.

2.2 Host-pathogen interactions during dormancy

After aerosol inhalation, *M.tb* is phagocytosed primarily by alveolar macrophages and resident dendritic cells (Cohen et al., 2018). The bacteria are then killed by phagolysosomes and antigen processing occurs to mediate the immune response. However, *M.tb* is a successful pathogen that has evolved various alternative strategies to survive within the hostile environment of host. *M.tb* can escape phagolysosome fusion and utilizes the autophagy pathway to replicate. The maintenance of dormant bacterial state is a dual relationship between the pathogen and the host. The bacteria modulate host factors to ensure successful immune evasion and survival. Upon infection, some bacteria attain non-replicative form and survive in the dormant state within the, granuloma. The granuloma is the inflammation site formed majorly by immune cells such as macrophages NK cells, T cells, B cells, fibroblasts, and neutrophils (Ehlers and Schaible, 2013). These granulomas are heterogenous and the environment within them is skewed towards pro-inflammatory milieu rather than anti-inflammatory. Bacteria persists within the granulomas in extracellular form. *M.tb* replication is obstructed in these sites and thus they are rendered protected from antibiotics. Apart from being a niche for dormant *M.tb*, solid granuloma prevents active disease, the reduced vascularisation restricts dissemination, while caseation results in reactivation as shown in Figure 1 (Bold and Ernst, 2009). Therefore, during immunosuppression, such as in case of HIV co-infection, there is a caseation of granulomas resulting in reactivation and dissemination of *M.tb* (Pawlowski et al., 2012).

Little is known about the host factors that enable *M.tb* dormancy, yet there are some reports on the host and environmental factors that allow bacteria to become dormant. Most such studies are focussed on *M.tb* and macrophage interaction. The bacteria interfere with the trafficking pathways within the macrophage to inhibit its degradation *via* lysosomal fusion and autophagy (Flynn and Chan, 2003). Macrophages secrete various pro-inflammatory cytokines and chemokines that attract various mononuclear cells including T cells to contain the bacteria within the granuloma. The host factors such as TNF-α and IFN-γ enables the bacteria to survive in acidic conditions, thus providing the aid to the bacteria to reside within the granuloma. Higher TNF-α and apoptosis have been reported to maintain the dormant state of bacteria (Gautam et al., 2014). The macrophage reprogramming is mediated by certain mycobacterial latency proteins such as DosS (DevR), hypoxic response protein 1 (hrp1), latency-associated protein

TABLE 1 List of genes upregulated during dormancy in various *in-vitro* and *in-vivo* models.

Model	Method of study	Selected genes upregulated during dormancy	Ref
Hypoxia	qPCR	Dormancy regulon gene- *devR, acr, tgs1* *fad26* gene required for cell wall lipid phthioceroldimycocerosate's (PDIM) synthesis Sigma factors- *sigB, SigE, rpoB,* (*trxB*1)- for antioxidant defense Hexose monophosphate shunt (HMP) for maintaining carbon homeostasis during dormancy *narX* is a nitrate reductase involved in anaerobic respiration.	(Iona et al., 2016)
Hypoxia	RNA-seq	*DosRST, MprAB*- two-component systemalternative sigma factors *SigE, SigH icl-1*- with role in glyoxylate shunt pathway, methylcitrate lyase, KstR regulated genes involved in lipid degradation and cholesterol catabolism *Mce* transport systems: encodes ABC transporters involved in lipid transportation and utilization.	(Du et al., 2016)
Lung from Mice model- *Balb/c* and SCID were compared with invitro grown bacterium under hypoxic conditions	Micro array	Core *in-vivo* regulated genes with role in dormancy were found to be *rubB, dinF*, and *fdxA*. *In-vitro* regulated genes-*cstA* (carbon starvation-induced stress response protein), cysW (sulfate transport system permease protein), *Rv3383c* (transferase involved in lipid biosynthesis), *sigJ* and *Rv1167c* or *Rv1994c* (transcriptional regulators).	(Talaat et al., 2004)
Lung from C57BL/6 mice model	Quantitative real time PCR	*Icl, pckA, hspX*	(Iona et al., 2016)
Non-human primate model (NHP)	Intra- granulomatous gene expression study using transcriptomics	Genes belonging to *dosR* regulon, toxin-antitoxin genes, alternate sigma factors- *sigF, sigD, sigJ, sigI, sigB, sigK*, and *sigH*	(Hudock et al., 2017)
Human lung granuloma	RNA-RNA *in-situ* hybridization	*Icl, narX* *Rv2557* and *Rv2558*- carbon starvation inducible genes *iniB* and *kasA*- upregulation due to isoniazid exposure.	(Fenhalls et al., 2002)

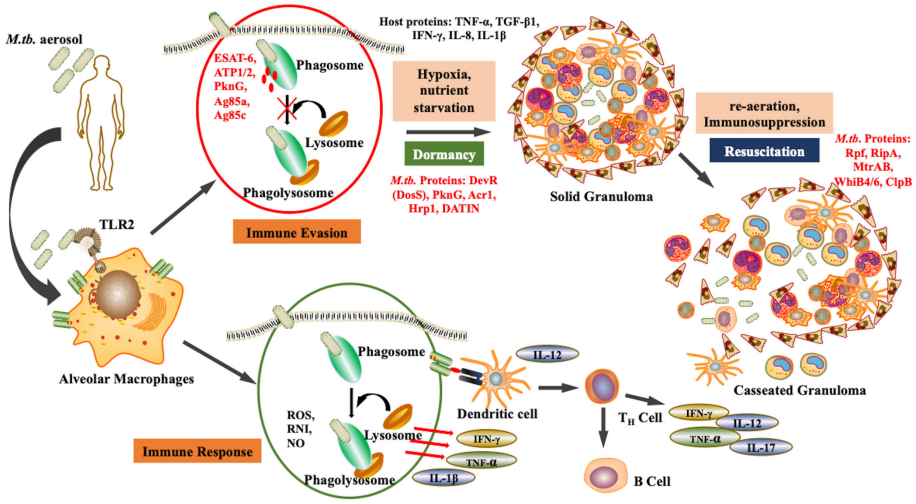

FIGURE 1
Pathogenesis of *M.tb*: Upon aerosol inhalation, alveolar macrophages degrade bacteria through ROS production and phagolysosomal degradation, which activates other immune cells such as T cells and B cells, further providing defense against the pathogen. However, *M.tb.* adapts the ability to inhibit phagolysosomal degradation, and therefore under unfavorable conditions such as hypoxia undergo dormancy. As the environmental conditions become favorable, the bacteria resuscitate, resulting in active disease. (Red represents *M.tb.* antigens).

Rv2660c, DATIN, etc., which augments the production of proinflammatory cytokines such as TNF-α, IFN-γ, IL-8, and IL-1β (Kumar et al., 2013; Yihao et al., 2015). There is another study that suggests interaction of *M.tb* with TREM2 receptor of macrophages which reduces antibacterial state in macrophages. This is mediated *via* decrease in TNF-α and ROS levels, enhancing the *M.tb* survival. This is also accompanied by upregulation of anti-inflammatory cytokines such as IFN-β and IL-10 (Iizasa et al., 2021).. The exact mechanism of how these proteins modulate the macrophages to form granuloma is yet to be elucidated. Another study reveals that during dormancy, the alpha-crystallin protein-1 (Acr-1) of *M.tb* provides immunogenic tolerance by inhibiting the maturation of dendritic cells (Siddiqui et al., 2014). In contrast to this, Mubin et al. in 2018 reported that Acr-1 regulates and inhibits the maturation of differentiated macrophages while activating naïve macrophages *via* phosphorylation of STAT-1 and STAT-4. This is accompanied by the generation of *M.tb*-specific T cells that can prevent disease (Mubin et al., 2018). Being a dormancy-associated gene, Acr-1 primes the host immune system to mount an immune response against the bacteria.

M.tb has benefitted by exploiting resident mesenchymal stem cells. Unlike macrophages, mesenchymal stem cells (MSCs) provide cytosol as the niche for bacterial replication and rapid lipid synthesis for maintaining dormancy (Fatima et al., 2020). Bacteria live longer in MSCs in a dormant state by hiding themselves in lipid droplets and rendering themselves resistant to combination antibiotics therapy (Fatima et al., 2020) (Jain et al., 2020). It has also been suggested that MSCs are less tolerant to bacterial replication, unlike macrophages, but rather promote dormancy. In turn, *M.tb* induces expression of genes accountable for the quiescent state of MSCs that includes Sox-9, NOTCH-1, and FOXO3a. RNA-seq analysis conferred that autophagy inhibition is one of the strategies employed by the bacteria to maintain a dormant state (Fatima et al., 2020). A recent comparative study suggested that ABCG2 efflux pumps of bone marrow-derived MSCs are upregulated in presence of rifampicin, conferring resistant phenotype to the bacteria. Therefore, targeting these pumps will augment the action of rifampicin (Kaur et al., 2021), however, this observation needs further characterization and analysis.

Yet, there are a lot of other host cells and factors participating in *M.tb* pathogenesis including dormancy and persistence. Host environmental factors such as hypoxia, nutrient deprivation such as depletion of potassium, and availability of Vitamin C are major drivers of the dormancy of the bacteria. It has been stated that Vitamin C (Ascorbic acid) forages oxygen and induces *DevR* regulon to create a hypoxic environment and thereby dormancy (Taneja et al., 2010). Vitamin C promotes growth arrest, while vitamin C removal leads to reactivation of the Viable but non-culturable (VBNC) state of the bacteria. Thus, Vitamin C adjunctive therapy accompanied by anti-TB drugs can help eliminate the disease (Sikri et al., 2018).

2.3 BPaL incorporation in MDR treatment regimen

WHO has improvised the treatment regimen for TB known as Direct Observed Treatment Short Course (DOTS) containing the following antibiotics- Isoniazid (H), Rifampicin (R), Ethambutol (E), and Pyrazinamide (Z). As per WHO guidelines 2020, patients with rifampicin resistance or Multi Drug Resistant (MDR) TB are treated, with a combination of drugs which generally include Levofloxacin, Bedaquiline, Linezolid, Clofazimine and Cycloserine. If these drugs cannot be used, then other drugs like Ethambutol, Delamanid, Pyrazinamide, Meropenam, Amikacin, Ethionamide, p-aminosalicylic acid are added to complete the regimen (Andries et al., 2005). For treatment of LTBI, combination (Andries et al., 2005)mbination of Isoniazid, Rifapentine and Rifampin is recommended (World Health Organization, 2020).

According to the latest WHO 2022 guidelines, a new regimen is on a roll out in several countries including India for MDR TB (with resistance Fluoroquinolones) consisting of Bedaquiline, Pretomanid, and Linezolid (BPaL). This drug combination has been found to reduce the treatment regimen from eighteen months to six months (Migliori and Tiberi, 2022). The search for drugs to eliminate latent and persistent bacilli populations is continuing. The recently rolled out BPal regimen can be one of such possible leads in this direction. Studies by Andries et al. proposed the necessity of ATP synthase in *M.tb* survival despite its downregulation as compared to log-state replicating bacilli, thus making it a suitable target for dormant bacteria. Therefore, Bedaquiline which is a diarylquinolone with the ability to target the F0-F1 ATP synthase of the pathogen can target dormant bacilli. Several *in vitro* and *in vivo* models of dormancy have found a significant decline in CFU using this drug (Andries et al., 2005). Pretomanid, a nitroimidazole has also been documented to have positive correlates in the reduction of the bacteria in *in vitro* and *in vivo* dormancy models (Egorova et al., 2021). It is a pro-drug, and is known to release NO within mycobacterial cells. Apart from targeting mycolic acid synthesis, it also results in respiratory poisoning for the bacterium, and NO targets various enzymes in *M.tb* such as ATP synthase, Pks13,and RNA polymerase (Singh et al., 2008; Manjunatha et al., 2009). Linezolid is another antibiotic known to inhibit bacterial protein synthesis by binding to 23S rRNA in the bacterial 50S ribosome. It was found to have potent bactericidal activity against non-replicating bacterial cells in the murine model of latent infection (Zhang et al., 2014). With these promising results on the above-mentioned drugs. WHO has rolled out a new regimen for MDR TB (with

resistance Fluoroquinolones) consisting of Bedaquiline, Pretomanid, and Linezolid (BPaL). This drug combination has been found to reduce the treatment regimen from eighteen months to six months (Migliori and Tiberi, 2022).

2.4 Drugs and vaccines in evolution against dormant *M.tb*

A. Drugs: Several of the drugs currently in use for TB target actively replicating bacteria. There has been a lag in studying and developing drugs that specifically target dormant phase bacteria and this has been a major turn-off for developing effective short-course therapies. The various models – *in vitro* or *in vivo*, which are used to study dormancy fail to fully capture the entire clinical situation of dormancy. In this direction, meta-analysis studies can be quite helpful to predict druggable targets by integrating various results which help in better capture of granuloma heterogeneity (Murphy and Brown, 2007). Few molecules have entered the drug discovery pipeline with efficacy in eliminating the non-replicating form of the bacilli and are in the preliminary stages of study as presented in Table 2.

- **CPZEN-45:** It is a nucleoside analog that targets mycobacterial WecA enzyme, which is involved in the synthesis of the arabinogalactan layer of the mycobacterial cell wall and has been found effective against replicating and non-replicating form of the bacteria (Takahashi et al., 2013). It is a derivative of caprazamycin and it is in late-stage preclinical development (Ishizaki et al., 2013).
- **Nitrobenzothiazinone (BTZ-043):** It is a covalent inhibitor of DprE1, an enzyme that is involved in -epimerization of decaprenylphosphoryl ribose (DPR) to decaprenylphosphoryl arabinose (DPA) during arabinan synthesis of the mycobacterial cell wall. Nitrobenzothiazione derivatives have been found to effectively inhibit replicating and non-replicating *M.tb*. It is currently in phase Ia/IIb trial (Makarov et al., 2009).
- **Thioquinazoline (CBR3465), 2-mercapto-quinazolinones:** These are known to inhibit bacterial NADH dehydrogenase-2 (NDH-2), which has a role during both aerobic and anaerobic growth of the bacterium. These are in the lead identification stages.
- **Allylaminomethanone-A, 7-methoxy-2-naphthol:** Menaquinone biosynthesis is an attractive target for dormant stage bacterium. Consequently, inhibitors targeting enzymes, such as MenA of menaquinone biosynthesis are currently in the lead identification stage (Shetye et al., 2020).
- **Salicylanilide esters:** This inhibits ICL, which is found to be upregulated in non-replicating *M.tb*. This inhibitor is currently in the lead identification stage. Despite the importance of ICL in dormant TB infection, no chemical inhibitor is currently in clinical trials (Krátký et al., 2012). The already available small molecule inhibitors such as itaconate, itaconic anhydride, 3-bromopyruvate, oxalate, malate, and 3- nitropropionate (3-NP) are highly cytotoxic (Lee et al., 2015).

Based on data from various models, efforts are underway to synthesize and test small molecule inhibitors specifically targeting dormant and non-replicating bacilli. A few of them are mentioned below-

- **HC106A, 1-(4-fluorophenyl)-3-(isoxazol-5-yl)urea:** These are known to inhibit *DosRST* and were identified through chemical library screening using the *DosRST* regulon fluorescent *M.tb* reporter strain CDC1551 (Zheng et al., 2017).
- **PDKA analogs:** They target malate synthase which is involved in the second step of the glyoxylate shunt

TABLE 2 List of drugs under clinical trials trial against dormant *M.tb*.

Drug	Target	Developmental stage	Ref
CPZEN-45	WecA enzyme	Late-stage pre-clinical development	(Takahashi et al., 2013; Zhang et al., 2014)
Nitrobenzothiazinone (BTZ-043)	DprE1	Ia/IIb stage trial	(Ishizaki et al., 2013)
Allylaminomethanone-A, 7-methoxy-2-naphthol	MenA	Lead identification stage	(Makarov et al., 2009)
Salicylanilide esters	ICL	Not entered clinical trial	(Shetye et al., 2020)
HC106A	DosRST	Hit identification stage	(Lee et al., 2015)
PDKA analogues	Malate synthase	Hit identification stage	(Zheng et al., 2017)
(3-(3,4-Dichlorophenyl) ureido) benzoic acid	Cysteine synthase	Hit identification stage	(Schnell et al., 2015)
4-methoxy-2-(pyridin-4-yl) thiazole-5-carboxylic acid	Lysine ϵ-Aminotransferase (LAT)	Hit identification stage	(Betts et al., 2002)

pathway after the ICL step, and thereby inducing dormancy. Krieger et al. have synthesized methyl ester prodrug of (Z)-2-hydroxy-4-oxo-4-phenyl but-2-enoic acid (PDKA) analogs (Krieger et al., 2012).

- **(3-(3,4-Dichlorophenyl) ureido) benzoic acid:** Cysteine is known to play role in mycothiol biosynthesis, which helps in maintaining redox balance during *M.tb* dormancy. Cysteine synthase is an enzyme involved in the synthesis of cysteine using O-phosphoserine and a sulfur carrier protein CysO (Schnell et al., 2015). Urea-based compounds such as 3-(3-(3,4-Dichlorophenyl) ureido) benzoic acid have been identified as hit compounds to target cysteine synthase by Brunner et al. by using a nutrient starved model of *M.tb* dormancy (Brunner et al., 2016).
- **4-methoxy-2-(pyridin-4-yl) thiazole-5-carboxylic acid:** Lysine ϵ-Aminotransferase (LAT) enzyme has been found to have a role in persister population formation in mycobacterium (Duan et al., 2016). Studies by Betts et al., have shown this enzyme to be highly upregulated during nutrient starved model of dormancy (Betts et al., 2002). Sriram et al., have identified several hits against this target such as 4-methoxy-2-(pyridin-4-yl) thiazole-5-carboxylic acid, 1-((4-methoxyphenyl) sulfonyl)-40,50 -dihydrospiro[piperidine-4,70 -thieno[2,3-c]pyran], 2,20-oxybis(N0-(4-fluorobenzylidene) acetohydrazide). These compounds have shown positive results in *in-vitro* dormancy model (Devi et al., 2015).
- Several compounds such as quinoxaline-based molecule (6-(4-(4-fluorophenyl)piperazin-1-yl)-3-(methoxycarbonyl)-2-(trifluoromethyl)quinoxaline 1,4-dioxide), 3-triazenoindole-based molecule TU112(ethyl ester of 3-((4-methylpiperazin-1-yl) diazenyl)-1H-indole-2-carboxylic acid), thiazole derivative (ethyl ester of 2-cyclohexyl-5-(quinoxalin-6-yl)thiazole-4-carboxylic acid; compound), benzimidazole–acrylonitrile hybrid (2-(1H-benzo[d]imidazol-2-yl)-3-(4-(4-(ptolyl)piperazin-1-yl)phenyl)acrylonitrile), pyrano [3,2-b] indolones (2-oxo-2,5-dihydropyrano [3,2-b]indole-3-carbonitrile), PAMCHD (2-(((2-hydroxyphenyl)amino)methylene)-5,5-dimethylcyclohexane-1,3-dione) have been synthesized or identified as hit compounds by several research groups with proven effectiveness inhibiting dormant mycobacterium in *in-vitro* studies. But further research is required to convert these molecules into the lead compounds and test their efficacy in *in-vivo* models, and to elucidate the mechanism of action and target sites of these compounds (Egorova et al., 2021).

B. Vaccines: BCG, the only approved vaccine currently in use for TB fails to provide long-term immunity in adults. The waning immunity in the long term is due to failure in the generation of memory T cell response, and inadequate response to latency-associated antigens. BCG only generates cell-mediated immunity to secretory antigens which are mainly expressed by the rapidly growing bacterium (Dey et al., 2011). The deleted RD1 region of BCG contains several genes that are upregulated during hypoxia and nutrient-starved model of *in vitro* dormancy; thus BCG vaccine, does not prevent the establishment of latent TB infection (Andersen, 2007). Since the maximum population is vaccinated with BCG, vaccination strategies that can complement it and improve the long-term immunological response are being searched for. In this direction, researchers have proposed vaccine strategies such as the first stage use of BCG vaccine followed by second-stage use of vaccine several years after BCG such that this vaccine can act as BCG prime-boost and boost memory responses. A third stage post-exposure vaccine can be administered to prevent reactivation of latent TB (Ottenhoff and Kaufmann, 2012; Weiner and Kaufmann, 2014).

At present several prophylactic subunit vaccines are in clinical trial against TB as tabulated in Table 3, but they are based on antigens secreted by actively replicating bacilli thus undermining their utility against reactivation of LTBI (Khademi et al., 2018). Two subunit vaccines have used dormancy antigens and are in phase 1 of clinical trials. These vaccines are H56 + IC31 (H56 is a subunit vaccine candidate formulated with TLR9-agonist cationic adjuvant IC31)and ID93 + GLA-SE (ID93 is a subunit vaccine candidate with TLR4-agonist adjuvant known as Glucopyranosyl Lipid A [GLA] in a nano emulsion

TABLE 3 List of vaccines currently under study against dormant *M.tb*.

Vaccine	Vaccine type	Ref
H56 + IC31 and ID93 + GLA-SE	Prophylactic subunit vaccines	(Andersen, 2007; Ottenhoff and Kaufmann, 2012)
Rv3131	Antigen for multi-antigenic subunit vaccine	(Lu et al., 2022)
AEC/BC02	Subunit vaccine	(Rai et al., 2018)
L91	Lipidated multistage epitope-based vaccine	(Khademi et al., 2018)
Latency antigens incorporated in Modified ankara virus vector	Multi-antigenic, multiphasic vaccine	(Kwon et al., 2017)
RUTI	Therapeutic vaccine	(Cardona, 2006; Leung-Theung-Long et al., 2015)

formulation), and have been found to generate multifunctional $CD4^+$T cell response, strong Th1 response, and limit reactivation of latent TB in animal models (Weiner and Kaufmann, 2014; Luabeya et al., 2015; Khademi et al., 2018; The TBVPX-113 Study Team et al., 2018; Kaufmann, 2020).

Kwon et al. have identified Rv3131, a nitro reductase, as a suitable antigen for use in multi-antigenic subunit vaccines. This antigen was found to be upregulated during exponential as well as hypoxic growth conditions. Rv3131 administration along with GLA-SE which is a TLR4 adjuvant displayed a significant reduction in bacterial number, less extensive lung inflammation, improved multifunctional and specific $CD4^+$ T cells, effector/memory T cell expansion, improved serum IgG2c response in mice model (Kwon et al., 2017).

Subunit vaccine AEC/BC02 developed by. Lu J et al., has been found effective in reducing tissue lesions and providing protection in latently *M.tb* infected mice. The vaccine candidate also inhibited *M.tb* infection in latently infected guinea pigs. Th1-mediated immune response was predominately observed. This vaccine candidate can be further researched as a post-exposure candidate for latent *M.tb* infection (Lu et al., 2022).

Rai et al., have designed a lipidated multistage epitope-based vaccine L91 which comprises a promiscuous $CD4^+$ T cell epitope of latently associated Acr1 antigen of *M.tb* and TLR-2 agonist Pam2Cys. This candidate showed better antigen processing and presentation by DC, improved release of IFN-γ by peptide-specific $CD4^+$ T cells, and generated significant memory T cell responses. L91 immunization had better protection than BCG in mice, guinea pig, and PBMC derived from PPD^+ healthy volunteers. This construct was further refined using $CD8^+$ T cell epitope from *M.tb* antigen (TB10.4) and renamed as L4.8 (Rai et al., 2018).

Leung-Theung et al. have designed a multi-antigenic, multiphasic vaccine based on the modified Ankara virus. This construct contained 14 antigens representative of the active, latent and resuscitation phases of TB. The 3 protein fusions used were - RpfB-RpfD-Ag85B-TB10.4-ESAT-6, SF-Rv2029-Rv2626-Rv1733-Rv0111(SF- signal peptide of measles virus), and SR-Rv0569-Rv1813-Rv3407-Rv3478-Rv1807-TMR (SR-glycoprotein precursor of rabies ERA strain, TMR-membrane anchoring peptide from rabies glycoprotein). This construct was found effective in the generation of $CD4^+$T cell response, $CD8^+$T cell response, and effective cytokine generation in mice and non-human primate models (Leung-Theung-Long et al., 2015).

Therapeutic vaccine such as RUTI is currently under phase 1 clinical trial. It is a semi-purified and detoxified fragment of *M.tb* that had been cultured under stress and starvation conditions that can result in the enrichment of dormancy antigens (Cardona, 2006; Vilaplana et al., 2010).

3 Resuscitation of dormant *M.tb*

Depending upon several genetic and environmental factors, the latent bacteria are capable of undergoing reactivation or resuscitation leading to a clinically characterized state. Clinically known as resuscitation, reactivation is the active phenotype of *M.tb* after exiting the dormancy and may take up to months or years to happen. Of those latently infected with TB, about 10% of individuals re-develop the disease and are clinically diagnosed with active disease. This state is determined by the ability of the bacteria to re-grow and multiply conferring active disease upon forbearing conditions. Coinfections like HIV, metabolic disorders like diabetes or other drug-induced immune suppression as in organ transplant patients are the major drivers of resuscitation.

Resuscitation-promoting factors (Rpfs) are secreted by Actinobacteria and were initially identified in *Micrococcus luteus* (Mukamolova et al., 2002). These factors are indispensable for exiting dormancy but are not crucial for bacterial growth (Wang et al., 2021). In *M.tb*, there are five factors- rpfA-E, sharing a conserved domain known as Domains of Unknown Functions (DUF) and while RpfB and RpfE have G5 domains in addition to DUF that bind some cytoplasmic proteins. The distinguishing feature of *M.tb* rpfs is the presence of the lysozyme C and lytic transglycolase domain, possibly important in cell wall metabolism. Researchers have shown that rpfs show their catalytic activity in hydrolyzing peptidoglycan. This implies that rpfs comprise enzymatic features that allow the transition of bacteria from dormancy to reactivation (Kana and Mizrahi, 2010). There have been numerous attempts to find the other factors that participate in the resuscitation process. To date, only one factor known as the Resuscitation-promoting factor interacting protein (RipA), is discovered that interacts with RpfB to allow cell division. These two factors are known to act synergistically to modify the peptidoglycan at specific regions, thus exiting the dormancy (Nikitushkin et al., 2015). It is also reported that the deletion of protein kinase G (*pknG*) boosted the bactericidal activity of anti-TB drugs and subsequently attenuated the ability of the bacteria to resuscitate in antibiotic treated mice, thus contributing as one of the important adjunct therapy to prevent resuscitation (Khan and Nandicoori, 2021). However, there should be other supporting bacterial factors that interact with Rpfs to allow the transition to resuscitation, therefore, this area of research should be explored.

It is worth acknowledging how RpfB is functional in dormant cells to promote reactivation. Therefore, some studies have explored the bacterial components and have identified the role of one of the essential two-component systems in the regulation of RpfB. These include the MtrAB two-component system that regulates the transcription control of RpfB. MtrA is a response regulator that represses the expression of *rpfB* by binding to the promoter region of *rpfb* (Sharma et al., 2015). Apart from MtrAB, the balance of RpfB activity is maintained by co-regulation of cell wall synthesis, ribosome maturation, and resuscitation, preventing cellular toxicity. This regulation is performed by the RNA switch that permits co-transcription of

ksgA, a methyltransferase that plays a crucial role in ribosome maturation, and a kinase, *ispE* important in cell wall synthesis. This is essential for the efficient protein synthesis, thus easing in transition to resuscitation (Schwenk et al., 2018). Hence, the process of resuscitation is under multidimensional control involving early and co-transcriptional regulation but a detailed investigation is further required.

3.1 Transcriptional regulation

It is believed that during different phases of *M. tb* replication, dormancy and resuscitation, there are alterations in the transcriptional and translational state of the bacteria. Minimal efforts are put to identify such changes and reports have shown that there is an immediate transcriptomic burst of coding and non-coding RNA during resuscitation. During dormancy, there is less lipid content in bacterial cells as compared to replicating cells (Gengenbacher and Kaufmann, 2012). Hence to combat the stress, bacteria tend to upregulate the fatty acid synthase, ensuring the higher synthesis of mycolic acid that assist in cell wall synthesis for replication (Choi et al., 2000). Another major upregulation was observed in the expression of heat shock proteins and endopeptidase ClpB, which plays a crucial role in degrading misfolded proteins and maintaining protein turnover, thereby increasing the probability of reactivation (Sherrid et al., 2010). To support the growth, there is an increase in the expression of genes involved in metabolic pathways to allow cell division. WhiB6 is a transcriptional regulator that controls the metabolism and virulence of *M.tb* and is a dormancy related factor (Chen et al., 2016). These genes are involved in the early stages of resuscitation, yet some genes are more upregulated in the late stages of reactivation. These included genes responsible for aerobic respiration, ATP synthesis, and the TCA cycle to meet the energy demands of the cell to replicate (Salina et al., 2014). Iona et al., (2016), reported that several genes were upregulated during resuscitation similarly to the exponential phase (Salina et al., 2019).

3.2 Translational regulation

Despite the upregulation in transcription, minimal efforts have been made to identify the changes at the proteome level during resuscitation. SWATH-MS is a modified technique that provides the advantage of absolute quantification of the proteome in a cell. Through this technique, the absolute protein concentration of the whole cell lysate was estimated. It was observed that intracellular levels of ATP were significantly higher during the exponential phase, gradually decreasing upon hypoxia-stress i.e., dormancy. However, after re-aeration, ATP levels increased but were not equivalent to the exponential phase. Despite differences in ATP levels, F0-F1 ATP synthase levels were unaffected while other enzymes involved in energy production and metabolism were significantly upregulated. For example, NADH dehydrogenase I/II, cytochrome c reductase, cytochrome b oxidase, cytochrome c oxidase, and nitrate reductase were downregulated during resuscitation as compared to dormancy. Also, it is worth noting that enzymes involved in the methylcitrate cycle were present in higher copies during 2 days after re-aeration, suggesting that these enzymes are involved in the early phase of resuscitation. These enzymes were PrpC and PrpD. Other proteins were also upregulated during dormancy that included sigma factors such as SigE and Sig B, as well as the transcriptional regulator ClgR that regulates ClpP (Gopinath et al., 2015) (Schubert et al., 2015). However, the proteome experiments were performed on *in vitro* cultures. Since the host environment is crucial to the growth of bacteria, *in vivo* proteome study is essential and thus should be explored.

There are still missing gaps that are required to be filled to comprehend the mechanism of resuscitation. Understanding the minute changes at the transcriptional and translational levels will assist in designing the therapies against reactivation, preventing disease transmission.

3.3 Host factors responsible for resuscitation

Progression of *M.tb* in the host is mediated by various immune processes including innate and adaptive arms of the immune system. As discussed earlier, the bacteria hijack the host system to hide in latent form and thus is an escape mechanism of the pathogen from the immune system. Immune cells provide the niche for the extracellular bacteria to be contained in the granuloma. TNF-α is one of the host factors that enable the containment of bacteria in granulomas (Mezouar et al., 2019). However, due to certain environmental and genetic factors, and co-morbidities, suppression of the immune system leads to the dissemination of the bacteria resulting in disease reactivation. Upon resuscitation, the immune system is re-stimulated and generates strong T- cell responses. Researchers have put efforts to understand the antigenic stimulation of such T- cells and observed that Rpfs carry the antigenic determinants triggering the immune system in LTBI. Mutants of Rpfs have been shown to induce greater Th1 immune response and a significant decrease in bacterial load and lung pathology (Kim et al., 2013). Anti- TNF-α induces resuscitation of the bacteria and results in an increase in bacterial load. These TNF-α antagonists such as Adalimumab induce TGF-β1 to promote resuscitation, whereas lymphotoxin-α neutralization prevents reactivation (Arbués et al., 2020). DOTS therapy antibiotics such as isoniazid, rifampicin, pyrazinamide and ethambutol leads to reactivation of the dormant bacteria as it damps the immune

system causing decrease in $CD4^+$T cells (Skakun and Shman'ko, 1985; Younossian et al., 2005; Singh et al., 2021).

Despite the existing data, this is unclear how host proteins and environment support bacterial reactivation and growth. Therefore, it is one of the fascinating research areas to identify the host factors promoting resuscitation and the immune response toward resuscitated bacteria.

3.4 Existing strategies and prospects to combat resuscitation

Understanding the transition from dormancy to resuscitation is key to developing strategies to combat all the phases of disease transmission. Today's existing knowledge is less sufficient to devise a better therapy against TB reactivation, yet researchers have put forward to bring diverse ways of battling the disease.

Vaccines: There are several shreds of evidence showing that Rpf is a vital therapeutic target that has been studied to date. Few antigenic determinants of RpfD have been shown to induce polyfunctional $CD4^+$T cells while memory and effector subsets of $CD8^+$T cells were also observed (Arroyo et al., 2016). One of the mutants of Rpf is Rpfd2 which can serve as a potential vaccine target due to its ability to induce a higher Th1 response (Kim et al., 2013). Also, of all the Rpfs tested, RpfB has been a promising candidate for the DNA vaccine. It has been shown to induce a modest but significant cellular immune response against TB with higher levels of IL-2 and IFN-γ (Romano et al., 2012). Fan et al., in 2010, have shown that the RpfB domain has the ability to induce humoral response, and thereby, monoclonal antibodies against rpfs may inhibit TB recurrence (Fan et al., 2010). Collectively, Rpfs are suggested to be novel vaccine candidates but require further characterization and analysis to serve as a sub-unit vaccine. It is well-known that only available vaccine against TB is BCG that fails to induce long term memory and thereby insufficient to prevent resuscitation (Negi et al., 2022). Therefore, a potential adjunct complex, termed as peptide-TLR agonist-liposome (PTL) when administered with BCG enhances the long-term memory and reduces the rate of reactivation, thereby reduction in bacterial burden in the lungs of mice (Kumar et al., 2021).

Inhibitors: The biological activity of RpfB is dependent on LysM and LytM domains (Sexton et al., 2020), therefore inhibition of Rpf is the potential way to prevent resuscitation and thereby transmission. Further, deletion of *pknG* along with anti-TB drugs has been shown to inhibit resuscitation, suggesting that it can be targeted to prevent resuscitation (Khan and Nandicoori, 2021). Inhibition of TNF-α and lymphotoxin-α with Adalimumab and Etanercept, respectively, have been shown to induce resuscitation *via* TGF-β1 (Arbués et al., 2020). Therefore, suppressing TGF-β1 may show inhibition in resuscitation. On the other hand, computational approaches are utilised to identify small molecule inhibitors such as phytochemicals to inhibit rpfs and thereby resuscitation (Dwivedi et al., 2020). Bergenin is one of the phytochemicals that has been experimentally validated to show the modulation of the existing TB therapy and reduces immune suppression. Thus, bergenin acts as an adjunct to prevent resuscitation or reactivation of *M.tb* (Kumar et al., 2019). Curcumin is another bioactive molecule which when formulated in nanoparticles and administered as adjunct therapy prevents reactivation of the dormant bacteria (Tousif et al., 2017). Similarly, Luteolin has also been shown to provide sterile immunity when given as an adjunct to DOTS therapy and prevents reactivation (Singh et al., 2021).

It is worth noting that inhibitors preventing resuscitation may serve as an important therapeutic intervention to restrict the bacteria in dormant state. This is because it has been known that LTBI can reactivate within 2-5 years of infection (Behr et al., 2018). Thus, sustaining the bacteria in a dormant state would prevent TB transmission, thereby reducing the disease burden globally.

Since the existing anti-TB drugs are ineffective against LTBI, and as mentioned earlier, they are proven to dampen the immune system, therefore, combining inhibitors of resuscitation along with standard anti-TB drugs can prevent the further reactivation and progression of the disease.

Repurposed drugs: The repurposing of drugs has proven to be highly efficient in preventing pulmonary TB and thereby, reactivation. One such drug is statins, inhibitors of HMG-CoA reductase. It is known that *M.tb* utilizes cholesterol to infect the immune cells and therefore survive within them (Istvan and Deisenhofer, 2001). Therefore, statins are used as host-directed therapy. It is given as an adjunct with anti-TB drugs that depletes the cholesterol, making environmental conditions harsh for the bacteria survival (Lobato et al., 2014). Similarly, anti-diabetic drug, metformin is also administered along with statins to reduce the prevalence of LTBI and thus, prevents resuscitation (Magee et al., 2019). Along with this, corticosteroids such as dexamethasone is also used an adjunct with standard TB drugs. Dexamethasone inhibits the *M.tb*- induced necrotic cell death in the host thus preventing disease reactivation (Gräb et al., 2019).

Taken together, more understanding of the mechanism of transition from dormancy to resuscitation is required to invent therapies against TB. Also, there are possible host factors that promote reactivation, thus discovering them and modulating them is essential to have definitive host-directed strategies to combat this highly infectious disease.

4 Concluding remarks

Of all the infected individuals, 90% of individuals develop LTBI while in 10% of them, the bacteria resuscitate and develop active disease. Thus, controlling the infection at the state of dormancy or resuscitation is important to prevent transmission.

Nonetheless, the mechanism of transition from dormancy to resuscitation is less explored due to the lack of a perfect model of dormancy, hence it is a drawback in devising prophylactic and therapeutic strategies. In this direction, bioinformatic studies such as meta-analysis can be a powerful tool to integrate and score results arising from different models of dormancy and thus bridge the limitations prevailing amongst the current dormancy models. Resolving the dilemma over LTBI i.e., whether lifelong latency is associated with TB or it is majorly a transmissible disease from active TB patients can be the key towards the WHO End TB goal. Epidemiological studies and newer biomarker discoveries can help attain this goal by directing resources towards the most definitive cause and eventually reduction in the global TB burden.

Targeting the host factors to battle the disease may provide a better way of preventing disease as compared to the drugs against bacterial factors due to the high chances of emergence of drug resistance. Targeting the host factors as discussed in this review, such as factors responsible for a hypoxic environment that drives granuloma formation seems to be crucial in eradicating the bacteria. Thus, accompanying anti-TB drugs with host-directed therapies can be one of the crucial strategies to prevent TB. Employing combinatorial therapies is the key to fight with drug-resistant TB.

Author contributions

AB designed the theme of the manuscript. AV and AG conducted the literature search and wrote the manuscript. AV drew the schematic diagram and AG made the tables. AB and VD critically reviewed and edited the final version of the manuscript. All authors read and approved the final manuscript.

Conflict of interest

The authors declare that the research was conducted in the absence of any commercial or financial relationships that could be construed as a potential conflict of interest.

Publisher's note

All claims expressed in this article are solely those of the authors and do not necessarily represent those of their affiliated organizations, or those of the publisher, the editors and the reviewers. Any product that may be evaluated in this article, or claim that may be made by its manufacturer, is not guaranteed or endorsed by the publisher.

References

Alnimr, A. M. (2015). Dormancy models for mycobacterium tuberculosis: A minireview. *Braz. J. Microbiol.* 46 (3), 641–647. doi: 10.1590/S1517-838246320140507

Andersen, P. (2007). Vaccine strategies against latent tuberculosis infection. *Trends Microbiol.* 15 (1), 7–13. doi: 10.1016/j.tim.2006.11.008

Andries, K., Verhasselt, P., Guillemont, J., Göhlmann, H. W. H., Neefs, J. M., Winkler, H., et al. (2005). A diarylquinoline drug active on the ATP synthase of mycobacterium tuberculosis. *Science.* 307 (5707), 223–227. doi: 10.1126/science.1106753

Arbués, A., Brees, D., Chibout, S. D., Fox, T., Kammüller, M., and Portevin, D. (2020). TNF-α antagonists differentially induce TGF-β1-dependent resuscitation of dormant-like mycobacterium tuberculosis. *PloS Pathog.* 16 (2), e1008312. doi: 10.1371/journal.ppat.1008312

Arroyo, L., Rojas, M., Franken, K. L. M. C., Ottenhoff, T. H. M., and Barrera, L. F. (2016). Multifunctional T cell response to DosR and rpf antigens is associated with protection in long-term mycobacterium tuberculosis-infected individuals in Colombia. *Clin. Vaccine Immunol.* 23 (10), 813–824. doi: 10.1128/CVI.00217-16

Bañuls, A. L., Sanou, A., Van Anh, N. T., and Godreuil, S. (2015). Mycobacterium tuberculosis: ecology and evolution of a human bacterium. *J. Med. Microbiol.* 64 (11), 1261–1269. doi: 10.1099/jmm.0.000171

Barberis, I., Bragazzi, N. L., Galluzzo, L., and Martini, M. (2017). The history of tuberculosis: from the first historical records to the isolation of koch's bacillus. *J. Prev. Med. Hyg.* 58 (1), E9–12.

Behr, M. A., Edelstein, P. H., and Ramakrishnan, L. (2018). Revisiting the timetable of tuberculosis. *BMJ* 23, k2738. doi: 10.1136/bmj.k2738

Behr, M. A., Edelstein, P. H., and Ramakrishnan, L. (2019). Is mycobacterium tuberculosis infection life long? *BMJ.* 24, l5770. doi: 10.1136/bmj.l5770

Behr, M. A., Kaufmann, E., Duffin, J., Edelstein, P. H., and Ramakrishnan, L. (2021). Latent tuberculosis: Two centuries of confusion. *Am. J. Respir. Crit. Care Med.* 204 (2), 142–148. doi: 10.1164/rccm.202011-4239PP

Beste, D. J. V., Espasa, M., Bonde, B., Kierzek, A. M., Stewart, G. R., and McFadden, J. (2009). The genetic requirements for fast and slow growth in mycobacteria. neyrolles O, editor. *PloS One* 4 (4), e5349. doi: 10.1371/journal.pone.0005349

Betts, J. C., Lukey, P. T., Robb, L. C., McAdam, R. A., and Duncan, K. (2002). Evaluation of a nutrient starvation model of mycobacterium tuberculosis persistence by gene and protein expression profiling: Nutrient starvation of m. *tuberculosis*. *Mol. Microbiol.* 43 (3), 717–731. doi: 10.1046/j.1365-2958.2002.02779.x

Bhaskar, A., Dwivedi, V. P., and Nandicoori, V. K. (2019). "Eliminating mycobacterial persistence: Novel targets for anti-TB therapy," in *Pathogenicity and drug resistance of human pathogens*. Eds. S. Hameed, Z. Fatima, et al (Singapore: Springer Singapore), 57–79. Available at: http://link.springer.com. doi: 10.1007/978-981-32-9449-3_3

Bold, T. D., and Ernst, J. D. (2009). Who benefits from granulomas, mycobacteria or host? *Cell.* 136 (1), 17–19. doi: 10.1016/j.cell.2008.12.032

Boom, W. H., Schaible, U. E., and Achkar, J. M. (2021). The knowns and unknowns of latent mycobacterium tuberculosis infection. *J. Clin. Invest.* 131 (3), 136222. doi: 10.1172/JCI136222

Brandt, L., Feino Cunha, J., Weinreich Olsen, A., Chilima, B., Hirsch, P., Appelberg, R., et al. (2002). Failure of the mycobacterium bovis BCG vaccine: some species of environmental mycobacteria block multiplication of BCG and induction of protective immunity to tuberculosis. *Infect. Immun.* 70 (2), 672–678. doi: 10.1128/IAI.70.2.672-678.2002

Brunner, K., Maric, S., Reshma, R. S., Almqvist, H., Seashore-Ludlow, B., Gustavsson, A. L., et al. (2016). Inhibitors of the cysteine synthase CysM with antibacterial potency against dormant mycobacterium tuberculosis. *J. Med. Chem.* 59 (14), 6848–6859. doi: 10.1021/acs.jmedchem.6b00674

Cambau, E, and Drancourt, M. (2014). Steps towards the discovery of Mycobacterium tuberculosis by Robert Koch, 1882. *Clinical Microbiology and Infection* 20 (3), 196–201. doi: 10.1111/1469-0691.12555

Cardona, P. J. (2006). RUTI: A new chance to shorten the treatment of latent tuberculosis infection. *Tuberculosis.* 86 (3–4), 273–289. doi: 10.1016/j.tube.2006.01.024

Chen, Z., Hu, Y., Cumming, B. M., Lu, P., Feng, L., Deng, J., et al. (2016). Mycobacterial WhiB6 differentially regulates ESX-1 and the dos regulon to modulate granuloma formation and virulence in zebrafish. *Cell Rep.* 16 (9), 2512–2524. doi: 10.1016/j.celrep.2016.07.080

Choi, K. H., Kremer, L., Besra, G. S., and Rock, C. O. (2000). Identification and substrate specificity of beta -ketoacyl (acyl carrier protein) synthase III (mtFabH) from mycobacterium tuberculosis. *J. Biol. Chem.* 275 (36), 28201–28207. doi: 10.1074/jbc.M003241200

Cohen, S. B., Gern, B. H., Delahaye, J. L., Adams, K. N., Plumlee, C. R., Winkler, J. K., et al. (2018). Alveolar macrophages provide an early mycobacterium tuberculosis niche and initiate dissemination. *Cell Host Microbe* 24 (3), 439–446.e4. doi: 10.1016/j.chom.2018.08.001

de Oliveira Rodrigues, M., de Almeida Testa, L. H., dos Santos, A. C. F., Zanetti, L. P., da Silva Ruiz, L., de Souza, M. P., et al. (2021). Latent and active tuberculosis infection in allogeneic hematopoietic stem cell transplant recipients: a prospective cohort study. *Bone Marrow Transplant.* 56 (9), 2241–2247. doi: 10.1038/s41409-021-01329-3

Devi, P. B., Sridevi, J. P., Kakan, S. S., Saxena, S., Jeankumar, V. U., Soni, V., et al. (2015). Discovery of novel lysine ε-aminotransferase inhibitors: An intriguing potential target for latent tuberculosis. *Tuberculosis.* 95 (6), 786–794. doi: 10.1016/j.tube.2015.04.010

Dey, B., Jain, R., Gupta, U. D., Katoch, V. M., Ramanathan, V. D., and Tyagi, A. K. (2011). A booster vaccine expressing a latency-associated antigen augments BCG induced immunity and confers enhanced protection against tuberculosis. chakravortty d, editor. *PloS One* 6 (8), e23360. doi: 10.1371/journal.pone.0023360

Duan, X., Li, Y., Du, Q., Huang, Q., Guo, S., Xu, M., et al. (2016). Mycobacterium lysine ε-aminotransferase is a novel alarmone metabolism related persister gene *via* dysregulating the intracellular amino acid level. *Sci. Rep.* 6 (1), 19695. doi: 10.1038/srep19695

Du, P., Sohaskey, C. D., and Shi, L. (2016). Transcriptional and physiological changes during mycobacterium tuberculosis reactivation from non-replicating persistence. *Front. Microbiol.* 7. doi: 10.3389/fmicb.2016.01346/abstract. http://journal.frontiersin.org/Article/.

Dwivedi, V. D., Arya, A., Sharma, T., Sharma, S., Patil, S. A., and Gupta, V. K. (2020). Computational investigation of phytomolecules as resuscitation-promoting factor b (RpfB) inhibitors for clinical suppression of mycobacterium tuberculosis dormancy reactivation. *Infect. Genet. Evol.* 83, 104356. doi: 10.1016/j.meegid.2020.104356

Egorova, A., Salina, E. G., and Makarov, V. (2021). Targeting non-replicating mycobacterium tuberculosis and latent infection: Alternatives and perspectives (Mini-review). *IJMS.* 22 (24), 13317. doi: 10.3390/ijms222413317

Ehlers, S., and Schaible, U. E. (2013). The granuloma in tuberculosis: Dynamics of a host–pathogen collusion. *Front. Immun.* 3. doi: 10.3389/fimmu.2012.00411/.

Ehrt, S., Schnappinger, D., and Rhee, K. Y. (2018). Metabolic principles of persistence and pathogenicity in mycobacterium tuberculosis. *Nat. Rev. Microbiol.* 16 (8), 496–507. doi: 10.1038/s41579-018-0013-4

Fan, A., Jian, W., Shi, C., Ma, Y., Wang, L., Peng, D., et al. (2010). Production and characterization of monoclonal antibody against mycobacterium tuberculosis RpfB domain. *Hybridoma (Larchmt).* 29 (4), 327–332. doi: 10.1089/hyb.2010.0007

Fatima, S., Kamble, S. S., Dwivedi, V. P., Bhattacharya, D., Kumar, S., Ranganathan, A., et al. (2020). Mycobacterium tuberculosis programs mesenchymal stem cells to establish dormancy and persistence. *J. Clin. Invest.* 130 (2), 655–661. doi: 10.1172/JCI128043

Fenhalls, G., Stevens, L., Moses, L., Bezuidenhout, J., Betts, J. C., Helden, Pv P.v., et al. (2002). *In situ* detection of mycobacterium tuberculosis transcripts in human lung granulomas reveals differential gene expression in necrotic lesions. *Infect. Immun.* 70 (11), 6330–6338. doi: 10.1128/IAI.70.11.6330-6338.2002

Flynn, J. L., and Chan, J. (2003). Immune evasion by mycobacterium tuberculosis: living with the enemy. *Curr. Opin. Immunol.* 15 (4), 450–455. doi: 10.1016/s0952-7915(03)00075-x

Gaonkar, S., Bharath, S., Kumar, N., Balasubramanian, V., and Shandil, R. K. (2010). Aerosol infection model of tuberculosis in wistar rats. *Int. J. Microbiol.* 2010, 1–6. doi: 10.1155/2010/426035

Gautam, U. S., Mehra, S., Ahsan, M. H., Alvarez, X., Niu, T., and Kaushal, D. (2014). Role of TNF in the altered interaction of dormant mycobacterium tuberculosis with host macrophages. *PloS One* 9 (4), e95220. doi: 10.1371/journal.pone.0095220

Gengenbacher, M., and Kaufmann, S. H. E. (2012). Mycobacterium tuberculosis: success through dormancy. *FEMS Microbiol. Rev.* 36 (3), 514–532. doi: 10.1111/j.1574-6976.2012.00331.x

Gopinath, V., Raghunandanan, S., Gomez, R. L., Jose, L., Surendran, A., Ramachandran, R., et al. (2015). Profiling the proteome of mycobacterium tuberculosis during dormancy and reactivation. *Mol. Cell Proteomics.* 14 (8), 2160–2176. doi: 10.1074/mcp.M115.051151

Gräb, J., Suárez, I., van Gumpel, E., Winter, S., Schreiber, F., Esser, A., et al. (2019). Corticosteroids inhibit mycobacterium tuberculosis-induced necrotic host cell death by abrogating mitochondrial membrane permeability transition. *Nat. Commun.* 10 (1), 688. doi: 10.1038/s41467-019-08405-9

Harper, J., Skerry, C., Davis, S. L., Tasneen, R., Weir, M., Kramnik, I., et al. (2012). Mouse model of necrotic tuberculosis granulomas develops hypoxic lesions. *J. Infect. Diseases.* 205 (4), 595–602. doi: 10.1093/infdis/jir786

Hmama, Z., Peña-Díaz, S., Joseph, S., and Av-Gay, Y. (2015). Immunoevasion and immunosuppression of the macrophage by mycobacterium tuberculosis. *Immunol. Rev.* 264 (1), 220–232. doi: 10.1111/imr.12268

Hudock, T. A., Foreman, T. W., Bandyopadhyay, N., Gautam, U. S., Veatch, A. V., LoBato, D. N., et al. (2017). Hypoxia sensing and persistence genes are expressed during the intragranulomatous survival of mycobacterium tuberculosis. *Am. J. Respir. Cell Mol. Biol.* 56 (5), 637–647. doi: 10.1165/rcmb.2016-0239OC

Hu, Y., Zheng, X., Davies Forsman, L., Ning, Z., Chen, C., Gao, Y., et al. (2021). Emergence of additional drug resistance during treatment of multidrug-resistant tuberculosis in China: a prospective cohort study. *Clin. Microbiol. Infect.* 27 (12), 1805–1813. doi: 10.1016/j.cmi.2021.04.001

Iizasa, E., Chuma, Y., Uematsu, T., Kubota, M., Kawaguchi, H., Umemura, M., et al. (2021). TREM2 is a receptor for non-glycosylated mycolic acids of mycobacteria that limits anti-mycobacterial macrophage activation. *Nat. Commun.* 12 (1), 2299. doi: 10.1038/s41467-021-22620-3

Iona, E., Pardini, M., Mustazzolu, A., Piccaro, G., Nisini, R., Fattorini, L., et al. (2016). Mycobacterium tuberculosis gene expression at different stages of hypoxia-induced dormancy and upon resuscitation. *J. Microbiol.* 54 (8), 565–572. doi: 10.1007/s12275-016-6150-4

Ishizaki, Y., Hayashi, C., Inoue, K., Igarashi, M., Takahashi, Y., Pujari, V., et al. (2013). Inhibition of the first step in synthesis of the mycobacterial cell wall core, catalyzed by the GlcNAc-1-phosphate transferase WecA, by the novel caprazamycin derivative CPZEN-45. *J. Biol. Chem.* 288 (42), 30309–30319. doi: 10.1074/jbc.M113.492173

Istvan, E. S., and Deisenhofer, J. (2001). Structural mechanism for statin inhibition of HMG-CoA reductase. *Science.* 292 (5519), 1160–1164. doi: 10.1126/science.1059344

Jain, N., Kalam, H., Singh, L., Sharma, V., Kedia, S., Das, P., et al. (2020). Mesenchymal stem cells offer a drug-tolerant and immune-privileged niche to mycobacterium tuberculosis. *Nat. Commun.* 11 (1), 3062. doi: 10.1038/s41467-020-16877-3

Kana, B. D., and Mizrahi, V. (2010). Resuscitation-promoting factors as lytic enzymes for bacterial growth and signaling. *FEMS Immunol. Med. Microbiol.* 58 (1), 39–50. doi: 10.1111/j.1574-695X.2009.00606.x

Kaufmann, S. H. E. (2020). Vaccination against tuberculosis: Revamping BCG by molecular genetics guided by immunology. *Front. Immunol.* 11, 316. doi: 10.3389/fimmu.2020.00316

Kaur, S., Angrish, N., Gupta, K., Tyagi, A. K., and Khare, G. (2021). Inhibition of ABCG2 efflux pumps renders the mycobacterium tuberculosis hiding in mesenchymal stem cells responsive to antibiotic treatment. *Infect. Genet. Evol.* 87, 104662. doi: 10.1016/j.meegid.2020.104662

Khademi, F., Derakhshan, M., Yousefi-Avarvand, A., Tafaghodi, M., and Soleimanpour, S. (2018). Multi-stage subunit vaccines against mycobacterium tuberculosis: an alternative to the BCG vaccine or a BCG-prime boost? *Expert Rev. Vaccines* 17 (1), 31–44. doi: 10.1080/14760584.2018.1406309

Khan, M. Z., and Nandicoori, V. K. (2021). Deletion of pknG abates reactivation of latent mycobacterium tuberculosis in mice. *Antimicrob. Agents Chemother.* 65 (4), e02095–e02020. doi: 10.1128/AAC.02095-20

Kim, J. S., Kim, W. S., Choi, H. G., Jang, B., Lee, K., Park, J. H., et al. (2013). Mycobacterium tuberculosis RpfB drives Th1-type T cell immunity *via* a TLR4-dependent activation of dendritic cells. *J. Leukoc. Biol.* 94 (4), 733–749. doi: 10.1189/jlb.0912435

Krátký, M., Vinšová, J., Novotná, E., Mandíková, J., Wsól, V., Trejtnar, F., et al. (2012). Salicylanilide derivatives block mycobacterium tuberculosis through inhibition of isocitrate lyase and methionine aminopeptidase. *Tuberculosis.* 92 (5), 434–439. doi: 10.1016/j.tube.2012.06.001

Krieger, I. V., Freundlich, J. S., Gawandi, V. B., Roberts, J. P., Gawandi, V. B., Sun, Q., et al. (2012). Structure-guided discovery of phenyl-diketo acids as potent inhibitors of m. tuberculosis malate synthase. *Chem. Biol.* 19 (12), 1556–1567. doi: 10.1016/j.chembiol.2012.09.018

Kumar, S., Bhaskar, A., Patnaik, G., Sharma, C., Singh, D. K., Kaushik, S. R., et al. (2021). Intranasal immunization with peptide-based immunogenic complex enhances BCG vaccine efficacy in a murine model of tuberculosis. *JCI Insight* 6 (4), 145228. doi: 10.1172/jci.insight.145228

Kumar, A., Lewin, A., Rani, P. S., Qureshi, I. A., Devi, S., Majid, M., et al. (2013). Dormancy associated translation inhibitor (DATIN/Rv0079) of mycobacterium

tuberculosis interacts with TLR2 and induces proinflammatory cytokine expression. *Cytokine.* 64 (1), 258–264. doi: 10.1016/j.cyto.2013.06.310

Kumar, S., Sharma, C., Kaushik, S. R., Kulshreshtha, A., Chaturvedi, S., Nanda, R. K., et al. (2019). The phytochemical bergenin as an adjunct immunotherapy for tuberculosis in mice. *J. Biol. Chem.* 294 (21), 8555–8563. doi: 10.1074/jbc.RA119.008005

Kwon, K. W., Kim, W. S., Kim, H., Han, S. J., Hahn, M. Y., Lee, J. S., et al. (2017). Novel vaccine potential of Rv3131, a DosR regulon-encoded putative nitroreductase, against hyper-virulent mycobacterium tuberculosis strain K. *Sci. Rep.* 7 (1), 44151. doi: 10.1038/srep44151

Lee, Y. V., Wahab, H. A., and Choong, Y. S. (2015). Potential inhibitors for isocitrate lyase of mycobacterium tuberculosis and non- m. *tuberculosis: A Summary. BioMed. Res. Int.* 2015, 1–20. doi: 10.1155/2015/895453

Leung-Theung-Long, S., Gouanvic, M., Coupet, C. A., Ray, A., Tupin, E., Silvestre, N., et al. (2015). A novel MVA-based multiphasic vaccine for prevention or treatment of tuberculosis induces broad and multifunctional cell-mediated immunity in mice and primates. *PloS One* 10 (11), e0143552. doi: 10.1371/journal.pone.0143552

Lobato, L. S., Rosa, P. S., Ferreira J da, S., Neumann A da, S., da Silva, M. G., do Nascimento, D. C., et al. (2014). Statins increase rifampin mycobactericidal effect. *Antimicrob. Agents Chemother.* 58 (10), 5766–5774. doi: 10.1128/AAC.01826-13

Luabeya, A. K. K., Kagina, B. M. N., Tameris, M. D., Geldenhuys, H., Hoff, S. T., Shi, Z., et al. (2015). First-in-human trial of the post-exposure tuberculosis vaccine H56:IC31 in mycobacterium tuberculosis infected and non-infected healthy adults. *Vaccine.* 33 (33), 4130–4140. doi: 10.1016/j.vaccine.2015.06.051

Lu, J., Guo, X., Wang, C., Du, W., Shen, X., Su, C., et al. (2022). Therapeutic effect of subunit vaccine AEC/BC02 on mycobacterium tuberculosis post-chemotherapy relapse using a latent infection murine model. *Vaccines (Basel).* 10 (5), 825. doi: 10.3390/vaccines10050825

Magee, M. J., Salindri, A. D., Kornfeld, H., and Singhal, A. (2019). Reduced prevalence of latent tuberculosis infection in diabetes patients using metformin and statins. *Eur. Respir. J.* 53 (3), 1801695. doi: 10.1183/13993003.01695-2018

Makarov, V., Manina, G., Mikusova, K., Möllmann, U., Ryabova, O., Saint-Joanis, B., et al. (2009). Benzothiazinones kill mycobacterium tuberculosis by blocking arabinan synthesis. *Science.* 324 (5928), 801–804. doi: 10.1126/science.1171583

Manjunatha, U., Boshoff, H. I. M., and Barry, C. E. (2009). The mechanism of action of PA-824: Novel insights from transcriptional profiling. *Communicative Integr. Biol.* 2 (3), 215–218. doi: 10.4161/cib.2.3.7926

Mezouar, S., Diarra, I., Roudier, J., Desnues, B., and Mege, J. L. (2019). Tumor necrosis factor-alpha antagonist interferes with the formation of granulomatous multinucleated giant cells: New insights into mycobacterium tuberculosis infection. *Front. Immunol.* 10, 1947. doi: 10.3389/fimmu.2019.01947

Migliori, G. B., and Tiberi, S. (2022). WHO drug-resistant TB guidelines 2022: what is new? *Int. J. tuberc Lung Dis.*, 26(7)590–591. doi: 10.5588/ijtld.22.0263

Mothé, B. R., Lindestam Arlehamn, C. S., Dow, C., Dillon, M. B. C., Wiseman, R. W., Bohn, P., et al. (2015). The TB-specific CD4+ T cell immune repertoire in both cynomolgus and rhesus macaques largely overlap with humans. *Tuberculosis.* 95 (6), 722–735. doi: 10.1016/j.tube.2015.07.005

Mubin, N., Pahari, S., Owais, M., and Zubair, S. (2018). Mycobacterium tuberculosis host cell interaction: Role of latency associated protein acr-1 in differential modulation of macrophages. rottenberg ME, editor. *PloS One* 13 (11), e0206459. doi: 10.1371/journal.pone.0206459

Mukamolova, G. V., Turapov, O. A., Kazarian, K., Telkov, M., Kaprelyants, A. S., Kell, D. B., et al. (2002). The rpf gene of micrococcus luteus encodes an essential secreted growth factor. *Mol. Microbiol.* 46 (3), 611–621. doi: 10.1046/j.1365-2958.2002.03183.x

Murphy, D. J., and Brown, J. R. (2007). Identification of gene targets against dormant phase mycobacterium tuberculosis infections. *BMC Infect. Dis.* 7 (1), 84. doi: 10.1186/1471-2334-7-84

Negi, K., Bhaskar, A., and Dwivedi, V. P. (2022). Progressive host-directed strategies to potentiate BCG vaccination against tuberculosis. *Front. Immunol.* 13, 944183. doi: 10.3389/fimmu.2022.944183

Nikitushkin, V. D., Demina, G. R., Shleeva, M. O., Guryanova, S. V., Ruggiero, A., Berisio, R., et al. (2015). A product of RpfB and RipA joint enzymatic action promotes the resuscitation of dormant mycobacteria. *FEBS J.* 282 (13), 2500–2511. doi: 10.1111/febs.13292

Ottenhoff, T. H. M., and Kaufmann, S. H. E. (2012). Vaccines against tuberculosis: where are we and where do we need to go? *PloS Pathog.* 8 (5), e1002607. doi: 10.1371/journal.ppat.1002607

Pawlowski, A., Jansson, M., Sköld, M., Rottenberg, M. E., and Källenius, G. (2012). Tuberculosis and HIV co-infection. *PloS Pathog.* 8 (2), e1002464. doi: 10.1371/journal.ppat.1002464

Poh, X. Y., Hong, J. M., Bai, C., Miow, Q. H., Thong, P. M., Wang, Y., et al. (2022). Nos2–/– mice infected with m. tuberculosis develop neurobehavioral changes and immunopathology mimicking human central nervous system tuberculosis. *J. Neuroinflammation.* 19 (1), 21. doi: 10.1186/s12974-022-02387-0

Rai, P. K., Chodisetti, S. B., Maurya, S. K., Nadeem, S., Zeng, W., Janmeja, A. K., et al. (2018). A lipidated bi-epitope vaccine comprising of MHC-I and MHC-II binder peptides elicits protective CD4 T cell and CD8 T cell immunity against mycobacterium tuberculosis. *J. Transl. Med.* 16 (1), 279. doi: 10.1186/s12967-018-1653-x

Rao, S. P. S., Alonso, S., Rand, L., Dick, T., and Pethe, K. (2008). The protonmotive force is required for maintaining ATP homeostasis and viability of hypoxic, nonreplicating mycobacterium tuberculosis. *Proc. Natl. Acad. Sci. U.S.A.* 105 (33), 11945–11950. doi: 10.1073/pnas.0711697105

Rodrigues-Junior, V. S., Cintra, L., Machado, P., Dadda, A., Basso, L. A., Mafra, A. C. C. N., et al. (2017). Toxicological profile of IQG-607 after single and repeated oral administration in minipigs: An essential step towards phase I clinical trial. *Regul. Toxicol. Pharmacol.* 90, 78–86. doi: 10.1016/j.yrtph.2017.08.015

Romano, M., Aryan, E., Korf, H., Bruffaerts, N., Franken, C. L. M. C., Ottenhoff, T. H. M., et al. (2012). Potential of mycobacterium tuberculosis resuscitation-promoting factors as antigens in novel tuberculosis sub-unit vaccines. *Microbes Infect.* 14 (1), 86–95. doi: 10.1016/j.micinf.2011.08.011

Salina, E. G., Grigorov, A. S., Bychenko, O. S., Skvortsova, Y. V., Mamedov, I. Z., Azhikina, T. L., et al. (2019). Resuscitation of dormant "Non-culturable" mycobacterium tuberculosis is characterized by immediate transcriptional burst. *Front. Cell Infect. Microbiol.* 9, 272. doi: 10.3389/fcimb.2019.00272

Salina, E. G., Waddell, S. J., Hoffmann, N., Rosenkrands, I., Butcher, P. D., and Kaprelyants, A. S. (2014). Potassium availability triggers mycobacterium tuberculosis transition to, and resuscitation from, non-culturable (dormant) states. *Open Biol.* 4 (10), 140106. doi: 10.1098/rsob.140106

Schnell, R., Sriram, D., and Schneider, G. (2015). Pyridoxal-phosphate dependent mycobacterial cysteine synthases: Structure, mechanism and potential as drug targets. *Biochim. Biophys. Acta (BBA) - Proteins Proteomics.* 1854 (9), 1175–1183. doi: 10.1016/j.bbapap.2014.11.010

Schubert, O. T., Ludwig, C., Kogadeeva, M., Zimmermann, M., Rosenberger, G., Gengenbacher, M., et al. (2015). Absolute proteome composition and dynamics during dormancy and resuscitation of mycobacterium tuberculosis. *Cell Host Microbe* 18 (1), 96–108. doi: 10.1016/j.chom.2015.06.001

Schwenk, S., Moores, A., Nobeli, I., McHugh, T. D., and Arnvig, K. B. (2018). Cell-wall synthesis and ribosome maturation are co-regulated by an RNA switch in mycobacterium tuberculosis. *Nucleic Acids Res.* 46 (11), 5837–5849. doi: 10.1093/nar/gky226

Sexton, D. L., Herlihey, F. A., Brott, A. S., Crisante, D. A., Shepherdson, E., Clarke, A. J., et al. (2020). Roles of LysM and LytM domains in resuscitation-promoting factor (Rpf) activity and rpf-mediated peptidoglycan cleavage and dormant spore reactivation. *J. Biol. Chem.* 295 (27), 9171–9182. doi: 10.1074/jbc.RA120.013994

Sharma, A. K., Chatterjee, A., Gupta, S., Banerjee, R., Mandal, S., Mukhopadhyay, J., et al. (2015). MtrA, an essential response regulator of the MtrAB two-component system, regulates the transcription of resuscitation-promoting factor b of mycobacterium tuberculosis. *Microbiol. (Reading).* 161 (6), 1271–1281. doi: 10.1099/mic.0.000087

Sherrid, A. M., Rustad, T. R., Cangelosi, G. A., and Sherman, D. R. (2010). Characterization of a clp protease gene regulator and the reaeration response in mycobacterium tuberculosis. *PloS One* 5 (7), e11622. doi: 10.1371/journal.pone.0011622

Shetye, G. S., Franzblau, S. G., and Cho, S. (2020). New tuberculosis drug targets, their inhibitors, and potential therapeutic impact. *Trans. Res.* 220, 68–97. doi: 10.1016/j.trsl.2020.03.007

Siddiqui, K. F., Amir, M., Gurram, R. K., Khan, N., Arora, A., Rajagopal, K., et al. (2014). Latency-associated protein Acr1 impairs dendritic cell maturation and functionality: a possible mechanism of immune evasion by mycobacterium tuberculosis. *J. Infect. Dis.* 209 (9), 1436–1445. doi: 10.1093/infdis/jit595

Sikri, K., Duggal, P., Kumar, C., Batra, S. D., Vashist, A., Bhaskar, A., et al. (2018). Multifaceted remodeling by vitamin c boosts sensitivity of mycobacterium tuberculosis subpopulations to combination treatment by anti-tubercular drugs. *Redox Biol.* 15, 452–466. doi: 10.1016/j.redox.2017.12.020

Singh, R., Dwivedi, S. P., Gaharwar, U. S., Meena, R., Rajamani, P., and Prasad, T. (2020). Recent updates on drug resistance in mycobacterium tuberculosis. *J. Appl. Microbiol.* 128 (6), 1547–1567. doi: 10.1111/jam.14478

Singh, R., Manjunatha, U., Boshoff, H. I. M., Ha, Y. H., Niyomrattanakit, P., Ledwidge, R., et al. (2008). PA-824 kills nonreplicating mycobacterium tuberculosis by intracellular NO release. *Science.* 322 (5906), 1392–1395. doi: 10.1126/science.1164571

Singh, V. K., Mishra, A., Bark, S., Mani, A., Subbian, S., Hunter, R. L., et al. (2020). Human mesenchymal stem cell based intracellular dormancy model of mycobacterium tuberculosis. *Microbes Infection.* 22 (9), 423–431. doi: 10.1016/j.micinf.2020.05.015

Singh, D. K., Tousif, S., Bhaskar, A., Devi, A., Negi, K., Moitra, B., et al. (2021). Luteolin as a potential host-directed immunotherapy adjunct to isoniazid treatment of tuberculosis. *PloS Pathog.* 17 (8), e1009805. doi: 10.1371/journal.ppat.1009805

Skakun, N. P., and Shman'ko, V. V. (1985). Synergistic effect of rifampicin on hepatotoxicity of isoniazid. *Antibiot Med. Biotekhnol.* 30 (3), 185–189.

Smith, I. (2003). Mycobacterium tuberculosis pathogenesis and molecular determinants of virulence. *Clin. Microbiol. Rev.* 16 (3), 463–496. doi: 10.1128/CMR.16.3.463-496.2003

Takahashi, Y., Igarashi, M., Miyake, T., Soutome, H., Ishikawa, K., Komatsuki, Y., et al. (2013). Novel semisynthetic antibiotics from caprazamycins a–G: caprazene derivatives and their antibacterial activity. *J. Antibiot.* 66 (3), 171–178. doi: 10.1038/ja.2013.9

Talaat, A. M., Lyons, R., Howard, S. T., and Johnston, S. A. (2004). The temporal expression profile of mycobacterium tuberculosis infection in mice. *Proc. Natl. Acad. Sci. U.S.A.* 101 (13), 4602–4607. doi: 10.1073/pnas.0306023101

Taneja, N. K., Dhingra, S., Mittal, A., Naresh, M., and Tyagi, J. S. (2010). Mycobacterium tuberculosis transcriptional adaptation, growth arrest and dormancy phenotype development is triggered by vitamin c. *PloS One* 5 (5), e10860. doi: 10.1371/journal.pone.0010860

The TBVPX-113 Study Team, Coler, R. N., Day, T. A., Ellis, R., Piazza, F. M., Beckmann, A. M., et al. (2018). The TLR-4 agonist adjuvant, GLA-SE, improves magnitude and quality of immune responses elicited by the ID93 tuberculosis vaccine: first-in-human trial. *NPJ Vaccines* 3 (1), 34. doi: 10.1038/s41541-018-0057-5

Timm, J., Post, F. A., Bekker, L. G., Walther, G. B., Wainwright, H. C., Manganelli, R., et al. (2003). Differential expression of iron-, carbon-, and oxygen-responsive mycobacterial genes in the lungs of chronically infected mice and tuberculosis patients. *Proc. Natl. Acad. Sci. U.S.A.* 100 (24), 14321–14326. doi: 10.1073/pnas.2436197100

Tousif, S., Singh, D. K., Mukherjee, S., Ahmad, S., Arya, R., Nanda, R., et al. (2017). Nanoparticle-formulated curcumin prevents posttherapeutic disease reactivation and reinfection with mycobacterium tuberculosis following isoniazid therapy. *Front. Immunol.* 8, 739. doi: 10.3389/fimmu.2017.00739

Via, L. E., England, K., Weiner, D. M., Schimel, D., Zimmerman, M. D., Dayao, E., et al. (2015). A sterilizing tuberculosis treatment regimen is associated with faster clearance of bacteria in cavitary lesions in marmosets. *Antimicrob. Agents Chemother.* 59 (7), 4181–4189. doi: 10.1128/AAC.00115-15

Via, L. E., Weiner, D. M., Schimel, D., Lin, P. L., Dayao, E., Tankersley, S. L., et al. (2013). Differential virulence and disease progression following mycobacterium tuberculosis complex infection of the common marmoset (Callithrix jacchus). *Infect. Immun.* 81 (8), 2909–2919. doi: 10.1128/IAI.00632-13

Vilaplana, C., Montané, E., Pinto, S., Barriocanal, A. M., Domenech, G., Torres, F., et al. (2010). Double-blind, randomized, placebo-controlled phase I clinical trial of the therapeutical antituberculous vaccine RUTI®. *Vaccine.* 28 (4), 1106–1116. doi: 10.1016/j.vaccine.2009.09.134

Wang, Y., Shi, J., Tang, L., Zhang, Y., Zhang, Y., Wang, X., et al. (2021). Evaluation of rpf protein of micrococcus luteus for cultivation of soil actinobacteria. *Systematic Appl. Microbiol.* 44 (5), 126234. doi: 10.1016/j.syapm.2021.126234

Weiner, J., and Kaufmann, S. H. E. (2014). Recent advances towards tuberculosis control: vaccines and biomarkers. *J. Intern. Med.* 275 (5), 467–480. doi: 10.1111/joim.12212

World Health Organization (2020). *WHO consolidated guidelines on tuberculosis: module 4: treatment: drug-resistant tuberculosis treatment* (Geneva: World Health Organization). Available at: https://apps.who.int/iris/handle/10665/332397.

Yihao, D., Hongyun, H., and Maodan, T. (2015). Latency-associated protein Rv2660c of mycobacterium tuberculosis augments expression of proinflammatory cytokines in human macrophages by interacting with TLR2. *Infect. Dis. (Lond).* 47 (3), 168–177. doi: 10.3109/00365548.2014.982167

Younossian, A. B., Rochat, T., Ketterer, J. P., Wacker, J., and Janssens, J. P. (2005). High hepatotoxicity of pyrazinamide and ethambutol for treatment of latent tuberculosis. *Eur. Respir. J.* 26 (3), 462–464. doi: 10.1183/09031936.05.00006205

Zellweger, J. P., Sotgiu, G., Corradi, M., and Durando, P. (2020). The diagnosis of latent tuberculosis infection (LTBI): currently available tests, future developments, and perspectives to eliminate tuberculosis (TB). *Med. Lav.* 111 (3), 170–183. doi: 10.23749/mdl.v111i3.9983

Zhan, L., Ding, H., Lin, S., Tang, J., Deng, W., Xu, Y., et al. (2014). Experimental mycobacterium tuberculosis infection in the Chinese tree shrew. *FEMS Microbiol. Lett.* 360 (1), 23–32. doi: 10.1111/1574-6968.12524

Zhang, M., Sala, C., Dhar, N., Vocat, A., Sambandamurthy, V. K., Sharma, S., et al. (2014). *In vitro* and *In vivo* activities of three oxazolidinones against nonreplicating mycobacterium tuberculosis. *Antimicrob. Agents Chemother.* 58 (6), 3217–3223. doi: 10.1128/AAC.02410-14

Zheng, H., Colvin, C. J., Johnson, B. K., Kirchhoff, P. D., Wilson, M., Jorgensen-Muga, K., et al. (2017). Inhibitors of mycobacterium tuberculosis DosRST signaling and persistence. *Nat. Chem. Biol.* 13 (2), 218–225. doi: 10.1038/nchembio.2259

frontiers | Frontiers in Cellular and Infection Microbiology

TYPE Original Research
PUBLISHED 26 January 2023
DOI 10.3389/fcimb.2022.957512

OPEN ACCESS

EDITED BY
Bavesh Kana,
University of the Witwatersrand, South Africa

REVIEWED BY
Abhilasha Madhvi,
Rutgers University, Newark, United States
Nathella Pavan Kumar,
National Institute of Research in Tuberculosis (ICMR), India

*CORRESPONDENCE
Sadhna Sharma
sadhnabiochem@gmail.com

SPECIALTY SECTION
This article was submitted to Bacteria and Host, a section of the journal Frontiers in Cellular and Infection Microbiology

RECEIVED 31 May 2022
ACCEPTED 28 December 2022
PUBLISHED 26 January 2023

CITATION
Verma A, Kaur M, Luthra P, Singh L, Aggarwal D, Verma I, Radotra BD, Bhadada SK and Sharma S (2023) Immunological aspects of host–pathogen crosstalk in the co-pathogenesis of diabetes and latent tuberculosis. *Front. Cell. Infect. Microbiol.* 12:957512. doi: 10.3389/fcimb.2022.957512

Immunological aspects of host–pathogen crosstalk in the co-pathogenesis of diabetes and latent tuberculosis

Arpana Verma[1], Maninder Kaur[1], Princy Luthra[1], Lakshyaveer Singh[2], Divya Aggarwal[3], Indu Verma[1], Bishan D. Radotra[3], Sanjay Kumar Bhadada[4] and Sadhna Sharma[1]*

[1]Department of Biochemistry, Post Graduate Institute of Medical Education and Research, Chandigarh, India, [2]Tuberculosis Aerosol Challenge Facility (TACF), International Centre for Genetic Engineering and Biotechnology, New Delhi, India, [3]Department of Histopathology, Post Graduate Institute of Medical Education and Research, Chandigarh, India, [4]Department of Endocrinology, Post Graduate Institute of Medical Education and Research, Chandigarh, India

Introduction: Diabetes is a potent risk factor for the activation of latent tuberculosis and worsens the tuberculosis (TB) treatment outcome. The major reason for mortality and morbidity in diabetic patients is due to their increased susceptibility to TB. Thus, the study was conducted to understand the crosstalk between *M. tuberculosis* and its host upon latent tuberculosis infection and under hyperglycemic conditions or diabetes.

Methods: An animal model was employed to study the relationship between latent tuberculosis and diabetes. BCG immunization was done in mice before infection with *M. tuberculosis*, and latency was confirmed by bacillary load, histopathological changes in the lungs and gene expression of *hspX, tgs1, tgs3* and *tgs5*. Diabetes was then induced by a single high dose of streptozotocin (150 mg/kg body weight). Host factors, like various cytokines and MMPs (Matrix metalloproteinases), which play an important role in the containment of mycobacterial infection were studied *in vivo* and *in vitro*.

Results: A murine model of latent TB was developed, which was confirmed by CFU counts ($<10^4$ in the lungs and spleen) and granuloma formation in lungs in the latent TB group. Also, the gene expression of *hspX, tgs1*, and *tgs5* was upregulated, and after diabetes induction, blood glucose levels were >200 mg/dl. An *in vitro* study employing a THP-1 macrophage model of latent and active tuberculosis under normal and high glucose conditions showed that dormant bacilli were better contained in the presence of 5.5 mM glucose concentration as compared with active bacilli. However, the killing and restriction efficiency of macrophages decreased, and CFU counts increased significantly with an increase in glucose concentration.

Discussion: The decreased levels of MCP-1, decreased expression of *mmp-9*, and increased expression of *mmp-1* in the latent group at high glucose concentrations could explain the failure of granuloma formation at high glucose conditions.

KEYWORDS

Latent tuberculosis, diabetes, triglyceride synthase, matrix metalloproteinases, cytokines

1 Introduction

Diabetic patients are twice as vulnerable to *M. tuberculosis* infection compared to non-diabetics, and diabetes also increases the risk of premature death in tuberculosis patients (Faurholt-Jepsen et al., 2013). There is a two-way association between tuberculosis and diabetes. Although diabetes is a potent risk factor for TB and affects treatment outcomes (Baker et al., 2011), tuberculosis, on the other hand, influences glycemic control in diabetic patients as well (Fisher-Hoch et al., 2013). At present, the mechanisms behind the association between tuberculosis and diabetes are not completely known. Compromised immunological condition plays a crucial role in the susceptibility to the tuberculosis. As diabetes is a pandemic, it is now among the well-known causes for an immune compromised state, which facilitates TB development along with HIV, aging, malnutrition, and smoking (Fox and Menzies, 2013; Rieder, 2014). In diabetes, the immunity of the host against *M. tuberculosis* is "dysfunctional" to be precise instead of "compromised" as in the case of other risk factors with exaggerated or delayed immune responses against *M. tuberculosis*, which renders the host susceptible for activation of latent tuberculosis.

Monocytes play a crucial role in tuberculosis by migrating to the lungs in response to *M. tuberculosis* exposure and differentiating into macrophages and dendritic cells that act as antigen-presenting cells and release cytokines. Chronic hyperglycemia alters the expression of various chemokines and cytokines, causes phagocytic dysfunction in monocytes, and inhibits the complement system, thereby affecting the immune system directly (Stegenga et al., 2008; Hair et al., 2012; Restrepo et al., 2014). The immune susceptibility of diabetics to TB is not clearly understood. Increased TB susceptibility in diabetes patients can be attributed to multiple factors, with direct effects linked to insulin resistance and hyperglycemia, whereas indirect effects have been linked to lymphocyte and macrophage function (Dooley and Chaisson, 2009; Restrepo and Schlesinger, 2013; Martinez and Kornfeld, 2014). Compromised immunity in diabetic patients, which either reactivates latent tuberculosis or promotes primary infection of tuberculosis, could be a possible explanation for overall impaired immunity (Ponce-de-Leon et al., 2004).

MMPs are tightly regulated by various growth factors, hormones, cytokines and are also controlled by tissue inhibitors of MMPs (TIMPs) and endogenous MMP inhibitors (MMPIs). Cytokines modulate MMPs production at the gene level *via* negative or positive regulatory elements (Woessner, 1991), and may affect the proteolytic enzymes production that inhibit or activate MMPs (Ries and Petrides, 1995; Galboiz et al., 2002). Thus, during *M. tuberculosis* infection, where cytokine levels are upscaled, the activity and regulation of MMPs is expected to be controlled by cytokines. MMPs intercede in the immunological response toward infectious pathogens (Turner et al., 2001; Lee et al., 2005). MMPs, particularly MMP-9, have been reported to be expressed during various types of tuberculosis, including meningitis (Matsuura et al., 2000; Price et al., 2001; Thwaites et al., 2003; Lee et al., 2004), active cavitary tuberculosis (Chang et al., 1996; Price et al., 2001; Hrabec et al., 2002), and pleuritis (Hoheisel et al., 2001; Hrabec et al., 2002; Jin et al., 2004). Inhibition of MMP-9 along with the TB treatment has shown increased bacillary clearance and inhibited inflammation in tuberculosis meningitis (Majeed et al., 2016). Thus, the emerging data suggest an important role of MMPs in tuberculosis and its various associated pathological states. Extracellular matrix (ECM) plays a vital role in the structural composition of granuloma in terms of leucocyte trafficking in and out of this dynamic environment (Rhoades, 1997; Gonzalez-Juarrero et al., 2001), but the underlying events during this structural reorganization to establish a stable granuloma or advancement toward a pathological lesion as the granuloma dissolves are unfolding slowly. Interestingly, MMPs are the key factors involved in both the granuloma creation and lung tissue destruction (Salgame, 2011). So, the present study was focused on understanding the crosstalk between *M. tuberculosis* and host upon latent TB infection under hyperglycemic conditions/diabetes with respect to various cytokines and MMPs involved in granuloma formation in TB diabetes copathogenesis.

2 Materials and methods

2.1 Animal procurement and ethics statement

All animal procedures were performed in the Bio-Safety Level-III (BSL-III) facility at the International Centre for Genetic Engineering and Biotechnology (ICGEB), New Delhi. Animal procedures were approved by the Institutional Animal Ethical Committee with ref. no. 89/90/IAEC/616 and also by the Animal Ethical Committee of the ICGEB, New Delhi, with ref. no. ICGEB/IAEC/02042019/TACF-PGIMER-16 (Verma et al., 2021).

2.2 *M. tuberculosis* H_{37}Rv culture and maintenance

M. tuberculosis H_{37}Rv (NCTC-7416), originally procured from the national collection of type culture in London, UK, was cultured in Soutan's media containing 2% glycerol and 0.05% Tween 80 under shaking conditions at 200 rpm. Logarithmically growing cultures were enumerated by comparing with McFarland standards and stored at −80°C till further use.

2.3 Mouse model of latent tuberculosis and diabetes

The mouse model of latent tuberculosis was developed by infecting 5 to 6-week-old Balb/c mice with BCG through aerosolization at 0.5 O.D. (600 nm), and after six weeks, *M. tuberculosis* H37Rv infection was given at 1.1 O.D. (600 nm). Latency was confirmed by CFU counts after 4 and 6 weeks of infection with *M. tuberculosis*. Six weeks post infection with *M. tuberculosis*, latently infected animals were divided into three groups, i.e., Group-I: latent tuberculosis only (n = 24), Group-II: latent tuberculosis with diabetes (n = 24), and Group-III: latent tuberculosis with immunosuppression (n = 24). Group-I animals were kept untreated. Group-II animals were induced with diabetes by a single dose of streptozotocin (150 mg/kg body weight), and Group-III animals were induced with immunosuppression by dexamethasone (Ahmad et al., 2006). Animals were sacrificed at weeks 9 and 13 of diabetes induction.

2.4 Histopathological studies

Aseptically removed lungs and spleen were transferred to 10% buffered formalin and further processed for paraffin embedding and sectioning (Ramos-Vara, 2011). Paraffin sections were deparaffinized and stained with the standard hematoxylin and eosin (H&E) and the acid-fast bacilli (AFB) stain.

2.5 Culture and maintenance of THP-1 cell line

The human leukemic monocytic cell line THP-1 was obtained from the cell repository at the National Centre for Cell Science (NCCS) Pune, India, and was routinely maintained as suspended cells in RPMI 1640 media, supplemented with 10% fetal bovine serum, 2 mM glutamine, and 100 µg/ml of an antibiotic–antimycotic cocktail from Sigma (penicillin, streptomycin, and gentamycin) at 37°C and 5% CO_2 in a humidified incubator. Cells were grown to a density of 2–5 × 10^6 cells/ml in 25 cm^2 flat-bottom tissue culture flasks and passaged every third day.

2.6 *In vitro* model of latent tuberculosis

An *in vitro* nutritional starvation model of latent tuberculosis was developed according to the method described by Betts et al. (2002). Briefly, *M. tuberculosis* H_{37}Rv was cultured and grown in nutrition-rich media, i.e., Soutan's media containing 2% glycerol and 0.05% Tween 80, under constant shaking conditions at 200 rpm for 7 days. After 7 days, the culture was centrifuged at 5,000×*g* for 10–15 min, and the bacterial pellet was washed and transferred to PBS containing 0.05% Tween 80 (PBST) for 6 weeks under shaking conditions at 200 rpm in an incubator shaker. After 6 weeks of incubation, it was used as a latent TB culture and stored at −80°C until further use.

2.7 Infection of THP-1 derived macrophages with *M. tuberculosis* H_{37}Rv

For infection experiments, 3 × 10^5 THP-1 cells/well were plated in complete RPMI-1640 media containing 5% FBS and different glucose concentrations, i.e., 5.5 mM (normoglycemic condition), 15 mM, and 25 mM (hyperglycemic condition). D-mannitol was used as an osmotic control at the same molar concentrations. Approximately 20 ng/ml of phorbol myristate acetate (MP Biomedicals, USA) was added to the media for 24 h for differentiation of monocytes to macrophages. After 24 h, cell monolayers were then covered with fresh RPMI media containing no antibiotics and respective glucose concentrations, supplemented with 2% FBS, and incubated at 37°C and 5% CO_2 for 24 h. After 48 h of cell plating, cells were divided into three groups, i.e., an uninfected group, an active TB group, and a latent TB group. Active *M. tuberculosis* culture was used to infect cells of the active TB group, whereas dormant *M. tuberculosis* culture was used to infect THP-1 cells of the latent TB group at a multiplicity of infection (MOI) of 1:5 (5 bacteria/1 cell) for 3 h (Iona et al., 2012). After 3 h, cells were washed twice with warm RPMI 1640 and replenished with complete RPMI 1640 medium containing different glucose concentrations and amikacin (50 µg/ml) to prevent extracellular replication of mycobacteria.

2.8 Colony forming units enumeration

Lungs and spleen were aseptically removed and homogenized in phosphate buffer saline (PBS) and plated on Middlebrook 7H11 agar (Becton-Dickinson, USA) containing 10% oleic acid-albumin-dextrose-catalase (OADC) (Difco-Becton Dickinson, USA). For the latent group, where BCG was given to animals prior to *M. tuberculosis* infection, 4 mg/ml of 2-thiophenecarboxylic acid hydrazide (TCH) (Sigma Aldrich) was added to 7H11 agar media to select for *M. tuberculosis* (Lecoeur et al., 1989). The latently and actively infected THP-1 cells grown under the above-mentioned glucose concentrations were lysed in 0.1% Triton X-100 for 5 min at different time points, i.e., 0 day, 1 day, 3 day, and 6 day of infection. Lysates were plated on Middlebrook 7H11 agar plates supplemented with 10% OADC in triplicate. Plates were incubated at 37°C in a 5% CO_2 environment, and CFU counts were determined after 28 days of incubation.

2.9 Gene expression analysis of matrix metalloproteinases

The uninfected, latently, and actively infected THP-1 cells grown under different glucose concentrations were washed with FBS-free RPMI media and treated with a Trypsin-EDTA solution. After centrifugation at 1,600×*g* for 3 min, the cell pellet was resuspended in TRIzol. For gene expression studies in animals, lung tissue was directly transferred to 2–3 ml of TRIzol, depending on the size of the tissue. RNA was then isolated with the standard phenol–chloroform method (Adilakshmi et al., 2006). For quantitative real-time polymerase chain reaction (qRT-PCR), RNA (500 ng) was reverse transcribed using the Revert Aid First Strand cDNA Synthesis Kit (Thermo Scientific, USA). qRT-PCR amplification was done using SYBR® Green chemistry on Roche LightCycler® 96 Real-Time PCR Systems. The sequence of primers used for the amplification of different genes is given in Table 1.

2.10 Cytokine determination

Cytokines were determined in THP-1 culture supernatants by using the Cytometric Bead Array (CBA) Human Soluble Protein Master Buffer Kit (Becton Dickinson, USA) and in mouse serum by using the CBA Mouse Th1/Th2/Th17 cytokine kit. In the serum and culture supernatants, protein inhibitor cocktail (Sigma Aldrich, USA) was added and stored at −80°C. The cytokine assay was performed according to the manufacturer's protocol.

2.11 Matrix metalloproteinase determination

Matrix metalloproteinases were determined in the serum of mice using ELISA kits from ImmunoTag, USA. Protein inhibitor cocktail

TABLE 1 Primer sequence for various genes.

Gene	Primer Sequence		Annealing temperature
16srRNA	GTGGCGAACGGGTGAGTAAC ATGCATCCCGTGGTCCTATC	(Forward) (Reverse)	60°C
hspX	CACCACCCTTCCCGTTCAG TGGACCGGATCTGAATGTGC	(Forward) (Reverse)	56°C
tgs1	TCGTTAATGCTGCCCAACCT CCGAATTGTCTCTGTCCCCC	(Forward) (Reverse)	56°C
tgs3	GACATCACCTACCACGTCCG TACATCTCCCACAATGGCCG	(Forward) (Reverse)	64°C
tgs5	GATGGGCCAGAAGATGGACC CTTGGTAAACAGCAGCACGG	(Forward) (Reverse)	53°C
mmp1 (Human)	ATGCACAGCTTTCCTCCACTG CAGCCCAAAGAATTCCTGCATT	(Forward) (Reverse)	57°C
mmp2 (Human)	AACTACGATGATGACCGCAA CTCCTGAATGCCCTTGATGT	(Forward) (Reverse)	54°C
mmp9 (Human)	GCCACTACTGTGCCTTTGAG AGAATCGCCAGTACTTCCCA	(Forward) (Reverse)	58°C
β-actin (Human)	AGAGCCTCGCCTTTGCCGATC CCCACCATCACGCCCTGGTGC	(Forward) (Reverse)	64°C
mmp1 (Mouse)	ACTACAACTGACAACCCAAGAAAG AGGAGATGCCTAGAATCACAGT	(Forward) (Reverse)	62°C
mmp2 (Mouse)	AACGGTCGGGAATACAGCAG AAACAAGGCTTCATGGGGGC	(Forward) (Reverse)	63°C
mmp9 (Mouse)	CTCTCCTGGCTTTCGGCTG TCCGTGAGGTTGGAGGTTTTC	(Forward) (Reverse)	63°C
gapdh (Mouse)	AGCTTGTCATCAACGGGAAG TTTGATGTTAGTGGGGTCTCG	(Forward) (Reverse)	60°C

(PIC) (Sigma Aldrich, USA) was added to the serum and stored at −80°C. The assay was performed according to the manufacturer's protocol.

2.12 Statistical analysis

The level of significance was determined by the Mann–Whitney test and the Kruskal–Wallis test using the GraphPad Prism package, version 8.0 (GraphPad Software, San Diego, USA) (Verma et al., 2021).

3 Results

3.1 Bacillary load in latent tuberculosis mice model

Mice were infected with BCG through aerosol, and one day after immunization, the mean CFU counts of BCG in the lungs were found to be 1.92 ± 0.04 $\log_{10}$ (data not shown). After six weeks, the mean *M. tuberculosis* CFU counts after 1 day of infection were 1.84 ± 0.03 $\log_{10}$ (data not shown). Four weeks after challenge, the mean *M. tuberculosis* CFU counts in the lungs and spleen of the latent TB group were found to be significantly decreased as compared to the active TB group (Figures 1A, B). Similarly, after 6 weeks of infection, the mean CFU counts in the lungs and spleen were significantly lower in the latent TB group as compared to the active TB group (Figures 1C, D). Further, the mean CFU count of the lungs and spleen after 8 weeks of infection in the latent TB group were 3.79 ± 0.034 $\log_{10}$ and 3.02 ± 0.04 $\log_{10}$, respectively (Figure 1E). The CFU counts of the latent TB group after 4 and 6 weeks post-infection with *M. tuberculosis* confirmed the establishment of latent tuberculosis. The latent infection was sustained up to week 8 post-infection, as well, a stable CFU count was observed in the lungs and spleen of latent TB group animals.

3.2 Granuloma formation in the lungs of latent TB infected mice

After 4 and 6 weeks of infection, peri-bronchial and peri-vascular inflammation was observed in the lungs of animals from the active TB group (Figures 2A, C) whereas in the latent TB group, the lungs were presented with parenchymal inflammation and inflammatory cell collection in air spaces. Also, histiocytic collection leading to the formation of sparse granulomas was observed after 4 weeks of infection in the latent TB group (Figure 2B). After 6 weeks of infection, collection of inflammatory cells at the pleural surface in the air spaces of the lungs was observed and ill-formed granulomas

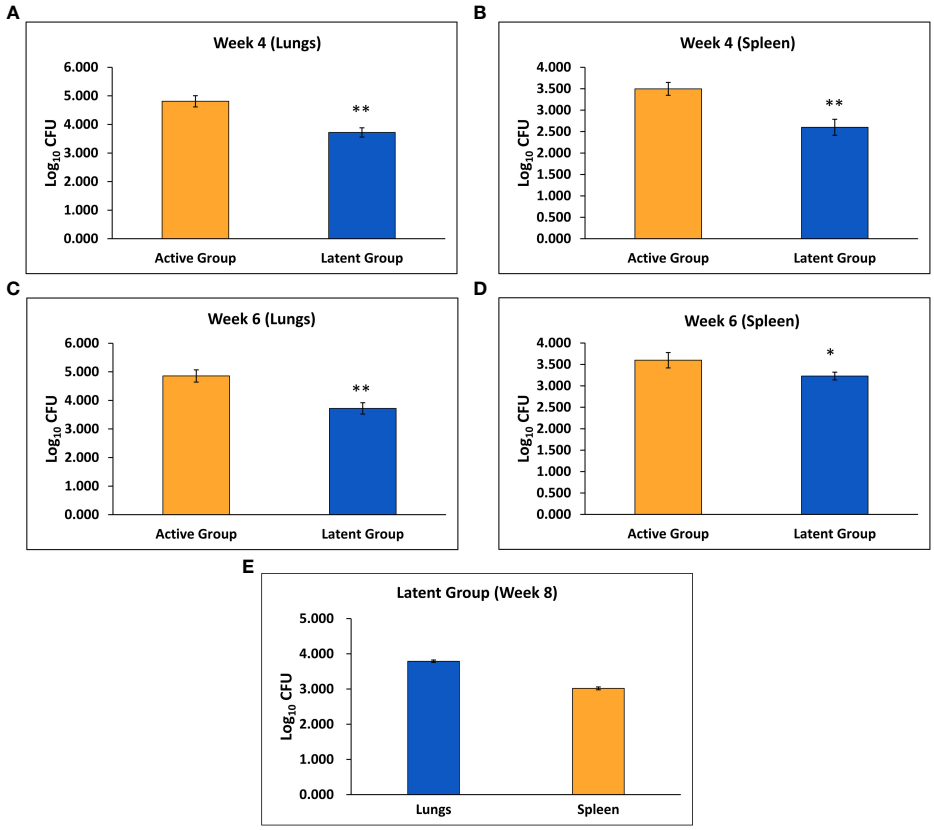

FIGURE 1
Log_{10} CFU counts of *M. tuberculosis* $H_{37}Rv$ in the active TB and latent TB groups. **(A)** After 4 weeks of infection in the lungs. **(B)** After 4 weeks of infection in the spleen. **(C)** After 6 weeks of infection in the lungs. **(D)** After 6 weeks of infection in the spleen. **(E)** After 8 weeks of infection in the lungs and spleen of the latent group. Values are Mean ± SE of five animals from each group. *p ≤0.05, **p ≤0.01 as compared to the active group.

were observed in the latent TB group (Figure 2D). Lung tissues of animals from the latent TB group after 8 weeks of infection also displayed lymphoid and histiocytic collections, which indicated the formation of ill-formed granulomas (Figure 2E).

3.3 Expression of dormancy associated genes in lungs of latent TB model

The expression of various latency-associated genes of *M. tuberculosis* was studied, including *hspX, tgs1, tgs3*, and *tgs5*. The gene expression of the *tgs1* and *tgs5* was found to be 3.8-fold and 2.6-fold upregulated, respectively, in the latent TB group as compared to the active TB group, and no significant change was observed in the expression of the *hspX* gene after 4 weeks of infection (Figures 3A–C). However, the expression of the *hspX* was found to be approximately 3.5-fold upregulated, and an approximately 1.4-fold increase in the expression of the *tgs5* was observed in the latent TB group as compared to the active TB group after 6 weeks of *M. tuberculosis* infection (Figures 3D, F), signifying the development of latency in the latent TB group. Also, the expression of *tgs1* was found to be increased non-significantly in latent TB group as compared to active TB group at week 6 (Figure 3E). No significant change was observed in the expression of *tgs3* after 4 and 6 weeks of infection between the latent and active TB groups (data not shown).

3.4 Development of diabetes in latently infected mice

Initially we tried to establish diabetes in latently infected mice with multiple low doses of streptozotocin and blood glucose levels were measured. However, diabetes in latently infected animals could not be established as blood glucose levels were found to be below 200 mg/dl until week 7 of their streptozotocin treatment at this dose (Figure 4). Thus, another single high dose of streptozotocin was given to these animals at week 7 of first streptozotocin treatment, and diabetes was found to have been successfully established in the latent TB group animals at week 8 as blood glucose levels were found to be greater than 200 mg/dl (Figure 4). Also, the pancreatic tissues of animals with latent TB and diabetes showed inflammation at weeks 9 (two weeks after diabetes development) and 13 (six weeks after diabetes development). The islets of Langerhans were densely inflamed, and loss of cellularity, necrosis, and admixture of cells were observed (Supplementary Figures 1B, D).

3.5 Expression analysis of matrix metalloproteinases

After the establishment of diabetes in latently infected mice, the animals were divided into three groups, i.e., Group-I (latent

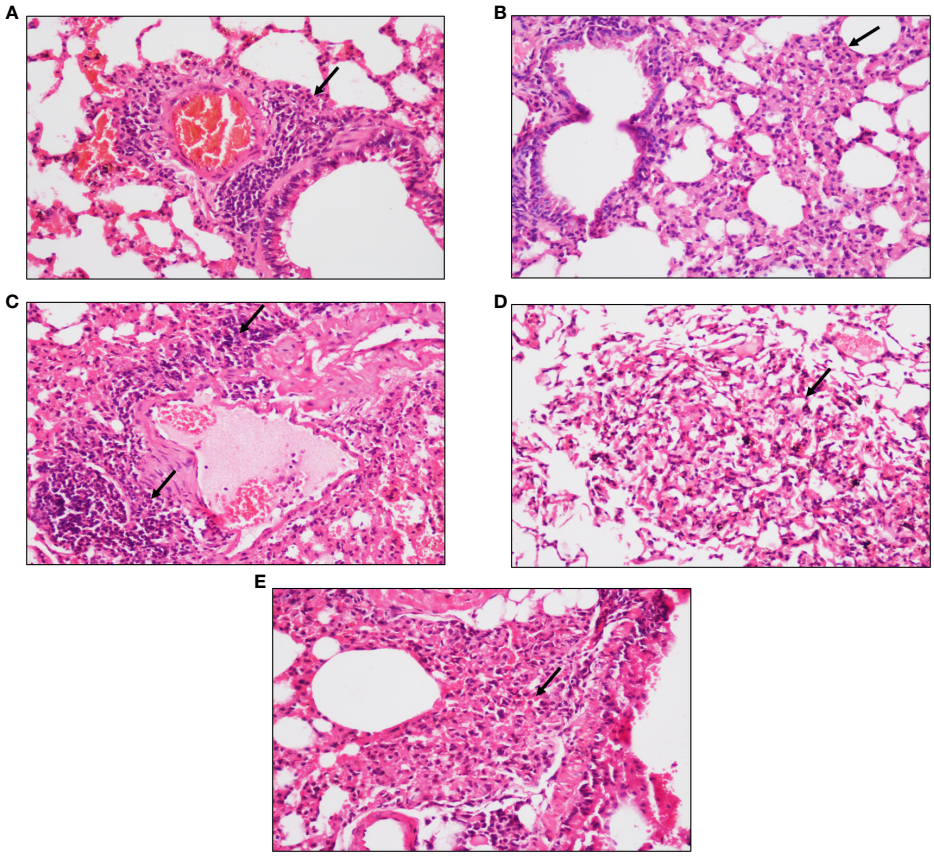

FIGURE 2
Representative images of hematoxylin and eosin staining of lung tissue of mice after 4, 6, and 8 weeks of infection with *M. tuberculosis* at ×20 magnification. **(A)** Section of the active TB group mice after 4 weeks. **(B)** Section of the latent TB group mice after 4 weeks. **(C)** Section of the active TB group mice after 6 weeks. **(D)** Section of the latent TB group mice after 6 weeks. **(E)** Section of the latent TB group mice after 8 weeks. Arrows indicate granulomas in the latent group and inflammation in the active group.

tuberculosis only), Group-II (latent tuberculosis with diabetes), and Group-III (latent tuberculosis with immunosuppression). Two weeks after the development of diabetes, i.e., week 9, the expression of the *mmp-1* was found to be significantly downregulated in Group-II as compared to Group-I, and no significant change in expression was observed in Group-III (Supplementary Figure 2A). Also, no significant change was observed in the gene expression of *mmp-2* and *mmp-9* in Groups-II and -III as compared to Group-I (data not shown). After six weeks of diabetes development, i.e., at week 13, an increase was observed in the expression of *mmp-1* in Group-II as compared to Group-I, but the increase was not significant (Supplementary Figure 2B). Moreover, no significant change was observed in the expression of *mmp-2* and *mmp-9* genes in Groups-I, -II, and -III respectively (data not shown). Thus, an increase in expression of *mmp-1* was observed in the diabetes group co-infected with latent tuberculosis, although the increase was non-significant. The levels of MMP-1, MMP-2, and MMP-9 were also measured in the serum of animals. At week 9, no significant change in the levels of MMP-1, MMP-2, and MMP-9 was observed between Groups-I, -II, and -III (data not shown). At week 13, the levels of MMP-1 were found to be significantly higher in Group-III in comparison to Groups-I and -II. The levels of MMP-1 and MMP-2 were significantly reduced in Group-II as compared to Group-I (Supplementary Figures 2C, D). The levels of MMP-9 were found to be the same between Group-I and Group-II. In Group-III, the levels of MMP-9 were significantly raised as compared to Group-II (Supplementary Figure 2E).

3.6 Cytokine levels in blood

At week 9, the levels of TNF-α were higher in Group-I, but the increase was not significant. The levels of IL-10, IFN-γ, IL-4, and IL-17 were found to be significantly increased in Group-III as compared to the control group, Group-I, and Group-II, but no change was found in the levels between Group-I and Group-II (data not shown). The levels of IL-6 were found to be significantly reduced in Group-II as compared to Group-I (Supplementary Figure 3A). No significant change was observed in the levels of IL-2 and TNF-α in any group (data not shown). At week 13, no significant change was observed in the levels of IL-10, TNF-α, IFN-γ, and IL-17 in any group (data not shown). A significant decrease was observed in the levels of IL-2 and IL-6 in Group-III as compared to the control group, Group-I, and Group-II (Supplementary Figures 3B, C). The levels of IL-4 were found to be significantly higher in Group-III as compared to Group-I, but no change was observed in the levels between the other groups (Supplementary Figure 3D).

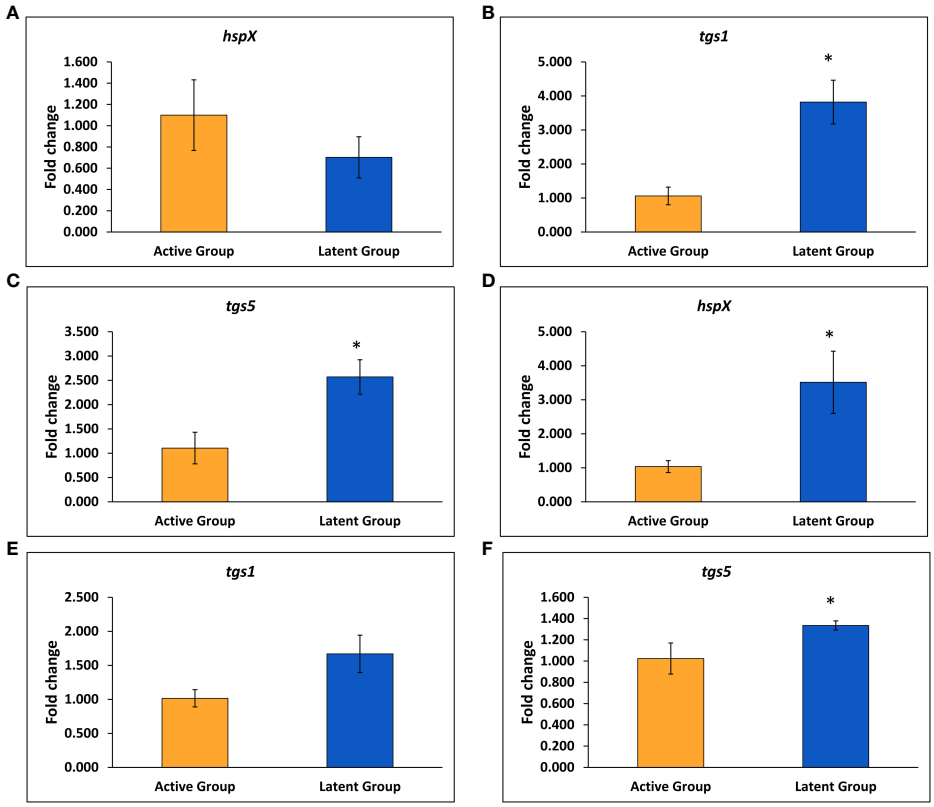

FIGURE 3
Expression of various genes in the latent TB group and active TB group. **(A)** *hspX* after 4 weeks. **(B)** *tgs1* after 4 weeks. **(C)** *tgs5* after 4 weeks. **(D)** *hspX* after 6 weeks. **(E)** *tgs1* after 6 weeks. **(F)** *tgs5* after 6 weeks. Values are Mean ± SE of three animals from each group. *p ≤0.05 as compared to the active TB and latent TB groups. 16srRNA was used as constitutive gene.

3.7 High glucose conditions affects the macrophage bacterial clearing efficiency

In THP-1 cells infected with active and latent cultures of *M. tuberculosis* H37Rv, the mean CFU counts were found to be significantly increased in the active as well as the latent group in the presence of 25 mM glucose concentration as compared to 5.5 mM and 15 mM glucose concentration on day 0 and day 1 (Figures 5A, B). On day 3, the mean CFU counts in the active group at 25 mM glucose were significantly increased as compared to 5.5 mM glucose, whereas in the latent group, the mean CFU counts were significantly increased in the presence of 15 mM and 25 mM glucose concentration as compared to 5.5 mM glucose concentration (Figure 5C). Similarly, on day 6 also the mean CFU counts in the active and latent groups were significantly increased with an increase in glucose concentration (Figure 5D). The CFU data indicated that as the glucose concentration is increased, the bacterial clearing capacity of macrophages is decreased in both active and latent infection.

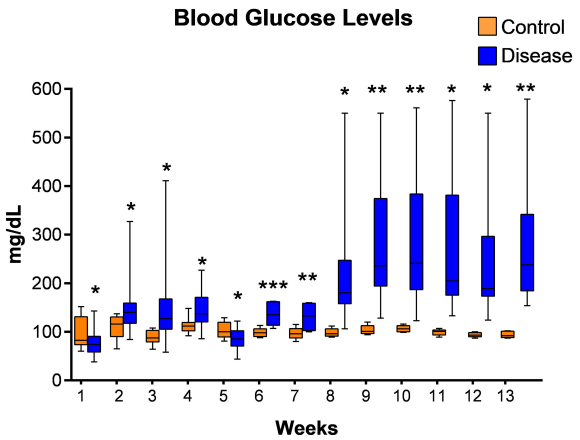

FIGURE 4
Blood glucose levels of mice from latent tuberculosis with diabetes group after streptozotocin treatment. Values are Mean ± SE of 24 animals until week 6, and 8–22 animals from week 7 until week 13. *p ≤0.05, **p ≤0.01, ***p ≤0.001 as compared to the control group. Blue bars indicate the streptozotocin treated group (latent tuberculosis with diabetes) and orange bars indicate the control group (healthy group without TB infection or diabetes).

3.8 *In vitro* expression analysis of matrix metalloproteinases

With an increase in glucose concentration, the expression of the *mmp-1* gene was found to be upregulated in both active and latent groups as compared to the uninfected group at all time points, i.e., day 0, day 1, day 3, and day 6. At 25 mM glucose concentration, expression was observed to be 21-fold upregulated in the active group and approximately 29-fold upregulated in the latent group on day 0, whereas a 16.7-fold increase in the active group and a 19.7-fold increase in the latent group was observed on day 1 as compared

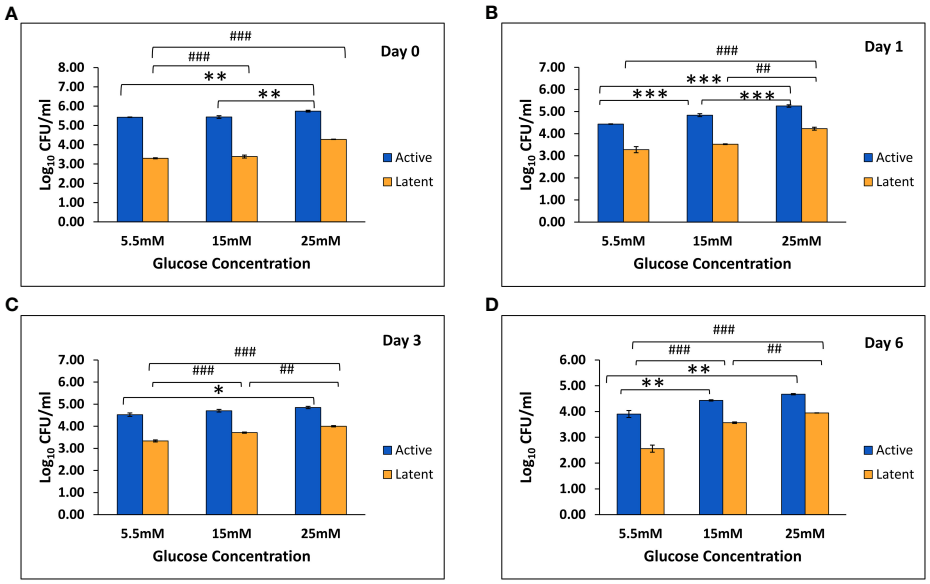

FIGURE 5
Log_{10} CFU counts of *M. tuberculosis* $H_{37}Rv$ in THP-1 cells infected with active and latent bacilli in the presence of different glucose concentrations at different time intervals. **(A)** On day 0 of infection. **(B)** On day 1 of infection. **(C)** On day 3 of infection. **(D)** On day 6 of infection. Values are Mean ±SE of three independent experiments. *p ≤0.05, **p ≤0.01, and ***p ≤0.001 represent the comparison between different glucose concentrations in the active group. $^{##}$p ≤0.01 and $^{###}$p ≤0.001 represent the comparison between different glucose concentrations in the latent group.

to the uninfected group (Figures 6A–D). The expression of the *mmp-9* was found to be downregulated in the active and latent groups at 25 mM as compared to 15 mM glucose concentration at all time points, but the expression was significantly downregulated in the latent group as compared to the active group at later time points at high glucose conditions (Figures 7A–D). At higher glucose concentrations, the gene expression of *mmp-2* was found to be significantly increased in the active group at earlier time points, whereas at later time points it was observed to be downregulated. However, in the latent group a significant decrease in expression was observed on day 6 at 25 mM glucose concentration as compared to 5.5 mM and 15 mM glucose concentration (Figures 8A–D).

3.9 *In vitro* analysis of cytokines

The levels of different cytokines, i.e., IL-12, MCP-1, TNF-α, and MIP-1α, were determined in the THP-1 cell culture supernatants of the uninfected, active, and latent groups at different time intervals, i.e., 0 h, 6 h, 18 h, and 24 h of infection, in the presence of different glucose concentrations. With an increase in glucose concentration, the levels of MCP-1 were found to be decreased in the uninfected, active, and latent groups at all time points. This decrease in MCP-1 levels was more drastic in the active group as compared to the uninfected group with an increase in glucose concentration, which further explains reduced chemotaxis with an increase in glucose concentrations (Supplementary Figures 4A–D). The levels of TNF-α were found to be very high in both the active and latent groups with an increase in glucose concentrations (Supplementary Figures 5A–D). However, the levels of MIP-1α and IL-12 were found to be approximately similar in all the groups at 5.5 mM, 15 mM, and 25 mM glucose (data not shown).

4 Discussion

Diabetes is considered as a contributing factor to the dissemination of tuberculosis. Diabetes and active tuberculosis are well associated, yet the link between latent tuberculosis and diabetes has not been explored. Thus, a mice model of latent tuberculosis, developed by Zhang et al. (2009) was used and simultaneously diabetes was induced after establishment of latency which was confirmed by the CFU counts in lungs and spleen after infection with *M. tuberculosis*. The CFU counts were less than 10^4 and remained stable, which affirmed the establishment of latent tuberculosis. The bacterial load in LTBI is presumed to be ≤10^4 CFU, as the lower limit of detection for acid-fast smears is 10^4 CFU/ml (Nuermberger et al., 2004; Zhang et al., 2009). Histological studies also supported the establishment of a latent tuberculosis model as granulomas were detected in the lungs after *M. tuberculosis* challenge. The results were supported by a study conducted by Dutta et al. (2014) wherein necrotic lung granulomas were observed after infection with *M. tuberculosis* in C3HeB/FeJ mice that were previously immunized with BCG. The development of granulomatous lesions after 2 and 10 weeks of low-aerosol infection with *M. tuberculosis* in the lungs of C57BL/6 mice has also been reported (Botha and Ryffel, 2002).

Alpha crystallin sustains the tubercle bacilli during the dormant or latent phase of infection, therefore qualifying HspX as a potential biomarker for latent TB infection (Mustafa et al., 1999; Botha and

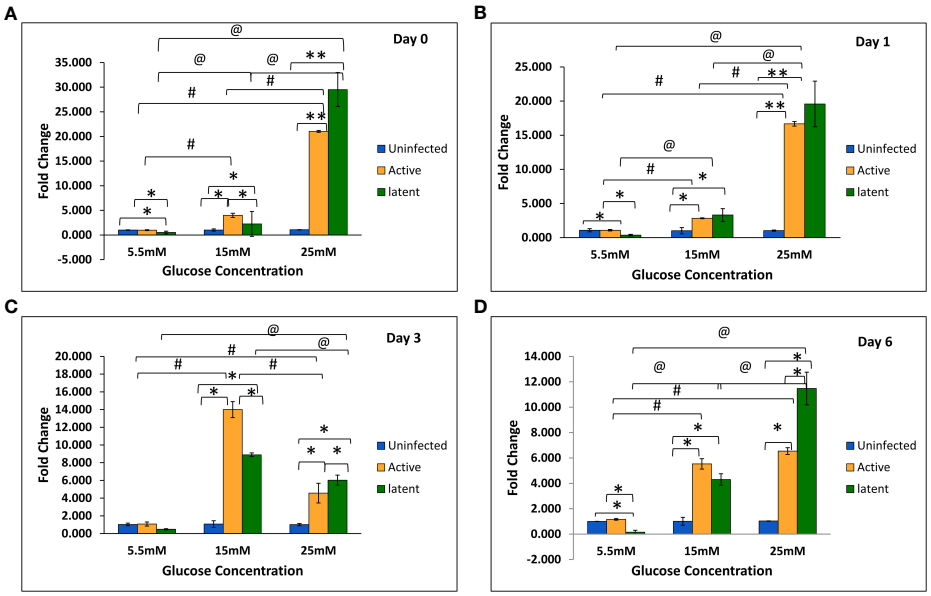

FIGURE 6
Expression of the *mmp-1* gene in the uninfected, active, and latent groups of THP-1 cells in the presence of different glucose concentrations at different time intervals. **(A)** On day 0 of infection. **(B)** On day 1 of infection. **(C)** On day 3 of infection. **(D)** On day 6 of infection. Values are Mean ±SE of three independent experiments. *p ≤0.05 represents the comparison between the uninfected, active, and latent groups within the same glucose concentration. **p ≤0.01 represents the comparison between the uninfected, active, and latent groups within the same glucose concentration. $^{\#}$p ≤0.05 represents the comparison between different glucose concentrations in the active group. $^{@}$p ≤0.05 represents the comparison between different glucose concentrations in the latent group.

Ryffel, 2002). In our study, the gene expression of *hspX* was significantly upregulated in the latent TB group in comparison with the active TB group. This observation was in accordance with a study that revealed elevated HspX levels by tubercle bacilli in the latent state and its reversal to normal levels when exponential growth was resumed (Hu et al., 2006). It is known that *M. tuberculosis* can synthesize or accumulate triacylglycerol (TG), which leads to its long-term survival or persistence or dormancy under stress conditions (Daniel et al., 2004). *M. tuberculosis* synthesizes different TG synthases, which are responsible for the accumulation of TG under different stress conditions (Sirakova et al., 2006). The expression of the *tgs1* and *tgs5* genes has been observed to be upregulated in the latent TB group as compared to the active TB group. The results were supported by a study wherein the *tgs1* gene was found to be the prime contributor to TG synthesis in *M. tuberculosis* cultures grown under hypoxic and nitric oxide stress conditions (Daniel et al., 2004).

Further, diabetes was induced in latently infected mice using multiple, low doses of streptozotocin. A multiple, low-dose streptozotocin-induced diabetes model was developed by Leiter in 1982 using C57BL/6 mice (Leiter, 1982). After that, many researchers have also used this multiple, low-dose model to develop diabetes (McEvoy et al., 1984; Sun et al., 2005; Ventura-Sobrevilla et al., 2011). However, diabetes was not induced using multiple, low doses of streptozotocin in this study, which was thought to be due to BCG immunization as it has an important role in protection against diabetes. Various studies have observed that diabetes was not induced by multiple, low doses of streptozotocin in mice previously immunized with BCG (Baik et al., 1999; Rosa et al., 2013). Therefore, another single high dose of streptozotocin was given to the animals. and diabetes was successfully induced in latently infected mice.

To understand the crosstalk between intracellular mycobacteria and host macrophages, the THP-1 monocytic cell line was grown under hyperglycemic conditions and infected with latent as well as active cultures of *M. tuberculosis* for 3 h. Accordingly, mycobacterial phagocytosis by macrophages under high glucose conditions was studied. THP-1 cells were used as model phagocytic cells (Ranaivomanana et al., 2018; Riaz et al., 2020). CFU enumeration at normal glucose conditions suggested that the dormant bacilli were better contained within the macrophages as compared to the active bacilli. The data was supported by a study wherein the growth of dormant bacilli was better suppressed by macrophages as compared to aerobic bacilli (Iona et al., 2012). However, as the glucose concentration increased, the CFU counts in both the active and latent TB groups increased significantly as compared to normal glucose conditions at each time point. Similar results were obtained in a study in which bacterial internalization and killing were reduced by macrophages isolated from diabetic mice (Alim et al., 2017). Also, Gomez et al. observed that the monocytes isolated from diabetic patients had reduced intake of *M. tuberculosis* in comparison to monocytes isolated from nondiabetic patients (Gomez et al., 2013).

Cytokines play a critical role in active and latent TB infection. Th1 cytokines differentiate between latent tuberculosis and active tuberculosis, as their levels are higher in LTBI (Wu et al., 2017). A study by Kumar et al. found that latent tuberculosis infection and diabetes co-pathology are characterized by decreased systemic Th1 cytokine levels (Kumar et al., 2014). In this study, the levels of TNF-α

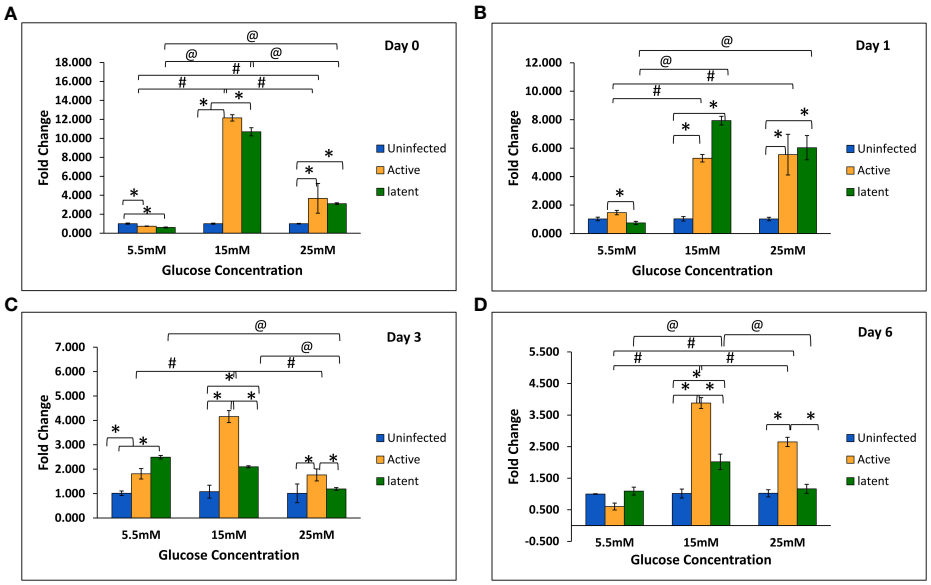

FIGURE 7
Expression of the *mmp-9* gene in the uninfected, active, and latent groups of THP-1 cells in the presence of different glucose concentrations at different time intervals. **(A)** On day 0 of infection. **(B)** On day 1 of infection. **(C)** On day 3 of infection. **(D)** On day 6 of infection. Values are Mean ±SE of three independent experiments. *p ≤0.05 represents the comparison between the uninfected, active, and latent groups within the same glucose concentration. $^{\#}$p ≤0.05 represents the comparison between different glucose concentrations in the active group. $^{@}$p ≤0.05 represents the comparison between different glucose concentrations in the latent group.

were found to be lower in the latent group as compared to the active group at 0 h. However, with an increase in time, the levels of TNF-α were found to be higher in the latent group as compared to the active group at high glucose conditions. In a mouse model of latent tuberculosis, TNF-α levels were found to be decreased non-significantly in the latent tuberculosis with diabetes group at week 9 of diabetes induction as compared to latent tuberculosis alone; however, levels were comparable between both groups at week 13. The results were in contrast to a study in which reduced levels of type-1 and type-17 cytokines along with diminished circulating levels of pro-inflammatory cytokines were reported in individuals with latent tuberculosis and diabetes as compared to individuals with latent tuberculosis without diabetes (Kumar and Babu, 2017). The possible reasons for this variation could be the species difference as the present study was performed on mice, and another possible reason could be the early time points as the sacrifice was done after the second (week 9) and sixth (week 13) weeks of diabetes establishment. Th2 cytokines, i.e., IL-4, IL-6, IL-10, IL-13, etc., inhibit Th1 responses and thus cross-regulate and influence the progression to active tuberculosis (O'Garra et al., 2013). In the mouse model, the levels of IL-6 and IL-10 were found to be significantly decreased in the latent tuberculosis with diabetes group in comparison to the latent tuberculosis only group. The results were supported by a study in which no difference in the levels of IL-4, IL-5, IL-6, and IL-13 and a decrease in IL-10 levels were reported between latently infected individuals with diabetes and those without diabetes (Kumar et al., 2014).

Along with the cytokines, levels of chemokines, i.e., monocyte chemotactic protein-1 (MCP-1) and macrophage inflammatory protein-1a (MIP-1α), were measured. MCP-1 plays an important role in latent infection, primarily in the establishment and maintenance of granulomas by recruiting leukocytes at the site of infection (Deshmane et al., 2009). In this study, the levels of MCP-1 were found to be decreased in the culture supernatants of the active group as compared to the latent and uninfected groups, and the levels were greatly reduced at higher glucose concentrations as compared to normal glucose concentrations in both the active and latent groups. Results were supported by a study in diabetic mice infected with *M. tuberculosis*, which showed reduced levels of MCP-1 in lung lysates, resulting in delayed migration of dendritic cells from the lungs to lymph nodes (Vallerskog et al., 2010). Chemokines like MIP-1α, CCL4, and CCL5 function in synergy with IFN-γ as pro-inflammatory chemokines (Dorner et al., 2002). However, no change in the levels of MIP-1α in the culture supernatants was observed between the uninfected, active, and latent groups or between normal glucose and high glucose conditions. The results were supported by a study in which no difference was observed in the secretion and mRNA expression of CCL3 upon *M. tuberculosis* infection between extrapulmonary and pulmonary TB patients (Hasan et al., 2009).

ECM plays a vital role in the structural composition of granulomas in terms of leucocyte trafficking in and out of this dynamic environment (Gonzalez-Juarrero et al., 2001). Interestingly, MMPs appear to play a key role in both granuloma formation and in lung tissue destruction. In the present study, the expression of the *mmp-1* gene was observed to be increased non-significantly at week 13 in latently infected mice with diabetes in comparison with non-diabetic mice. Similarly, in *in vitro* studies, the gene expression of *mmp-1* was observed to be significantly

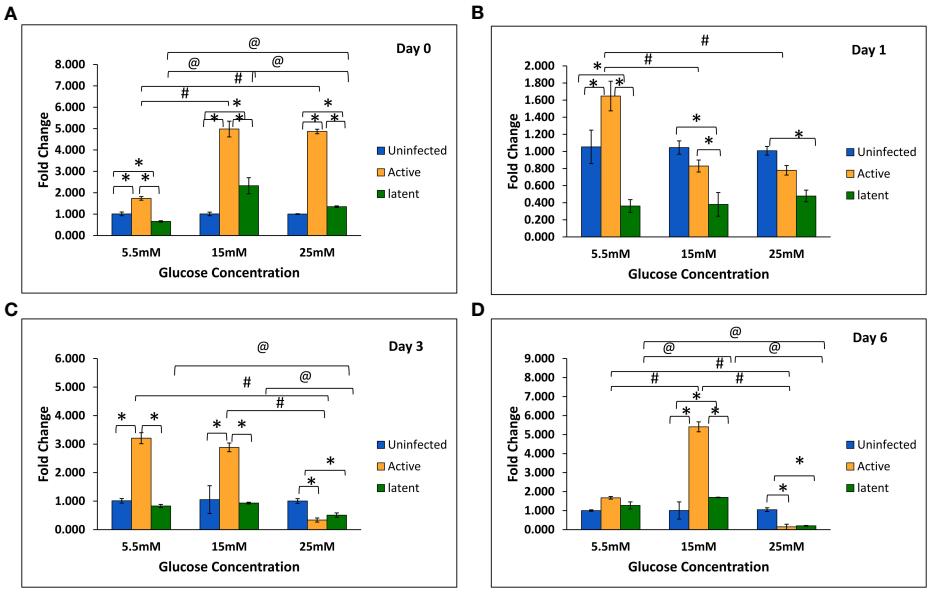

FIGURE 8
Expression of the *mmp-2* gene in the uninfected, active, and latent groups of THP-1 cells in the presence of different glucose concentrations at different time intervals. **(A)** On day 0 of infection. **(B)** On day 1 of infection. **(C)** On day 3 of infection. **(D)** On day 6 of infection. Values are Mean ±SE of three independent experiments. *p ≤0.05 represents the comparison between the uninfected, active, and latent groups within the same glucose concentration. #p ≤0.05 represents the comparison between different glucose concentrations in the active group. @p ≤0.05 represents the comparison between different glucose concentrations in the latent group.

upregulated in the latent group as compared to the active group at high glucose concentrations. The results were supported by a study wherein the circulating levels of MMP-1 were found to be elevated in active pulmonary TB patients as compared to individuals with LTBI (Andrade et al., 2015). However, no significant change was observed in the protein levels of MMP-1 at week 9, and a significant decrease was observed in levels at week 13 in the serum of latently infected mice with diabetes compared to those without diabetes. Results were comparable to a study in which no significant difference was observed in the plasma levels of MMP-1 between tuberculosis patients with or without diabetes (Andrade et al., 2014). The MMP-9 elevation was related with monocyte and macrophage recruitment, which is essential for the maturation of granulomas (Volkman et al., 2010). In this study, the gene expression of *mmp-9* was found to be significantly decreased in the latent group as compared to the active group at high glucose concentrations in THP-1 cells. The results were in accordance with a study on HIV-TB in which the concentrations of MMP-1, -2, -3, and -9 were decreased in the sputum of TB patients with HIV as compared to those without HIV (Walker et al., 2017). However, *in vivo* studies did not show any significant difference either in gene expression or in the serum levels of MMP-9 in actively infected mice or in latently infected mice with or without diabetes. The results were supported by another study in which no changes in the circulating levels of MMP-9 were observed between TB patients with or without diabetes (Kumar et al., 2018).

In conclusion, an animal model was employed to study latent tuberculosis and diabetes. Although animal models of tuberculosis and diabetes co-morbidity have been developed in the past, no animal model of latent tuberculosis and diabetes has been developed so far. This model of latent tuberculosis and diabetes was further used to study the role of diabetes in the activation of latent tuberculosis (Verma et al., 2021). Further, diabetes and hyperglycemic conditions lead to a decrease in levels of MCP-1, increased gene expression of *mmp-1*, and decreased gene expression of *mmp-9*, which together may lead to a disruption in the process of granuloma formation and in the activation of latent TB infection.

Data availability statement

The original contributions presented in the study are included in the article/Supplementary Material. Further inquiries can be directed to the corresponding author.

Ethics statement

The animal study was reviewed and approved by the Institutional Animal Ethical Committee, PGIMER, Chandigarh with ref. no. 89/90/IAEC/616 and the Animal Ethical Committee, ICGEB, New Delhi with ref. no. ICGEB/IAEC/02042019/TACF-PGIMER-16.

Author contributions

AV—Conception & design of the work, acquisition, analysis, and interpretation of data, wrote the main manuscript text and prepared figures. MK, PL, LS—Acquisition of data. DA, IV, BR, SB—Interpretation of data. SS—Conception and design of the work, interpretation of data and substantively revised the work. All

authors listed have made a substantial, direct, and intellectual contribution to the work and approved it for publication.

Acknowledgments

The authors are grateful to the Indian Council of Medical Research (wide no. 5/8/5/14/2014/ECD-1 and 3/1/3 JRF-2015/HRD-LS/20/10882/33) for financially supporting this work.

Conflict of interest

The authors declare that the research was conducted in the absence of any commercial or financial relationships that could be construed as a potential conflict of interest.

Publisher's note

Supplementary material

The Supplementary Material for this article can be found online at: https://www.frontiersin.org/articles/10.3389/fcimb.2022.957512/full#supplementary-material

References

Adilakshmi, T., Lease, R. A., and Woodson, S. A. (2006). Hydroxyl radical footprinting in vivo: Mapping macromolecular structures with synchrotron radiation. *Nucleic Acids Res* 34 (8), e64. doi: 10.1093/nar/gkl291

Ahmad, Z., Sharma, S., and Khuller, G. K. (2006). The potential of azole antifungals against Latent/Persistent tuberculosis. *FEMS Microbiol. Lett.* 258 (2), 200–2035. doi: 10.1111/j.1574-6968.2006.00224.x

Alim, M. A., Sikder, S., Bridson, T. L., Rush, C. M., Govan, B. L., and Ketheesan, N. (2017). Anti-mycobacterial function of macrophages is impaired in a diet induced model of type 2 diabetes. *Tuberculosis* 102, 47–54. doi: 10.1016/j.tube.2016.12.002

Andrade, B. B., Kumar, N. P., Amaral, E. P., Riteau, N., Mayer-Barber, K. D., Tosh, K. W., et al. (2015). Heme oxygenase-1 regulation of matrix metalloproteinase-1 expression underlies distinct disease profiles in tuberculosis. *J. Immunol.* 195 (6), 2763–73. doi: 10.4049/jimmunol.1500942

Andrade, B. B., Kumar, N. P., Sridhar, R., Banurekha, V. V., Jawahar, M. S., Nutman, T. B., et al. (2014). Heightened plasma levels of heme oxygenase-1 and tissue inhibitor of metalloproteinase-4 as well as elevated peripheral neutrophil counts are associated with TB-diabetes comorbidity. *Chest* 145 (6), 1244–1254. doi: 10.1378/chest.13-1799

Baik, S. H., Park, I. B., Choi, K. M., Kim, Y. H., Kim, N. H., Kim, S. J., et al. (1999). BCG Vaccine prevents insulitis in low dose streptozotocin-induced diabetic mice. *Diabetes Res. Clin. Practice* 46 (2), 91–7. doi: 10.1016/S0168-8227(99)00079-0

Baker, M. A., Harries, A. D., Jeon, C. Y., Hart, J. E., Kapur, A., Lönnroth, K., et al. (2011). The impact of diabetes on tuberculosis treatment outcomes: A systematic review. *BMC Med.* 9 (1), 815. doi: 10.1186/1741-7015-9-81

Betts, J. C., Lukey, P. T., Robb, L. C., McAdam, R. A., and Duncan, K. (2002). Evaluation of a nutrient starvation model of mycobacterium tuberculosis persistence by gene and protein expression profiling. *Mol. Microbiol.* 43 (3), 717–315. doi: 10.1046/j.1365-2958.2002.02779.x

Botha, T., and Ryffel, B. (2002). Reactivation of latent tuberculosis by an inhibitor of inducible nitric oxide synthase in an aerosol murine model. *Immunology* 107 (3), 350–7. doi: 10.1046/j.1365-2567.2002.01511.x

Chang, J. C., Wysocki, A., Tchou-Wong, K. M., Moskowitz, N., Zhang, Y., and Rom, W. N. (1996). Effect of mycobacterium tuberculosis and its components on macrophages and the release of matrix metalloproteinases. *Thorax* 51 (3), 306–11. doi: 10.1136/thx.51.3.306

Daniel, J., Deb, C., Dubey, V. S., Sirakova, T. D., Abomoelak, B., Morbidoni, H. R., et al. (2004). Induction of a novel class of diacylglycerol acyltransferases and triacylglycerol accumulation in mycobacterium tuberculosis as it goes into a dormancy-like state in culture. *J. Bacteriol* 186 (15), 5017–30. doi: 10.1128/JB.186.15.5017-5030.2004

Deshmane, S. L., Kremlev, S., Amini, S., and Sawaya, B. E. (2009). Monocyte chemoattractant protein-1 (MCP-1): An overview. *J. Interferon Cytokine Res* 29 (6), 313–26. doi: 10.1089/jir.2008.0027

Dooley, K. E., and Chaisson, R. E. (2009). Tuberculosis and diabetes mellitus: Convergence of two epidemics. *Lancet Infect. Dis* 9 (12), 737–46. doi: 10.1016/S1473-3099(09)70282-8

Dorner, B. G., Scheffold, A., Rolph, M. S., Huser, M. B., Kaufmann, S. H., Radbruch, A., et al. (2002). MIP-1alpha, MIP-1beta, RANTES, and ATAC/Lymphotactin function together with IFN-gamma as type 1 cytokines. *Proc. Natl. Acad. Sci. U.S.A* 99 (9), 6181–6. doi: 10.1073/pnas.092141999\n092141999

Dutta, N. K., Illei, P. B., Jain, S. K., and Karakousis, P. C. (2014). Characterization of a novel necrotic granuloma model of latent tuberculosis infection and reactivation in mice. *Am. J. Pathol.* 184 (7), 2045–55. doi: 10.1016/j.ajpath.2014.03.008

Faurholt-Jepsen, D., Nyagosya, R., Praygod, G., Jeremiah, K., Faurholt-Jepsen, M., Aabye, M. G., et al. (2013). Diabetes is a strong predictor of mortality during tuberculosis treatment: A prospective cohort study among tuberculosis patients from mwanza, Tanzania. *Trop. Med. Int. Health* 18 (7), 822–9. doi: 10.1111/tmi.12120

Fisher-Hoch, S. P., Mathews, C. E., and Mccormick, J. B. (2013). Obesity, diabetes and pneumonia: The menacing interface of non-communicable and infectious diseases. *Trop. Med. Int. Health* 18 (12), 1510–9. doi: 10.1111/tmi.12206

Fox, G. J., and Menzies, D. (2013). Epidemiology of tuberculosis immunology. *Adv. Exp. Med. Biol.* 783, 1–32. doi: 10.1007/978-1-4614-6111-1_1

Galboiz, Y., Shapiro, S., Lahat, N., and Miller, A. (2002). Modulation of monocytes matrix metalloproteinase-2, MT1-MMP and TIMP-2 by interferon-γ and -β: Implications to multiple sclerosis. *J. Neuroimmunol* 131 (1-2), 191–200. doi: 10.1016/S0165-5728(02)00266-7

Gomez, D. I., Twahirwa, M., Schlesinger, L. S., and Restrepo, B. I. (2013). Reduced mycobacterium tuberculosis association with monocytes from diabetes patients that have poor glucose control. *Tuberculosis* 93 (2), 192–7. doi: 10.1016/j.tube.2012.10.003

Gonzalez-Juarrero, M., Turner, O. C., Turner, J., Marietta, P., Brooks, J. V., and Orme, I. M. (2001). Temporal and spatial arrangement of lymphocytes within lung granulomas induced by aerosol infection with mycobacterium tuberculosis. *Infect. Immun.* 69 (3), 1722–8. doi: 10.1128/IAI.69.3.1722-1728.2001

Hair, P. S., Echague, C. G., Rohn, R. D., Krishna, N. K., Nyalwidhe, J. O., and Cunnion, K. M. (2012). Hyperglycemic conditions inhibit C3-mediated immunologic control of staphylococcus aureus. *J. Trans. Med* 10, 35. doi: 10.1186/1479-5876-10-35

Hasan, Z., Cliff, J. M., Dockrell, H. M., Jamil, B., Irfan, M., Ashraf, M., et al. (2009). CCL2 responses to mycobacterium tuberculosis are associated with disease severity in tuberculosis. *PloS One* 4 (12), e8459. doi: 10.1371/journal.pone.0008459

Hoheisel, G., Sack, U., Hui, D. S. C., Huse, K., Chan, K. S., Chan, K. K., et al. (2001). Occurrence of matrix metalloproteinases and tissue inhibitors of metalloproteinases in tuberculous pleuritis. *Tuberculosis* 81 (3), 203–9. doi: 10.1054/tube.2000.0276

Hrabec, E., Strek, M., Zieba, M., Kwiatkowska, S., and Hrabec, Z. (2002). Circulation level of matrix metalloproteinase-9 is correlated with disease severity in tuberculosis patients. *Int. J. Tuberculosis Lung Dis* 6 (8), 713–9.

Hu, Y., Movahedzadeh, F., Stoker, N. G., and Coates, A. R. M. (2006). Deletion of the mycobacterium tuberculosis α-crystallin-like HspX gene causes increased bacterial growth *in vivo*. *Infect. Immun.* 74 (2), 861–8. doi: 10.1128/IAI.74.2.861-868.2006

Iona, E., Pardini, M., Gagliardi, M. C., Colone, M., Stringaro, A. R., Teloni, R., et al. (2012). Infection of human THP-1 cells with dormant mycobacterium tuberculosis. *Microbes Infect.* 14 (11), 959–675. doi: 10.1016/j.micinf.2012.04.003

Jin, H. Y., Lee, K. S., Jin, S. M., and Lee, Y. C. (2004). Vascular endothelial growth factor correlates with matrix metalloproteinase-9 in the pleural effusion. *Respir. Med.* 98 (2), 115–212. doi: 10.1016/j.rmed.2003.09.002

Kumar, N. P., and Babu, S. (2017). Influence of diabetes mellitus on immunity to human tuberculosis. *Immunology* 152 (1), 13–245. doi: 10.1111/imm.12762

Kumar, N. P., George, P. J., Kumaran, P., Dolla, C. K., Nutman, T. B., and Babu, S. (2014). Diminished systemic and antigen-specific type 1, type 17, and other proinflammatory cytokines in diabetic and prediabetic individuals with latent mycobacterium tuberculosis infection. *J. Infect. Dis* 210 (10), 1670–8. doi: 10.1093/infdis/jiu329

Kumar, N. P., Moideen, K., Viswanathan, V., Shruthi, B. S., Sivakumar, S., Menon, P. A., et al. (2018). Elevated levels of matrix metalloproteinases reflect severity and extent of disease in tuberculosis-diabetes Co-morbidity and are predominantly reversed following

standard anti-tuberculosis or metformin treatment. *BMC Infect. Dis.* 18 (1), 345. doi: 10.1186/s12879-018-3246-y

Lecoeur, H. F., Truffot-Pernot, C., and Grosset, J. H. (1989). Experimental short-course preventive therapy of tuberculosis with rifampin and pyrazinamide. *Am. Rev. Respir. Dis* 140 (5), 1189–93. doi: 10.1164/ajrccm/140.5.1189

Lee, K. Y., Kim, E. H., Yang, W. S., Ryu, H., Cho, S. N., Lee, B. I., et al. (2004). Persistent increase of matrix metalloproteinases in cerebrospinal fluid of tuberculous meningitis. *J. Neurol. Sci* 220 (1-2), 73–8. doi: 10.1016/j.jns.2004.02.008

Lee, M. M., Yoon, B. J., Osiewicz, K., Preston, M., Bundy, B., Heeckeren, A. M. V., et al. (2005). Tissue inhibitor of metalloproteinase 1 regulates resistance to infection. *Infect. Immun.* 73 (1), 661–5. doi: 10.1128/IAI.73.1.661-665.2005

Leiter, E. H. (1982). Multiple low-dose streptozotocin-induced hyperglycemia and insulitis in C57BL mice: Influence of inbred background, sex, and thymus. *Proc. Natl. Acad. Sci.* 79 (2), 630–634. doi: 10.1073/pnas.79.2.630

Majeed, S., Radotra, B. D., and Sharma, S. (2016). Adjunctive role of MMP-9 inhibition along with conventional anti-tubercular drugs against experimental tuberculous meningitis. *Int. J. Exp. Pathol.* 97 (3), 230–7. doi: 10.1111/iep.12191

Martinez, N., and Kornfeld, H. (2014). Diabetes and immunity to tuberculosis. *Eur. J. Immunol.* 44 (3), 617–26. doi: 10.1002/eji.201344301

Matsuura, E., Umehara, F., Hashiguchi, T., Fujimoto, N., Okada, Y., and Osame, M. (2000). Marked increase of matrix metalloproteinase 9 in cerebrospinal fluid of patients with fungal or tuberculous meningoencephalitis. *J. Neurol. Sci.* 173 (1), 45–52. doi: 10.1016/S0022-510X(99)00303-2

McEvoy, R. C., Andersson, J., Sandler, S., and Hellerstrom, C. (1984). Multiple low-dose streptozotocin-induced diabetes in the mouse. evidence for stimulation of a cytotoxic cellular immune response against an insulin-producing beta cell line. *J. Clin. Invest.* 74 (3), 715–722. doi: 10.1172/JCI111487

Mustafa, T., Phyu, S., Nilsen, R., Jonsson, R., and Bjune, G. (1999). A mouse model for slowly progressive primary tuberculosis. *Scandinavian J. Immunol.* 50 (2), 127–136. doi: 10.1046/j.1365-3083.1999.00596.x

Nuermberger, E. L., Yoshimatsu, T., Tyagi, S., Bishai, W. R., and Grosset, J. H. (2004). Paucibacillary tuberculosis in mice after prior aerosol immunization with mycobacterium bovis BCG. *Infect. Immun.* 72 (2), 1065–71. doi: 10.1128/IAI.72.2.1065-1071.2004

O'Garra, A., Redford, P. S., McNab, F. W., Bloom, C. I., Wilkinson, R. J., and Berry, M. P. R. (2013). The immune response in tuberculosis. *Annu. Rev. Immunol.* 31, 475–527. doi: 10.1146/annurev-immunol-032712-095939

Ponce-de-Leon, A., Garc°a-Garc°a, M., Gomez-Perez, F. J., Valdespino-G¢mez, J. L., Olaiz-Fernandez, G., Rojas, R., et al. (2004). Tuberculosis and diabetes in southern Mexico. *Diabetes Care* 27, 1584–1590. doi: 10.2337/diacare.27.7.1584

Price, N. M., Farrar, J., Thi Hong Chau, T., Thi Hoang Mai, N., Tinh Hien, T., and Friedland, J. S. (2001). Identification of a matrix-degrading phenotype in human tuberculosis in vitro and *In vivo*. *J. Immunol.* 166 (6), 4223–30. doi: 10.4049/jimmunol.166.6.4223

Ramos-Vara, J. A. (2011). Principles and methods of immunohistochemistry. *Methods Mol. Biol.* 691, 83–96. doi: 10.1007/978-1-60761-849-2_5

Ranaivomanana, P., Raberahona, M., Rabarioelina, S., Borella, Y., Machado, A., De Dieu Randria, M. J., et al. (2018). Cytokine biomarkers associated with human extra-pulmonary tuberculosis clinical strains and symptoms. *Front. Microbiol.* 9, 275. doi: 10.3389/fmicb.2018.00275

Restrepo, B. I., and Schlesinger, L. S. (2013). Host-pathogen interactions in tuberculosis patients with type 2 diabetes mellitus. *Tuberculosis* 93 (Suppl 0), S10–4. doi: 10.1016/S1472-9792(13)70004-0

Restrepo, B. I., Twahirwa, M., Rahbar, M. H., and Schlesinger, L. S. (2014). Phagocytosis *via* complement or fc-gamma receptors is compromised in monocytes from type 2 diabetes patients with chronic hyperglycemia. *PloS One* 9 (3), e92977. doi: 10.1371/journal.pone.0092977

Rhoades, E. R. (1997). Progression of chronic pulmonary tuberculosis in mice aerogenically infected with virulent mycobacterium tuberculosis. *Tubercle Lung Dis* 78 (1), 57–66. doi: 10.1016/S0962-8479(97)90016-2

Riaz, M. S., Kaur, A., Shwayat, S. N., Behboudi, S., Kishore, U., and Pathan, A. A. (2020). Dissecting the mechanism of intracellular mycobacterium smegmatis growth inhibition by platelet activating factor c-16. *Front. Microbiol.* 11, 1046. doi: 10.3389/fmicb.2020.01046

Rieder, H. L. (2014). The dynamics of tuberculosis epidemiology. *Indian J. Tuberculosis* 61 (1), 19–29.

Ries, C., and Petrides, P. E. (1995). Cytokine regulation of matrix metalloproteinase activity and its regulatory dysfunction in disease. *Biol. Chem. Hoppe-Seyler* 376 (6), 345–55.

Rosa, L., Chiuso-Minicucci, F., Zorzella-Pezavento, S. F. G., França, T. G. D., Ishikawa, L. L. W., Colavite, P. M., et al. (2013). Bacille calmette-Guérin/DNAhsp65 prime-boost is protective against diabetes in non-obese diabetic mice but not in the streptozotocin model of type 1 diabetes. *Clin. Exp. Immunol.* 173 (3), 430–437. doi: 10.1111/cei.12140

Salgame, P. (2011). MMPs in tuberculosis: Granuloma creators and tissue destroyers. *J. Clin. Invest.* 121 (5), 1686–1688. doi: 10.1172/JCI57423

Sirakova, T. D., Dubey, V. S., Deb, C., Daniel, J., Korotkova, T. A., and Abomoelak, B. (2006). Identification of a diacylglycerol acyltransferase gene involved in accumulation of triacylglycerol in mycobacterium tuberculosis under stress. *Microbiology* 152 (Pt 9), 2717–2725. doi: 10.1099/mic.0.28993-0

Stegenga, M. E., van der Crabben, S. N., Dessing, M. C., Pater, J. M., van den Pangaart, P. S., de Vos, A. F., et al. (2008). Effect of acute hyperglycaemia and/or hyperinsulinaemia on proinflammatory gene expression, cytokine production and neutrophil function in humans. *Diabetic Med.* 25 (2), 157–164. doi: 10.1111/j.1464-5491.2007.02348.x

Sun, N., Yang, G., Zhao, H., Savelkoul, H. F. J., and An, L. (2005). Multidose streptozotocin induction of diabetes in BALB/c mice induces a dominant oxidative macrophage and a conversion of TH1 to T H2 phenotypes during disease progression. *Mediators Inflammation* 4, 202–209. doi: 10.1155/MI.2005.202

Thwaites, G. E., Simmons, C. P., Quyen, N. T. H., Thi Hong Chau, T., Mai, P. P., and Thi Dung, N. (2003). Pathophysiology and prognosis in Vietnamese adults with tuberculous meningitis. *J. Infect. Dis.* 188 (8), 1105–15. doi: 10.1086/378642

Turner, J., Gonzalez-Juarrero, M., Saunders, B. M., Brooks, J. V., Marietta, P., Ellis, D. L., et al. (2001). Immunological basis for reactivation of tuberculosis in mice. *Infect. Immun.* 69 (5), 3264–70. doi: 10.1128/IAI.69.5.3264-3270.2001

Vallerskog, T., Martens, G. W., and Kornfeld, H. (2010). Diabetic mice display a delayed adaptive immune response to mycobacterium tuberculosis. *J. Immunol.* 184 (11), 6275–82. doi: 10.4049/jimmunol.1000304

Ventura-Sobrevilla, J., Boone-Villa, V. D., Aguilar, C. N., Román-Ramos, R., Vega-Avila, E., Campos-Sepúlveda, E., et al. (2011). Effect of varying dose and administration of streptozotocin on blood sugar in Male CD1 mice. *Proc. Western Pharmacol. Soc.* 54, 5–9.

Verma, A., Kaur, M., Singh, L. V., Aggarwal, D., Verma, I., Radotra, B. D., et al. (2021). Reactivation of latent tuberculosis through modulation of resuscitation promoting factors by diabetes. *Sci. Rep.* 11 (1), 197005. doi: 10.1038/s41598-021-99257-1

Volkman, H. E., Pozos, T. C., Zheng, J., Davis, J. M., Rawls, J. F., and Ramakrishnan, L. (2010). Tuberculous granuloma induction *via* interaction of a bacterial secreted protein with host epithelium. *Science* 327 (5964), 466–9. doi: 10.1126/science.1179663

Walker, N. F., Wilkinson, K. A., Meintjes, G., Tezera, L. B., Goliath, R., Peyper, J. M., et al. (2017). Matrix degradation in human immunodeficiency virus type 1-associated tuberculosis and tuberculosis immune reconstitution inflammatory syndrome: A prospective observational study. *Clin. Infect. Dis.* 65 (1), 121–132. doi: 10.1093/cid/cix231

Woessner, J. F. (1991). Matrix metalloproteinases and their inhibitors in connective tissue remodeling. *FASEB J* 5 (8), 2145–54. doi: 10.1096/fasebj.5.8.1850705

Wu, J., Wang, S., Lu, C., Shao, L., Gao, Y., Zhou, Z., et al. (2017). Multiple cytokine responses in discriminating between active tuberculosis and latent tuberculosis infection. *Tuberculosis* 102, 68–75. doi: 10.1016/j.tube.2016.06.001

Zhang, T., Zhang, M., Rosenthal, I. M., Grosset, J. H., and Nuermberger, E. L. (2009). Short-course therapy with daily rifapentine in a murine model of latent tuberculosis infection. *Am. J. Respir. Crit. Care Med.* 180 (11), 1151–1585. doi: 10.1164/rccm.200905-0795OC

frontiers | Frontiers in Cellular and Infection Microbiology

TYPE Original Research
PUBLISHED 09 March 2023
DOI 10.3389/fcimb.2023.1144210

OPEN ACCESS

EDITED BY
Elena G. Salina,
Research Center of Biotechnology of the Russian Academy of Sciences, Russia

REVIEWED BY
Martin I. Voskuil,
University of Colorado Denver, United States
Brian Weinrick,
Trudeau Institute, United States

*CORRESPONDENCE
Kyle H. Rohde
Kyle.rohde@ucf.edu

SPECIALTY SECTION
This article was submitted to Bacteria and Host, a section of the journal Frontiers in Cellular and Infection Microbiology

RECEIVED 13 January 2023
ACCEPTED 15 February 2023
PUBLISHED 09 March 2023

CITATION
Simcox BS, Tomlinson BR, Shaw LN and Rohde KH (2023) *Mycobacterium abscessus* DosRS two-component system controls a species-specific regulon required for adaptation to hypoxia. *Front. Cell. Infect. Microbiol.* 13:1144210. doi: 10.3389/fcimb.2023.1144210

Mycobacterium abscessus DosRS two-component system controls a species-specific regulon required for adaptation to hypoxia

Breven S. Simcox[1], Brooke R. Tomlinson[2], Lindsey N. Shaw[2] and Kyle H. Rohde[1]*

[1]Division of Immunology and Pathogenesis, Burnett School of Biomedical Sciences, College of Medicine, University of Central Florida, Orlando, FL, United States, [2]Department of Cell Biology, Microbiology and Molecular Biology, University of South Florida, Tampa, FL, United States

Mycobacterium abscessus (*Mab*), an emerging opportunistic pathogen, predominantly infects individuals with underlying pulmonary diseases such as cystic fibrosis (CF). Current treatment outcomes for *Mab* infections are poor due to *Mab's* inherent antibiotic resistance and unique host interactions that promote phenotypic tolerance and hinder drug access. The hypoxic, mucus-laden airways in the CF lung and antimicrobial phagosome within macrophages represent hostile niches *Mab* must overcome *via* alterations in gene expression for survival. Regulatory mechanisms important for the adaptation and long-term persistence of *Mab* within the host are poorly understood, warranting further genetic and transcriptomics study of this emerging pathogen. DosRS$_{Mab}$, a two-component signaling system (TCS), is one proposed mechanism utilized to subvert host defenses and counteract environmental stress such as hypoxia. The homologous TCS of *Mycobacterium tuberculosis* (*Mtb*), DosRS$_{Mtb}$, is known to induce a ~50 gene regulon in response to hypoxia, carbon monoxide (CO) and nitric oxide (NO) *in vitro* and *in vivo*. Previously, a small DosR$_{Mab}$ regulon was predicted using bioinformatics based on DosR$_{Mtb}$ motifs however, the role and regulon of DosRS$_{Mab}$ in *Mab* pathogenesis have yet to be characterized in depth. To address this knowledge gap, our lab generated a *Mab dosRS* knockout strain (*Mab*$_{\Delta dosRS}$) to investigate differential gene expression, and phenotype in an *in vitro* hypoxia model of dormancy. qRT-PCR and lux reporter assays demonstrate *Mab_dosR* and 6 predicted downstream genes are induced in hypoxia. In addition, RNAseq revealed induction of a much larger hypoxia response comprised of >1000 genes, including 127 differentially expressed genes in a *dosRS* mutant strain. Deletion of DosRS$_{Mab}$ led to attenuated growth under low oxygen conditions, a shift in morphotype from smooth to rough, and down-regulation of 216 genes. This study provides the first look at the global transcriptomic response of *Mab* to low oxygen conditions encountered in the airways of CF patients and within macrophage phagosomes. Our data also demonstrate the importance of DosRS$_{Mab}$ for adaptation of *Mab* to hypoxia,

highlighting a distinct regulon (compared to *Mtb)* that is significantly larger than previously described, including both genes conserved across mycobacteria as well as *Mab*-specific genes.

KEYWORDS

nontuberculous mycobacteria (NTM), *Mycobacterium abcessus*, hypoxia, two-component system (TCS), RNAseq, DosR

Introduction

Mycobacterium abscessus (*Mab*) is an opportunistic pathogen capable of causing skin, soft tissue and pulmonary infections in immunocompromised individuals and individuals with pre-existing lung disease such as cystic fibrosis (CF) and bronchiectasis (Brown-Elliott and Wallace, 2002; Olivier et al., 2003; Harris and Kenna, 2014; Lee et al., 2015; Lopeman et al., 2019). Impaired innate immune defenses and viscous mucus within the CF lung contribute to reduced clearance of bacterial pathogens leading to increased rates of infections and morbidity (Lyczak et al., 2002; Chmiel and Davis, 2003). *Mab* is the most common rapidly-growing mycobacterial (RGM) species recovered from the lungs of CF patients (Esther et al., 2010). Within the CF population and patients with underlying lung dysfunction, infections caused by *Mab* are associated with lung function decline, increased hospital visits, prolonged hospital stays and in some cases exclusion from lung transplants (Olivier et al., 2003; Esther et al., 2010; Lopeman et al., 2019). Due to *Mab's* inherent antibiotic resistance, treatment options are limited, resulting in extremely low cure rates of less than 50% (Greendyke and Byrd, 2008; Hurst-Hess et al., 2017; Molina-Torres et al., 2018; Story-Roller et al., 2018; Lopeman et al., 2019).

The development of effective treatment strategies for *Mab* is hindered by discrepancies between *in vitro* and *in vivo* susceptibilities associated with *Mab's* unique lifestyle (Greendyke and Byrd, 2008; Philley et al., 2016; Molina-Torres et al., 2018). Akin to *Mycobacterium tuberculosis* (*Mtb*), the causative agent of tuberculosis, *Mab* resides within pulmonary macrophages and within granulomas which limit antibiotic accessibility and promote drug tolerance, making treatment of an inherently antibiotic resistant pathogen even more difficult (Bernut et al., 2016; Peddireddy et al., 2017). The viscous mucus in the CF lung represents an additional hostile niche within the host to which *Mab* must adapt (Lyczak et al., 2002; Chmiel and Davis, 2003; Miranda-CasoLuengo et al., 2016; Dubois et al., 2019). One key host-derived stress encountered by *Mab* in all three of these microenvironments is decreased oxygen tension, with oxygen tension estimated to be ~1% O_2 within these niches (Worlitzsch et al., 2002; Cunningham-Bussel et al., 2013; Hudock et al., 2017). Thus, to successfully cause an infection, *Mab* must encode mechanisms to adapt and persist under hypoxic conditions. Transcriptional responses to host-derived cues/stresses are not well-defined in this NTM pathogen, requiring further studies to understand how *Mab* adapts its physiology and virulence factor expression to cause insidious, persistent infections.

Two-component signaling (TCS) is a mechanism commonly utilized by prokaryotes to regulate virulence gene expression in response to host-derived cues (Yarwood et al., 2001; Walters et al., 2006; Gonzalo-Asensio et al., 2008; Gooderham and Hancock, 2009). A typical TCS consists of a sensor histidine kinase (HK) responsible for signal recognition and subsequent phosphorylation of a cognate response regulator (RR) which binds DNA motifs within promoter regions to drive alterations in gene expression (Stock et al., 1989; West and Stock, 2001; Mascher et al., 2006; Salazar and Laub, 2015). *Mab* encodes 11 TCS, 5 orphan RRs and 1 orphan HK each with a corresponding ortholog in *Mtb*; however, in-depth studies of *Mab* TCS have not been performed (Bretl et al., 2011). The well-documented atypical TCS DosRS/T_{Mtb}, is known to control a ~50 gene regulon to counteract hypoxic and nitrosative stress encountered within macrophages and granulomas (Sherman et al., 2001; Park et al., 2003; Voskuil et al., 2003; Leistikow et al., 2010; Rohde et al., 2012; Cunningham-Bussel et al., 2013; Peterson et al., 2020; Kundu and Basu, 2021). DosRS/$T_{Mtb,}$contains 2 HKs (DosS and DosT) rather than one which are responsible for phosphorylating the RR DosR at different stages of hypoxia (Roberts et al., 2004). Although *Mtb dosT* contributes to signaling in early stages of hypoxia, it is constitutively expressed and is not part of the $DosR_{Mtb}$ regulon (Honaker et al., 2009). The $DosR_{Mtb}$ regulon includes autoregulation of *dosRS* itself, as well as heat shock proteins, triacylglycerol synthases, ferrodoxins, universal stress proteins, diacylglycerol acyltransferases, and nitroreductase which are implicated in dormancy, resuscitation, phenotypic drug tolerance and increased lipid metabolism (Park et al., 2003; Voskuil et al., 2003; Leistikow et al., 2010; Galagan et al., 2013; Aguilar-Ayala et al., 2017). Induction of *Mtb dosR* within animal models capable of forming hypoxic granulomas (rhesus macaques, guinea pigs, and C3HeB/FeJ mice) and attenuation of mutants lacking $DosRS_{Mtb}$ highlight the importance of this TCS for *Mtb* pathogenesis (Converse et al., 2009; Gautam et al., 2015a, Gautam et al., 2015b; Mehra et al., 2015).

According to whole genome sequence data, *Mab* encodes a DosR ortholog (*Mab*_3891c) with a high level of homology with $DosR_{Mtb}$ (~72% identity) adjacent to and upstream of $DosS_{Mab}$ (*Mab*_3890c) with lower similarity (~51% identify) to its counterpart in *Mtb*. *Mab* does not appear to encode a secondary orphan HK analogous to DosT, with the closest homolog to *dosT* being $dosS_{Mab}$/*Mab*_3890C (53% identity). At the time this study

was initiated, only two reports made mention of DosRS$_{Mab}$. A bioinformatics study by Gerasimova et al. used *Mtb* DosR promoter motifs to predict a small DosR$_{Mab}$ regulon consisting of only 6 genes (Gerasimova et al., 2011). A subsequent transcriptomics study by Miranda Caso-Luengo et al. demonstrated induction of the 6 predicted DosR$_{Mab}$ regulated genes plus 56 other genes upon exposure to nitric oxide (NO) (Miranda-CasoLuengo et al., 2016). It remained unclear whether induction of these genes occurs through signaling of DosRS$_{Mab}$ or whether hypoxia is an induction cue.

Although there is considerable overlap in the repertoires of TCS encoded by different mycobacteria, few cross-species transcriptomic studies are available comparing TCS regulons and regulatory networks between e.g. *Mtb* and NTM pathogens. Given the diversity of conditions encountered by *Mab* as an environmental, opportunistic pathogen, and larger genome (compared to *Mtb)* comprised of ~800 species-specific genes, the potential for unique gene sets in *Mab* TCS regulons is high (Malhotra et al., 2017; Wee et al., 2017). A hypoxia model mimicking the physiologic conditions in the mucus of CF airways, within granulomas and intramacrophage compartments was used to evaluate the role of DosRS$_{Mab}$ and assess transcriptional regulation mediated by this TCS. Our work demonstrates DosRS$_{Mab}$ is important for maximal growth and survival in hypoxia and regulates a potentially larger set of genes than previously predicted. RNAseq revealed upregulation of >1000 genes in hypoxia including 127 putative DosRS$_{Mab}$ regulated genes. Information gained from this study identifies the importance of the DosRS$_{Mab}$ TCS in adaptation to hypoxia for survival and provides valuable knowledge of a novel set of hypoxia-induced genes in this species for future studies.

Methods

Mycobacterium abscessus cloning

Mab$_{\Delta dosRS}$ was generated *via* recombineering as described by van Kessell and Hatfull in the strain *Mab* 390S obtained from the Thomas Byrd lab (Byrd and Lyons, 1999; van Kessel and Hatfull, 2007). In brief, an allelic exchange substrate (AES) was engineered containing an apramycin resistance cassette flanked by ~1000 nucleotides upstream and downstream of the *dosRS* operon *via* round the horn PCR and fast cloning (Moore and Prevelige, 2002; Li et al., 2011). *Mab*::pJV53 competent cells induced with .02% acetamide for 4 hours were electroporated with 100ng AES, recovered in 7H9 OADC media for 24 hours, and plated on 7H10 agar supplemented with apramycin 50 µg/ml. Complement strain, *Mab*$_{\Delta dosRS+C}$, containing *dosRS* with its native promoter was engineered using round the horn (Moore and Prevelige, 2002) and fast cloning (Li et al., 2011) in the integrating vector pUAB400 followed by electroporation into *Mab*$_{\Delta dosRS}$ (Singh et al., 2006). *Mab* 390S and *Mab*$_{\Delta dosRS}$ were transformed with pMV306hspG13lux (Addgene #26161) to generate the constitutive lux strains, *Mab* 390S P$_{hsp60}$-lux and *Mab*$_{\Delta dosRS}$ P$_{hsp60}$-lux. Lux reporters under the control of P$_{dosR}$ and P$_{2489}$ were constructed in the background plasmid pMV306hspG13lux to generate Mab 390S P$_{dosR}$-lux, *Mab*$_{\Delta dosRS}$ P$_{dosR}$-lux, *Mab* 390S P$_{2489}$-lux, and *Mab*$_{\Delta dosRS}$ P$_{2489}$-lux, *via* replacement of P$_{hsp60}$ (hsp60 promoter) using round-the horn cloning (Moore and Prevelige, 2002; Andreu et al., 2010; Li et al., 2011). Refer to Table S1 for strains, plasmids and primers used for cloning.

Hypoxic and re-aeration culture models

Cultures were grown in 7H9-OADC+.05% tyloxapol from glycerol stocks at 37°C while shaking unless otherwise noted. For growth kinetics assays, strains were inoculated from mid-log phase starter cultures into 13ml of media in filter-capped T-25 flasks to an OD$_{600}$ = 0.02. Hypoxic cultures were grown standing in a hypoxic incubator set at 1% O_2 while aerated controls were cultured at 20% O_2 while shaking at 100 rpm. Re-aeration studies were conducted after cultures were subjected to hypoxia or grown at 20% O_2 for 30 days. Optical density readings (OD$_{600nm}$) were taken on days 2, 3, 5, 8 and 10.

RNA experiments

RNA was extracted as previously described (Rohde et al., 2007) in triplicate from hypoxic cultures (1% O_2) and normoxic cultures (20% O_2) for qRT-PCR and RNAseq. At designated time points, cultures were pelleted at 4300 rpm for 5 minutes, resuspended in guanidine thiocyanate buffer, pelleted again at 12,000 rpm for 5 min, and stored at -80°C until processing. Thawed pellets were resuspended in 65°C Trizol then lysed using 0.1mM silicon beads in a BeadBeater at max speed for 1 minute 2x followed by cooling on ice for 1 minute between bead beating. Isolation of total RNA from Trizol lysates was performed using chloroform extraction and Qiagen RNeasy column purification. Total RNA was treated with Turbo DNase (Invitrogen) to eliminate DNA contamination. 50 ng/µl of total RNA was used to generate cDNA using iScript^{TM} cDNA synthesis kit (Bio-Rad) for qRT-PCR reactions carried out in a QuantStudio7 thermocycler. Primers used for qRT-PCR are listed in Table S1. RNA samples for RNAseq analysis were pooled at equal RNA concentrations from three biological experiments as previously described (Tomlinson et al., 2021; Tomlinson et al., 2022) prior to library preparation at a concentration of 50 ng/µl in 20 µl. Only RNA samples with RIN>6 as determined by Tapestation analysis were utilized. RNA samples were sequenced by Microbial Genome Sequencing Center (MiGs) using Illumina sequencing protocol aligning reads to the *Mab* ATCC19977 genome (accession #CU458896). RNAseq data reflects a minimum of 12M paired end reads per sample. Due to incompatibility of Ribo-zero rRNA removal kit (Illumina) with *Mab* which resulted in high levels of rRNA, MiGS designed custom depletion probes (Table S2) for rRNA depletion. Raw data was received from MiGs as fastq files followed by analysis using CLC Genomics Workbench 12 (Qiagen Bioinformatics). Illumina paired importer tool was used to eliminate failed reads using the quality score parameter option set to Illumina Pipelines 1.8. Expression browser tool (v1.1) was used to calculate gene expression with an output of transcript per million (TPM). Differential gene expression is expressed as a $\log_2$FC of ≤-1 or ≥1 and visualized as scatter plots created in GraphPad Prism 9.

Lux reporter assays

Bio-luminescent reporter strains were grown to mid-log phase, diluted to .02 OD in 13ml in T25 flasks and grown in either 20% O_2 or 1% O_2 for 1, 5 and 20 days. 200 ul of each culture was aliquoted in triplicate into 96 well white bottomed plate to measure luminescence *via* Synergy H4 reader (Biotek). Fold change of luminescence was analyzed comparing individual strains in 1% O_2 to 20% O_2 using *Mab* 390S P_{hsp60}-lux or $Mab_{\Delta dosRS}$ P_{hsp60}-lux as internal controls (1%O_2(P_{dosR} or P_{2489}/P_{hsp60}))/(20% O_2(P_{dosR} or P_{2489}/P_{hsp60})).

Results

Growth and transcriptome remodeling of *Mab* in a defined hypoxia model

Our first goal was to develop a tractable *in vitro* model to investigate the mechanisms employed by *Mab* to persist under physiologically relevant oxygen-limited conditions. To do this, *Mab* 390S was grown under standing conditions in a 1% O_2 atmosphere to mimic the pO_2 observed within the CF lung, macrophages and granulomas (Worlitzsch et al., 2002; Cunningham-Bussel et al., 2013; Hudock et al., 2017). *Mab* 390S grew steadily at 1% O_2, reaching OD_{600} ~0.7 by day 5 with continued increase to ~0.9 by day 10 (Figure S1). Somewhat unexpectedly, the intended aerobic control culture (20% O_2 atmosphere, standing) had a very similar growth profile, reaching only a slightly higher OD ~1.2 by day 10 (Figure S1). In contrast, *Mab* 390S grown in 20% O_2 with shaking (100rpm) reached a maximum density by day 5 (OD_{600}~1.6) and subsequently plateaued up to day 10 (Figure S1). This difference is likely due to the microaerobic conditions experienced by bacilli growing below the media surface, as previously seen with *Mtb* and BCG strains grown in standing conditions (Cunningham and Spreadbury, 1998; Purkayastha et al., 2002). To maximize the contrast between aerobic and hypoxic conditions, *Mab* cultures shaking in 20% O_2 served as references for all hypoxia experiments. Thus, *Mab* is not only able to survive but to actively replicate under *in-vivo* like hypoxia conditions. It is worth noting that exposure of *Mab* to sudden hypoxia using BD Gaspack anaerobic pouches led to rapid sterilization of the cultures (data not shown). This may indicate a lower threshold of O_2 levels needed for *Mab* viability was exceeded or that slower, adaptive responses are necessary to survive.

Exploiting this model to profile *Mab* differential gene expression (DGE) in response to hypoxia, RNAseq transcriptomic analysis was conducted on wild-type *Mab* 390S cultured at 1% O_2 and 20% O_2 on day 5. This time point reflects the maximal difference in OD_{600nm} between hypoxic and aerated cultures and precedes the plateau in growth curves (Figure S1). The scatter plot in Figure 1A graphically depicts the dramatic genome-wide alterations in *Mab* 390S gene expression induced by *in vivo*-like low oxygen condition. The *Mab* hypoxia response included induction of 1,190 genes (≥ 1 log_2 fold change compared to 20% O_2) and downregulation of 1,062 genes (≤ 1 log_2 fold change compared to 20% O_2). This represented a larger set of hypoxia-induced genes than observed in *Mtb* in two studies under similar 1% O_2 hypoxia conditions (induction of ~400 genes detected *via* microarray and ~682 *via* RNAseq) (Rustad et al., 2009; Vilcheze et al., 2022). These data highlight the functional genomic differences between *Mab* and *Mtb*, in particular their distinct patterns of gene regulation in response to hypoxia which are discussed in detail below.

To identify putative regulators of hypoxia adaptation in *Mab*, we assessed the differential expression of TCSs and other annotated transcription factors in the 1% hypoxia model. Of the 11 TCS orthologous to *Mtb*, only *dosRS*, *mtrA*, *narS* and the orphan RRs *Mab_2133* and *Mab_3520c* displayed DGE (Figure 1B). *Mab_dosRS* exhibited the largest magnitude of gene induction with log_2FC of 3.9 and 4.5, respectively, pointing to $DosRS_{Mab}$ as an important TCS facilitating adaptation to hypoxic stress. The other TCS components were minimally induced with a log_2FC of 1.6 for *narS*, 1.2 for *mtrA* and 1.1 for the orphan RR *Mab_2133*. The roles of *narS, mtrA* and *Mab_2133* have not been determined in *Mab*. However, in the context of *Mtb*, the regulons of DosRS and NarLS TCS display partial overlap and protein-protein interactions between the RR from these two TCSs, DosR and NarL, have been detected (Malhotra et al., 2015). *mtrA* is essential in *Mtb* due its role in replication, whereas in *Mab mtrA* was reported to be non-essential, pointing to potential differences in the role of this TCS between the two species (Fol et al., 2006; Akusobi et al., 2022). The *Mtb* ortholog (Rv3143) of orphan RR *Mab_2133* is implicated in nitrate metabolism in the absence of oxygen, binds to *nuo* subunits required for electron transport and is within nuo operon (Plocinska et al., 2022). *Mab's* nuo operon displays synteny with the *Mtb nuo* operon including the orphan RR *Mab_2133*. Whereas Rv3143 was moderately induced by hypoxia in a DosR-dependent manner (Kendall et al., 2004), the upregulation of *Mab_2133* in our hypoxia model was not altered in the absence of DosRS (Table S3). The only TCS gene displaying substantial downregulation was *Mab_3520c* (log_2FC = -9.7). The *Mtb* ortholog of *Mab_3520c*, Rv0260c, is known to be upregulated in hypoxia and to interact with DosS *via* protein-protein interaction independent of DosR; however, the function of *Rv0260c* has not been identified (Gautam et al., 2019; Vilcheze et al., 2022). The opposite pattern of regulation of Rv0260c (induced) and *Mab*_3520c (repressed) in hypoxia implies they are utilized differently for adaptation to hypoxia. Thus, our transcriptomic analyses of *Mab* under physiologic hypoxia conditions point to *Mab* DosRS as an important TCS aiding in adaptation to hypoxia.

In addition to induction of the *Mab_dosRS* TCS, we also observed upregulation of 80 single component transcription factors (TF) in hypoxia (Table S3). Due to the high number of TF, only the genes with a log_2FC ≥ 3 are included in Table S4 with the most highly induced genes being *Mab_4180* (lclR), *Mab_2606c* (TetR family), *Mab_4332* (TetR family) and *Mab_3018* (GntR family). The *Mtb* orthologs for *Mab_4332* (Rv0273c) and *Mab_3018* (Rv0586) have 64.14% and 45.53% identity, respectively. Rv0273c has been identified as a regulator of *inhA*, an enoyl-ACP reductase involved in mycolic acid synthesis, and

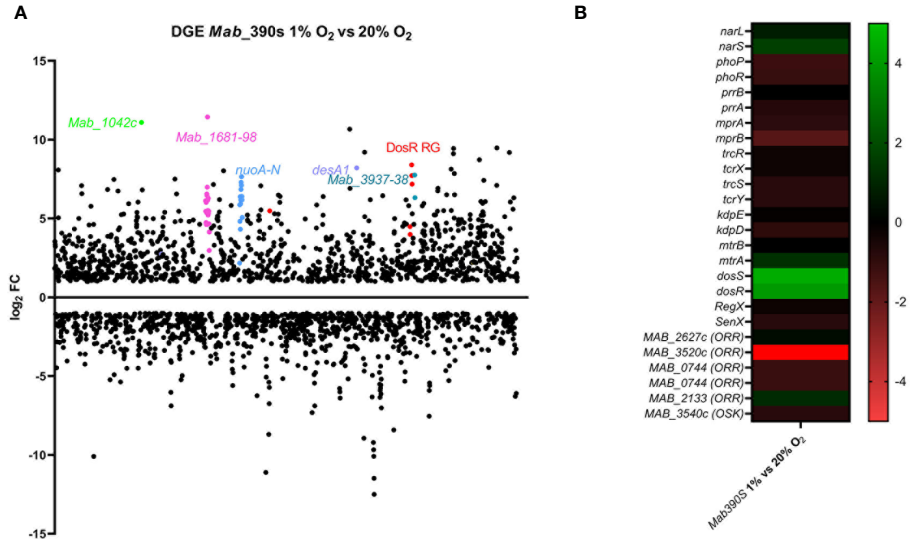

FIGURE 1
Transcriptome analysis of *Mab*390S in defined hypoxia model. DGE is visualized as **(A)** scatter plot depicting changes in gene expression reported as TPM with ≥ or ≤ log_2FC on Day 5 for *Mab* 390S 1% O_2 vs *Mab* 390S 20% O_2. Dots represent individual genes (neon green=*Mab_1042C*, pink=*Mab_1681-1698*, blue=*nuo* operon, purple= *desA1*, turquoise=*Mab_3937 & 3938*, red= predicted DosR regulated genes (RG). **(B)** Heat map showing DGE of TCS of *Mab* 390S in 1% O_2 vs 20% O_2. In gene names, orphan response regulators and orphan sensor kinases are denoted as ORR and OSK, respectively.

Rv0586 is known to mediate lipid metabolism in *Mtb* (Santangelo Mde et al., 2009; Yousuf et al., 2018; Zhu et al., 2018). Both *Mab_4180* and *Mab_2606c* share less than 30% sequence homology with the *Mtb* orthologs and no known function has been identified. Although few *Mab* transcriptional regulators have been characterized, the large number of regulators with altered expression under hypoxic stress are likely key nodes in the regulatory networks needed to adapt *in vivo*.

Due to the number of TFs and their magnitude of modulation in response to hypoxia, including upregulation of *Mab_dosRS*, the broad scope of transcriptional changes was not surprising. The list of hypoxia-induced genes included loci involved in fatty acid and cholesterol metabolism, components of the NADH-quinone oxidoreductase subunits (*nuoA-N*), 6 epoxide hydrolases (*ephD*), ATP synthase subunits, 5 mammalian cell entry operons (MCE), members of the glycopeptidolipid locus (GPL), and 520 hypothetical genes (Tables S3, 4). Several pathways critical for pathogenesis of *Mtb*, such as fatty acid and cholesterol metabolism, are also induced in various hypoxia models (Wayne model, 1% O_2) and within granulomas (Wilburn et al., 2018; Yang et al., 2021; Vilcheze et al., 2022). All four MCE loci in *Mtb* are differentially expressed in response to hypoxia, suggesting an important role for this family of lipid/cholesterol transporters in adaptation to this stress. While *mce2* and *mce3* were induced in a hypoxia model similar to ours (1% O_2, 5 days), *mce1* was repressed, and *mce4* expression remained unchanged (Vilcheze et al., 2022). A separate study by Rathor et al. found that *mce4* was upregulated after much longer durations of hypoxia stress (Rathor et al., 2016). Mce1 and Mce4 are known to play a role in the transport of fatty acids and cholesterol (Wilburn et al., 2018; Klepp et al., 2022), whereas the function of Mce2 and Mce3 have not been determined yet. In contrast, five of the seven MCE systems encoded by *Mab* were upregulated in 1% O_2 after 5 days (Tables S3, 4). Although the biological role of MCE complexes in *Mab* have not been studied, their distinct expression profile suggest they may be important for *in vivo* survival. The *Mab* hypoxia-induced gene set also included a large number of genes implicated in β-oxidation pathways - 14 *fadE* genes, 8 *fadD* genes, and one of each *fadA* and *fadH* (Tables S3, 4). Upregulation of 6 *ephD* genes (an epoxide hydrolase predicted to alter the amount of epoxymycolates in the cell wall), members of the GPL locus accounting for smooth morphology (Tables S3, 4), and arabinosyltransferases A and B (Supplemental Table 1) involved with arabinogalactan synthesis indicate *Mab* may undergo cell wall remodeling in response to hypoxia (Amin et al., 2008; Gutierrez et al., 2018; Madacki et al., 2018).

In addition to β-oxidation, metabolic pathway induction included *nuo* subunits *A-N*, ATPase subunits, and cytochrome P450 genes (Tables S3, 4). NuoA-N are subunits of the proton pumping NADH dehydrogenase type 1 responsible for transferring electrons to menaquinone in the electron transport chain (ETC) in an energy conserving manner to generate a PMF (Weinstein et al., 2005). Although these genes are upregulated in the RGM *Mycobacterium smegmatis* (*Msmeg*) during slowed growth and in *E.coli* in anaerobic conditions, this is not a feature observed in the hypoxic response of slow-growing mycobacteria (SGM) like *Mtb* (Unden and Bongaerts, 1997; Berney and Cook, 2010). In contrast to *Mab*, the nuo operon and ATPase subunits are downregulated in hypoxic *Mtb*, further highlighting the distinct stress responses and energy metabolism of these two species in response to hypoxia (Cook et al., 2014; Vilcheze et al., 2022). Of the 25 *Mab* cytochrome P450s, 14 were induced in hypoxia (Supplemental Table 1). This data is consistent with hypoxic induction a large number of

cytochrome P450s in the RGM *Msmeg* but not in the SGM *Mtb* with the exception of only 2 cytochrome P450s (Sherman et al., 2001; Berney and Cook, 2010; Ortega Ugalde et al., 2019). The roles of individual *Mab* cytochrome P450s remain unknown but the functions of the *Mtb* orthologs are dependent on their ferredoxin redox partners and include cholesterol degradation, redox balance, and virulence (Capyk et al., 2009). Our data supports hypoxic induction of 2 ferredoxins (*Mab_0914c* & *Mab_2049c*) and 3 ferredoxin reductases (*Mab_0930*, *Mab_2047c* and *Mab_4356c*) (Table S3). Induction of *nuo*A-N, ATPAse subunits, the large number of cytochrome P450s and ferredoxins implies *Mab* may employ different sets of genes for anaerobic respiration in its response to hypoxia and adapation.

Mab's transcriptional adaptation to hypoxia also comprised a large set of downregulated genes including but not limited to multiple TF, tRNAs, 30S and 50S ribosomal proteins, alternative sigma factors, and 431 hypothetical proteins (Table S3). Downregulation of genes involved in essential processes such as protein synthesis (e.g. tRNAs, ribosomal proteins and sigma factors) are consistent with the slowed growth observed in hypoxic *Mab* cultures. Included among the most downregulated genes in hypoxia (Table S3) is the orphan response regulator *Mab_3520c* (Figure 1B) and three adjacent upstream genes (nirD/MAB_3521c, nirB/MAB_3522c), and nark3/MAB_3523c) predicted to be involved in nitrite reduction and extrusion (Malm et al., 2009). *Mtb nirB* and *nirD* orthologs are reportedly induced in nutrient starvation but minimal to no DGE occurred in hypoxia at 1% O_2 (Vilcheze et al., 2022). However, in the Wayne model of hypoxia *Mtb nirB* displayed induction and functional *nirBD* genes were required for growth in hypoxia when nitrite was used as the sole nitrogen source (Akhtar et al., 2013).

Construction and validation of *Mab*$_{\Delta dosRS}$ and *Mab*$_{\Delta dosRS+C}$

Elucidation of the global transcriptional responses of *Mab* to hypoxia for the first time revealed the DosRS TCS is employed during hypoxic adaptation, yet much remains unknown about the role of DosRS in gene regulation and *Mab* pathogenesis. The DosR$_{Mab}$ regulon was previously predicted to consist of only 6 genes - *Mab_*3890 (*dosS*), *Mab_*3891 (*dosR*), *Mab_*2489 (universal stress protein, USP), *Mab_*3902c (ortholog of Rv2004c), *Mab_*3903 (nitroreductase) and *Mab_*3904 (USP) – based solely on bioinformatic analysis (Gerasimova et al., 2011). However, at the time this study was initiated, the role of DosRS$_{Mab}$ signaling in gene regulation, including induction of this gene set, remained to be experimentally demonstrated. To enable determination of the DosRS$_{Mab}$ regulon and role of this TCS in *Mab* adaptation to hypoxia, we generated *Mab*$_{\Delta dosRS}$(knockout mutant) using recombineering and the corresponding complemented strain (*Mab*$_{\Delta dosRS+C}$) expressing a single, integrated *dosRS* allele driven by its native promoter (van Kessel and Hatfull, 2007). In addition to confirming strain genotypes by PCR and DNA sequencing (data not shown), the absence of *dosRS* transcripts in *Mab*$_{\Delta dosRS}$ and restoration to wild-type levels in *Mab*$_{\Delta dosRS+C}$ was validated by qRT-PCR (Figure 2A). We next assessed transcript levels of 4 genes (in addition to *dosRS* operon itself) previously predicted to be DosR-dependent. Loss of a functional DosRS system resulted in down-regulation of all predicted DosR$_{Mab}$-regulated genes by >2 log (*MAB_2489, MAB_3902c, MAB_3903)* or > 1 log in the case of *MAB_3904* with restoration to wild-type levels in the complemented strain (Figure 2B), consistent with DosR-mediated induction of these genes.

DosRS$_{Mab}$ is required for maximal growth in hypoxia

As detailed above, to verify the role of DosRS under *in vivo* relevant conditions, we compared the growth kinetics assays of *Mab* 390S, *Mab*$_{\Delta dosRS}$, and *Mab*$_{\Delta dosRS+C}$ in hypoxic (1% O_2, standing) versus aerobic (20% O_2, shaking) conditions. Strains were monitored over a 30-day period using CFU/ml as the readout at day 5, 20, and 30 and grown in normoxic conditions after plating. Cultures grown in 20% O_2 reached maximum growth on day 5 with no difference in

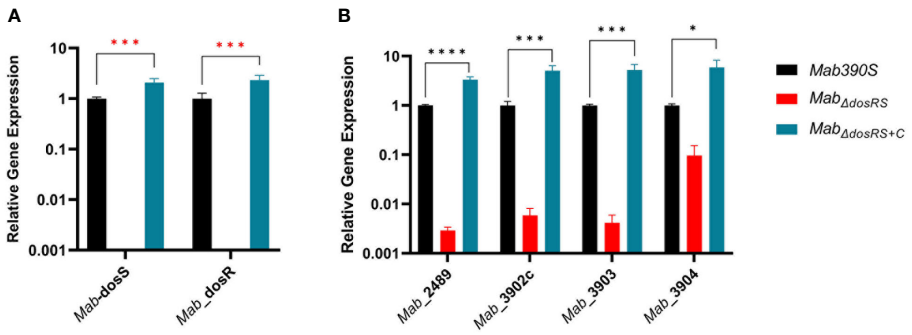

FIGURE 2
Validation of *Mab*$_{\Delta dosRS}$ and *Mab*$_{\Delta dosRS+C}$. qRT-PCR was performed to **(A)** confirm the deletion and restoration of *dosS* and *dosR* in *Mab*$_{\Delta dosRS}$ and *Mab*$_{\Delta dosRS+C}$, respectively, and **(B)** assess the effect on predicted downstream genes. *Mab 390S* (black), *Mab*$_{\Delta dosRS}$ (red) and *Mab*$_{\Delta dosRS+C}$ (blue). Data is representative of 3 experiments performed in triplicate. *P* values were calculated *via* one -way ANOVA using GraphPad. Red stars indicate C_t values were not detected for *Mab dosR* nor *dosS* in the mutant strain. **P*-value <.05, ****P*-value <.001 *****P*-value <.0001.

growth between strains at any time point confirming fully aerated cultures are not dependent on DosRS for replication (Figure 3A). At 1% O_2 maximum growth was achieved by day 20 in *Mab* 390S with a ~2-log decrease in $Mab_{\Delta dosRS}$and ~log decrease in $Mab_{\Delta dosRS+C}$ (Figure 3B) suggesting a functional DosRS is required for maximal growth and survival during hypoxic stress. By day 30 in 1% O_2, *Mab* 390S displayed a slight decrease in CFU compared to day 20 however, this decline was also observed in fully aerated cultures indicating that hypoxic stress was not the cause (Figures 3A, B). These data support the conclusion that $DosRS_{Mab}$ is necessary for growth in hypoxic environments that mimic the physiologic environments of the CF lung, within macrophages and granulomas (Worlitzsch et al., 2002; Cunningham-Bussel et al., 2013; Hudock et al., 2017). Unexpectedly, a morphotype transition from smooth to rough occurred in $Mab_{\Delta dosRS}$ after pro-longed exposure to 1% O_2. On day 20 and 30 an observable change in morphology occurred only in the mutant strain resulting in a heterogenous population of smooth and rough colonies (Figures 4A–D), indicating a DosR-dependent inducible alteration in cell wall composition for $Mab_{\Delta dosRS}$. This is corroborated by the fact that in hypoxic liquid culture assays, $Mab_{\Delta dosRS}$ alone adopted a biofilm-like pellicle layer that was resistant to disruption, whereas other strains maintained a homogeneous composition (data not shown).

Prompted by the inability of $Mtb_{\Delta dosR}$ to resuscitate after re-aeration from hypoxia (Leistikow et al., 2010; Veatch and Kaushal, 2018), we investigated the ability of $Mab_{\Delta dosRS}$ to resuscitate after 30 days in hypoxia. Day 30 cultures taken from 20% O_2 and 1% O_2 were diluted to an OD_{600nm} of 0.02 and grown in 20% O_2 while shaking to evaluate the recovery of $Mab_{\Delta dosRS}$ after prolonged exposure to hypoxia. OD_{600nm} was taken over a 10-day period (Day 0, 2, 3, 5, 8, and 10) to monitor growth kinetics after re-introduction of O_2. All strains originating from aerobic conditions displayed similar growth curves after re-culturing and reached maximal OD by day 5 (Figure 5A). In contrast, after being subjected to hypoxia for 30 days, $Mab_{\Delta dosRS}$ displayed reduced growth compared to *Mab* 390S and $Mab_{\Delta dosRS+C}$ taken from 1% O_2 (Figure 5B). Attenuated growth in 1% O_2 and the inability to resuscitate after re-aeration for $Mab_{\Delta dosRS}$ supports a critical role for $DosRS_{Mab}$ in mediating adaptation to changing oxygen levels encountered within the host during both dormancy and reactivation.

Identification of a large and unique gene set regulated by $DosRS_{Mab}$

We next analyzed DGE between *Mab*390S and $Mab_{\Delta dosRS}$ in hypoxia *via* RNAseq to experimentally identify DosRS regulated genes (Figure 6A). Cultures of *Mab* 390S and $Mab_{\Delta dosRS}$ were grown at 1% O_2 for 5 days at which point RNA was extracted from three independent experiments for analysis. In the absence of DosRS, 216 genes were expressed at lower levels relative to *Mab* 390S after exposure to 1% O_2 (Figure 6A), of which 127 genes were also induced in *Mab* 390S by hypoxia (Table S3). This pattern is consistent with DosRS-dependent hypoxia induction, suggesting that *Mab* DosR may control a much larger regulon than previously predicted. In subsequent analyses, we defined putative DosRS-dependent hypoxia induced genes as those whose transcript levels were decreased by $\log_2FC \geq 1$ in the $Mab_{\Delta dosRS}$ in 1% O_2 and were induced by $\log_2FC \geq 1$ in *Mab* 390S 1% O_2 (Table S3). The top 20 putative DosRS-dependent genes induced most highly by hypoxia (Table S5) include 4 of the genes previously predicted *in silico* to be members of the $DosRS_{Mab}$ regulon. Notably, two of the most highly upregulated genes, *Mab_3937* and *Mab_3354* (*desA1*), appear to be *Mab*-specific members of this regulon. *Mab_3937*, a hypothetical protein with no known ortholog, is predicted to be in an operon with *Mab_3938* and *Mab_3939*, encoding a clp protease subunit (ClpC2) with orthologous counterparts in *Mtb* and *Msmeg* which are essential genes. (Sassetti et al., 2003; Miranda-CasoLuengo et al., 2016; Kester et al., 2021). Both *desA1* (*Mab_3354*) and *desA2* (*Mab_1237*), desaturase enzymes with predicted roles in the biosynthesis of the mycolic acid component of mycobacterial cell walls, exhibited hypoxic DGE in the *dosRS* mutant (Yeruva et al., 2016; Bailo et al., 2022). Recently *desA2* but not *desA1* was predicted to be an essential gene in *Mab*, *Mtb* and *Msmeg* suggesting even slight downregulation could lead to detrimental alterations in the cell wall (Akusobi et al., 2022; Bailo et al., 2022). Although *Mtb* has orthologs of these genes (ClpC2, *desA1*, and *desA2)*, there is no evidence of regulation by $DosR_{Mtb}$, illustrating the potential for conserved TCS to interact with conserved target genes in distinct ways. Additionally, no known $DosR_{Mtb}$-regulated genes have been deemed essential, further highlighting the unique nature of $DosRS_{Mab}$-mediated hypoxia response. Among the 127 hypoxia-

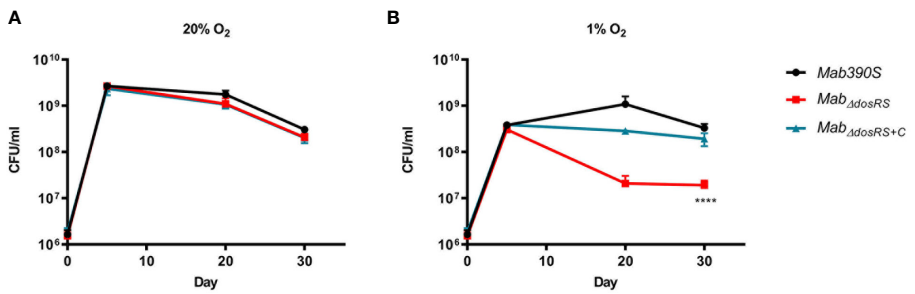

FIGURE 3
$Mab_{\Delta dosRS}$ is attenuated in hypoxia. Growth kinetics in hypoxia were assessed *via* serial dilutions, spot plating and enumeration of CFU/ml on day 5, 20 and 30. **(A)** Growth kinetics at 20% O_2 **(B)** Growth kinetics at 1% O_2. *Mab 390S* (black), $Mab_{\Delta dosRS}$ (red) and $Mab_{\Delta dosRS+C}$ (blue). Data reflects 3 independent experiments performed in triplicate. *P*-values were calculated *via* one-way ANOVA using GraphPad, ****P-value <.0001.

10.3389/fcimb.2023.1144210

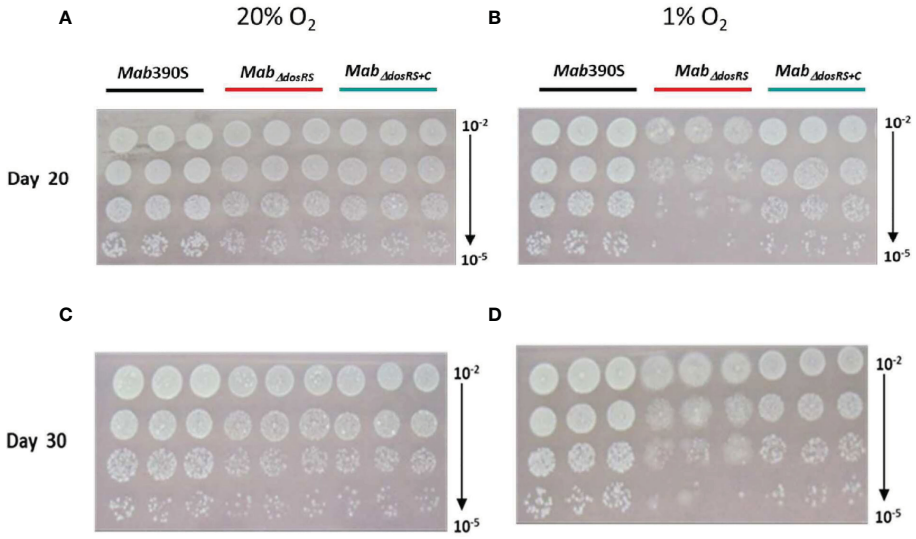

FIGURE 4
Hypoxia-induced morphological changes in $Mab_{\Delta dosRS}$. Cultures grown at 20% or 1% O_2 were spot plated on Day 20 and Day 30 and incubated under normoxic conditions. **(A)** Day 20 at 20% O_2 **(B)** Day 20 at 1% O_2 **(C)** Day 30 at 20% O_2 **(D)** Day 30 at 1% O_2.

induced putative $DosR_{Mab}$-dependent genes is a large gene cluster (*Mab_1681-1698)* containing hypothetical proteins, daunorubicin resistance efflux pump subunit (*drrA)*, and a putative *mce* operon (Table S5). Whereas some putative *Mab* MCE gene clusters have clear orthologs in *Mtb* (e.g. MAB_4146c-4155c with Mce4, Rv3492c-3501c), the predicted *Mab* MCE proteins encoded by MAB_*1681-1698* do not directly correspond to a specific MCE loci in *Mtb*. Rather, they share low homology with components of different *Mtb* MCE complexes, necessitating further research to fully assess the role of this *Mab*-specific MCE during hypoxia.

Comparing the ~ 50 genes of the $DosR_{Mtb}$ regulon with the putative $DosR_{Mab}$ regulated genes identified in this study (Supplemental Table 3), we only discovered 6 shared orthologs including 4 conserved hypothetical proteins (CHPs) plus DosR (*Mab_3891c*) and DosS (*Mab_3890c)*. In addition to the transcriptional regulator *Mab_3891c*, we found nine other transcriptional regulators to be induced by hypoxia in a putative DosR-dependent manner (Tables S3–5) with none of their *Mtb* orthologs regulated by $DosR_{Mtb}$. The transcriptional response of Mab to hypoxia is further differentiated from Mtb by the lack of regulation of any of the 7 putative triacylglycerol synthases (Tgs) by hypoxia or DosR, a characteristic of in vitro dormancy and hypoxia for Mtb (Table S3) (Voskuil et al., 2004; Deb et al., 2009). Hypoxic *Mtb* positively regulates *tgs1 via* DosR for synthesis of triacylglycerol (TAG) for energy storage and utilization. The absence of $DosR_{Mab}$ mediated induction of any Tgs enzymes under hypoxic stress points to a different mechanism for energy storage and utilization in *Mab* vs *Mtb* (Park et al., 2003; Daniel et al., 2004). The scope of the *Mab* DosR regulon precludes a comprehensive discussion of every downstream gene, many of which encode uncharacterized conserved hypothetical proteins. However, this RNAseq dataset is evidence for a species-specific regulon larger than predicted bioinformatically that likely contains novel mechanisms of hypoxia adaptation and pathogenesis.

Comparative transcriptomics also revealed upregulation of 200 genes in $Mab_{\Delta dosRS}$ compared to *Mab* 390S (Figure 6A and Table S3),

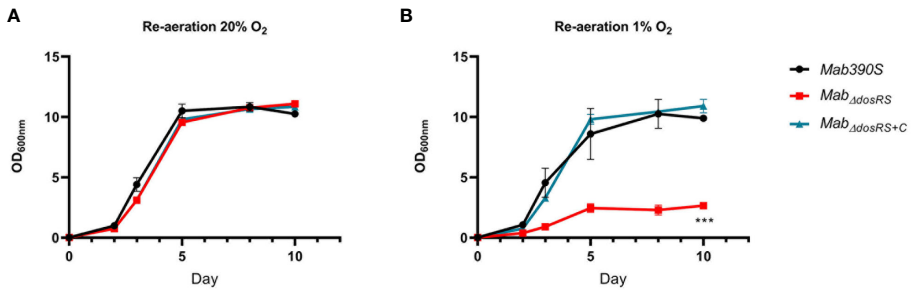

FIGURE 5
DosRS is required for resuscitation after hypoxia. OD_{600nm} was taken over a 10-day period of re-aerated cultures after 30 days of growth in either **(A)** 20% O_2 or **(B)** 1% O_2. *Mab390S* (black), $Mab_{\Delta dosRS}$ (red) and $Mab_{\Delta dosRS+C}$ (blue). Data reflects 2 independent experiments performed in triplicate. *P*-values were calculated *via* one-way ANOVA using GraphPad, ****P*-value <.001.

10.3389/fcimb.2023.1144210

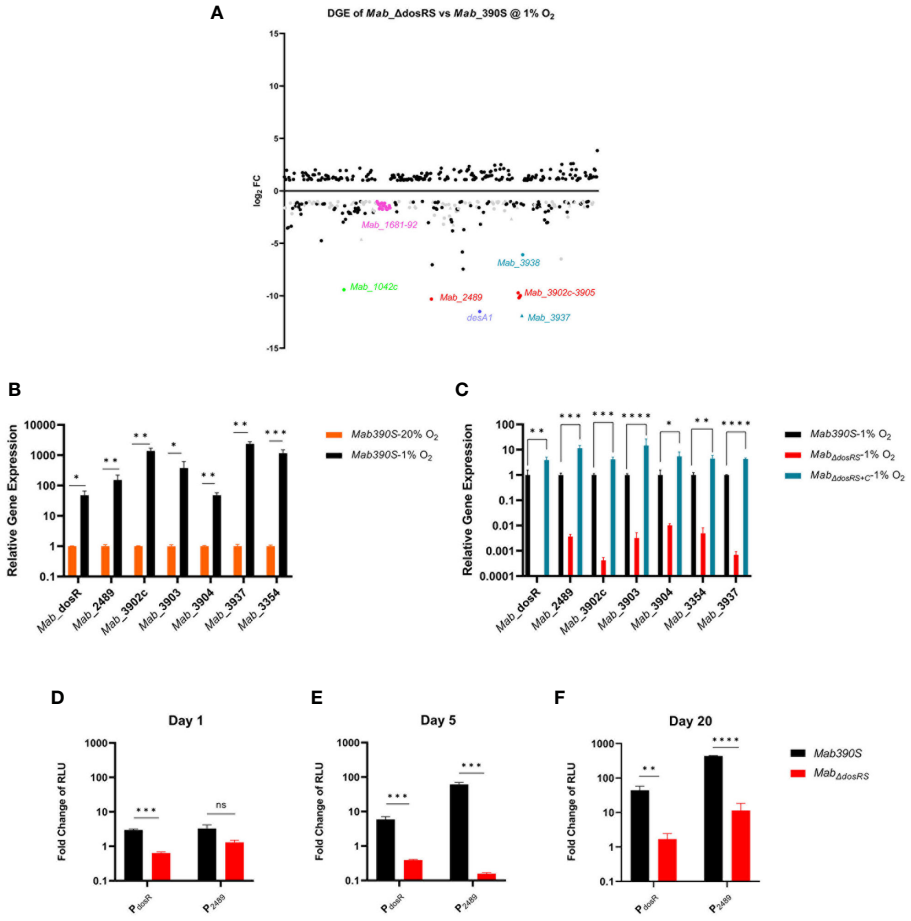

FIGURE 6
Mab DosR dependent DGE in 1% O_2. **(A)** Scatter plot of RNAseq analysis of $Mab_{\Delta dosRS}$ vs *Mab* 390S after 5 days in 1% O_2. Figure shows genes with $log_2FC \leq -1$ and ≥ 1. Gray circles are conserved hypothetical genes and gray triangles are *Mab* genes with no ortholog in *Mtb*. Names of select genes of interest are labeled (neon green=*Mab_1042C*, pink=*Mab_1681-1698*, purple= *desA1*, turquoise (triangle denotes no known ortholog in *Mtb*) =*Mab_3937 & 3938*, red= predicted DosR regulated genes (RG). **(B, C)** qRT-PCR assessment of select DosR-dependent genes. Gene expression was calculated as relative quantitation *via* the $2^{-\Delta\Delta Ct}$ method using *sigA* as the reference gene. **(B)** Hypoxia induced gene expression. Transcript levels of select genes in *Mab* 390S 20% O_2 (orange bars) and *Mab* 390S 1% O_2 (black bars). **(C)** DosR dependent gene expression. Transcript levels of select genes in $Mab_{\Delta dosRS}$ (red bars) and $Mab_{\Delta dosRS+C}$(blue bars) were compared to *Mab* 390S (black bars) in 1% O_2 on Day 5. **(D-F)** Kinetics of DosR-dependent gene induction measured luciferase reporter assays. Promoter activity in 1% O_2 was quantified by measuring luminescence compared to 20% O_2 cultures and normalized to lux-hsp60 constitutive promoter as a reference signal, $(1\%O_2(P_{dosR}$ or $P_{2489}/P_{hsp60}))/(20\%\ O_2(P_{dosR}$ or $P_{2489}/P_{hsp60}))$ and expressed as fold change of relative light units (RLU) **(D)** 24hours, **(E)** Day 5, and **(F)** Day 20. *Mab* 390S (black bars) and $Mab_{\Delta dosRS}$ (red bars). qRT-PCR and luciferase assay data are representative of 3 independent assays performed in triplicate. *P*-values were calculated using t-test **(B, D–F)** and one-way ANOVA **(C)**. *P*-values were calculated *via* GraphPad, **P*-value <.05, ** *P*-value <.01, ****P*-value <.001, *****P*-value. Not significant is denoted as ns.

however the magnitude of induction was low ranging between log_2FC of 1-3.6. Among the upregulated genes are 81 hypothetical proteins, 5 transcription factors, 30S and 50S ribosomal proteins. Included in the top 20 most highly induced genes in $Mab_{\Delta dosRS}$ are *Mab_3521c* (nitrite reductase) and *Mab_3523c* (nitrite extrusion protein) which were observed to be highly downregulated in hypoxic *Mab* 390S (Table S3). These data suggests that DosRS may act as a repressor of a subset of genes in hypoxic conditions, a hypothesis that remains to be experimentally validated. The low-level induction of other genes in the knockout strain may also result from indirect effects of DosRS on mycobacterial physiology under hypoxic stress.

To validate RNAseq results, two of the putative *Mab* DosR-dependent genes most differentially expressed in the mutant strain (*Mab_3354* and *Mab_3937*) were assessed *via* qRT-PCR along with 5 of the predicted *Mab* DosR genes (Figures 6B, C). Similar to RNAseq studies, the effect of hypoxia on gene expression was assessed in *Mab* 390S (1% vs 20% O_2) and the requirement for DosRS for DGE in response to hypoxia by comparing *Mab* 390S, $Mab_{\Delta dosRS}$ and $Mab_{\Delta dosRS+C}$. All genes assessed *via* qRT-PCR were induced by ≥ 10-fold in 1% O_2 compared to 20% O_2 for *Mab* 390S with *Mab_3937*, *Mab_3902c*, and *Mab_3354* having the highest gene induction consistent with RNAseq results (Figure 6B). These same genes displayed loss of induction in $Mab_{\Delta dosRS}$ by ≥ 10-fold similar to RNAseq results with restoration by $Mab_{\Delta dosRS+C}$ in hypoxia (Figure 6C). The most dramatic change in gene expression in $Mab_{\Delta dosRS}$ was *Mab_3902c* and *Mab_3937* with > 100-fold reduction compared to *Mab* 390S. Results from qRT-PCR corroborate RNAseq results and accentuate the magnitude of differential gene expression of predicted and newly discovered hypoxia-induced $DosRS_{Mab}$ regulated genes.

In addition to qRT-PCR, bacterial luciferase (Lux) reporter strains were used to evaluate the kinetics of hypoxia-dependent changes in gene expression across a broader time course. The integrating shuttle plasmid pMV306 luxG13 optimized for mycobacteria consists of the constitutive P_{hsp60} and P_{G13} promoters driving expression of *luxAB* and *luxCDE*, respectively (Andreu et al., 2010). Lux reporter constructs in which the constitutive P_{hsp60} promoter was replaced with promoters from two hypoxia inducible genes, DosR and *Mab*_2489 (P_{DosR} and P_{2489}) were introduced into *Mab* 390S and $Mab_{\Delta dosRS}$. Reporter assays performed on Days 1, 5, 20 identified temporal changes in gene expression with both promoters for *Mab* 390S but not in $Mab_{\Delta dosRS}$ (Figures 6D–F). The lux reporter under the control of P_{dosR} shows sustained induction over time, indicating that *dosR* is expressed throughout early and late stages of hypoxia, a trait not observed in *Mtb* (Rustad et al., 2008). Although the *Mab* 390S P_{2489}-lux reporter displays modest induction of ~ 3-fold change on day 1, there is not a significant difference compared to $Mab_{\Delta dosRS}P_{2489}$ (Figure 6D). However, on days 5 and 20 *Mab* 390S P_{2489}-lux was highly induced compared to $Mab_{\Delta dosRS}$ P_{2489}-lux with fold changes of 61 and 433, respectively (Figures 6E, F). It should be noted that $Mab_{\Delta dosRS}$ P_{2489}-lux did exhibit low-level induction on Day 20, which may be attributable to the activity of other transcription factors. However, as noted previously, there was a significant difference compared to the expression of P_{2489} in wild-type *Mab* 390S. Lux reporters facilitated dynamic monitoring of DosRS activation by hypoxia and provide a valuable tool to explore DosR-mediated gene regulation *in vitro* and *in vivo* in response to various stresses (e.g. NO, CO, antibiotics) or host microenvironments (e.g intramacrophage, granuloma, airway mucus).

Discussion

Infections caused by *Mab*, particularly within the CF population, are a major cause of concern due to the lack of efficacious antibiotics and the resulting inability to clear the infections from the airways. The poor correlation between *in vitro* drug susceptibility profiles and *in vivo* efficacy when treating *Mab* infections suggest that host-driven adaptations of *Mab* may contribute to treatment failures (Nessar et al., 2012). Host-derived cues encountered by *Mab* within the viscous mucus layer of CF airways, phagosomal compartments of macrophages, and during residence within granulomas may trigger upregulation of antimicrobial resistance mechanisms (Lyczak et al., 2002; Worlitzsch et al., 2002; Cunningham-Bussel et al., 2013; Hudock et al., 2017). Extrapolating from studies on *Mtb* (Gold and Nathan, 2017; Boldrin et al., 2020; Joshi et al., 2021), *in vivo* stresses such as hypoxia may also promote the development of phenotypically drug-tolerant persisters. Thus, a better understanding of *Mab's* physiological states and stress responses required for long-term persistence within the human host may lead to more effective treatment strategies.

Successful bacterial pathogens like *Mtb* and *Mab* employ extensive repertoires of transcription factors, including TCS, for coordinating gene expression to counteract host antimicrobial factors and immune pressure. The transcriptional regulatory networks and role of TCS of *Mtb* have been extensively characterized in multiple *in vitro* and *in vivo* models of infection (Bacon and Marsh, 2007; Rohde et al., 2012; Li et al., 2019; Stupar et al., 2022; Vilcheze et al., 2022). In contrast, few transcriptomic studies defining *Mab* stress responses, or the role of specific transcription factors have been reported (Miranda-CasoLuengo et al., 2016; Dubois et al., 2019). Given the well-documented relevance of hypoxia during *Mab*-host interactions (e.g. mucus of CF airway, macrophage phagosome, granuloma) (Lyczak et al., 2002; Worlitzsch et al., 2002; Cunningham-Bussel et al., 2013; Hudock et al., 2017), we sought to identify molecular mechanisms that enable *Mab* to adapt to these low-oxygen niches. In the better characterized pathogen *Mtb*, the master regulator of hypoxia adaptation is the atypical TCS DosRS/T, which regulates a ~50 gene regulon upon induction by hypoxia and NO stress (Park et al., 2003; Voskuil et al., 2003). *Mab* encodes orthologs of eleven of the twelve TCS found in *Mtb*, including DosRS (*dosT* homolog missing). However, as detailed in this study, the scope and content of *Mab* regulons controlled by these TCS may be less conserved. Prior to initiation of our study, only two reports had mentioned *Mab* DosRS: i) a bioinformatics study predicting a 6 gene regulon based on previously known *Mtb* DosR binding motifs (Gerasimova et al., 2011) and ii) transcriptomic study assessing the affect of NO exposure on the predicted genes (Miranda-CasoLuengo et al., 2016). These studies, however, did not directly demonstrate DosRS-mediated regulation of the predicted genes, define the transcriptional response of *Mab* to hypoxia nor the full extent of the DosR regulon, or identify a DosRS phenotype. To begin to address these knowledge gaps we developed a hypoxic model of 1% O_2 to mimic physiologically relevant oxygen tensions *Mab* encounters *in vivo* (Worlitzsch et al., 2002; Cunningham-Bussel et al., 2013; Hudock et al., 2017) to assess transcriptomics and growth kinetics of *Mab* in the presence or absence of $DosRS_{Mab}$.

Genome wide transcriptomics identified DosRS as the main TCS activated during hypoxia and analysis of a defined mutant lacking DosRS revealed a potentially larger regulon than previously predicted. We identified 216 genes to be downregulated in $Mab_{\Delta dosRS}$versus *Mab* 390S, 127 of which were upregulated in hypoxia. This gene set was deemed the putative hypoxia-induced DosR regulon-*Mab_3902c*, *Mab_3903* and Mab_*3904*), 2 novel genes displaying the highest DGE (MAB_3937 and *desA1*), 9 transcription factors, and 57 hypothetical genes among others. 22 of the 57 hypothetical genes are species-specific, further illustrating the unique nature of the regulons controlled by orthologous TCS. Not only is the *Mab* DosRS regulon likely larger than previously predicted, but it also appears to be notably larger than the well-studied *Mtb* DosR regulon. Surprisingly, the only orthologs in common between the *Mtb* DosR and *Mab* DosR regulons were the 6 genes originally predicted from the bioinformatics study and *Mab_1040*, an ortholog of the hypothetical protein *Rv3129* which is documented as an antigen in tuberculosis patients with latent infections (Park et al., 2003; Black et al., 2009; Lin et al., 2009). One of the hallmarks of *Mtb* hypoxia adaptations *in vivo* and *in vitro* is the marked upregulation of *tgs1* for energy storage and utilization (Garton et al., 2008; Deb et al., 2009). The induction of *Mab_3551c*, the primary TAG synthase gene in *Mab* (Viljoen et al.,

2016), is not observed in our *Mab in vitro* hypoxia model, suggesting *Mab* mechanisms of hypoxia adaptation or cues for regulation of lipid storage are distinctive from *Mtb*. Studies are underway to discriminate between genes whose expression is altered directly by DosR (DosR binding to promoter) versus indirectly (promoter regulated by secondary TF).

During the course of our study, Belardinelli et al. also reported on characterization of the *Mab* DosR regulon as part of efforts to repurpose antimalarial drugs that inhibit *Mtb* DosR as therapeutics for *Mab* (Belardinelli et al., 2022). Their transcriptomic comparison of *Mab* ATCC 19977 and $Mab_{\Delta dosRS}$ in microaerobic conditions identified 180 genes downregulated in a DosRS-dependent manner. Of these 180 genes, only 45 overlapped with our list of 216 genes downregulated in the *dosRS* mutant at 1% O_2. Both studies included the 6 previously predicted genes and the 2 genes most highly differentially expressed on our list (*Mab_3937*, *desA1*) plus 37 other genes. Of the 45 genes in common between these 2 studies, Belardinelli et al., reported 38 DosR binding motifs supporting the assertion that *Mab* DosR regulon is larger than previously predicted. Discrepant findings between this report and our study could be attributable to differences in strains (ATCC 19977 vs 390S), hypoxic models (20% O_2 standing vs 1% O_2 standing), time points (24hr vs 5 days), or media (Dubos-Tween albumin vs 7H9-OADC+.05% tyloxapol). Regardless, both clearly highlight the broad scope and unique nature of the $DosRS_{Mab}$ regulon and provide a framework for future studies to fully elucidate the role of this important two-component system.

The importance of DosR-regulated genes for hypoxia adaptation was evident from growth deficits seen on day 20 and 30 and impaired resuscitation after reaeration in $Mab_{\Delta dosRS}$ compared to *Mab* 390S (Figure 3). *Mab_ΔdosRS* differentially expressed genes in hypoxia contain 7 genes predicted to be essential in a recent TnSeq study under aerobic conditions (Akusobi et al., 2022), possibly accounting for these phenotypes. Included in this list is *desA2*, a desaturase enzyme that is responsible for mycolic acid biosynthesis and is essential for growth in the RGM *Msmeg* (Bailo et al., 2022). Strong induction of *desA1* in hypoxia suggests that it, along with *desA2*, may play role in cell wall modification in response to this stress. It is worth noting that, despite exclusion from the list of *Mab* predicted essential genes, the orthologous desaturase in *Msmeg* was deemed essential (Singh et al., 2016). Additionally, the MCE operon *Mab*_1693-*Mab*_1698 was differentially expressed in the mutant strain and may contribute to decreased importation of mycolic acids further disrupting cell wall integrity. The 6 other predicted essential genes possibly contributing to the $Mab_{\Delta dosRS}$ growth phenotype are 2 conserved hypothetical proteins (*Mab_3268c-Mab_3269c*), a DNA helicase (*Mab_3511c*), a protoporphyrinogen oxidase, a prephenate dehydratase (*Mab_0132*), and phosphoribosylformylglycinamidine synthase (*Mab_0698*).

In addition to growth/survival deficits and the inability to resuscitate, we also observed DosRS-dependent hypoxia-induced morphological changes. After 20 days in hypoxia, $Mab_{\Delta dosRS}$ displayed heterogeneous morphology consisting of smooth and rough colonies. This phenotype was not present in strains expressing DosRS or in fully aerated cultures, evidence that this TCS mediates dramatic remodeling of the cell wall in response hypoxia. The smooth and rough morphotypes of *Mab*, reflective of different compositions of the outer cell wall, have been shown to impact interactions with macrophages, immune stimulation and inflammation, antibiotic susceptibility, and virulence (Jonsson et al., 2007; Catherinot et al., 2009; Ruger et al., 2014; Roux et al., 2016; Li et al., 2020). Rough strains are able to trigger apoptosis of macrophages and grow extracellularly as aggregates known as cords, and are associated with worse clinical outcomes (Li et al., 2020) Mechanisms involved in smooth to rough transitions have not been fully elucidated. However, genomic comparisons between the two morphotypes revealed SNPs and indels in the *gpl* locus and in *mmpl4b* and *mps1* genes (Pawlik et al., 2013). In addition to total or partial loss of GPL due to mutations affecting its biosynthesis or transport, recent studies including identification of GPL+ rough clinical isolates suggest other mechanisms may also govern S➔R morphotype switching (Gutierrez et al., 2021). For example, Daher et al. reported that glycosylation patterns of GPL can alter *Mab* surface properties (Daher et al., 2022). An inducible transition from smooth to rough was also observed following exposure to subinhibitory doses of aminoglycoside antibiotics providing evidence for transcriptional modulation of morphotype in response to stress (Tsai et al., 2015). Belardinelli et al. reported no differences in GPL content between *Mab* ATCC 19977 and isogenic *ΔdosRS* mutant after microaerobic culture for 24 hours (Belardinelli et al., 2022). Our observation of a switch to rough morphotype in a *ΔdosRS* mutant after extended culture at 1% O_2 may reflect either adaptive cell wall remodeling triggered by lower O_2 levels or longer duration of stress in our model. Alternatively, rather than affecting GPL levels per se, inactivation of the DosRS regulon may impact GPL modifications or biosynthesis of unique cell wall constituents. Intriguingly, Pawlik et al. reported that expression of *dosR* was elevated in an R versus S strain (Pawlik et al., 2013). This seems to contrast with our data suggesting that DosRS positively regulates GPLs, or at least the smooth phenotype (e.g. loss of DosRS➔rough phenotype in hypoxia). Whether this is a direct correlation or stress induced side-effect stemming from the loss of GPL remains to be determined. It is clear that much remains to be learned regarding how *Mab* regulates the composition of its complex cell wall during infection and the roles of TCS like DosRS in host-pathogen interactions.

In addition to determination of the DosRS-dependent component of *Mab* hypoxia adaptation, this is the first transcriptomics study designed to identify genome-wide changes in *Mab* gene expression in a defined, physiologically relevant model of hypoxia. RNAseq analysis of wild-type *Mab*390S in 1% O_2 versus 20% O_2 identified an additional 1,063 DosRS-independent hypoxia-induced genes with putative roles in *Mab* adaptation in hypoxia. Differential gene expression of such a large group of genes in hypoxia outside of the DosR regulon points to a sophisticated mechanism of regulation for adaptation beyond TCS. This gene set included 80 TF, lipid metabolism and transport, energetics, secondary metabolism, cell wall synthesis plus induction of 540 hypothetical proteins, (Table S3). Our data highlights the necessity of adaptation to hypoxia *via* a large repertoire of genes including but not limited to the TCS DosRS. Further investigation of unique *Mab* DosR regulated genes and species-specific *Mab* genes employed for hypoxic adaptation will provide beneficial insights into *Mab* pathogenesis.

Data availability statement

The datasets presented in this study are deposited in the NCBI database, accession number PRJNA932814 (https://www.ncbi.nlm.nih.gov/bioproject/?term=PRJNA932814).

Author contributions

BS and KR: Conception and design of experiments. BS and BT: Analysis and interpretation of data for RNAseq experiments. BS and KR: Preparation and revision of manuscript. KR and LS: Approval of final manuscript. All authors contributed to the article and approved the submitted version.

Funding

LS acknowledges funding from the National Health Institute grant AI124458.

Acknowledgments

We would like to thank George Walters-Marrah for assistance with construction of luciferase reporter plasmids. We also thank Dr. Rushmi Gupta and Dr. Mollie Jewett for technical support and guidance.

Conflict of interest

The authors declare that the research was conducted in the absence of any commercial or financial relationships that could be construed as a potential conflict of interest.

Publisher's note

Supplementary material

The Supplementary Material for this article can be found online at: https://www.frontiersin.org/articles/10.3389/fcimb.2023.1144210/full#supplementary-material

References

Aguilar-Ayala, D. A., Tilleman, L., Van Nieuwerburgh, F., Deforce, D., Palomino, J. C., Vandamme, P., et al. (2017). The transcriptome of mycobacterium tuberculosis in a lipid-rich dormancy model through RNAseq analysis. *Sci. Rep.* 7 (1), 17665. doi: 10.1038/s41598-017-17751-x

Akhtar, S., Khan, A., Sohaskey, C. D., Jagannath, C., and Sarkar, D. (2013). Nitrite reductase NirBD is induced and plays an important role during *in vitro* dormancy of mycobacterium tuberculosis. *J. Bacteriol* 195 (20), 4592–4599. doi: 10.1128/JB.00698-13

Akusobi, C., Benghomari, B. S., Zhu, J., Wolf, I. D., Singhvi, S., Dulberger, C. L., et al. (2022). Transposon mutagenesis in mycobacterium abscessus identifies an essential penicillin-binding protein involved in septal peptidoglycan synthesis and antibiotic sensitivity. *Elife* 11. doi: 10.7554/eLife.71947.sa2

Amin, A. G., Goude, R., Shi, L., Zhang, J., Chatterjee, D., and Parish, T. (2008). EmbA is an essential arabinosyltransferase in mycobacterium tuberculosis. *Microbiol. (Reading)* 154 (Pt 1), 240–248. doi: 10.1099/mic.0.2007/012153-0

Andreu, N., Zelmer, A., Fletcher, T., Elkington, P. T., Ward, T. H., Ripoll, J., et al. (2010). Optimisation of bioluminescent reporters for use with mycobacteria. *PloS One* 5 (5), e10777. doi: 10.1371/journal.pone.0010777

Bacon, J., and Marsh, P. D. (2007). Transcriptional responses of mycobacterium tuberculosis exposed to adverse conditions *in vitro*. *Curr. Mol. Med.* 7 (3), 277–286. doi: 10.2174/156652407780598566

Bailo, R., Radhakrishnan, A., Singh, A., Nakaya, M., Fujiwara, N., and Bhatt, A. (2022). The mycobacterial desaturase DesA2 is associated with mycolic acid biosynthesis. *Sci. Rep.* 12 (1), 6943. doi: 10.1038/s41598-022-10589-y

Belardinelli, J. M., Verma, D., Li, W., Avanzi, C., Wiersma, C. J., Williams, J. T., et al. (2022). Therapeutic efficacy of antimalarial drugs targeting DosRS signaling in mycobacterium abscessus. *Sci. Transl. Med.* 14 (633), eabj3860. doi: 10.1126/scitranslmed.abj3860

Berney, M., and Cook, G. M. (2010). Unique flexibility in energy metabolism allows mycobacteria to combat starvation and hypoxia. *PloS One* 5 (1), e8614. doi: 10.1371/journal.pone.0008614

Bernut, A., Nguyen-Chi, M., Halloum, I., Herrmann, J. L., Lutfalla, G., and Kremer, L. (2016). Mycobacterium abscessus-induced granuloma formation is strictly dependent on TNF signaling and neutrophil trafficking. *PloS Pathog.* 12 (11), e1005986. doi: 10.1371/journal.ppat.1005986

Black, G. F., Thiel, B. A., Ota, M. O., Parida, S. K., Adegbola, R., Boom, W. H., et al. (2009). Immunogenicity of novel DosR regulon-encoded candidate antigens of mycobacterium tuberculosis in three high-burden populations in Africa. *Clin. Vaccine Immunol.* 16 (8), 1203–1212. doi: 10.1128/CVI.00111-09

Boldrin, F., Provvedi, R., Cioetto Mazzabo, L., Segafreddo, G., and Manganelli, R. (2020). Tolerance and persistence to drugs: A main challenge in the fight against mycobacterium tuberculosis. *Front. Microbiol.* 11, 1924. doi: 10.3389/fmicb.2020.01924

Bretl, D. J., Demetriadou, C., and Zahrt, T. C. (2011). Adaptation to environmental stimuli within the host: Two-component signal transduction systems of mycobacterium tuberculosis. *Microbiol. Mol. Biol. Rev.* 75 (4), 566–582. doi: 10.1128/MMBR.05004-11

Brown-Elliott, B. A., and Wallace, R. J.Jr. (2002). Clinical and taxonomic status of pathogenic nonpigmented or late-pigmenting rapidly growing mycobacteria. *Clin. Microbiol. Rev.* 15 (4), 716–746. doi: 10.1128/CMR.15.4.716-746.2002

Byrd, T. F., and Lyons, C. R. (1999). Preliminary characterization of a mycobacterium abscessus mutant in human and murine models of infection. *Infect. Immun.* 67 (9), 4700–4707. doi: 10.1128/IAI.67.9.4700-4707.1999

Capyk, J. K., Kalscheuer, R., Stewart, G. R., Liu, J., Kwon, H., Zhao, R., et al. (2009). Mycobacterial cytochrome p450 125 (cyp125) catalyzes the terminal hydroxylation of c27 steroids. *J. Biol. Chem.* 284 (51), 35534–35542. doi: 10.1074/jbc.M109.072132

Catherinot, E., Roux, A. L., Macheras, E., Hubert, D., Matmar, M., Dannhoffer, L., et al. (2009). Acute respiratory failure involving an r variant of mycobacterium abscessus. *J. Clin. Microbiol.* 47 (1), 271–274. doi: 10.1128/JCM.01478-08

Chmiel, J. F., and Davis, P. B. (2003). State of the art: Why do the lungs of patients with cystic fibrosis become infected and why can't they clear the infection? *Respir. Res.* 4, 8. doi: 10.1186/1465-9921-4-8

Converse, P. J., Karakousis, P. C., Klinkenberg, L. G., Kesavan, A. K., Ly, L. H., Allen, S. S., et al. (2009). Role of the dosR-dosS two-component regulatory system in mycobacterium tuberculosis virulence in three animal models. *Infect. Immun.* 77 (3), 1230–1237. doi: 10.1128/IAI.01117-08

Cook, G. M., Hards, K., Vilcheze, C., Hartman, T., and Berney, M. (2014). Energetics of respiration and oxidative phosphorylation in mycobacteria. *Microbiol. Spectr.* 2 (3). doi: 10.1128/9781555818845.ch20

Cunningham, A. F., and Spreadbury, C. L. (1998). Mycobacterial stationary phase induced by low oxygen tension: Cell wall thickening and localization of the 16-kilodalton alpha-crystallin homolog. *J. Bacteriol* 180 (4), 801–808. doi: 10.1128/JB.180.4.801-808.1998

Cunningham-Bussel, A., Zhang, T., and Nathan, C. F. (2013). Nitrite produced by mycobacterium tuberculosis in human macrophages in physiologic oxygen impacts bacterial ATP consumption and gene expression. *Proc. Natl. Acad. Sci. U.S.A.* 110 (45), E4256–E4265. doi: 10.1073/pnas.1316894110

Daher, W., Leclercq, L. D., Johansen, M. D., Hamela, C., Karam, J., Trivelli, X., et al. (2022). Glycopeptidolipid glycosylation controls surface properties and pathogenicity in mycobacterium abscessus. *Cell Chem. Biol.* 29 (5), 910–924 e917. doi: 10.1016/j.chembiol.2022.03.008

Daniel, J., Deb, C., Dubey, V. S., Sirakova, T. D., Abomoelak, B., Morbidoni, H. R., et al. (2004). Induction of a novel class of diacylglycerol acyltransferases and triacylglycerol accumulation in mycobacterium tuberculosis as it goes into a dormancy-like state in culture. *J. Bacteriol* 186 (15), 5017–5030. doi: 10.1128/JB.186.15.5017-5030.2004

Deb, C., Lee, C. M., Dubey, V. S., Daniel, J., Abomoelak, B., Sirakova, T. D., et al. (2009). A novel *in vitro* multiple-stress dormancy model for mycobacterium tuberculosis generates a lipid-loaded, drug-tolerant, dormant pathogen. *PloS One* 4 (6), e6077. doi: 10.1371/journal.pone.0006077

Dubois, V., Pawlik, A., Bories, A., Le Moigne, V., Sismeiro, O., Legendre, R., et al. (2019). Mycobacterium abscessus virulence traits unraveled by transcriptomic profiling in amoeba and macrophages. *PloS Pathog.* 15 (11), e1008069. doi: 10.1371/journal.ppat.1008069

Esther, C. R.Jr., Esserman, D. A., Gilligan, P., Kerr, A., and Noone, P. G. (2010). Chronic mycobacterium abscessus infection and lung function decline in cystic fibrosis. *J. Cyst Fibros* 9 (2), 117–123. doi: 10.1016/j.jcf.2009.12.001

Fol, M., Chauhan, A., Nair, N. K., Maloney, E., Moomey, M., Jagannath, C., et al. (2006). Modulation of mycobacterium tuberculosis proliferation by MtrA, an essential two-component response regulator. *Mol. Microbiol.* 60 (3), 643–657. doi: 10.1111/j.1365-2958.2006.05137.x

Galagan, J. E., Minch, K., Peterson, M., Lyubetskaya, A., Azizi, E., Sweet, L., et al. (2013). The mycobacterium tuberculosis regulatory network and hypoxia. *Nature* 499 (7457), 178–183. doi: 10.1038/nature12337

Garton, N. J., Waddell, S. J., Sherratt, A. L., Lee, S. M., Smith, R. J., Senner, C., et al. (2008). Cytological and transcript analyses reveal fat and lazy persister-like bacilli in tuberculous sputum. *PloS Med.* 5 (4), e75. doi: 10.1371/journal.pmed.0050075

Gautam, U. S., McGillivray, A., Mehra, S., Didier, P. J., Midkiff, C. C., Kissee, R. S., et al. (2015a). DosS is required for the complete virulence of mycobacterium tuberculosis in mice with classical granulomatous lesions. *Am. J. Respir. Cell Mol. Biol.* 52 (6), 708–716. doi: 10.1165/rcmb.2014-0230OC

Gautam, U. S., Mehra, S., and Kaushal, D. (2015b). In-vivo gene signatures of mycobacterium tuberculosis in C3HeB/FeJ mice. *PloS One* 10 (8), e0135208. doi: 10.1371/journal.pone.0135208

Gautam, U. S., Mehra, S., Kumari, P., Alvarez, X., Niu, T., Tyagi, J. S., et al. (2019). Mycobacterium tuberculosis sensor kinase DosS modulates the autophagosome in a DosR-independent manner. *Commun. Biol.* 2, 349. doi: 10.1038/s42003-019-0594-0

Gerasimova, A., Kazakov, A. E., Arkin, A. P., Dubchak, I., and Gelfand, M. S. (2011). Comparative genomics of the dormancy regulons in mycobacteria. *J. Bacteriol* 193 (14), 3446–3452. doi: 10.1128/JB.00179-11

Gold, B., and Nathan, C. (2017). Targeting phenotypically tolerant mycobacterium tuberculosis. *Microbiol. Spectr.* 5 (1). doi: 10.1128/microbiolspec.TBTB2-0031-2016

Gonzalo-Asensio, J., Mostowy, S., Harders-Westerveen, J., Huygen, K., Hernandez-Pando, R., Thole, J., et al. (2008). PhoP: A missing piece in the intricate puzzle of mycobacterium tuberculosis virulence. *PloS One* 3 (10), e3496. doi: 10.1371/journal.pone.0003496

Gooderham, W. J., and Hancock, R. E. (2009). Regulation of virulence and antibiotic resistance by two-component regulatory systems in pseudomonas aeruginosa. *FEMS Microbiol. Rev.* 33 (2), 279–294. doi: 10.1111/j.1574-6976.2008.00135.x

Greendyke, R., and Byrd, T. F. (2008). Differential antibiotic susceptibility of mycobacterium abscessus variants in biofilms and macrophages compared to that of planktonic bacteria. *Antimicrob. Agents Chemother.* 52 (6), 2019–2026. doi: 10.1128/AAC.00986-07

Gutierrez, A. V., Baron, S. A., Sardi, F. S., Saad, J., Coltey, B., Reynaud-Gaubert, M., et al. (2021). Beyond phenotype: The genomic heterogeneity of co-infecting mycobacterium abscessus smooth and rough colony variants in cystic fibrosis patients. *J. Cyst Fibros* 20 (3), 421–423. doi: 10.1016/j.jcf.2021.02.002

Gutierrez, A. V., Viljoen, A., Ghigo, E., Herrmann, J. L., and Kremer, L. (2018). Glycopeptidolipids, a double-edged sword of the mycobacterium abscessus complex. *Front. Microbiol.* 9, 1145. doi: 10.3389/fmicb.2018.01145

Harris, K. A., and Kenna, D. T. (2014). Mycobacterium abscessus infection in cystic fibrosis: molecular typing and clinical outcomes. *J. Med. Microbiol.* 63 (Pt 10), 1241–1246. doi: 10.1099/jmm.0.077164-0

Honaker, R. W., Leistikow, R. L., Bartek, I. L., and Voskuil, M. I. (2009). Unique roles of DosT and DosS in DosR regulon induction and mycobacterium tuberculosis dormancy. *Infect. Immun.* 77 (8), 3258–3263. doi: 10.1128/IAI.01449-08

Hudock, T. A., Foreman, T. W., Bandyopadhyay, N., Gautam, U. S., Veatch, A. V., LoBato, D. N., et al. (2017). Hypoxia sensing and persistence genes are expressed during the intragranulomatous survival of mycobacterium tuberculosis. *Am. J. Respir. Cell Mol. Biol.* 56 (5), 637–647. doi: 10.1165/rcmb.2016-0239OC

Hurst-Hess, K., Rudra, P., and Ghosh, P. (2017). Mycobacterium abscessus WhiB7 regulates a species-specific repertoire of genes to confer extreme antibiotic resistance. *Antimicrob. Agents Chemother.* 61 (11). doi: 10.1128/AAC.01347-17

Jonsson, B. E., Gilljam, M., Lindblad, A., Ridell, M., Wold, A. E., and Welinder-Olsson, C. (2007). Molecular epidemiology of mycobacterium abscessus, with focus on cystic fibrosis. *J. Clin. Microbiol.* 45 (5), 1497–1504. doi: 10.1128/JCM.02592-06

Joshi, H., Kandari, D., and Bhatnagar, R. (2021). Insights into the molecular determinants involved in mycobacterium tuberculosis persistence and their therapeutic implications. *Virulence* 12 (1), 2721–2749. doi: 10.1080/21505594.2021.1990660

Kendall, S. L., Movahedzadeh, F., Rison, S. C., Wernisch, L., Parish, T., Duncan, K., et al. (2004). The mycobacterium tuberculosis dosRS two-component system is induced by multiple stresses. *Tuberculosis (Edinb)* 84 (3-4), 247–255. doi: 10.1016/j.tube.2003.12.007

Kester, J. C., Kandror, O., Akopian, T., Chase, M. R., Zhu, J., Rubin, E. J., et al. (2021). ClpX is essential and activated by single-strand DNA binding protein in mycobacteria. *J. Bacteriol* 203 (4). doi: 10.1128/JB.00608-20

Klepp, L. I., Sabio, Y. G. J., and FabianaBigi, (2022). Mycobacterial MCE proteins as transporters that control lipid homeostasis of the cell wall. *Tuberculosis (Edinb)* 132, 102162. doi: 10.1016/j.tube.2021.102162

Kundu, M., and Basu, J. (2021). Applications of transcriptomics and proteomics for understanding dormancy and resuscitation in mycobacterium tuberculosis. *Front. Microbiol.* 12, 642487. doi: 10.3389/fmicb.2021.642487

Lee, M. R., Sheng, W. H., Hung, C. C., Yu, C. J., Lee, L. N., and Hsueh, P. R. (2015). Mycobacterium abscessus complex infections in humans. *Emerg. Infect. Dis.* 21 (9), 1638–1646. doi: 10.1126/scitranslmed.abj3860

Leistikow, R. L., Morton, R. A., Bartek, I. L., Frimpong, I., Wagner, K., and Voskuil, M. I. (2010). The mycobacterium tuberculosis DosR regulon assists in metabolic homeostasis and enables rapid recovery from nonrespiring dormancy. *J. Bacteriol* 192 (6), 1662–1670. doi: 10.1128/JB.00926-09

Li, X., Lv, X., Lin, Y., Zhen, J., Ruan, C., Duan, W., et al. (2019). Role of two-component regulatory systems in intracellular survival of mycobacterium tuberculosis. *J. Cell Biochem.* 120 (8), 12197–12207. doi: 10.1002/jcb.28792

Li, C., Wen, A., Shen, B., Lu, J., Huang, Y., and Chang, Y. (2011). FastCloning: a highly simplified, purification-free, sequence- and ligation-independent PCR cloning method. *BMC Biotechnol.* 11, 92. doi: 10.1186/1472-6750-11-92

Li, B., Ye, M., Zhao, L., Guo, Q., Chen, J., Xu, B., et al. (2020). Glycopeptidolipid genotype correlates with the severity of mycobacterium abscessus lung disease. *J. Infect. Dis.* 221 (Suppl 2), S257–S262. doi: 10.1093/infdis/jiz475

Lin, M. Y., Reddy, T. B., Arend, S. M., Friggen, A. H., Franken, K. L., van Meijgaarden, K. E., et al. (2009). Cross-reactive immunity to mycobacterium tuberculosis DosR regulon-encoded antigens in individuals infected with environmental, nontuberculous mycobacteria. *Infect. Immun.* 77 (11), 5071–5079. doi: 10.1128/IAI.00457-09

Lopeman, R. C., Harrison, J., Desai, M., and Cox, J. A. G. (2019). Mycobacterium abscessus: Environmental bacterium turned clinical nightmare. *Microorganisms* 7 (3). doi: 10.3390/microorganisms7030090

Lyczak, J. B., Cannon, C. L., and Pier, G. B. (2002). Lung infections associated with cystic fibrosis. *Clin. Microbiol. Rev.* 15 (2), 194–222. doi: 10.1128/CMR.15.2.194-222.2002

Madacki, J., Laval, F., Grzegorzewicz, A., Lemassu, A., Zahorszka, M., Arand, M., et al. (2018). Impact of the epoxide hydrolase EphD on the metabolism of mycolic acids in mycobacteria. *J. Biol. Chem.* 293 (14), 5172–5184. doi: 10.1074/jbc.RA117.000246

Malhotra, V., Agrawal, R., Duncan, T. R., Saini, D. K., and Clark-Curtiss, J. E. (2015). Mycobacterium tuberculosis response regulators, DevR and NarL, interact *in vivo* and co-regulate gene expression during aerobic nitrate metabolism. *J. Biol. Chem.* 290 (13), 8294–8309. doi: 10.1074/jbc.M114.591800

Malhotra, S., Vedithi, S. C., and Blundell, T. L. (2017). Decoding the similarities and differences among mycobacterial species. *PloS Negl. Trop. Dis.* 11 (8), e0005883. doi: 10.1371/journal.pntd.0005883

Malm, S., Tiffert, Y., Micklinghoff, J., Schultze, S., Joost, I., Weber, I., et al. (2009). The roles of the nitrate reductase NarGHJI, the nitrite reductase NirBD and the response regulator GlnR in nitrate assimilation of mycobacterium tuberculosis. *Microbiol. (Reading)* 155 (Pt 4), 1332–1339. doi: 10.1099/mic.0.023275-0

Mascher, T., Helmann, J. D., and Unden, G. (2006). Stimulus perception in bacterial signal-transducing histidine kinases. *Microbiol. Mol. Biol. Rev.* 70 (4), 910–938. doi: 10.1128/MMBR.00020-06

Mehra, S., Foreman, T. W., Didier, P. J., Ahsan, M. H., Hudock, T. A., Kissee, R., et al. (2015). The DosR regulon modulates adaptive immunity and is essential for mycobacterium tuberculosis persistence. *Am. J. Respir. Crit. Care Med.* 191 (10), 1185–1196. doi: 10.1164/rccm.201408-1502OC

Miranda-CasoLuengo, A. A., Staunton, P. M., Dinan, A. M., Lohan, A. J., and Loftus, B. J. (2016). Functional characterization of the mycobacterium abscessus genome coupled with condition specific transcriptomics reveals conserved molecular strategies for host adaptation and persistence. *BMC Genomics* 17, 553. doi: 10.1186/s12864-016-2868-y

Molina-Torres, C. A., Tamez-Pena, L., Castro-Garza, J., Ocampo-Candiani, J., and Vera-Cabrera, L. (2018). Evaluation of the intracellular activity of drugs against mycobacterium abscessus using a THP-1 macrophage model. *J. Microbiol. Methods* 148, 29–32. doi: 10.1016/j.mimet.2018.03.020

Moore, S. D., and Prevelige, P. E.Jr. (2002). A P22 scaffold protein mutation increases the robustness of head assembly in the presence of excess portal protein. *J. Virol.* 76 (20), 10245–10255. doi: 10.1128/JVI.76.20.10245-10255.2002

Nessar, R., Cambau, E., Reyrat, J. M., Murray, A., and Gicquel, B. (2012). Mycobacterium abscessus: A new antibiotic nightmare. *J. Antimicrob. Chemother.* 67 (4), 810–818. doi: 10.1093/jac/dkr578

Olivier, K. N., Weber, D. J., Wallace, R. J.Jr., Faiz, A. R., Lee, J. H., Zhang, Y., et al. (2003). Nontuberculous mycobacteria. I: Multicenter prevalence study in cystic fibrosis. *Am. J. Respir. Crit. Care Med.* 167 (6), 828–834. doi: 10.1164/rccm.200207-678OC

Ortega Ugalde, S., Boot, M., Commandeur, J. N. M., Jennings, P., Bitter, W., and Vos, J. C. (2019). Function, essentiality, and expression of cytochrome P450 enzymes and their cognate redox partners in mycobacterium tuberculosis: Are they drug targets? *Appl. Microbiol. Biotechnol.* 103 (9), 3597–3614. doi: 10.1007/s00253-019-09697-z

Park, H. D., Guinn, K. M., Harrell, M. I., Liao, R., Voskuil, M. I., Tompa, M., et al. (2003). Rv3133c/dosR is a transcription factor that mediates the hypoxic response of mycobacterium tuberculosis. *Mol. Microbiol.* 48 (3), 833–843. doi: 10.1046/j.1365-2958.2003.03474.x

Pawlik, A., Garnier, G., Orgeur, M., Tong, P., Lohan, A., Le Chevalier, F., et al. (2013). Identification and characterization of the genetic changes responsible for the characteristic smooth-to-rough morphotype alterations of clinically persistent mycobacterium abscessus. *Mol. Microbiol.* 90 (3), 612–629. doi: 10.1111/mmi.12387

Peddireddy, V., Doddam, S. N., and Ahmed, N. (2017). Mycobacterial dormancy systems and host responses in tuberculosis. *Front. Immunol.* 8, 84. doi: 10.3389/fimmu.2017.00084

Peterson, E. J. R., Abidi, A. A., Arrieta-Ortiz, M. L., Aguilar, B., Yurkovich, J. T., Kaur, A., et al. (2020). Intricate genetic programs controlling dormancy in mycobacterium tuberculosis. *Cell Rep.* 31 (4), 107577. doi: 10.1016/j.celrep.2020.107577

Philley, J. V., DeGroote, M. A., Honda, J. R., Chan, M. M., Kasperbauer, S., Walter, N. D., et al. (2016). Treatment of non-tuberculous mycobacterial lung disease. *Curr. Treat Options Infect. Dis.* 8 (4), 275–296. doi: 10.1007/s40506-016-0086-4

Plocinska, R., Wasik, K., Plocinski, P., Lechowicz, E., Antczak, M., Blaszczyk, E., et al. (2022). The orphan response regulator Rv3143 modulates the activity of the NADH dehydrogenase complex (Nuo) in mycobacterium tuberculosis *via* protein-protein interactions. *Front. Cell Infect. Microbiol.* 12, 909507. doi: 10.3389/fcimb.2022.909507

Purkayastha, A., McCue, L. A., and McDonough, K. A. (2002). Identification of a mycobacterium tuberculosis putative classical nitroreductase gene whose expression is coregulated with that of the acr aene within macrophages, in standing versus shaking cultures, and under low oxygen conditions. *Infect. Immun.* 70 (3), 1518–1529. doi: 10.1128/IAI.70.3.1518-1529.2002

Rathor, N., Garima, K., Sharma, N. K., Narang, A., Varma-Basil, M., and Bose, M. (2016). Expression profile of mce4 operon of mycobacterium tuberculosis following environmental stress. *Int. J. Mycobacteriol* 5 (3), 328–332. doi: 10.1016/j.ijmyco.2016.08.004

Roberts, D. M., Liao, R. P., Wisedchaisri, G., Hol, W. G., and Sherman, D. R. (2004). Two sensor kinases contribute to the hypoxic response of mycobacterium tuberculosis. *J. Biol. Chem.* 279 (22), 23082–23087. doi: 10.1074/jbc.M401230200

Rohde, K. H., Abramovitch, R. B., and Russell, D. G. (2007). Mycobacterium tuberculosis invasion of macrophages: linking bacterial gene expression to environmental cues. *Cell Host Microbe* 2 (5), 352–364. doi: 10.1016/j.chom.2007.09.006

Rohde, K. H., Veiga, D. F., Caldwell, S., Balazsi, G., and Russell, D. G. (2012). Linking the transcriptional profiles and the physiological states of mycobacterium tuberculosis during an extended intracellular infection. *PloS Pathog.* 8 (6), e1002769. doi: 10.1371/journal.ppat.1002769

Roux, A. L., Viljoen, A., Bah, A., Simeone, R., Bernut, A., Laencina, L., et al. (2016). The distinct fate of smooth and rough mycobacterium abscessus variants inside macrophages. *Open Biol.* 6 (11). doi: 10.1098/rsob.160185

Ruger, K., Hampel, A., Billig, S., Rucker, N., Suerbaum, S., and Bange, F. C. (2014). Characterization of rough and smooth morphotypes of mycobacterium abscessus isolates from clinical specimens. *J. Clin. Microbiol.* 52 (1), 244–250. doi: 10.1128/JCM.01249-13

Rustad, T. R., Harrell, M. I., Liao, R., and Sherman, D. R. (2008). The enduring hypoxic response of mycobacterium tuberculosis. *PloS One* 3 (1), e1502. doi: 10.1371/journal.pone.0001502

Rustad, T. R., Sherrid, A. M., Minch, K. J., and Sherman, D. R. (2009). Hypoxia: a window into mycobacterium tuberculosis latency. *Cell Microbiol.* 11 (8), 1151–1159. doi: 10.1111/j.1462-5822.2009.01325.x

Salazar, M. E., and Laub, M. T. (2015). Temporal and evolutionary dynamics of two-component signaling pathways. *Curr. Opin. Microbiol.* 24, 7–14. doi: 10.1016/j.mib.2014.12.003

Santangelo Mde, L., Blanco, F., Campos, E., Soria, M., Bianco, M. V., Klepp, L., et al. (2009). Mce2R from mycobacterium tuberculosis represses the expression of the mce2 operon. *Tuberculosis (Edinb)* 89 (1), 22–28. doi: 10.1016/j.tube.2008.09.002

Sassetti, C. M., Boyd, D. H., and Rubin, E. J. (2003). Genes required for mycobacterial growth defined by high density mutagenesis. *Mol. Microbiol.* 48 (1), 77–84. doi: 10.1046/j.1365-2958.2003.03425.x

Sherman, D. R., Voskuil, M., Schnappinger, D., Liao, R., Harrell, M. I., and Schoolnik, G. K. (2001). Regulation of the mycobacterium tuberculosis hypoxic response gene encoding alpha -crystallin 98, 13, 7534–7539. doi: 10.1073/pnas.121172498

Singh, A., Mai, D., Kumar, A., and Steyn, A. J. (2006). Dissecting virulence pathways of mycobacterium tuberculosis through protein-protein association. *Proc. Natl. Acad. Sci. U.S.A.* 103 (30), 11346–11351. doi: 10.1073/pnas.0602817103

Singh, A., Varela, C., Bhatt, K., Veerapen, N., Lee, O. Y., Wu, H. H., et al. (2016). Identification of a desaturase involved in mycolic acid biosynthesis in mycobacterium smegmatis. *PloS One* 11 (10), e0164253. doi: 10.1371/journal.pone.0164253

Stock, J. B., Ninfa, A. J., and Stock, A. M. (1989). Protein phosphorylation and regulation of adaptive responses in bacteria. *Microbiol. Rev.* 53 (4), 450–490. doi: 10.1128/mr.53.4.450-490.1989

Story-Roller, E., Maggioncalda, E. C., Cohen, K. A., and Lamichhane, G. (2018). Mycobacterium abscessus and beta-lactams: Emerging insights and potential opportunities. *Front. Microbiol.* 9, 2273. doi: 10.3389/fmicb.2018.02273

Stupar, M., Furness, J., De Voss, C. J., Tan, L., and West, N. P. (2022). Two-component sensor histidine kinases of mycobacterium tuberculosis: Beacons for niche navigation. *Mol. Microbiol.* 117 (5), 973–985. doi: 10.1111/mmi.14899

Tomlinson, B. R., Denham, G. A., Torres, N. J., Brzozowski, R. S., Allen, J. L., Jackson, J. K., et al. (2022). Assessing the role of cold-shock protein c: a novel regulator of acinetobacter baumannii biofilm formation and virulence. *Infect. Immun.* 90 (10), e0037622. doi: 10.1128/iai.00376-22

Tomlinson, B. R., Malof, M. E., and Shaw, L. N. (2021). A global transcriptomic analysis of staphylococcus aureus biofilm formation across diverse clonal lineages. *Microb. Genom* 7 (7). doi: 10.1099/mgen.0.000598

Tsai, S. H., Lai, H. C., and Hu, S. T. (2015). Subinhibitory doses of aminoglycoside antibiotics induce changes in the phenotype of mycobacterium abscessus. *Antimicrob. Agents Chemother.* 59 (10), 6161–6169. doi: 10.1128/AAC.01132-15

Unden, G., and Bongaerts, J. (1997). Alternative respiratory pathways of escherichia coli: Energetics and transcriptional regulation in response to electron acceptors. *Biochim. Biophys. Acta* 1320 (3), 217–234. doi: 10.1016/S0005-2728(97)00034-0

van Kessel, J. C., and Hatfull, G. F. (2007). Recombineering in mycobacterium tuberculosis. *Nat. Methods* 4 (2), 147–152. doi: 10.1038/nmeth996

Veatch, A. V., and Kaushal, D. (2018). Opening pandora's box: Mechanisms of mycobacterium tuberculosis resuscitation. *Trends Microbiol.* 26 (2), 145–157. doi: 10.1016/j.tim.2017.08.001

Vilcheze, C., Yan, B., Casey, R., Hingley-Wilson, S., Ettwiller, L., and Jacobs, W. R.Jr. (2022). Commonalities of mycobacterium tuberculosis transcriptomes in response to defined persisting macrophage stresses. *Front. Immunol.* 13, 909904. doi: 10.3389/fimmu.2022.909904

Viljoen, A., Blaise, M., de Chastellier, C., and Kremer, L. (2016). MAB_3551c encodes the primary triacylglycerol synthase involved in lipid accumulation in mycobacterium abscessus. *Mol. Microbiol.* 102 (4), 611–627. doi: 10.1111/mmi.13482

Voskuil, M. I., Schnappinger, D., Visconti, K. C., Harrell, M. I., Dolganov, G. M., Sherman, D. R., et al. (2003). Inhibition of respiration by nitric oxide induces a mycobacterium tuberculosis dormancy program. *J. Exp. Med.* 198 (5), 705–713. doi: 10.1084/jem.20030205

Voskuil, M. I., Visconti, K. C., and Schoolnik, G. K. (2004). Mycobacterium tuberculosis gene expression during adaptation to stationary phase and low-oxygen dormancy. *Tuberculosis (Edinb)* 84 (3-4), 218–227. doi: 10.1016/j.tube.2004.02.003

Walters, S. B., Dubnau, E., Kolesnikova, I., Laval, F., Daffe, M., and Smith, I. (2006). The mycobacterium tuberculosis PhoPR two-component system regulates genes essential for virulence and complex lipid biosynthesis. *Mol. Microbiol.* 60 (2), 312–330. doi: 10.1111/j.1365-2958.2006.05102.x

Wee, W. Y., Dutta, A., and Choo, S. W. (2017). Comparative genome analyses of mycobacteria give better insights into their evolution. *PloS One* 12 (3), e0172831. doi: 10.1371/journal.pone.0172831

Weinstein, E. A., Yano, T., Li, L. S., Avarbock, D., Avarbock, A., Helm, D., et al. (2005). Inhibitors of type II NADH:menaquinone oxidoreductase represent a class of antitubercular drugs. *Proc. Natl. Acad. Sci. U.S.A.* 102 (12), 4548–4553. doi: 10.1073/pnas.0500469102

West, A. H., and Stock, A. M. (2001). Histidine kinases and response regulator proteins in two-component signaling systems. *Trends Biochem. Sci.* 26 (6), 369–376. doi: 10.1016/S0968-0004(01)01852-7

Wilburn, K. M., Fieweger, R. A., and VanderVen, B. C. (2018). Cholesterol and fatty acids grease the wheels of mycobacterium tuberculosis pathogenesis. *Pathog. Dis.* 76 (2). doi: 10.1093/femspd/fty021

Worlitzsch, D., Tarran, R., Ulrich, M., Schwab, U., Cekici, A., Meyer, K. C., et al. (2002). Effects of reduced mucus oxygen concentration in airway pseudomonas infections of cystic fibrosis patients. *J. Clin. Invest.* 109 (3), 317–325. doi: 10.1172/JCI0213870

Yang, H., Wang, F., Guo, X., Liu, F., Liu, Z., Wu, X., et al. (2021). Interception of host fatty acid metabolism by mycobacteria under hypoxia to suppress anti-TB immunity. *Cell Discovery* 7 (1), 90. doi: 10.1038/s41421-021-00301-1

Yarwood, J. M., McCormick, J. K., and Schlievert, P. M. (2001). Identification of a novel two-component regulatory system that acts in global regulation of virulence

factors of staphylococcus aureus. *J. Bacteriol* 183 (4), 1113–1123. doi: 10.1128/JB.183.4.1113-1123.2001

Yeruva, V. C., Savanagouder, M., Khandelwal, R., Kulkarni, A., Sharma, Y., and Raghunand, T. R. (2016). The mycobacterium tuberculosis desaturase DesA1 (Rv0824c) is a Ca(2+) binding protein. *Biochem. Biophys. Res. Commun.* 480 (1), 29–35. doi: 10.1016/j.bbrc.2016.10.014

Yousuf, S., Angara, R. K., Roy, A., Gupta, S. K., Misra, R., and Ranjan, A. (2018). Mce2R/Rv0586 of mycobacterium tuberculosis is the functional homologue of FadR(E. coli). *Microbiol. (Reading)* 164 (9), 1133–1145. doi: 10.1099/mic.0.000686

Zhu, C., Liu, Y., Hu, L., Yang, M., and He, Z. G. (2018). Molecular mechanism of the synergistic activity of ethambutol and isoniazid against mycobacterium tuberculosis. *J. Biol. Chem.* 293 (43), 16741–16750. doi: 10.1074/jbc.RA118.002693

frontiers | Frontiers in Cellular and Infection Microbiology

TYPE Original Research
PUBLISHED 24 March 2023
DOI 10.3389/fcimb.2023.1111997

OPEN ACCESS

EDITED BY
Elena G. Salina,
Research Center of Biotechnology of the Russian Academy of Sciences, Russia

REVIEWED BY
Ashima Bhaskar,
International Centre for Genetic Engineering and Biotechnology (India), India
Md Ataul Islam,
The University of Manchester, United Kingdom

*CORRESPONDENCE
Vivek Kumar Gupta
gupta.vk2@icmr.gov.in

†These authors have contributed equally to this work

SPECIALTY SECTION
This article was submitted to Bacteria and Host, a section of the journal Frontiers in Cellular and Infection Microbiology

RECEIVED 30 November 2022
ACCEPTED 06 March 2023
PUBLISHED 24 March 2023

CITATION
Sharma S, Chikhale R, Shinde N, Khan AM and Gupta VK (2023) Targeting dormant phenotype acquired mycobacteria using natural products by exploring its important targets: *In vitro* and *in silico* studies. *Front. Cell. Infect. Microbiol.* 13:1111997. doi: 10.3389/fcimb.2023.1111997

Targeting dormant phenotype acquired mycobacteria using natural products by exploring its important targets: *In vitro* and *in silico* studies

Shweta Sharma [1†], Rupesh Chikhale [2,3†], Nivedita Shinde [1], A. M. Khan [4] and Vivek Kumar Gupta [1*]

[1]Department of Biochemistry, ICMR-National JALMA Institute for Leprosy and Other Mycobacterial Diseases, Agra, India, [2]Division of Pharmacy and Optometry, University of Manchester, Manchester, United Kingdom, [3]Department of Pharmaceutical & Biological Chemistry, School of Pharmacy, University College London, London, United Kingdom, [4]Division of Clinical Trials and Implementation Research, ICMR-National JALMA Institute for Leprosy and Other Mycobacterial Diseases, Agra, India

The dormant phenotype of *Mycobacterium tuberculosis* that develops during infection poses a major challenge in disease treatment, since these bacilli show tolerance to front-line drugs. An *in vitro* hypoxia dormancy model was established, which produced phenotypically dormant *Mycobacterium smegmatis* after prolonged incubation under conditions of low oxygen, low pH, and nutrient limitation. Bacilli in this model displayed the classical dormancy characters, including loss of acid fastness, altered morphology, and, most importantly, tolerance to front-line drugs. The dormant form of *M. smegmatis* was treated with drugs and phytomolecules. Three phytomolecules exhibited activity against dormant bacilli, as shown by lack of regrowth in solid and liquid media. Further investigation of dormancy-active hits was carried out using *in silico* approaches to understand the druggable targets of these phytomolecules in dormant bacilli. For this study, molecular docking, molecular dynamics simulations (MDS), and molecular mechanics-generalized born solvent accessibility (MM-GBSA)-based binding energy (ΔG_{bind}) calculations were performed. Five different targets, namely, isocitrate lyase (ICL), GMP synthase, LuxR, DosR, and serine/threonine protein kinase (STPK), from *M. smegmatis* and *M. tuberculosis* were studied in details. DosR and STPK were found to be the common targets in both the species that were more prone to the phytomolecules. The standard DosR inhibitor, HC104A, showed a lower dock score and binding energy of −4.27 and −34.50 kcal/mol, respectively, compared to the natural products under study. The phytomolecule, icariin, showed better docking score (dock score = −5.92 kcal/mol with and binding energy ΔG_{bind}= −52.96 kcal/mol) with DosR compared to known DosR inhibitor, HC104A (dock score = −4.27 kcal/mol and binding energy ΔG_{bind} = −34.50 kcal/mol). Similarly, the known STPK inhibitor MRCT67127 showed a lower dock score and binding energy of −4.25 and −29.43 kcal/mol, respectively, compared to the phytomolecule, icariin (dock score = −5.74 kcal/mol and ΔG_{bind}= −43.41 kcal/

mol). These compounds might ultimately lead to new therapeutics or may be useful as adjuvants to the first-line drugs to reduce the lengthy anti-TB therapy in the future.

KEYWORDS

tuberculosis, mycobacterium, dormancy, drug targets, phytomolecules, LTBI (latent TB infection), homology modeling, molecular docking

Introduction

Tuberculosis (TB) is one of the main causes of death by an infectious disease worldwide. A large number of individuals latently infected with *Mycobacterium tuberculosis* (*Mtb*) delay the efforts to eliminate this disease (Ai et al., 2016). The dormant form of bacilli in latent TB infection (LTBI) also serves as a reservoir for the reactivation and transmission of the disease. The lifetime risk of reactivation of bacilli in LTBI is estimated to be 5%–10%, and this is 10–100 times more in HIV patients (Sterling et al., 2020). Targeting the dormant form of *Mtb* in LTBI is a big challenge for current chemotherapy (Dutta and Karakousis, 2014). The dormant state of *Mtb* is characterized by the presence of non-dividing or slowly replicating bacilli with low metabolic state, and such bacilli are also phenotypically resistant to standard anti-tuberculosis (anti-TB) agents (Gupta et al., 2017). Complete cure of TB requires the eradication of both replicating and dormant forms of *Mtb*. Most of the standard anti-TB agents are more than 45 years old and are mostly active against the replicating form of bacilli. A prolonged therapy is required due to dormancy-induced drug tolerance developed by *Mtb* (Evangelopoulos et al., 2015). The differences in altered physiology of the dormant bacilli from replicating bacilli can serve as therapeutic drug targets for the development of effective therapy against this disease.

The search for antimycobacterial compounds from natural sources is a historically authenticated approach. Plant molecules are the major component of traditional medicine system, which is well known to possess a wide range of biological activities, such as antioxidative, anti-inflammatory, antimicrobial, and anticancer effects (Cowan, 1999).

In this study, three plant molecules, namely, ursolic acid (UA), betulinic acid (BA), and icariin (IC), were tested against the dormant form of *Mycobacterium smegmatis*, which serves as a surrogate model strain for the pathogenic *Mtb* (Chaturvedi et al., 2007). An *in vitro* hypoxia dormancy model developed by Wayne and Hayes (1996) was used in this study, which produced dormant bacilli after prolonged incubation under conditions of low oxygen, low pH, and nutrient limitation (Wayne and Sramek, 1994). Bacilli in this model exhibited the typical dormancy traits, including loss of acid fastness, altered morphology, and, most importantly, tolerance to front-line anti-TB drugs.

Further investigation of dormancy-active hits was carried out using *in silico* approaches to understand the druggable targets of these phytomolecules in dormant bacilli, which may ultimately lead to new therapeutics that may be able to reduce the lengthy anti-TB therapy.

Materials and methods

Maintenance of *M. smegmatis*

Mycobacterium smegmatis strain (MTCC 994) was procured from Microbial Type Culture Collection (MTCC), Institute of Microbial Technology, (IMTECH), Chandigarh, India. *M. smegmatis* was maintained at pH 7 and temperature at 37°C in Middlebrook 7H9 (Difco) liquid culture medium supplemented with 10% oleic albumin dextrose catalase (OADC) (BD) and 0.1% Tween-80 (Merck). Nutrient agar (Hi-Media) was used as solid culture medium for the routine maintenance of culture.

Drugs and plant compounds

All antibiotics and compounds were purchased from Sigma-Aldrich Chemicals (St. Louis, MO, USA). The standard first-line antibiotics used included rifampicin (RIF) and isoniazid (INH). INH and metronidazole were each prepared in water to stock concentrations of 10 and 50 mg/ml, respectively, while RIF was dissolved in methanol (stock concentration, 10 mg/ml). The three phytomolecules were dissolved in dimethyl sulfoxide (DMSO) (Merck) to a stock concentration of 10 mg/ml. The final working concentration ranges for each antibiotic were prepared by twofold serial dilutions with appropriate solvents.

Generation of dormant bacilli

In order to generate *in vitro* dormancy, a hypoxic model developed by Wayne and Hayes (1996) was used for this study. Broth culture of *M. smegmatis* was taken in tubes (with tight-fitting rubber caps), which were then sealed and centrifuged at 6,000 rpm for 10 min at 10°C. The pellet was washed twice with phosphate-buffered saline (PBS) and then dissolved in PBS with Tween-80 (0.01% v/v). The culture was diluted in nutrient-deficient Sauton's medium (Mulyukin et al., 2010; Nikitushkin et al., 2016) (Supplementary Table S1) containing pH 6.0 to reach a dilution of 1:10. (1.0 McFarland suspension). The culture was divided into

two vacutainer tubes (5.0 ml) (Becton Dickinson) (Rathor et al., 2016; Imperiale et al., 2017), which were tightly screwed and sealed with parafilm. The methylene blue was added to the final concentration of 1.5 μg/ml to one of the tubes as an indicator of hypoxia (oxygen depletion). The optimal headspace ratio of air volume to liquid was maintained in the tubes throughout the experiment. The tubes were incubated at low stirring at 37°C to maintain a hypoxic environment. Regular observations were made for the reduction in methylene blue, and colony-forming units (CFU) counting was performed.

Ziehl–Neelsen staining

A thin bacterial smear was prepared from a hypoxic culture tube to perform Ziehl–Neelsen (Z–N) staining using carbol fuchsin (Van Deun et al., 2008). To decolorize the background, sulfuric acid (20% v/v) was used. Counterstaining was done using methylene blue, and slides were observed under a 100× oil immersion microscope.

Electron microscopy

Scanning electron microscopy (SEM) of *M. smegmatis* culture was performed to observe their morphology under stress environment. Cultures from above experiments were taken for this study. The cells were fixed overnight at 4°C in a mixture of 4% (v/v) paraformaldehyde (Sigma-Aldrich) and 2.5% (v/v) glutaraldehyde (Sigma-Aldrich) in 0.1 M phosphate buffer (pH 7.4). The sample suspension was then centrifuged, the supernatant was discarded, and the pellet was washed with 0.1 M phosphate buffer twice; the specimens were then fixed with 1% (w/v) osmium tetraoxide (Sigma-Aldrich) in 0.1 M phosphate buffer for 1 h. The cells were then dehydrated in ascending concentration using molecular grade ethanol (Merck) from 50%, 70%, and 100% (10 min at room temperature). The cells were transferred on a glass coverslip and air dried. All samples were coated with gold using a sputter coater (Quorm, SC7620) and examined using a scanning electron microscope (THERMO FEISEM, Volumescope) (Kim et al., 2017; Pawar et al., 2020). SEM was performed at the Advanced Technology Platform Centre (ATPC) facility, RCB, Faridabad, India.

Hypoxic resazurin reduction assay for screening of compounds against dormant bacilli

HyRRA was performed with slight modification as described by Taneja and Tyagi (2007). Briefly, vacutainer tubes (5.0 ml) were filled, using a syringe and needle (26½), with nutrient-deficient Sauton's medium. *Mycobacterium smegmatis* (from hypoxic culture of the above experiment) was inoculated in vacutainer tubes to a turbidity equivalent to 1.0 McFarland turbidity suspension.

The tubes were kept static at 37°C to allow for self-generation of hypoxia in the cultures (as described above). Fading/decolorization of the methylene blue dye (at final concentration of 1.5 μg/ml) was used to determine hypoxia. Various test compounds/drugs were subsequently injected at different concentrations by a needle without opening the tubes and further incubated for 48 h at 37°C under static conditions. Metronidazole (actively works on anaerobically grown microorganisms) and isoniazid (primarily acting on dividing cells) were used as positive control. Resazurin dye (0.02%) was added in each vacutainer tube. A reduction in dye color was noted after 24 h of incubation at 37°C. Minimum inhibitory concentrations (MICs) were determined for the test drugs in the same manner as for aerobic resazurin microtiter plate assay (REMA) (Martin et al., 2003).

Statistical analysis. GraphPad Prism 5 software (Graph Pad Software, San Diego, CA) was used for analysis of data.

Molecular docking

Homology modeling

The protein crystal structures for the *M. smegmatis* isocitrate lyase (ICL), GMP synthase, LuxR, DosR, and serine/threonine protein kinase (STPK) are not available. These structures were modeled by homology modeling using tools like Swiss-Model (https://swissmodel.expasy.org/) (Waterhouse et al., 2018) and AlfaFold (https://alphafold.ebi.ac.uk/) (Jumper et al., 2021; Varadi et al., 2022). The modeled structures were validated for their structural quality by means of Ramachandran Plot, Qmean, and MolProbity scores (Benkert et al., 2009, 2011)

Protein preparation

The crystal structures for DNA-binding transcriptional activator DosR/DevR (PDB: 3C3W) (Wisedchaisri et al., 2008) and intracellular STPK domain of *Mtb* PknB (PDB: 1MRU) (Young et al., 2003) from *Mtb* were obtained from the Protein Data Bank (PDB) (https://www.rcsb.org/). These were directly imported into the protein preparation wizard of Schrödinger Maestro version 2018-1 (Schrödinger, 2018). These structures were analyzed for any inconsistencies like breaks or missing residues and was prepared by adding hydrogen, treating the metal, deleting water molecules beyond 5 Å, correcting for protonation states, and assigning partial charges by using the OPLS-2005 force field. Both of these crystal structures are apo proteins; the binding site was determined using the SiteMap tool, and the top-ranking site was selected to prepare a grid using a protein–ligand docking grid generation tool in Maestro.

Ligand preparation

The 2D structure of ligands, namely, ursolic acid (UA), betulinic acid (BA), and icariin (IC), were downloaded from PubChem compound database (https://pubchem.ncbi.nlm.nih.gov) in SDF format and uploaded to the work space in Glide. The ligands HC104A and MRCT67127 were used as standard ligands. The LigPrep (Schrödinger, 2018) module in Maestro was used to generate three-dimensional conformations of these ligands with a higher limit of 200 conformations for each structure; all the conformations generated were further used for docking simulations.

Protein ligand docking

The molecular docking simulations were performed in the Glide module of the Schrödinger suite with the grid file for protein binding site and ligand conformations generated in earlier steps. The docking was performed in the extra precision mode (XP mode) and the poses with high docking score, protein–ligand interactions like hydrogen bond, and π–π interactions were selected. The results of simulations were analyzed using a glide XP visualizer, and the important active site interactions were analyzed along with the scoring functions.

Molecular dynamics simulations and molecular mechanics-generalized born solvent accessibility analysis

System preparation

All the 29 molecular dynamics simulations were calculated on AMBER 18 software package (Lee et al., 2018; Singh et al., 2020). ANTECHAMBR (Wang et al., 2001) was used for ligand preparation and for the determination of the charges on the ligand; further GAFF force field was used for parametrization, and the protein–ligand complexes were prepared in XLEAP (Wang et al., 2001). The protein receptor–ligand complex was solvated separately in truncated octahedron of TIP3P (Price and Brooks, 2004) box with water molecules; a sufficient number of counter ions Na^+ and Cl^- were added to neutralize the simulation system, and 0.1M of ionic strength was achieved (Mark and Nilsson, 2001; Price and Brooks, 2004). To parameterize the amino acids and to model the proteins, FF14SB force field was used (Maier et al., 2015).

Unbiased MD simulation

All simulations were performed for 100 ns on Nvidia V100-SXM2-16GB Graphic Processing Unit using the PMEMD.CUDA (Peramo, 2016) module installed on the Computational Shred Facility (CSF), University of Manchester, UK. Simulations were run at 1 atm constant pressure using Monte Carlo barostat and 300 K constant temperature by using Langevin thermostat with a collision frequency of 2 ps^{-1}, and the volume exchange was attempted for every 100 fs. An integration step of 2 fs was also used for the simulation of the hydrogen atoms involving bonds and were constrained by using SHAKE algorithm (Andersen, 1983). Long-range electrostatic interactions were computed by using the particle mesh Ewald method, while for short-range interaction, a cutoff of 8 Å was used. Equilibration consisted of rounds of NVT and NPT equilibrations, respectively, for 10 ns in total. CPPTRAJ (Roe and Cheatham, 2013) was used to analyze the interactions over full trajectory after taking configuration at every 4 ps. Root mean square deviation (RMSD), root mean square fluctuation (RMSF), and MM-GBSA binding free energy were determined after analyzing the trajectories.

MM-GBSA analysis

The MM-GBSA was performed on Amber18 and Amber18 tools. After simulation of the protein–ligand complexes, all the trajectories of 100 ns covering all the 10,000 frames were used for MM-GBSA analysis (Rastelli et al., 2010). All the results in the form of energies were tabulated and reported in kcal/mol.

Results and discussion

Evaluation of the *in vitro* dormancy model

In order to mimic the granuloma stress *in vitro* to generate dormancy, Wayne's hypoxia model was used in this study for the generation of dormant bacilli. The additional stress of nutrient starvation with slightly acidic pH (6.0) were also provided. With the use of this model, we observed bacterial growth in $1.75\pm0.52 \times 10^9$ CFU in vacutainer tubes at day 7, indicative of the replication stage of bacterial culture (Supplementary Figure S1). At this stage, the color of methylene blue was not changed, which showed the presence of normal environment in the culture vials. On the 14th day, the color of methylene blue was reduced, indicating a generation of hypoxia, which easily correlated with the decrease in the number of cells corresponding to the stress (Dick et al., 1998). A 100-fold reduction in CFU was observed in the vials at day 14. The growth of the bacteria became static from 21 days onward. The shifting of the environment from aerobic to hypoxic/anaerobic and nutrient limitation may be the cause of the decrease in CFU. Once bacteria adapt to the stress environment, the static condition is maintained for a long time. All the experiments were performed in triplicates.

The generation of dormancy was also validated through the Z-N staining method. The Z-N staining differences in cultures were observed in this study. The aerobic replicating culture showed a darker pink shade, while the hypoxic culture showed a lighter tone of pink (Supplementary Figure S2). The dormant cells contain less mycolic acid in their cell wall and thus take up a lower stain as compared to active cells (Deb et al., 2009).

Electron microscopic studies

Mycobacterium smegmatis cells from aerobic culture (Figures 1A, C) have smooth a surface and well-defined rigid shape. These cells were mostly rod-like proper length with septa or constrictions. In hypoxic culture, slight morphological changes were observed in comparison to the aerobic culture. The culture under hypoxic environment showed apical swelling, and the lengths of most of the bacilli were short (Figures 1B, D). Trutneva et al. (2020) observed altered morphology (small and ovoid appearance) of dormant cells of *Mtb* after 4.5 months of incubation in comparison to multiplying bacteria (typical rod-shaped appearance).

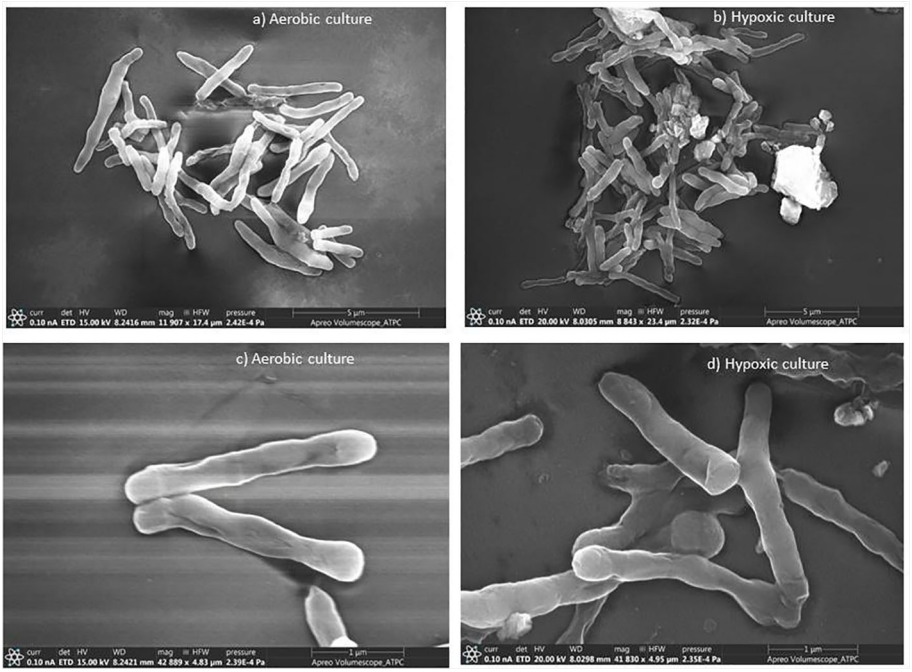

FIGURE 1
Scanning electron micrographs of *M. smegmatis* under aerobic and hypoxic environment: **(A, C)** aerobic culture and **(B, D)** hypoxic culture.

Evaluation of anti-TB activity of phytomolecules against dormant bacilli

The aim of our work was to determine the potent antibacterial activity of UA, BA, and IC, and their possible use as new agent against dormant bacterial population.

After the generation and validation of *in vitro* dormancy model, the dormant cells were used to screen the activities of phytomolecules to understand their efficiency. Three different concentrations (500, 250, and 125 µg/ml) of phytomolecules were used for the treatment of dormant cells (Table 1). At minimum inhibitory concentration (MIC) of phytomolecules, cultures remained blue post-resazurin (Supplementary Figure S3) addition and thereby confirmed their bactericidal activity against dormant *M. smegmatis*, and no growth was observed on solid and liquid media. Our results revealed that all the three phytomolecules exhibited significant anti-mycobacterial activity against dormant bacilli. UA, BA, and IC were effectively active against the dormant form of *M. smegmatis* in this study. UA, BA, and IC also exhibited activity against the replicating form of *M. smegmatis* with MICs of 125, 250, and 500 µg/ml, respectively.

Hence, our results agree with those from a previous study, which noticed that UA, BA, and IC were active against replicating form of *Mtb* (Jiménez-Arellanes et al., 2013; Lone et al., 2017).

Rifampicin and isoniazid were used as standard anti-TB drugs, while metronidazole was the positive control in the *in vitro* experiment. The dormant bacilli showed phenotypic drug resistance against standard drugs rifampicin and isoniazid. In the presence of metronidazole at 50 µg/ml, the blue color of resazurin did not change, which confirmed their activity under hypoxic environment (Wayne and Sramek, 1994; Murugasu-Oei and Dick, 2000).

TABLE 1 MIC of each compound against the *in vitro* generated dormant cells of *M. smegmatis*.

Sr. No.	Phytomolecules	MIC (µg/ml)
1	Betulinic acid	125
2	Icariin	500
3	Ursolic acid	125
4	Metronidazole (positive control)	50
5	Rifampicin (standard drug)	>60
6	Isoniazid (standard drug)	50

In silico study

In order to understand the molecular mechanism of inhibition taking place inside the dormant cell, *in silico* studies were also undertaken against important drug targets in dormant *M. smegmatis* and *Mtb*.

Mtb face depletion of oxygen and nutrients in the stress environment of the host's granuloma and survive in the form of non-replicating dormant cells. Isocitrate lyase (ICL) plays an important role in the survival of latent *Mtb* during chronic stage of infection (McKinney et al., 2000). ICL is a glyoxylate cycle enzyme, which converts isocitrate to succinate and glyoxylate, followed by the addition of acetyl-CoA to glyoxylate to form

malate by malate synthase, which help survival of *Mtb* in a carbon-deficient environment. Similarly, the two-component DOS (dormancy survival) regulon enables bacterial adaptation and survival in non-replicating persistence (NRP) stage during dormancy (Dasgupta et al., 2000). The expression of the ~50 gene regulon is coordinated by dormancy survival regulator (DosR), which binds to target sites on DNA and induces transcription of other genes, which help in survival (Sharma and Tyagi, 2016). Fang et al. (2013) detected the vital role of LuxR family regulator Rv0195 in *Mtb* dormancy, which affected the expression of more than 180 genes. Serine/threonine protein kinases (STPKs) play important roles in bacterial cellular processes including cell division, cell wall synthesis, cell metabolism, and dormancy exit (Chawla et al., 2014). Guanosine monophosphate synthase (GMP synthase), encoded by guaA gene (Rv3396c), catalyzes the conversion of xanthosine 5′-monophosphate (XMP) into guanosine 5′-monophosphate (GMP) and is a key enzyme in both purine *de novo* and salvage pathways of guanine nucleotides (Villela et al., 2015).

Considering the important role of the above-mentioned proteins in the dormant stage of the mycobacteria were selected for *in silico* studies. These targets were explored to understand which one of these could potentially be interacting with the ligands under investigation. We started with molecular docking studies to understand the drug–receptor interactions. These docked complexes were further explored by molecular dynamics studies to understand the stability of the complex. The binding energies were calculated by the MMGBSA method. In the docking studies, we docked BA, IC, UA, HC104A (a known DosR inhibitor), and MRCT67127 (a known STPK inhibitor). There are no known crystal structures for the *M. smegmatis* ICL, GMP synthase, LuxR, DosR, and STPK. To overcome this short fall, these proteins were modeled in the SWISS-MODEL using the sequences available on the Uniprot (https://www.uniprot.org/), and these were verified with the structures available in the AlphaFold database (https://alphafold.ebi.ac.uk/). The details of the sequences used for modeling the protein by homology modeling is provided in Supplementary Table S2, where the validation parameters like RC-plot, Q-mean scores, and MolProbility scores are provided in more detail. The modeled structures were found to be well within the acceptable ranges for structural quality. This was also verified by comparing the structures available in the AlphaFold database for structural identity. The protein structures were further refined by means of MDS for 100 ns and later used in the molecular docking and MDS studies. These refined protein structures were explored for possible binding sites by the SiteMap tool, the best site used for the generation of Grid for docking in the Glide. The ligands under study were subjected to conformation generation by LigPrep tool in the Glide software.

The docking of ligands BA, IC, UA, HC104A, and MRCT67127 showed several interactions with *M. smegmatis* ICL (Supplementary Figures 4A–C). The ligand BA docked in the binding site by forming a hydrogen bond interaction with the Lys189 (BA-O3—NZ-Lys, 2.81 Å) with a dock score of −2.85 kcal/mol. IC formed several interactions with the binding site residues of ICL, Thr347 (IC-O8—OG1-Thr, 2.81 Å), Glu285 (IC-O6—OE2-Glu, 2.79 Å), Asp108 (IC-O7—OD2-Glu, 2.61 Å), and Ala233 (IC-O15—O-Ala, 3.16 Å) with a dock score of −3.54 kcal/mol. The ligand UA docked inside the binding site with one hydrogen bond with the residues, Lys189 (UA-O3—NZ-Lys, 3.16 Å) and Asn313 (UA-O1—ND2-Asn, 2.77 Å) with a dock score of −5.95 kcal/mol (Supplementary Table S3), respectively. The docking experiment with *M. smegmatis* ICL shows best interaction with the ligand IC. The docking of ligands BA, IC, UA, HC104A, and MRCT67127 showed several interactions with *M. smegmatis* GMP synthase (Supplementary Figures S4D–F). To perform in-depth investigation on the binding of BA, IC, and UA with the GMP, we performed MDS for 100 ns on each of the respective complex and calculated the binding energies (Supplementary Table S3). These bound ligands showed high ligand RMSDs during the MDS with BA fluctuating from 3 to 15 Å and then lowered down to approximately 4 Å (Supplementary Figures S5A, D). IC had a stable initial phase of MDS for approximately 50 ns after which a steep rise to 16 Å was observed, which is probably due to the ligand's conformational change from its initial docked pose (Supplementary Figures S5B, E); its higher binding energy of (ΔG_{bind} = −32.90 (4.90) kcal/mol) indicates that the new conformation might be more favorable than the docked pose. UA-ICL complex was also studied by MDS for 100 ns; the ligand RMSD was found to show high fluctuation through the simulation. Initially, the UA RMSD was approximately 4.5 Å; this increased gradually over the period of 80 ns to approximately 10 Å and lowered to approximately 7.5 Å towards the end of the simulation. The UA–ICL protein RMSD also suggested for high protein RMSD to approximately 6 Å, and the protein RMSF showed high fluctuations for the residues between 350 and 375. The overall observations for UA–ICL complex showed week binding interactions, which was also supported by a low binding energy (ΔG_{bind} = −21.09 (3.79) kcal/mol) (Supplementary Figures 5C, F). The docked ligand–GMP synthase complex with BA did not show any hydrogen bond interaction. It has a very low dock score of −1.89 kcal/mol. The ligand UA bound to the *M. smegmatis* GMP synthase showed the formation of two hydrogen bonds, His176 (UA-O3—ND1-His, 2.79 Å) and Asp479 (UA-O1—OD1-Asp, 3.12 Å). The dock score for the *M. smegmatis* GMP synthase–UA complex was −2.72 kcal/mol. IC formed several interactions with the binding site residues of GMP synthase, Phe107 (IC-O15—N-Phe, 2.91 Å), Phe107 (IC-O14—N-Phe, 2.86 Å), Ser105 (IC-O14—O-Ser, 2.86 Å), and Asp479 (IC-O8—OD2-Asp, 2.74 Å) with a dock score of −5.29 kcal/mol. The BA, IC, and UA were also studied in more details for their binding modes with the GMP; the MDS calculations were performed, and binding energies were calculated (Supplementary Figures S6A–F). The MDS of GMP complexes for 100 ns showed varied results. The ligand BA's RMSD over the MDS showed large fluctuations with steep rise from 1 to 12 Å over a short period of 20 ns and kept fluctuating for the remaining time of simulation. Ligand IC showed a lower fluctuation during the MDS. It showed a gradual rise from 2 to 5 Å over a period of 45 ns, after which it stabilized for the rest of the MDS. The ligand UA presents large fluctuations for the initial 50 ns, after which it converged approximately 5 Å for rest of the period. The higher binding energies of ΔG_{bind} = -36.39 (5.41) kcal/mol for the IC–GMP complex supported the higher stability of this complex compared to other GMP complexes. The docking of ligands BA, IC, UA,

HC104A, and MRCT67127 showed several interactions with *M. smegmatis* LuxR (Supplementary Figures S4G–I). The ligand IC was the only one molecule that showed some hydrogen bond interactions with LuxR, the Trp37 (IC-O7—O-Trp, 2.92 Å) with a dock score of −4.41 Kcal/mol. The MDS for BA–LuxR showed an unstable complex with very high fluctuations. The ligand RMSD fluctuated as high as 80 Å, which lowered to 40 Å towards the end of the simulation (Supplementary Figures S7A, D). The IC–LuxR complex was found to be most stable complex with ligand RMSD approximately 3 Å throughout the simulation period; this was also supported by a high binding energy of ΔG_{bind} = −45.42 (5.15) kcal/mol. The UA–LuxR complex showed a low ligand RMSD but a high fluctuating protein RMSD; it showed a large variation of 1.5–5 Å through the MDS, suggesting that UA might not be able to stabilize the residues in the binding site. This was also observed in the protein RMSF with comparative higher fluctuations for residues between 80 and 100, and 130 and 150 of LuxR (Supplementary Figures S7B–F). These observations for binding of BA, IC, and UA to the *M. smegmatis* target receptors ICL, GMP, and LuxR by *in silico* methods indicated lower or no specificity towards these proteins.

The other studied target in *M. smegmatis* was DosR. The ligands under investigation were docked in the binding site of DosR to understand the ligand–receptor interactions. Compound BA docked in the binding site of the DosR to form a hydrogen bond interaction with Asn167 (BA-O3—ND2-Asn, 2.74 Å) with a dock score of −3.24 kcal/mol (Figure 2A and Table 2). IC docked in the binding site by interacting with various residues, namely, Arg56 (IC-O12—NH2-Arg, 3.10 Å), Pro58 (IC-O9—O-Pro, Asn61 (IC-O7—ND2-Asn, 3.26 Å), Glu195 (IC-OE2—NH2-Glu, 2.83 Å), and Asn167 (IC-O6—N-Asn, 2.96 Å) with a docking score of −5.92 kcal/mol (Figure 2B and Table 2). The ligand HC104A was docked in the binding site with few interactions with the surrounding residues, Gly60 (HC104A-O1—O-Gly, 2.84 Å) and Asn167 (HC104A-O1—ND2-Asn, 3.15 Å), and had a dock score of −4.27 kcal/mol (Figure 2C and Table 2). UA bound to the DosR showed a single hydrogen bond with the residue Leu161 (UA-O2—ND2-Leu, 2.79 Å) with dock score of −3.55 (Figure 2D and Table 2). The docking results suggest IC as the compound showing better interaction with the *M. smegmatis* DosR receptor as compared to other ligands. The final *M. smegmatis* target studied was STPK, the ligands under investigation were docked in the binding site of STPK to understand the ligand–receptor interactions. Compound BA docked in the binding site of the STPK showed a hydrogen bond interaction with Arg137(BA-O1—ND2-Arg, 2.88 Å) with a dock score of −2.24 kcal/mol (Figure 2E and Table 2). IC docked in the binding site by interacting with various residues of STPK; Ala188 (IC-O7—O-Ala, 2.83 Å), Gln187 (IC-O6—O-Gln, 2.86), Arg137 (IC-O2—NH1-Arg, 3.22 Å), Gly190 (IC-O14—O-Gly, 2.93 Å), and Arg161 (IC-O6—NH1-Arg, 2.68 Å) with a docking score of −4.74 kcal/mol (Figure 2F and Table 2). The ligand MRCT67127 was docked in the binding site where it showed few interactions with the surrounding residues, Arg189 (MRCT67127-N7—O-Arg, 3.04 Å). Arg137 (MRCT67127-N5—NH1-Arg, 2.85 Å), and Gln187 (MRCT67127-N1—NE-Gln, 3.04 Å), and it had a dock score of −4.25 kcal/mol (Figure 2H and Table 2). UA bound to the STPK showed a single hydrogen bond with the residue Arg137 (UA-O3—NH1-Arg, 2.94 Å) with a dock score of −2.65 kcal/mol (Figure 2G and Table 2). The docking studies showed a slightly higher binding of IC to STPK compared to the standard ligand MRCT67127.

To understand and compare the effect of the ligands on various important proteins and targets in the dormant state of the

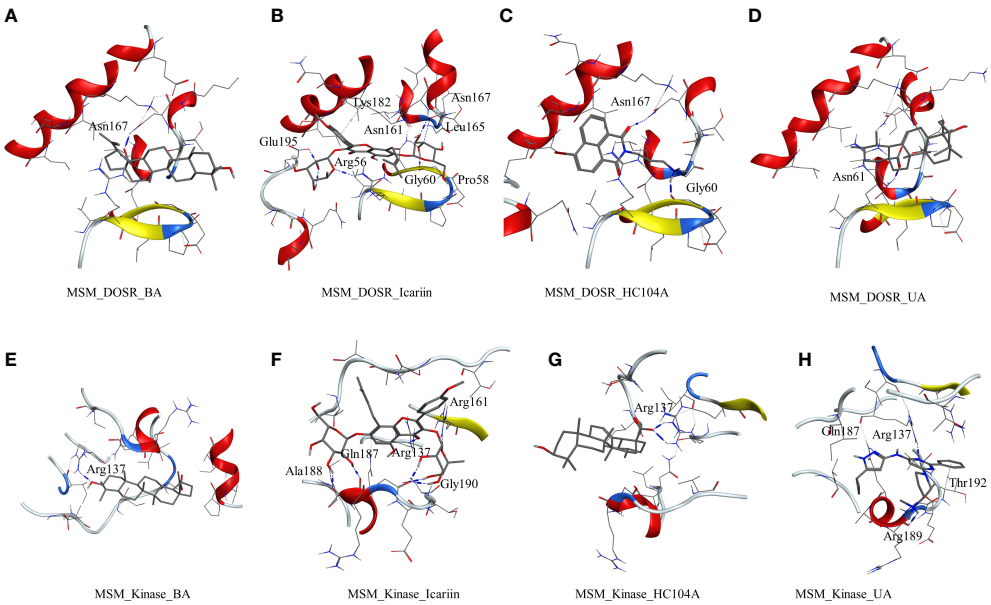

FIGURE 2
Molecular docking results for *M. smegmatis* dormancy survival regulator (DosR): **(A)** DosR–betulinic acid (BA), **(B)** DosR–icariin (IC), **(C)** DosR–HC104A, and **(D)** DosR–UA. Molecular docking results for *M. smegmatis* serine/threonine-protein kinase (STPK): **(E)** STPK – BA, **(F)** STPK–IC, **(G)** STPK–UA, and **(H)** STPK–MRCT67127.

TABLE 2 The dock scores and MM-GBSA binding energies for the ligands and reference compounds in complex with the DosR and STPK from *M. smegmatis* and *Mtb* all energies are in Kcal/mol with standard deviation in parenthesis.

Ligands	*M. smegmatis*				*M. tuberculosis*			
	DosR		STPK		DosR		STPK	
	Dock Score	MM-GBSA (ΔG_{bind})*	Dock Score	MM-GBSA (ΔG_{bind})	Dock Score	MM-GBSA (ΔG_{bind})	Dock Score	MM-GBSA (ΔG_{bind})
IC	-5.92	-52.96 (5.38)	-4.74	-43.41 (4.68)	-4.98	-31.76 (4.31)	-5.82	-24.30 (6.10)
UA	-3.55	-11.80 (5.89)	-2.65	-10.95 (4.77)	-2.35	-22.28 (7.33)	-3.61	-26.94 (4.09)
BA	-3.24	-30.66 (6.90)	-2.24	-24.84 (5.68)	-2.71	-17.13 (4.81)	-2.49	-33.86 (5.05)
HC104A	-4.27	-38.52 (2.87)	-4.25	-19.51 (3.47)	-3.97	-34.98 (6.11)	-5.11	-36.04 (7.94)
MRCT67127	-4.75	-34.50 (6.03)	-4.25	-29.43 (3.33)	-5.70	-33.45 (3.58)	-4.40	-50.83 (3.66)

*ΔG_{bind} = binding free energy (kcal/mol).

mycobacteria, we explored the *M. smegmatis* ICL, GMP synthase, LuxR, DosR, and STPK by docking experiments. DosR and STPK are reported to play a major role in the dormant state; hence, it was imperative to study these targets in *Mtb*. The crystal structure of DosR and STPK of *Mtb* are available in the PDB; hence, we explored these for the docking studies. The binding of ligand BA–DosR showed the formation of hydrogen bond and its interaction with the residue Arg56 (BA-O2—NH2-Arg, 2.70 Å) with a dock score of −2.71 kcal/mol (Figure 3A and Table 2). IC docked with the *Mtb* DosR and formed several hydrogen bond interactions owing to its free hydroxyl groups, Glu195 (IC-O13—OE2-Glu, 2.63 Å), Leu57 (IC-O9—O-Leu, 2.92 Å), Leu165 (IC-O8—O-Leu, 2.68 Å), Asn167 (IC-O6—OD1-Asn, 2.70 Å), and Asn61 (IC-O8—ND2-Asn, 3.12 Å), with a dock score of −4.98 kcal/mol (Figure 3B and Table 2). The ligand HC104A docked in the *Mtb* DosR with a dock score of −3.97 kcal/mol and formed a single hydrogen bond with the Asn167 (HC104A-O2—ND2-Asn, 2.86 Å) (Figure 3C and Table 2). The ligand UA did not form any hydrogen bond with the binding site residues of the *Mtb* DosR, and it showed a dock score of −2.35 kcal/mol (Figure 3D and Table 2). We also investigated the *Mtb* STPK to compare with the *M. smegmatis* STPK. The ligand BA did not form any interaction with the residues of the binding site of the *Mtb* STPK, for which the dock score was −2.49 kcal/mol (Figure 3E and Table 2). The ligand IC formed hydrogen bond interaction with the residues Thr179 (IC-O2—N-Thr, 3.07 Å), and it also coordinated with the magnesium ion present near the binding site near Asp156. IC showed a dock score of −5.82 kcal/mol (Figure 3F and Table 2). The ligand MRCT67127 docked in the binding site of *Mtb* STPK forming two hydrogen bond interactions with the residues Ala191 (MRCT67127-N2—O-Ala, 2.84 Å) and Arg140 (MRCT67127-N2—NH-Arg, 2.80 Å) with a dock score of −4.40 kcal/mol (Figure 3G). When UA was docked in the binding site of the *Mtb* STKP, it did not form any hydrogen bond interactions and showed a dock score of −3.61 kcal/mol (Figure 3H). These results from the docking of

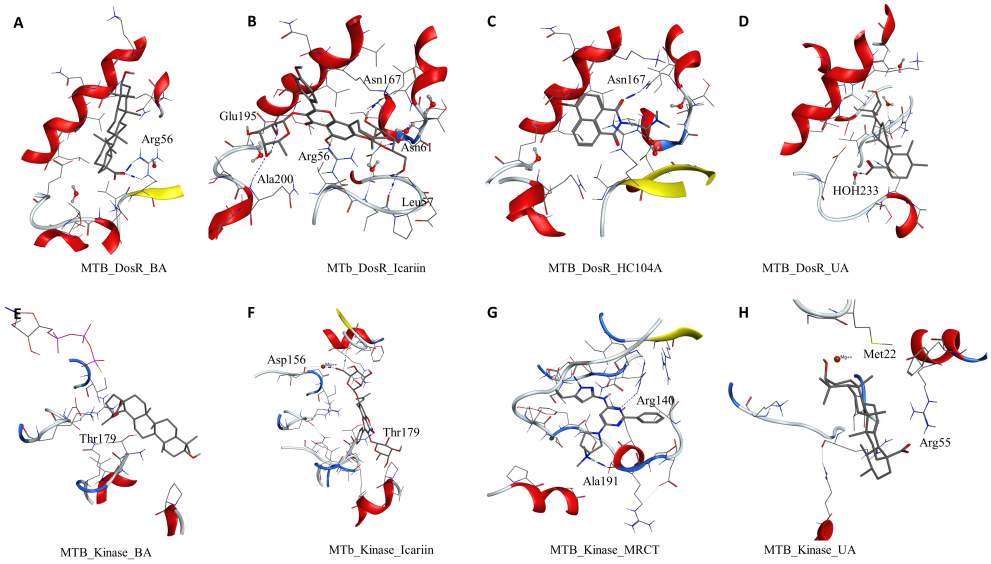

FIGURE 3
Molecular docking results for *M. tuberculosis* dormancy survival regulator (DosR) (PDB: 3C3W): **(A)** DosR–BA, **(B)** DosR–IC, **(C)** DosR–HC104A, and **(D)** DosR–UA. Molecular docking results for *M. tuberculosis* serine/threonine protein kinase (STPK) (PDB: 1MRU): **(E)** STPK–BA, **(F)** STPK–IC, **(G)** STPK–MRCT67127, and **(H)** STPK–UA.

various ligands into the *Mtb* STPK suggest that IC binds better than MRCT67127 with regard to binding interactions with the residues of the binding site and the dock score. These observations raised some questions about the nature of ligand binding, stability of the ligand–receptor complex, and the binding energies of these complexes. To answer these questions, we performed molecular dynamics simulations (MDS) on all the complexes using explicit solvent model for 100 ns and used this trajectory to calculate the binding energies by MM-GBSA method (Table 2).

The ligand RMSD for compounds bound to the *M. smegmatis* DosR showed variable RMSDs. The ligand HC104A had low RMSD, which fluctuated between 1 and 2.5 Å throughout the duration of the simulation (Figure 4A), whereas IC showed a fluctuating trend with RMSD between 1 and 4 Å. The compound BA had a low RMSD between 1 and 4 Å, which rose to 2–7 Å for the last 60 ns; however, it returned to the lower RMSD state towards the end of the simulation. The ligand UA did not remain in the complex, as it broke away from the complex and ended up to the walls of the periodic box (Figure 4G). The RMSD of the receptor participating in the ligand–receptor complex was calculated, except for the IC-bound complex where the protein RMSD stayed below 3 Å throughout the simulation. The IC-bound protein showed fluctuations throughout the simulation; it kept between 2 and 6 Å, suggesting high flexibility of the complex due to the shape of the IC and high binding affinity (Figure 4B and Table 2). The RMSF was calculated to understand the effect of ligand binding. The ligands bound in the region surrounded by residues Arg56, Leu57, Gly60, Gly164, Thr166, Lys182, and other binding site residues. The RMSF in the region of 150–200 residues showed lower RMSF for ligand-bound complexes, whereas, in case of the UA-bound complex, a high RMSD in this region of the plot was observed (Figure 4C). The protein–ligand complexes were analyzed at the end of the simulations. HC104A bound to the *M. smegmatis* DosR retained its interaction with the Gly60 and formed a new hydrogen bond interaction with Leu57 (HC104A-N2—O-Leu, 3.11 Å) (Figure 4D). Ligand BA was found to remain in the binding site of the *M. smegmatis* DosR, but it lost its interaction with the binding site residues (Figure 4E). IC formed a new interaction with Gly164 (IC-O7—O-Gly, 2.95 Å) while retaining most of its original interactions during the MDS (Figure 4F). The binding energies of the *M. smegmatis* DosR-bound ligands were calculated by MM-GBSA, which suggested the highest binding energy for IC (ΔG_{bind} = −52.96 (5.38)) followed by HC104A (ΔG_{bind} = −38.52 (2.87) kcal/mol) and BA (−38.52 (2.87) kcal/mol). UA formed a very unstable complex with the *M. smegmatis* DosR, which is reflected by a low binding energy (ΔG_{bind} = −11.80 (5.89) kcal/mol). The molecular docking studies, MDS, and binding energies suggest for a stable complex between IC and *M. smegmatis* DosR.

The ligand RMSD for those in complex with the *M. smegmatis* STPK showed a similar trend that we observed in an earlier case. Ligand MRCT67127 fluctuated between RMSD 1 and 7 Å; the RMSD for BA was found below 5 Å through the 100-ns MSD. Ligand IC showed a low fluctuation of <3 Å for the first 60 ns, after which it showed a gradual rise in the RMSD to 10 Å, and later, it reduced to 7.5 Å at the end of the MDS (Figure 5B). The ligand RMSD for UA was very high, as it leaves the complex right at the beginning of the MDS (Figure 5G). The protein RMSD for the complexes displayed a similar trend with an RMSD range between 1.5 and 4 Å, although the MDS was 100 ns. The protein RMSF for the complexes in the region of ligand binding show the effect of ligand binding. The binding site in the case of STPK lies in the region of residue numbers 160–200. The ligand-bound protein had a lower RMSF compared to the unbound one; the MRCT67127-, BA-, and IC-bound protein had lower fluctuations than the one bound to UA by approximately 1 Å (Figure 5A–C). The analysis of MDS trajectories towards the end of the simulations showed that

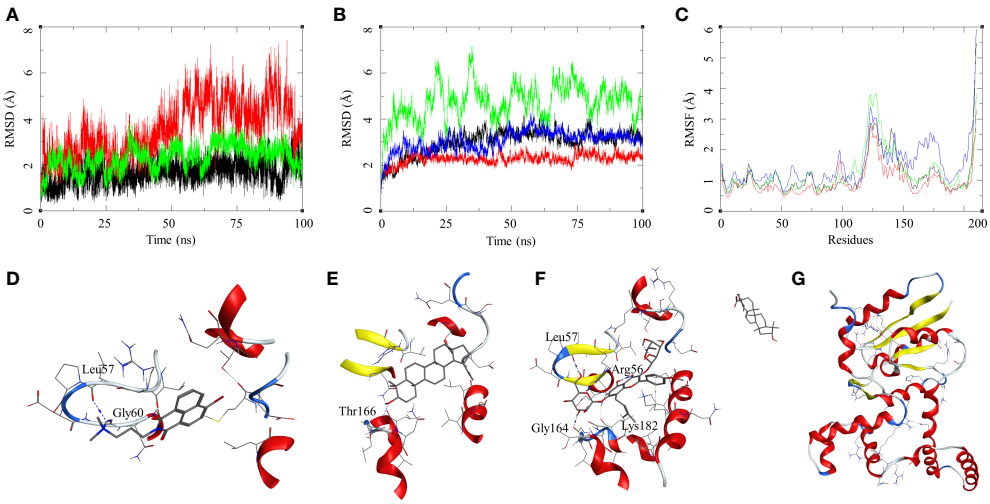

FIGURE 4
Molecular dynamics simulation results for *M. smegmatis* dormancy survival regulator (DosR) complexes: **(A)** ligand RMSD for HC104A (black), BA (red), and IC (green); **(B)** ligand-bound protein RMSD for HC104A (black), BA (red), IC (green), and UA (blue); **(C)** ligand-bound protein RMSF for HC104A (black), BA (red), IC (green), and UA (blue). Protein–ligand complex poses at the end of the 100-ns simulations, **(D)** DosR-HC104A, **(E)** DosR–BA, **(F)** DosR–IC, and **(G)** DosR–UA.

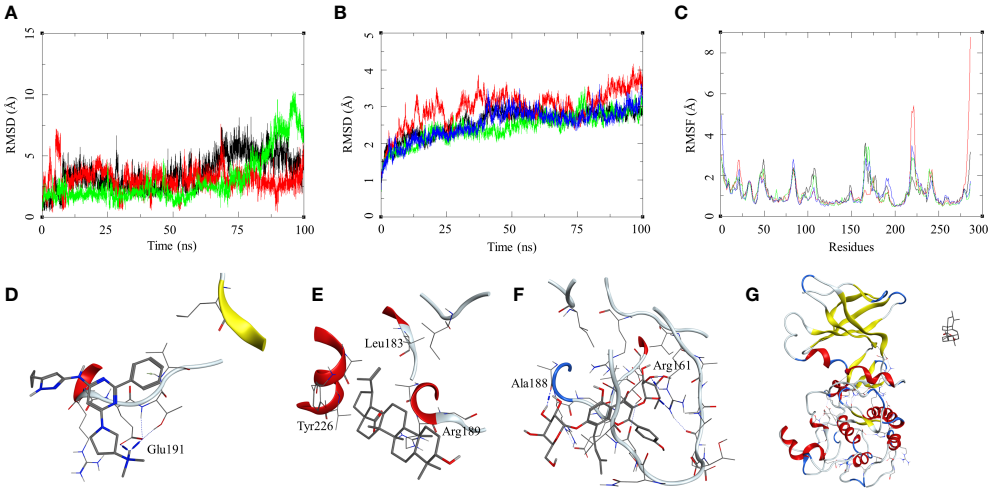

FIGURE 5
Molecular dynamics simulation results for *M. smegmatis* serine/threonine-protein kinase (STPK): **(A)** ligand RMSD for MRCT67127 (black), BA (red), and IC (green); **(B)** ligand-bound protein RMSD for MRCT67127 (black), BA (red), IC (green), and UA (blue); **(C)** ligand-bound protein RMSF for MRCT67127 (black), BA (red), IC (green), and UA (blue). Protein–ligand complex poses at the end of the 100-ns simulations, **(D)** STPK–MRCT67127, **(E)** STPK–BA, **(F)** STPK–IC, and **(G)** STPK–UA.

the interaction profile of the ligands with several modifications happened during the MDS (Figure 5D, E). The ligand MRCT67127 lost its original interactions and formed new and more stable interactions with the STPK binding site residues. It formed hydrogen bond interactions with the Glu191 (MRCT67127-OE2—N7-Glu, 2.80 Å) and an arene–backbone nitrogen interaction *via* hydrogen with the Val193. The ligand BA did not retain any interaction with the binding site residues, but it remained in the bound state towards the end of the MDS. The ligand IC, on the other hand, retained almost all interactions that were found in the initial state of MDS except for the hydrogen bond with the Ala188 (Figure 5F). The ligand UA did not retain its interaction with the *M. smegmatis* STPK in the MDS (Figure 5G). The binding energies for the protein–ligand complex reflected the same trend with the *M. smegmatis* STPK-IC complex showing the highest binding energy (ΔG_{bind} = -43.41 (4.68) kcal/mol). The ligands MRCT67127 (ΔG_{bind} = −29.43 (3.33) kcal/mol) and BA (ΔG_{bind} = −24.84 (5.68) kcal/mol) were the second and third, respectively, whereas the ligand UA (ΔG_{bind} = −10.95 (4.77) kcal/mol) showed the lowest binding energies. These results suggest that IC was the best binding ligand for *M. smegmatis* STPK from this set of compounds.

The protein–ligand interactions between the natural products and standard compounds under investigation with the *M. smegmatis* targets, ICL, GMP synthase, LuxR, DosR, and STPK, exhibited the potential pattern of interaction, which suggest DosR and STPK to be the leading target proteins for these molecules. The molecular docking and MDS results along with the binding energy calculations favored these two receptors from *M. smegmatis* as top interacting partners. Taking the hint from these calculations and observations, we decided to investigate further for their selectivity in the case of *Mtb*. The rationale behind this study is to identify ligands that are active in the dormant stage of the mycobacteria. Honaker et al. (2009) and Sharma and Tyagi (2016) reported the importance of DosR activation in *Mtb* for the anaerobic survival, latent infection, and drug tolerance. Based on our *in silico* finding with MSM, we decided to proceed further with investigating the *Mtb* DosR and STPK, and fortunately, the crystal structures for both these *Mtb* targets are available in the PDB. The details about these targets are provided in the materials section (Supplementary Table S2). The docking studies, molecular dynamics simulations, and binding energy calculations were performed on all the natural products and the standard drugs under investigation.

The ligand RMSD for compounds bound to the *Mtb* DosR showed variable RMSDs. The ligand HC104A and IC showed a low ligand RMSD between 1 and 4 Å. The ligand BA showed a gradually rising RMSD over a period of 20 ns from 1 to 12.5 Å, after which it converged and stayed within a fluctuating range of 1–5 Å for the rest of the MDS. The ligand UA had a similar trajectory with a gradual rise in the RMSD from 1 to 10 Å over a period of 30 ns followed by a convergence between 1 and 5 Å for rest of the MDS (Figure 6A). The protein RMSDs for these complexes was almost similar except for the protein bound to IC. The protein RMSD fluctuated between 2 and 5 Å for HC104A, BA, and UA complexes. The IC-bound protein showed a rise in RMSD between 30 and 75 ns of the MDS. The rise was of approximately 3–s4 Å from its initial state; after 75 ns, the RMSD went steeply back to its original state (Figure 6B). This also reflected in the RMSF of the IC-bound protein, which had an overall higher RMSF, and this could be attributed to the size and higher conformational flexibility of the IC ligand (Figure 6C). Analysis of ligand binding interaction towards the end of the MDS was performed to understand the interaction of ligands with the binding site residues. HC104A formed new interactions during the MDS. Apart from its hydrogen bonding with the Asn167, it formed new bonds with the residues Gly164 (HC104A-N2—O-Gly, 3.94 Å) and Glu64 (HC104A-N2—OE2-Glu, 2.90 Å) (Figure 6D). The ligand BA stayed within the binding site; it lost bonding with the Arg56 but forms a new

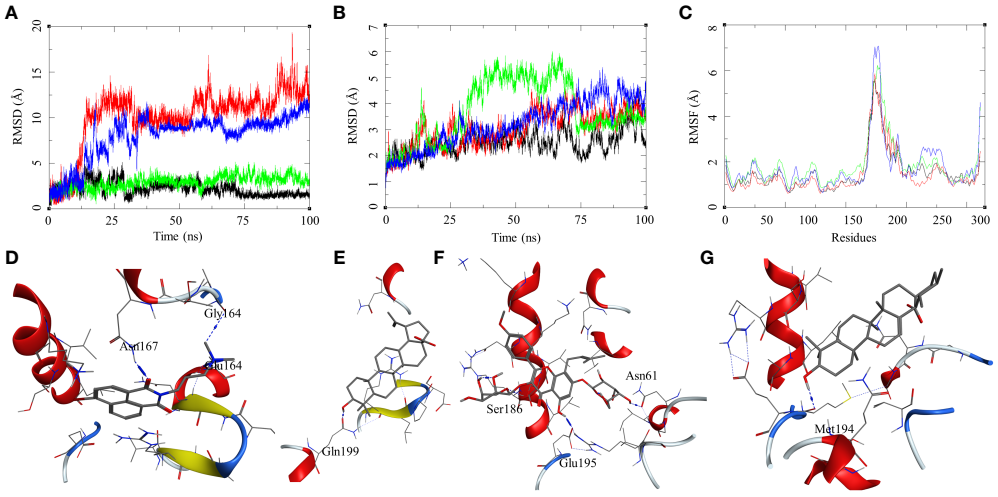

FIGURE 6
Molecular dynamics simulation results for *M. tuberculosis* dormancy survival regulator (DosR) (PDB: 3C3W): **(A)** ligand RMSD for HC104A (black), BA (red), IC (green), and UA (blue); **(B)** ligand-bound protein RMSD for HC104A (black), BA (red), IC (green), and UA (blue); **(C)** ligand-bound protein RMSF for HC104A (black), BA (Red), IC (green), and UA (blue). Protein–ligand complex poses at the end of the 100-ns simulations, **(D)** DosR–HC104A, **(E)** DosR–BA, **(F)** DosR–IC, and **(G)** DosR–UA.

interaction with Gln199 (BA-O1—OE1-Gln, 2.58 Å) (Figure 6E). IC was successful in maintaining its interactions with the binding site residues during the MDS with some conformational changes (Figure 6F). The ligand UA did not show any interactions with the binding site residues during the initial stage of the MDS, but it formed a hydrogen bond with Met194 (UA-O1—O-Met, 2.58 Å) towards the end of the MDS (Figure 6G). The binding energies of these complexes were calculated over all the frames of the MDS of which the standard ligand HC104A showed the highest binding energy of ΔG_{bind} = −34.98 (6.11) followed by IC (ΔG_{bind} = −31.76 (4.31) kcal/mol), UA (ΔG_{bind} = −22.28 (7.33) kcal/mol), and BA (ΔG_{bind} = −17.13 (4.81) kcal/mol) (Table 2). These results were expected because ligand HC104A is a known *Mtb* DosR inhibitor (Zheng et al., 2020); this also strengthens our experimental results about the efficacy of the IC as an inhibitor of DosR in the mycobacteria.

The ligand RMSD for compounds bound to the *Mtb* STPK showed variable RMSDs. The ligand RMSD for MRCT67127 remained low, between 1 and 5 Å, with very low fluctuations. However, BA showed a slightly higher fluctuation between 1 and 5 Å for approximately 75 ns of the MDS, after which there was a rise in the RMSD by approximately 5 Å till the end of the MDS (Figure 7A). In case of IC, there were high fluctuations throughout the MDS; it rose from 2.5 to 5 during first 20 ns and kept rising at an interval of 5 Å till the ligand showed very high deviation of approximately 20 Å. The visual inspection of the trajectory showed high conformational space exploration by IC. The ligand UA showed a stable RMSD initially, which was below 3 Å, but it gradually rose to approximately 6 Å around 60 ns and converged till the end of the MDS (Figure 7A). In case of the protein RMSD, the protein bound to MRCT67127 had high RMSD fluctuating between 1 and 5 Å throughout the MDS. The protein RMSD for the rest of the complexes was between 3 Å (Figure 7B). The protein RMSF for all the complexes showed a similar pattern for the ligand binding region of 150–200 residues, but in the case of the IC-bound protein, it was slightly higher by approximately 2 Å (Figure 7C). Analysis of ligand binding interaction towards the end of the MDS was performed to understand the interaction of ligands with the binding site residues. The ligand MRCT67127 retained its position in the binding site residues and formed a hydrogen bond interaction with the residue Arg135 (MRCT67127-N5—NH2-Arg, 2.80 Å), suggesting a stable complex that is supported by the ligand RMSD (Figure 7D). The ligand BA remained in the binding site of the *Mtb* STPK but did not participate in any interactions with the surrounding residues (Figure 7E). The ligand IC underwent large conformational change as evident from its ligand RMSD, towards the end of the MDS wherein it formed the hydrogen bond interaction with Lys255 (IC-O6—NZ-Lys, 2.92 Å) (Figure 7F). The ligand UA remained bound to the *Mtb* STPK through the MDS but did not form any hydrogen bond interactions (Figure 7G). The binding energies for these complexes was calculated over the MDS, the standard ligand MRCT67127 showed the highest binding energy of ΔG_{bind} = −50.83 (3.66) followed by BA (ΔG_{bind} = −33.86 (5.05) kcal/mol), UA (ΔG_{bind} = −26.94 (4.09) kcal/mol), and the IC (ΔG_{bind} = −24.30 (6.10) kcal/mol) (Table 2). These results were expected because ligand MRCT67127 is a known *Mtb* STPK inhibitor (Lougheed et al., 2011); this also strengthens our experimental results about the efficacy of the natural compounds as inhibitor of mycobacteria in its dormant state.

Conclusion

We demonstrated the generation of dormant bacilli under stress environment, which showed loss of acid fastness, altered morphology, and tolerance to isoniazid and rifampicin. UA, BA,

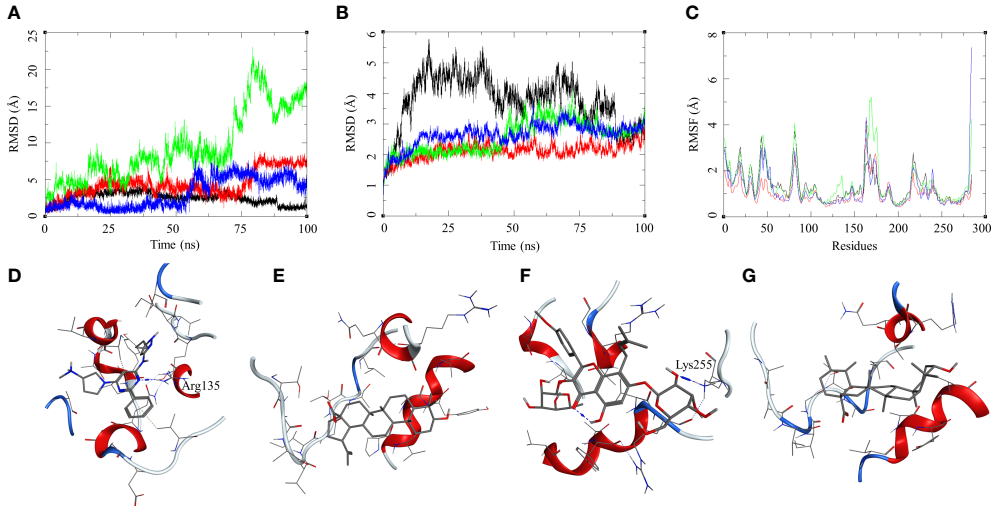

FIGURE 7
Molecular dynamics simulation results for *M. tuberculosis* serine/threonine-protein kinase (STPK) (PDB: 1MRU) complexes: **(A)** ligand RMSD for MRCT67127 (black), BA (red), IC (green), and UA (blue); **(B)** ligand-bound protein RMSD for MRCT67127 (black), BA (red), IC (green), and UA (blue); **(C)** ligand-bound protein RMSF for MRCT67127 (black), BA (red), IC (green), and UA (blue). Protein–ligand complex poses at the end of the 100-ns simulations, **(D)** STPK–MRCT67127, **(E)** STPK–BA, **(F)** STPK–IC, and **(G)** STPK–UA.

and IC effectively inhibited dormant population of *M. smegmatis*. For this study, an *in vitro* dormancy model for screening phytomolecules against a model strain of *M. smegmatis* was generated, and the activity was evaluated through hypoxic resazurin reduction assay.

In silico studies have provided deeper understanding about the possible interactions between the ligands and various targets investigated in this study. The molecular level interactions, binding modes of ligands with the binding site residues, and their behaviors in the solution phase helped in correlating the biological activities of the molecules on a structural basis. These investigations a part of this study have helped to determine important targets in the model strain of *M. smegmatis*, which have also been found in *M. tuberculosis*. DosR and STPK were found to be the targets common in both species that were more prone to these phytomolecules, which had promising inhibitory activity towards the dormant stage of *M. smegmatis*, and it could also be the case in *Mtb* as per the insights proved by the *in silico* studies.

Future prospective

The current anti-TB therapy contain important drugs to kill the replicating form of bacilli, but they do not effectively work against drug-tolerant dormant population of bacilli. The identification of drugs that can eradicate phenotypically drug-tolerant dormant population of *Mtb* is important for developing effective regimens to shorten the treatment duration for TB.

There are further needs for studying the efficacy of these phytomolecules against the non-replicating form of *Mtb*. These targets can also be explored for target-based study in an *in vitro* model, which can provide clear results regarding the efficacy of these phytomolecules. These compounds might ultimately lead to new therapeutics or adjuvants, which can be used with first-line drugs to reduce the duration of lengthy anti-TB therapy after evaluation through different experimental approaches in the future.

Data availability statement

The original contributions presented in the study are included in the article/Supplementary Material. Further inquiries can be directed to the corresponding author.

Author contributions

SS and NS performed *in vitro* studies and microscopic analysis. RC performed modeling studies. VG designed the study and analyzed data. AK reviewed the manuscript. All authors contributed to the article and approved the submitted version.

Acknowledgments

The authors would like to acknowledge the use of the Computational Shared Facility at the University of Manchester, Manchester, United Kingdom and Centre for High Performance Computing (CHPC), University of KwaZulu-Natal, Durban, South Africa, for the computational software support. We would also like to acknowledge Dr. M. Madhan Kumar, Department of Immunology, Indian Council of Medical Research - National JALMA Institute for Leprosy and Other Mycobacterial Disease, Agra-282004, India for assistance in correcting the manuscript.

Conflict of interest

The authors declare that the research was conducted in the absence of any commercial or financial relationships that could be construed as a potential conflict of interest.

Publisher's note

All claims expressed in this article are solely those of the authors and do not necessarily represent those of their affiliated organizations, or those of the publisher, the editors and the reviewers. Any product that may be evaluated in this article, or claim that may be made by its manufacturer, is not guaranteed or endorsed by the publisher.

Supplementary material

The Supplementary Material for this article can be found online at: https://www.frontiersin.org/articles/10.3389/fcimb.2023.1111997/full#supplementary-material

References

Ai, J. W., Ruan, Q. L., Liu, Q. H., and Zhang, W. H. (2016). Updates on the risk factors for latent tuberculosis reactivation and their managements. *Emerg. Microbes Infect.* 5, e10. doi: 10.1038/EMI.2016.10

Andersen, H. C. (1983). Rattle: A "velocity" version of the shake algorithm for molecular dynamics calculations. *J. Comput. Phys.* 52, 24–34. doi: 10.1016/0021-9991(83)90014-1

Benkert, P., Biasini, M., and Schwede, T. (2011). Toward the estimation of the absolute quality of individual protein structure models. *Bioinformatics* 27(3), 343-350. doi: 10.1093/bioinformatics/btq662

Benkert, P., Künzli, M., and Schwede, T. (2009). QMEAN server for protein model quality estimation. *Nucleic Acids Res.* 37(suppl_2), W510-W514. doi: 10.1093/nar/gkp322

Chaturvedi, V., Dwivedi, N., Tripathi, R. P., and Sinha, S. (2007). Evaluation of *Mycobacterium smegmatis* as a possible surrogate screen for selecting molecules active against multi-drug resistant *Mycobacterium tuberculosis*. *J. Gen. Appl. Microbiol.* 53 (6), 333–337. doi: 10.2323/jgam.53.333

Chawla, Y., Upadhyay, S., Khan, S., Nagarajan, S. N., Forti, F., and Nandicoori, V. K. (2014). Protein kinase b (PknB) of *Mycobacterium tuberculosis* is essential for growth of the pathogen *in vitro* as well as for survival within the host. *J. Biol. Chem.* 289, 13858–13875. doi: 10.1074/JBC.M114.563536

Cowan, M. M. (1999). Plant products as antimicrobial agents. *Clin. Microbiol. Rev.* 12 (4), 564–582. doi: 10.1128/CMR.12.4.564

Dasgupta, N., Kapur, V., Singh, K. K., Das, T. K., Sachdeva, S., Jyothisri, K., et al. (2000). Characterization of a two-component system, devR-devS, of *Mycobacterium tuberculosis*. *Tuber. Lung Dis.* 80, 141–159. doi: 10.1054/TULD.2000.0240

Deb, C., Lee, C. M., Dubey, V. S., Daniel, J., Abomoelak, B., Sirakova, T. D., et al. (2009). A novel *In vitro* multiple-stress dormancy model for *Mycobacterium tuberculosis* generates a lipid-loaded, drug-tolerant, dormant pathogen. *PloS One* 4 (6), e6077. doi: 10.1371/JOURNAL.PONE.0006077

Dick, T., Lee, B. H., and Murugasu-Oei, B. (1998). Oxygen depletion induced dormancy in *Mycobacterium smegmatis*. *FEMS Microbio. Lett.* 163 (2), 159–164. doi: 10.1111/j.1574-6968.1998.tb13040.x

Dutta, N. K., and Karakousis, P. C. (2014). Latent tuberculosis infection: Myths, models, and molecular mechanisms. *Microbiol. Mol. Biol. Rev.* 78 (3), 343–371. doi: 10.1128/MMBR.00010-14

Evangelopoulos, D., da Fonseca, J. D., and Waddell, S. J. (2015). Understanding anti-tuberculosis drug efficacy: Rethinking bacterial populations and how we model them. *Int. J. Infect. Dis.* 32, 76–80. doi: 10.1016/J.IJID.2014.11.028

Fang, H., Yu, D., Hong, Y., Zhou, X., Li, C., and Sun, B. (2013). The LuxR family regulator Rv0195 modulates *Mycobacterium tuberculosis* dormancy and virulence. *Tuberc. (Edinb)* 93, 425–431. doi: 10.1016/J.TUBE.2013.04.005

Gupta, V. K., Kumar, M. M., Singh, D., Bisht, D., and Sharma, S. (2017). Drug targets in dormant *Mycobacterium tuberculosis*: Can the conquest against tuberculosis become a reality? *Infect. Dis. (London England)* 50 (2), 81–94. doi: 10.1080/23744235.2017.1377346

Honaker, R. W., Leistikow, R. L., Bartek, I. L., and Voskui, M. I. (2009). Unique roles of DosT and DosS in DosR regulon induction and *Mycobacterium tuberculosis* dormancy. *Infect. Immun.* 77, 3258–3263. doi: 10.1128/IAI.01449-08/FORMAT/EPUB

Imperiale, B. R., Cataldi, Á. A., and Morcillo, N. S. (2017). *In vitro* anti-tuberculosis activity of azole drugs against *Mycobacterium tuberculosis* clinical isolates. *Rev. Argent Microbiol.* 49, 332–338. doi: 10.1016/J.RAM.2017.02.008

Jiménez-Arellanes, A., Luna-Herrera, J., Cornejo-Garrido, J., López-García, S., Castro-Mussot, M. E., Meckes-Fischer, M., et al. (2013). Ursolic and oleanolic acids as antimicrobial and immunomodulatory compounds for tuberculosis treatment. *BMC Complement Altern. Med.* 13. 258. doi: 10.1186/1472-6882-13-258

Jumper, J., Evans, R., Pritzel, A., Green, T., Figurnov, M., Ronneberger, O., et al. (2021). Highly accurate protein structure prediction with AlphaFold. *Nature* 596 (7873), 583–589. doi: 10.1038/s41586-021-03819-2

Kim, S., Seo, H., Mahmud, H. A., Islam, M. I., Kim, Y. S., Lyu, J., et al. (2017). *In vitro* effect of DFC-2 on mycolic acid biosynthesis in *Mycobacterium tuberculosis*. *J. Microbiol. Biotechnol.* 27 (11), 1932–1941. doi: 10.4014/JMB.1705.05013

Lee, T. S., Cerutti, D. S., Mermelstein, D., Lin, C., Legrand, S., Giese, T. J., et al. (2018). GPU-Accelerated molecular dynamics and free energy methods in Amber18: Performance enhancements and new features. *J. Chem. Inf Model.* 58, 2043–2050. doi: 10.1021/acs.jcim.8b00462

Lone, M. Y., Athar, M., Gupta, V. K., and Jha, P. C. (2017). Identification of *Mycobacterium tuberculosis* enoyl-acyl carrier protein reductase inhibitors: A combined in-silico and in-vitro analysis. *J. Mol. Graph Model.* 76, 172–180. doi: 10.1016/j.jmgm.2017.07.005

Lougheed, K. E., Osborne, S. A., Saxty, B., Whalley, D., Chapman, T., Bouloc, N., et al. (2011). Effective inhibitors of the essential kinase PknB and their potential as anti-mycobacterial agents. *Tuberc. (Edinburgh Scotland)* 91 (4), 277–286. doi: 10.1016/j.tube.2011.03.005

Maier, J. A., Martinez, C., Kasavajhala, K., Wickstrom, L., Hauser, K. E., and Simmerling, C. (2015). ff14SB: Improving the accuracy of protein side chain and backbone parameters from ff99SB. *J. Chem. Theory Comput.* 11 (8), 3696–3713. doi: 10.1021/acs.jctc.5b00255

Mark, P., and Nilsson, L. (2001). Structure and dynamics of the TIP3P, SPC, and SPC/E water models at 298 K. *J. Phys. Chem.* 105, 9954–9960. doi: 10.1021/jp003020w

Martin, A., Camacho, M., Portaels, F., and Palomino, J. C. (2003). Resazurin microtiter assay plate testing of *Mycobacterium tuberculosis* susceptibilities to second-line drugs: Rapid, simple, and inexpensive method. *Antimicrob. Agents Chemother.* 47 (11), 3616–3619. doi: 10.1128/AAC.47.11.3616-3619.2003

McKinney, J. D., Höner Zu Bentrup, K., Muñoz-Elias, E. J., Miczak, A., Chen, B., Chan, W. T., et al. (2000). Persistence of *Mycobacterium tuberculosis* in macrophages and mice requires the glyoxylate shunt enzyme isocitrate lyase. *Nature* 406, 735–738. doi: 10.1038/35021074

Mulyukin, A. L., Kudykina, Y. K., Shleeva, M. O., Anuchin, A. M., Suzina, N. E., Danilevich, V. N., et al. (2010). Intraspecies diversity of dormant forms of *Mycobacterium smegmatis*. *Microbiology* 79, 461–471. doi: 10.1134/S0026261710040089

Murugasu-Oei, B., and Dick, T. (2000). Bactericidal activity of nitrofurans against growing and dormant mycobacterium bovis BCG. *J. Antimicrob. Chemother.* 46 (6), 917–919. doi: 10.1093/jac/46.6.917

Nikitushkin, V. D., Shleeva, M. O., Zinin, A. I., Trutneva, K. A., Ostrovsky, D. N., and Kaprelyants, A. S. (2016). The main pigment of the dormant *Mycobacterium smegmatis* is porphyrin. *FEMS Microbiol. Lett.* 363 (19), fnw206. doi: 10.1093/FEMSLE/FNW206

Pawar, A., Jha, P., Chopra, M., Chaudhry, U., and Saluja, D. (2020). Screening of natural compounds that targets glutamate racemase of *Mycobacterium tuberculosis* reveals the anti-tubercular potential of flavonoids. *Sci. Rep.* 10 (1), 949. doi: 10.1038/s41598-020-57658-8

Peramo, A. (2016). Solvated and generalised born calculations differences using GPU CUDA and multi-CPU simulations of an antifreeze protein with AMBER. *Mol. Simulation* 42 (15), 1263–1273. doi: 10.1080/08927022.2016.1183000

Price, D. J., and Brooks, C. L. (2004). A modified TIP3P water potential for simulation with ewald summation. *J. Chem. Phys.* 121 (20), 10096–10103. doi: 10.1063/1.1808117

Rastelli, G., del Rio, A., Degliesposti, G., and Sgobba, M. (2010). Fast and accurate predictions of binding free energies using MM-PBSA and MM-GBSA. *J. Comput. Chem.* 31, 797–810. doi: 10.1002/JCC.21372

Rathor, N., Garima, K., Sharma, N. K., Narang, A., Varma-Basil, M., and Bose, M. (2016). Expression profile of mce4 operon of *Mycobacterium tuberculosis* following environmental stress. *Int. J. Mycobacteriol.* 5, 328–332. doi: 10.1016/J.IJMYCO.2016.08.004

Roe, D. R., and Cheatham, T. E. (2013). PTRAJ and CPPTRAJ: Software for processing and analysis of molecular dynamics trajectory data. *J. Chem. Theory Comput.* 9, 3084–3095. doi: 10.1021/CT400341P/SUPPL_FILE/CT400341P_SI_001.PDF

Schrödinger, E. (2018). *LigPrep | schrödinger*, Schrödinger Release 2018-1.

Sharma, S., and Tyagi, J. S. (2016). *Mycobacterium tuberculosis* DevR/DosR dormancy regulator activation mechanism: Dispensability of phosphorylation, cooperativity and essentiality of α10 helix. *PloS One* 11 (8), e0160723. doi: 10.1371/journal.pone.0160723

Singh, V., Bhoir, S., Chikhale, R. V., Hussain, J., Dwyer, D., Bryce, R. A., et al. (2020). Generation of phenothiazine with potent anti-TLK1 activity for prostate cancer therapy. *iScience* 23, 101474. doi: 10.1016/J.ISCI.2020.101474

Sterling, T. R., Njie, G., Zenner, D., Cohn, D. L., Reves, R., Ahmed, A., et al. (2020). Guidelines for the treatment of latent tuberculosis infection: Recommendations from the national tuberculosis controllers association and CDC 2020. *MMWR Recomm Rep.* 69 (1), 1–11. doi: 10.15585/mmwr.rr6901a1

Taneja, N. K., and Tyagi, J. S. (2007). Resazurin reduction assays for screening of anti-tubercular compounds against dormant and actively growing *Mycobacterium tuberculosis*, *Mycobacterium bovis* BCG and *Mycobacterium smegmatis*. *J. Antimicrob. Chemother.* 60 (2), 288–293. doi: 10.1093/jac/dkm207

Trutneva, K. A., Shleeva, M. O., Demina, G. R., Vostroknutova, G. N., and Kaprelyans, A. S. (2020). One-year old dormant, "non-culturable" *Mycobacterium tuberculosis* preserves significantly diverse protein profile. *Front. Cell Infect. Microbiol.* 10. doi: 10.3389/fcimb.2020.00026

Van Deun, A., Hossain, M. A., Gumusboga, M., and Rieder, H. L. (2008). Ziehl-neelsen staining: theory and practice. *Int. J. Tuberc. Lung Dis.* 12 (1), 108–110.

Varadi, M., Anyango, S., Deshpande, M., Nair, S., Natassia, C., Yordanova, G., et al. (2022). Alpha fold protein structure database: Massively expanding the structural coverage of protein-sequence space with high-accuracy models. *Nucleic Acids Res.* 50, D439–D444. doi: 10.1093/NAR/GKAB1061

Villela, A. D., Eichler, P., Pinto, A. F. M., Rodrigues-Junior, V., Yates, J. R., Bizarro, C. V., et al. (2015). Gene replacement and quantitative mass spectrometry approaches validate guanosine monophosphate synthetase as essential for *Mycobacterium tuberculosis* growth. *Biochem. Biophys. Rep.* 4, 277. doi: 10.1016/J.BBREP.2015.10.005

Wang, J., Wang, W., Kollman, P. A., and Case, D. A. (2001). Automatic atom type and bond type perception in molecular mechanical calculations. *J Mol Graph Model.* 25, 247–260. doi: 10.1016/j.jmgm.2005.12.005

Waterhouse, A., Bertoni, M., Bienert, S., Studer, G., Tauriello, G., Gumienny, R., et al. (2018). SWISS-MODEL: Homology modelling of protein structures and complexes. *Nucleic Acids Res.* 46, W296–W303. doi: 10.1093/NAR/GKY427

Wayne, L. G., and Hayes, L. G. (1996). An *in vitro* model for sequential study of shiftdown of *Mycobacterium tuberculosis* through two stages of nonreplicating persistence. *Infect. Immun.* 64 (6), 2062–2069. doi: 10.1128/iai.64.6.2062-2069

Wayne, L. G., and Sramek, H. A. (1994). Metronidazole is bactericidal to dormant cells of *Mycobacterium tuberculosis*. *Antimicrob. Agents Chemother.* 38, 2054–2058. doi: 10.1128/AAC.38.9.2054

Wisedchaisri, G., Wu, M., Sherman, D. R., and Hol, W. G. J. (2008). Crystal structures of the response regulator DosR from *Mycobacterium tuberculosis* suggest a helix rearrangement mechanism for phosphorylation activation. *J. Mol. Biol.* 378, 227–242. doi: 10.1016/J.JMB.2008.02.029

Young, T. A., Delagoutte, B., Endrizzi, J. A., Falick, A. M., and Alber, T. (2003). Structure of *Mycobacterium tuberculosis* PknB supports a universal activation mechanism for Ser/Thr protein kinases. *Nat. Struct. Biol.* 10 (3), 168–174. doi: 10.1038/nsb897

Zheng, H., Williams, J. T., Aleiwi, B., Ellsworth, E., and Abramovitch, R. B. (2020). Inhibiting *Mycobacterium tuberculosis* DosRST signaling by targeting response regulator DNA binding and sensor kinase heme. *ACS Chem. Biol.* 15 (1), 52–62. doi: 10.1021/acschembio.8b00849

Frontiers in
Cellular and Infection Microbiology

Investigates how microorganisms interact with their hosts

Explores bacteria, fungi, parasites, viruses, endosymbionts, prions and all microbial pathogens as well as the microbiota and its effect on health and disease in various hosts.

Discover the latest Research Topics

See more →

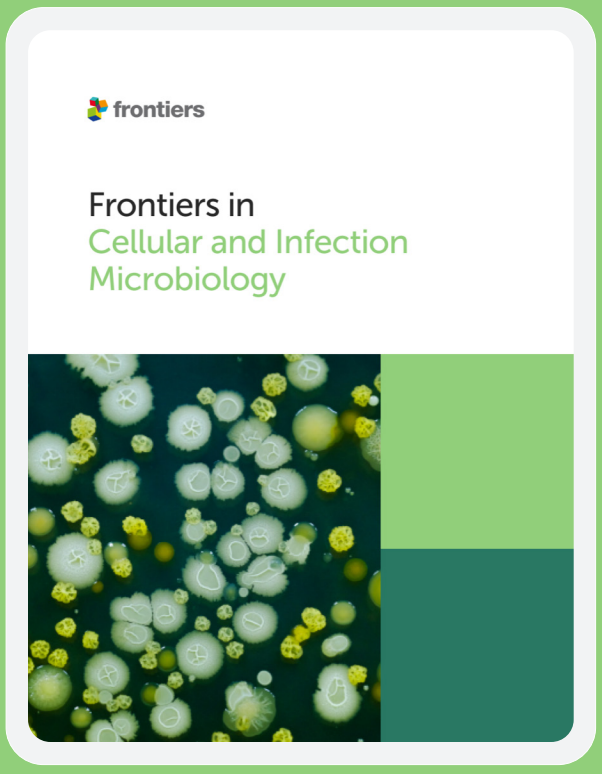

Frontiers

Avenue du Tribunal-Fédéral 34
1005 Lausanne, Switzerland
frontiersin.org

Contact us

+41 (0)21 510 17 00
frontiersin.org/about/contact